

D-A040 596

XONICS INC SANTA MONICA CALIF
THEORETICAL STUDIES OF HIGH-POWER ULTRAVIOLET AND INFRARED MATE--ETC(U)
DEC 76 M SPARKS, C J DUTHLER

F/G 20/5

DAHC15-73-C-0127

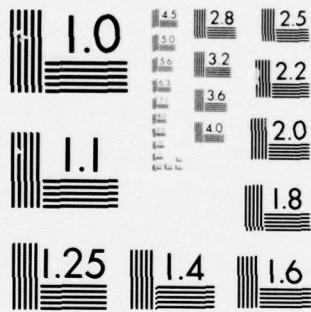
NL

UNCLASSIFIED

1 OF 4

AD
A040 596





AD A 040596

THEORETICAL STUDIES OF HIGH-POWER ULTRAVIOLET AND INFRARED MATERIALS

M. SPARKS, PRINCIPAL INVESTIGATOR, 213/451-9916
C. J. DUTHLER, PRINCIPAL SCIENTIST, 213/787-7380

XONICS, INCORPORATED
SANTA MONICA, CALIFORNIA 90401

EIGHTH TECHNICAL REPORT
31 DECEMBER 1976

DISTRIBUTION STATEMENT A
Approved for public release;
Distribution Unlimited

CONTRACT NO. DAHC 15-73-C-0127
EFFECTIVE DATE OF CONTRACT: 7 DECEMBER 1972
CONTRACT EXPIRATION DATE: 31 MARCH 1978

PREPARED FOR
DEFENSE SUPPLY SERVICE - WASHINGTON, D.C.

SPONSORED BY DEFENSE ADVANCED RESEARCH PROJECTS AGENCY
DARPA ORDER NO. 1969, AMENDMENT NO. 10, PROGRAM CODE NO. 6D10

AD NO. _____
DDC FILE COPY,

DDC
RECEIVED
JUN 15 1977
A

Unclassified

SECURITY CLASSIFICATION OF THIS PAGE (When Data Entered)

REPORT DOCUMENTATION PAGE		READ INSTRUCTIONS BEFORE COMPLETING FORM
1. REPORT NUMBER	2. GOVT ACCESSION NO.	3. RECIPIENT'S CATALOG NUMBER
4. TITLE (and Subtitle) THEORETICAL STUDIES OF HIGH-POWER ULTRAVIOLET AND INFRARED MATERIALS.		5. TYPE OF REPORT & PERIOD COVERED Eighth Technical Report, 1 July 1976 through 31 December 1976
		6. PERFORMING ORG. REPORT NUMBER
7. AUTHOR(s) M./Sparks and C. J./Duthler		8. CONTRACT OR GRANT NUMBER(s) DAHC 15-73-C-0127
9. PERFORMING ORGANIZATION NAME AND ADDRESS Xonics, Incorporated 1333 Ocean Avenue Santa Monica, California 90401		10. PROGRAM ELEMENT, PROJECT, TASK AREA & WORK UNIT NUMBERS 12937P.
11. CONTROLLING OFFICE NAME AND ADDRESS Defense Supply Service Room 1D245 - The Pentagon Washington, D. C. 20310		12. REPORT DATE 31 December 1976
		13. NUMBER OF PAGES 336
14. MONITORING AGENCY NAME & ADDRESS (if different from Controlling Office) Defense Advanced Research Projects Agency 1400 Wilson Boulevard Arlington, Virginia 22209		15. SECURITY CLASS. (of this report) Unclassified
15a. DECLASSIFICATION/DOWNGRADING SCHEDULE		
16. DISTRIBUTION STATEMENT (of this Report) This document may be further distributed only with specific prior approval of the Defense Supply Service, Washington, D. C. DISTRIBUTION STATEMENT A Approved for public release; Distribution Unlimited		
17. DISTRIBUTION STATEMENT (of the abstract entered in Block 20, if different from Report) Technical rept. no. 8, 1 Jul - 31 Dec 76,		
18. SUPPLEMENTARY NOTES		
19. KEY WORDS (Continue on reverse side if necessary and identify by block number) absorption, calcium fluoride, clusters of imperfections, coatings, damage threshold, electron-avalanche breakdown, film deposition, fracture, fused silica, heat-pipe mirrors, heat-transfer coefficient, heating, imperfections, intermediate-thermal layer, invar, localized damage sites, macroscopic inclusions, materials, melting, mirrors, molyb- denum, optical absorption, optical distortion, reflectors, sapphire, silicon carbide,		
20. ABSTRACT (Continue on reverse side if necessary and identify by block number) Theoretical results for the failure modes of reflectors and windows are derived and applied to a model system with $\lambda = 250$ to 350 nm, pulse duration $1 \mu s$, repetition rate 100 Hz (to 10^3 Hz), reflector absorptance 5×10^{-3} , extrinsic window-material absorp- tance 10^{-4} ($\beta = 10^{-4} \text{ cm}^{-1}$ for 1-cm thickness), and $\lambda/40$ allowed optical-phase distortion. (1) A low-thermal-expansion intermediate layer, such as ThF_4 (negative expansion)/ metal stack, between the optical coating and the substrate should give a near-zero single- phase contribution to the optical distortion threshold $(I_{tp})_0$. The remaining substrate- limited values of $(I_{tp})_0$ are greater than previously expected: $20 \text{ J/cm}^2/\text{pulse}$ for Mo and		

DD FORM 1 JAN 73 1473

EDITION OF 1 NOV 65 IS OBSOLETE

Unclassified

SECURITY CLASSIFICATION OF THIS PAGE (When Data Entered)

409 988

Unclassified

SECURITY CLASSIFICATION OF THIS PAGE(When Data Entered)

93 J/cm²/pulse for invar, both for state-of-the-art cooling (heat-transfer coefficient 10 W/cm² K and face-plate thickness 0.5 mm). Such great values of $(It_p)_0$, which seemed impractical at the beginning of the program, may be greater than the damage threshold $(It_p)_d$, which is expected to be between 10 and several hundred J/cm² in present coatings. Thus, increasing the damage threshold, by the same ultraclean deposition techniques suggested previously to decrease the coating absorptance, would further increase the system performance. A proposed cluster-of-microscopic-imperfections explanation of localized damage sites, which could explain previous localized damage when macroscopic inclusions could not be found, indicates this possibility of increasing the damage threshold. Invar and molybdenum are the two leading substrate candidates; Cu, Al, Ag, and Au have substrate-limited repeated-pulse and single-pulse thresholds below 10 J/cm², and SiC has potential reflector fabrication problems. A figure of merit $\beta K \ln(n_H/n_L)/\alpha(1+\nu)$ is less important than technical factors in choosing candidate coating materials, the optical coating material requirements being substantially reduced by the use of the intermediate-thermal-layer design. Tetrahedral-carbon films (so-called diamond films) recently developed at the Aerospace Corporation possibly could be superior optical-coating films. Two-photon absorption can be tolerated in coatings, but not in windows. Greater strength of materials in thin-film form possibly could make fracture a relatively unimportant failure mechanism. Measurements of the expansion coefficients α of coating materials in thin-film form are needed. The notion of a penetration depth of the irradiance into the coating is introduced to interpret and explain the coating-material absorptance, the substrate absorptance, the optical distortion from the change in phase of the reflection coefficient, and the optimum number of layers in the optical coating. Cooling the substrate, which is not effective for single pulses, is a major factor limiting the performance of repeated-pulse and cw reflectors. Possible solutions to the model reflector problem, in addition to the low α intermediate layer, include: lowering the absorptance, and possibly the damage threshold (see above), by considerably improving ultrapure deposition techniques; using an invar substrate; depositing an ultralow expansion coating; and such engineering solutions as adaptive optics (possibly with an uncooled invar substrate) and heat-pipe mirrors (possibly with adaptive optics). (2) The generally difficult problems of calculating the temperature distribution and stress components in layered structures with both radial and axial variation of temperature were solved in closed form with sufficient accuracy to be comparable with the assumptions and the accuracy with which the parameters are known by considering the stress as the sum of two terms. The detached-stress term is that of a reflector divided into many thin layers, and the attachment-stress term is the stress required to bring the layers back to their actual positions. Thickness changes, which cause optical distortion, tend to be more affected by the detachment stresses than by the attachment stresses. Neglecting the latter greatly simplifies the analysis and results and gives quite accurate results (five percent for the worst temperature distribution and of order $\sim \ell_F/4\ell_S$ for the best case of a currently used reflector) for many, but not all, reflectors. (3) Values of the failure thresholds for windows are calculated for the known important failure mechanisms. If an adaptive optical system (with a reasonable time constant of 10^{-3} s) can be developed, the value of $(It_p)_0$ for a window will be increased to the great single-pulse value of 3.3 J/cm²/pulse, as set by thermal optical distortion from extrinsic absorption, or possibly slightly lower from inclusions of clusters. Without adaptive optics the threshold is much lower: $(It_p)_0 = 3.3 \times 10^{-2}$ J/cm²/pulse, as set by extrinsic absorption (even assuming that β can be reduced to 10^{-4} cm⁻¹, which may not be easy). Technical considerations, including the position of F bands and other imperfection absorption bands as discussed by P. H. Klein, are more important than are figures of merit in choosing candidate window materials, as well as coating materials. The major difference between the two wavelength regions 250 nm and 350 nm is that two-photon absorption precludes the use at 250 nm of many materials that are useful at 350 nm (where they are limited by three-photon absorption). In a comparison of previous theoretical estimates of the two-photon absorption coefficient with eight experimental values, the absorption coefficient in alkali iodides and alkali

Unclassified

SECURITY CLASSIFICATION OF THIS PAGE(When Data Entered)

Unclassified

SECURITY CLASSIFICATION OF THIS PAGE (When Data Entered)

20. Abstract (Cont.)

bromides is typically underestimated by a factor of two, which is better agreement than previously predicted for the rough estimate. Reasonable materials that do not suffer two-photon absorption at 350 nm are LiF, MgF₂, CaF₂, BeO, NaF, SrF₂, BaF₂, Al₂O₃, SiO₂ (fused and crystalline), MgO, and possibly BeF₂. Of these materials, LiF, MgF₂, BeF₂, and perhaps CaF₂ and BeO, do not suffer two-photon absorption at 250 nm. Sapphire has an estimated fracture temperature that is a factor of 10 greater than that of other materials. Alkaline-earth fluorides tend to be less susceptible to thermal distortion than other materials. (4) In the first phase of the re-investigation of electron-avalanche breakdown, a classical transport equation is derived from the Boltzmann equation and is used to derive an expression for the average electron-multiplication rate Γ . The electron-phonon interaction parameters appearing in Γ are evaluated.

SECTION for	
White Section	<input checked="" type="checkbox"/>
Blue Section	<input type="checkbox"/>
UNCLASSIFIED	<input type="checkbox"/>
AUTHORIZATION	
<i>Letter on file</i>	
BY	
DISTRIBUTION/AVAILABILITY CODE	
Dist.	AVAIL. STATEMENT
A	

19. Key Words (Cont.)

strength of materials, stresses, substrate cooling, temperature, tetrahedral carbon, thermal expansion, thin films, thorium tetrafluoride, two-photon absorption, window materials

Unclassified

SECURITY CLASSIFICATION OF THIS PAGE (When Data Entered)

TABLE OF CONTENTS

<u>Section</u>	<u>Page</u>
Contents of Present and Previous Reports	xiii
Preface	xvii
A SUMMARY AND INTRODUCTION	1
Reflectors	1
Windows	4
Electron-Avalanche Breakdown	5
B OPTICAL DISTORTION AND FAILURE IN HIGH-POWER REFLECTORS	6
I. Introduction and Summary	9
Properties of the model system	10
Values of parameters	11
Approximations and assumptions	14
Reflectors considered	16
Summary of results	18
Possible solutions	19
Possibility of reducing optical distortion to a negligible value	20
Promising design using intermediate thermal layer . .	21
Possible explanation of single-pulse damage	22
Calculated failure thresholds	22
Figures of merit and material-selection guidelines . .	23
Candidate substrate materials	25
Candidate coating materials, including tetra- hedral carbon, SiO ₂ , and ThF ₄	25
Ultralow and negative thermal expansion coatings . .	27
Thin intermediate layers	28
Greater strength of films	28
Measurements of α are needed	29
Coating and reflector absorptance	29

TABLE OF CONTENTS (Cont.)

<u>Section</u>	<u>Page</u>
B	
Damage thresholds.	30
Optical distortion and absorption change from r	31
Cooling.	32
Engineering solutions	33
Optimum number of coating layers	33
Protective coatings	34
Stringent optical tolerance.	35
Miscellaneous	35
II. Uncoated Metallic Reflectors	37
Background.	37
Single-pulse temperature	39
Thermal-diffusion distances.	40
Repeated-pulse temperature distribution	41
Failure mechanism	44
Single-pulse optical distortion.	44
Continuously repeated-pulse optical distortion	47
III. Dielectric Coatings and Distortion	
Compensating Layers	50
Lowering the absorptance of coatings.	50
Possibility of obtaining near-zero thermally induced optical distortion	51
Clusters of microscopic imperfections	57
Single-pulse damage threshold	59
Two-photon absorption.	62
Strength of materials in thin-film form.	63
Experimental values of the expansion coefficients of deposited thin films are needed	63
Number of layers required	64
Theoretical absorptance of reflectors.	67
Obtaining an ultralow-thermal-expansion coating.	72

TABLE OF CONTENTS (Cont.)

<u>Section</u>	<u>Page</u>
B	
Coating failure modes.	76
Nonlinear effects	76
Material properties.	77
IV. Thermally Thick Dielectric Reflectors	78
Temperature distribution.	78
Thermally induced optical-distortion calculation . . .	79
Coating stresses and strength	82
Thermally induced stresses	83
Melting	87
V. Thermally Thin Dielectric Reflectors	89
Temperature distribution in a thermally thin coating .	89
Thermally induced optical distortion.	92
Coating stress and fracture analysis.	95
VI. Adaptive Optics and Substrate Materials and Cooling. . .	97
Typical values of heat-transfer coefficients h	97
Cobalt-iron-chromium negative-expansion substrate	98
Silicon carbide	99
Heat-pipe mirrors	99
Adaptive optics for lower h	100
Rapid interpulse cooling	102
Time constant for cooling.	102
Uncooled substrate with adaptive optics	103
VII. Continuous-Operation Reflectors	108
VIII. Thermally Induced Changes in the Reflection Coefficient	111

TABLE OF CONTENTS (Cont.)

<u>Section</u>		<u>Page</u>
B	IX. Applications.	124
	MgO/MgF ₂ : Mo	125
	MgO/MgF ₂ : Cu	127
	21-layer HfO ₂ /SiO ₂	127
	HfO ₂ /SiO ₂ : Mo	128
	X. Tabulation of Derived Results	132
	XI. Acknowledgments	144
	Appendix. Heat Flow in Many-Layered Structures	145
C	THERMAL STRESSES AND EXPANSION IN MULTILAYER DIELECTRIC REFLECTORS.	154
	I. Introduction and Summary	155
	Summary of results	157
	II. Temperature Distribution	159
	III. Simple Cases of Thermal Stresses	163
	IV. General Case of Stresses.	171
	V. Thermal Expansion.	180
	VI. Acknowledgments	184
	Appendix. Useful Thermal-Stress Results	185
D	FAILURE THRESHOLDS OF NEAR-ULTRAVIOLET TRANSPARENT MATERIALS	193
	I. Introduction.	196
	II. Absorption Coefficients.	200
	Extrinsic Absorption	200
	Two-Photon Absorption	201
	Three-Photon Absorption	209

TABLE OF CONTENTS (Cont.)

<u>Section</u>		<u>Page</u>
D	III. Free Carrier Creation and Recombination.	211
	IV. Free Carrier Optical Distortion and Absorption	225
	Free Carrier Absorption	227
	Free Carrier Optical Distortion.	233
	V. Thermal Distortion and Thermal Fracture	238
	VI. Nonlinear Refractive Index.	250
	VII. Absorbing Inclusions	252
	VIII. Summary of Single-Pulse Thresholds	254
	IX. Summary of Repeated-Pulse Thresholds.	260
E	LASER-INDUCED ELECTRON AVALANCHES IN INSULATING SOLIDS	267
	I. Introduction.	268
	II. Average Multiplication Rate β	272
	III. Electron-Phonon Interaction in Alkali-Halides.	281
	Appendix A. Deviation of the Classical Transport Equation	292
	Appendix B. Contribution of Electronically Inelastic Collisions to the Transport Equation.	301
F	OVERVIEW OF MATERIALS FOR HIGH-POWER VISIBLE AND ULTRAVIOLET LASERS.	305
	Metallic reflectors	305
	Multilayer-dielectric reflectors	309
	Transparent materials	310
	Electron-plasma defocusing	312
	Microscopic inclusions.	314
	Two-photon absorption	314
	Raman-scattering process	314
	Nonlinear-refractive-index mechanism	314

LIST OF ILLUSTRATIONS

<u>Section</u>	<u>Figure</u>	<u>Title</u>	<u>Page</u>
B	1	Thermally distorted mirror showing that the optical path distortion is equal to twice the physical distortion.	17
	2	Values of metallic absorptance plotted from data in the third edition of the American Institute of Physics Handbook.	38
	3	(a) Reflector or interest, and (b) a model reflector used in calculating the reflection coefficient of the reflector in (a).	113
	4	Schematic illustration showing the advance in phase of the reflected wave resulting from the change in position of the surface of the coating, and the retardation resulting from the phase ϕ_r of the reflector coefficient r (resulting from deeper penetration into the thermally expanded coating).	117
	A.1	Schematic illustration of the temperature distribution in a two-layer structure at various times.	147
	A.2	Schematic illustration of the temperature distribution in a many-layered structure.	148
C	1	Typical temperature distribution at the end of a pulse during repeated-pulse operation.	160
D	1	Two-photon absorption exciting an electron from the valence band to the conduction band with an upper-conduction band serving as the intermediate state.	203
	2	Other intermediate states for two-photon absorption.	204
	3	Time constant τ_R'' for impurity depletion as a function of laser intensity for two impurity-absorption cross sections.	214
	4	Free-carrier concentration as a function of time at five intensities for materials limited by donor-impurity absorption. N_0 is the concentration of donor impurities, τ_R is the intrinsic recombination time, and I_C is the characteristic intensity for depletion.	216

LIST OF ILLUSTRATIONS (Cont.)

<u>Section</u>	<u>Figure</u>	<u>Title</u>	<u>Page</u>
D	5	Electron-hole pair concentration as a function of time at five laser intensities for materials limited by intrinsic two-photon absorption. I_0 is the characteristic intensity where the two-photon absorption coefficient equals 1 cm^{-1} .	221
	6	Electron-hole pair concentration as a function of time at four laser intensities for materials limited by intrinsic three-photon absorption. I_{03} is the characteristic intensity where the three-photon absorption coefficient equals 1 cm^{-1} .	223
	7	Overall absorption coefficient as a function of time for materials containing donor impurities of various absorption cross sections, all having an initial absorption coefficient of 10^{-4} cm^{-1} .	229
	8	Overall absorption coefficient, including free-carrier absorption, as a function of time at five intensities for material limited by intrinsic two-photon absorption.	232
	9	Overall absorption coefficient, including free-carrier absorption, as a function of time at four intensities for a material limited by intrinsic three-photon absorption.	234
	10	Wavelength dependence of terms in the thermal distortion expression for CaF_2 demonstrating a possible cancellation in the visible and near uv spectral regions. (From Miles, Ref. 14.)	242
	11	Temperature rise as a function of time in materials limited by donor-impurity absorption having an initial absorption coefficient of 10^{-4} cm^{-1} and various impurity-absorption cross sections.	244
	12	Temperature rise as a function of time at four laser intensities in a material limited by intrinsic two-photon absorption.	246
	13	Temperature rise as a function of time at four laser intensities in a material limited by intrinsic three-photon absorption.	248

LIST OF ILLUSTRATIONS (Cont.)

<u>Section</u>	<u>Figure</u>	<u>Title</u>	<u>Page</u>
D	14	Summary of single-pulse thresholds for failure as a function of the pulse duration.	255
	15	Summary of single-pulse thresholds for a 10^{-6} sec duration pulse.	258
	16	Summary of repeated-pulse thresholds for failure as a function of pulse duration for a system pulsed at 10^3 Hz for 60 sec. The average intensities for failure are equal to the pulse intensity multiplied by the product of the pulse duration and the repetition rate.	261
	17	Summary of repeated-pulse thresholds for 10^{-6} sec duration pulses repeated at 10^3 Hz for 60 sec. The average intensities are 10^{-3} times the pulse intensities.	263
F	1	Schematic illustration of metallic absorptance in the free-electron approximation, showing the useful frequency range $0 < \omega < \omega_p$, and the great intrinsic values of absorptance on this range. Numbers in parentheses are for aluminum (neglecting the interband contribution to the absorptance).	308
	2	Schematic illustration of the frequency dependence of the absorption of a dielectric material, showing the useful range and the extrinsic absorption on this range.	311
	3	Impurity absorption in several alkali halides near the absorption edge, showing the long extrinsic absorption "tails" and the sample to sample variation. From Tomiki and Miyata. ¹³	313
	4	Schematic illustration of the effects of the nonlinear index of refraction $n_2 \langle E^2 \rangle$.	315
	5	Schematic illustration of the enhancement in the nonlinear refractive index $\delta n = n_2 \langle E^2 \rangle$.	316
	6	Intensities at which transparent materials fail by various mechanisms for a single 7.2 eV, 10 ns pulse. Changing the frequency or the pulse duration changes the values of the intensities and the relative importance of the mechanisms.	318

LIST OF TABLES

<u>Section</u>	<u>Table</u>		<u>Page</u>
B	I	Values of coating- and substrate-material parameters, and values of failure energy densities of uncoated substrates with $A = 5 \times 10^{-3}$ formally.	12
	II	Theoretical results for threshold energy densities, temperatures, heat-transfer coefficients, lengths, and times.	13
	III	Coating materials for possible use at 250 to 350 nm.	26
	IV	Number of coating layers required to give $1 - R = 5 \times 10^{-3}$ for various coating/substrate combinations.	68
D	I	Candidate transparent materials for use with a 350 nm wavelength laser.	199
	II	Comparison of experimental and theoretical values of the characteristic two-photon absorption intensity.	208
	III	Comparison of thermal distortion and thermal fracture parameters for some candidate materials.	241
F	I	Lowest measured values of absorptance of silver and aluminum, showing the great intrinsic values of metallic absorptance.	307

CONTENTS OF PRESENT AND PREVIOUS REPORTS

1. March 1972

1. Introduction
2. Calculation of Multiphonon Absorption Coefficients
3. Calculation of Extrinsic Absorption Coefficient
4. Effects of Pressure on Operation of Windows
5. Recommendations for an Experimental Program
6. Experimental Data from the Literature
7. Nonlinear Processes
- App. A. — Elementary Introduction to the Theory of Infrared Absorption Spectra

2. June 1972

1. Introduction
2. Calculation of Multiphonon Absorption Coefficient
3. Green's Function Analysis and Sjolander-Type Approximations
4. Rigid-Ion, Next-Near-Neighbor Model for the Scattering Hamiltonian
5. Pressure-Induced Optical Distortion in Laser Windows
6. Plans for Continued Research
- App. A. — Tabulation of Pressure-Induced Optical-Distortion Results
- App. B. — Eigenvectors for the Rigid-Ion, Next-Near-Neighbor Model

3. December 1972

- A. Introduction
- B. Theory of Multiphonon Infrared Absorption
- C. Theory of Infrared Absorption and Material Failure in Crystals
Containing Inclusions
- D. Collection of Experimental Results for $\beta(\omega)$
- E. References to Previous Multiphonon Calculations

4. June 1973

- A. Introduction
- B. Theory of Infrared Absorption and Material Failure in Crystals
Containing Inclusions
- C. Theory of Multiphonon Absorption in Insulating Crystals
- D. Temperature Dependence of Multiphonon Infrared Absorption
- E. Theory of Infrared Absorption by Crystals in the High Frequency Wing of
Their Fundamental Lattice Absorption
- F. Temperature Dependence of the Absorption Coefficient of Alkali Halides
in the Multiphonon Regime
- G. Temperature and Frequency Dependence of Infrared Absorption as a
Diagnostic Tool
- H. Short-Pulse Operation of Infrared Windows without Thermal Defocusing

5. December 1973

- A. Introduction
- B. Extrinsic Absorption
- C. Extrinsic Absorption in 10.6 μm Laser Window Materials Due to Molecular-Ion Impurities
- D. Very High-Intensity Effects
- E. Explanation of Laser-Damage Cone-Shaped Surface Pits
- F. Nonlinear Infrared Absorption from Parametric Instabilities of Phonons
- G. High-Power 2-6 μm Window-Material Figures of Merit with Edge Cooling and Surface Absorption Included
- H. High-Power 10.6 μm Window-Material Figures of Merit with Edge Cooling and Surface Absorption Included
- I. Explicit Exponential Frequency Dependence of Multiphonon Infrared Absorption
- J. Quasiselection Rule for Infrared Absorption by NaCl-Structure Crystals
- K. The Absorption Coefficient of Alkali Halides in the Multiphonon Regime: Effects
- L. Vertex Corrections for Multiphonon Absorption
- M. Negligible Intrinsic-Absorption Processes
- N. Summary of Publications and Results
- App.—Simple Pendulum Instability

6. June 1974

- A. Introduction and Summary
- B. Intensity Limits of High-Intensity Vacuum Ultraviolet Materials
- C. Multiphoton Absorption
- D. Calculated Reflectance of Aluminum in the Vacuum Ultraviolet
- E. Total-Internal-Reflection Devices
- F. The Scattering and Absorption of Electromagnetic Radiation by a Semi-Infinite Crystal in the Presence of Surface Roughness
- G. Infrared Absorption by the Higher-Order-Dipole-Moment Mechanism
- H. Stimulated Raman and Brillouin Scattering: Parametric Instability Explanation of Anomalies
- I. Extrinsic Absorption in 10.6 μm Laser Window Materials
- J. Erratum, High-Power 2- to 6- μm Window-Material Figures of Merit with Edge Cooling and Surface Absorption Included
- K. List of Recent Publications

7. December 1974

- A. Introduction and Summary
- B. Stimulated Raman Scattering: Enhanced Stokes Gain and Effects of Anti-Stokes and Parametric Phonon Processes
- C. Enhanced Stimulated Raman Scattering and General Three-Boson Parametric Instabilities
- D. Theory of Laser-Materials Damage by Enhanced Stimulated Raman Scattering
- E. Surface Roughness and the Optical Properties of a Semi-Infinite Material; The Effect of a Dielectric Overlayer
- E. App.—Construction of the Green's Functions for the Electromagnetic Wave Equation

7. December 1974 (Cont.)

- F. Theory of Laser Heating of Solids: I. Metals
- G. Current Status of High-Intensity Vacuum Ultraviolet Materials
- H. Impurity Absorption in Halide Window Materials
- I. List of Recent Publications

8. June 1975

- A. Introduction and Summary
- B. Current Status of Electron-Avalanche-Breakdown Theory
- C. Preliminary Theory of Electron-Avalanche Breakdown in Dielectric by Laser and dc Fields
- D. VUV Window Failure by Multiphoton Absorption and Electron Defocusing, Avalanche, and Absorption
- E. Optical Distortion from the Nonlinear Refractive Index
- F. Studies of Optical Properties of Alkali Halide Crystals
- G. A Possible Mechanism for Extrinsic Absorption in Insulators below the Fundamental Absorption Edge
- H. Multiphonon Absorption of Alkali Halides and Quasiselection Rules
- I. Enhanced Stimulated Raman Scattering and General Three-Boson Parametric Instabilities
- J. List of Publications

9. December 1975

- I. Summary of Results
- II. Near-Term Recommendations
- III. Background Information
- IV. Possible Sources of Additional Absorption in Coatings
- V. Suggested Measurements
- VI. Other Problems
- VII. Laser Heating of Coatings
- VIII. Laser Damage of Coatings
- IX. Laser Damage of Detached Coatings
- X. Guidelines for Selecting New Materials
- XI. Candidate 10.6 μm Coating Materials
- XII. Candidate 2-6 μm Coating Materials
- XIII. Excerpts and Results from Literature, with Comments

10. June 1976

- A. Introduction and Summary
- B. Polymer Coatings for Protection of Optical Components
- C. Electronic Properties of the LiF Valence Band; Surface States and the Local Density of States Near the Surface
- C. App.—Explicit Form of the Hamiltonian for the N Layer LiF Slab

10. June 1976 (Cont.)

- D. Localized Electronic States in Alkali Halides Associated with a Substitutional Anion Impurity
- E. Classical Transport Equation for Electron-Avalanche Breakdown
- F. Evaluation of Two-Center Integrals of Slater Atomic Orbitals
- G. Quasiselection Rules for Multiphonon Absorption in Alkali Halides
- H. Irradiance Limits for Vacuum-Ultraviolet Material Failure
- I. Materials for High-Power Window and Mirror Coatings and Multilayer-Dielectric Reflectors

11. December 1976

- A. Summary and Introduction
- B. Optical Distortion and Failure in High-Power Reflectors
 - B. App.—Heat Flow in Many-Layered Structures
- C. Thermal Stresses and Expansion in Multilayer Dielectric Reflectors
 - C. App.—Useful Thermal-Stress Results
- D. Failure Thresholds of Near-Ultraviolet Transparent Materials
- E. Laser-Induced Electron Avalanches in Insulating Solids
 - E. App. A—Deviation of the Classical Transport Equation
 - E. App. B—Contribution of Electronically Inelastic Collisions to the Transport Equation
- F. Overview of Materials for High-Power Visible and Ultraviolet Lasers

PREFACE

This Eighth Technical Report describes the work performed on Contract Number DAHC15-73-C-0127 on Theoretical Studies of High-Power Ultraviolet and Infrared Materials during the period from 1 July 1976 through 31 December, 1976. The work on the current contract is a continuation of that of the previous Contract Number DAHC15-72-C-0129.

The following investigators contributed to this report:

Dr. C. J. Duthler, principal research scientist

Mr. M. R. Flannery, research assistant

Dr. T. D. Holstein, consultant, University of California, Los Angeles

Dr. M. Sparks, principal investigator.

Previously reported results are not repeated in the present report, with the exception of Sec. F, which is a copy of an earlier paper presented at the DARPA Conference on Infrared Laser Window Materials, Boulder, Colorado, 12 July 1976. It is included for completeness; later results are compiled in Sec. D.

Sec. A

A. SUMMARY AND INTRODUCTION

✓
The main thrust of the program in the current report period has been on analyzing the expected performance of high-power reflectors and windows for use in the wavelength region from 250 to 350 nm, in anticipating potential problems for these reflectors and windows, and in seeking solutions. Several exciting new results were obtained. The abstracts and summaries in the Introduction and Summary subsections of the individual sections provide an outline of the central results. The following list is intended to provide an overview and a very brief summary of the results obtained to date.

(1) Theoretical results for the failure modes of reflectors and windows are derived and applied to a model system with wavelengths $\lambda = 250$ to 350 nm, pulse duration $t_p = 1 \mu s$, repetition rate 100 Hz (to 10^3 Hz), reflector absorptance 5×10^{-3} , extrinsic window material absorptance 10^{-4} (absorption coefficient $\beta = 10^{-4} \text{ cm}^{-1}$ for a one-centimeter-thick window), and $\lambda/40$ allowed optical phase distortion.

Handwritten notes:
microsec
1000
lambda
beta = .0001/cm
lambda

Reflectors

(2) A reflector design using a low thermal-expansion intermediate layer such as a ThF_4 (negative-expansion)/metallic stack between the optical coating and the substrate to obtain near-zero single-pulse contribution to the optical distortion should attain substrate-limited optical-distortion thresholds of $20 \text{ J/cm}^2/\text{pulse}$ for Mo or $93 \text{ J/cm}^2/\text{pulse}$ for invar, such high values appearing unattainable at the beginning of the program.

Sec. A

(3) Possibilities of increasing the overall system performance now exist since methods of increasing both the damage threshold and the optical-distortion threshold are suggested.

(4) A proposed damage mechanism of clusters of microscopic imperfections explains previously anomalous isolated damage sites.

(5) If the proposed damage mechanisms in (4) is correct, it may be possible to increase the damage threshold by the same ultrapure deposition techniques suggested previously to decrease the great coating absorptance.

(6) Materials possibly may have greater strength in thin-film form than in bulk form, which could result in the fracture threshold being relatively unimportant.

(7) The notion of a penetration depth of the irradiance into the coating is useful in explaining the coating material absorptance, the substrate absorptance, the optical distortion from the change in phase of the reflection coefficient, and the optimum number of layers in the optical coating.

(8) Tetrahedral carbon (so-called diamond), ThF_4 , and SiO_2 are good candidate materials for coatings.

(9) For coating materials, a figure of merit $\beta K \ln(n_H/n_L)/\alpha(1+\nu)$ is less important than technical considerations in selecting candidate materials.

(10) Two-photon absorption can be tolerated in coatings but not in windows.

(11) Invar and molybdenum are the most promising substrate-material candidates.

Sec. A

(12) A good figure of merit for substrate materials is $1/\alpha(1+\nu)$ for the typical case of poor cooling ($h \ll 3 K_S/\ell_S$), or $K/\alpha(1+\nu)$ for good cooling ($h \gg 3 K_S/\ell_S$).

(13) Measurements of the expansion coefficients of materials in thin-film form are needed in order to select and evaluate coating materials and to establish the viability of the proposed intermediate-thermal-layer design of (2).

(14) Possible solutions to the model reflector problem, in addition to that in (2), include: lowering the absorptance, and possibly the damage threshold (see (5)), by considerably improving ultrapure deposition techniques; using an invar substrate; depositing an ultralow expansion coating; and such engineering solutions as adaptive optics (possibly with an uncooled invar substrate) and heat-pipe mirrors (possibly with adaptive optics).

(15) Cooling the substrate, which is not effective for single pulses, is a major factor limiting the performance of repeated-pulse and cw reflectors.

(16) The state of the art for high-power (water cooled) mirrors is a heat-transfer coefficient $h = 10 \text{ W/cm}^2 \text{ K}$ and a face-plate thickness $\ell_S = 0.5 \text{ mm}$. These values were assumed in (2) above.

(17) The generally difficult problems of calculating the temperature distribution and stress components in layered structures with both radial and axial variation of the temperature were solved in closed form with sufficient accuracy to be compatible with the assumptions and accuracy with which the parameters are known by considering the stress as the sum of two terms, a detachment stress which is that of a reflector divided into many thin layers, and an attachment stress which is the stress required to bring the layers back to their actual positions.

Windows

(18) If an adaptive optical system (with a reasonable time constant of 10^{-3} s) can be developed, the value of $(It_p)_o$ for a window will be increased to the great single-pulse value of $3.3 \text{ J/cm}^2/\text{pulse}$, as set by thermal optical distortion from extrinsic absorption (with $\beta = 10^{-4} \text{ cm}^{-1}$), or possibly slightly lower from inclusions of clusters.

(19) Without adaptive optics, the threshold is much lower: $(It_p)_o = 3.3 \times 10^{-2} \text{ J/cm}^2/\text{pulse}$, as set by extrinsic absorption (even assuming that β can be reduced to 10^{-4} cm^{-1} , which may not be easy).

(20) Technical considerations, including the positions of the F bands and other imperfection absorption bands as discussed by P. Klein, are more important than the figures of merit in choosing candidate window materials, as well as coating materials.

(21) The major difference between the two wavelength regions 250 nm and 350 nm is that two-photon absorption precludes the use at 250 nm of many materials that are useful at 350 nm (where they are limited by three-photon absorption).

(22) In a comparison of previous theoretical estimates of the two-photon absorption coefficient with eight experimental values, the absorption coefficient in alkali iodides and alkali bromides is typically underestimated by a factor of two, which is better agreement than previously predicted for the rough estimate.

(23) Reasonable materials that do not suffer two-photon absorption at 350 nm are LiF , MgF_2 , CaF_2 , BeO , NaF , SrF_2 , BaF_2 , Al_2O_3 , SiO_2 (fused and crystalline), MgO , and possibly BeF_2 . Of these materials, LiF , MgF_2 , BeF_2 ,

Sec. A

and perhaps CaF_2 and BeO , do not suffer two-photon absorption at 250 nm. Sapphire has an estimated fracture temperature that is a factor of 10 greater than that of other materials. Alkaline-earth fluorides tend to be less susceptible to thermal distortion than other materials.

(24) Values of the failure thresholds, in $\text{J}/\text{cm}^2/\text{pulse}$ (or MW/cm^2 during the pulse), calculated for the important known window-failure mechanisms for the model system in (1) above are as follows. (Values in parentheses are for single-pulse operation.):

Thermal optical distortion, two photon	2.4×10^{-2}	(2.9)
Thermal optical distortion, extrinsic $\beta = 10^{-4} \text{ cm}^{-1}$	3.3×10^{-2}	(2×10^3)
Fracture, two-photon	0.22	(14)
Fracture, inclusion or clusters	~ 2 to ~ 500	(same)
Free-carrier optical distortion, two-photon	2.2	(same)
Fracture, extrinsic $\beta = 10^{-4} \text{ cm}^{-1}$	3.3	(2×10^5)
Thermal optical distortion, three-photon	28	(440)
Fracture, three-photon	89	(1.4×10^3)
Free-carrier optical distortion, extrinsic $\beta = 10^{-4} \text{ cm}^{-1}$	140	(same)
Free-carrier optical distortion, three-photon	1.8×10^3	(same)
Nonlinear refractive index optical distortion	3.1×10^3	(same)

Electron-Avalanche Breakdown

(25) In the first phase of the re-investigation of electron-avalanche breakdown, a classical transport equation is derived from the Boltzmann equation and used to derive an expression for the electron-avalanche multiplication rate Γ , and the electron-phonon-interaction parameters appearing in Γ are evaluated.

Sec. B

B. OPTICAL DISTORTION AND FAILURE IN HIGH-POWER REFLECTORS

M. Sparks

Xonics, Incorporated, Santa Monica, California 90401

- (1) Theoretical results for the melting, fracture, and optical distortion of dielectric reflectors deposited on metallic substrates, under single-pulse, repeated-pulse, and cw operation are derived and applied to high-power reflectors with absorptance $A = 5 \times 10^{-3}$ (absorption coefficient $\beta \cong 200 \text{ cm}^{-1}$, typically), pulse duration $t_p = 1 \mu\text{s}$, repetition rate = 100 Hz, and wavelength $\lambda = 250$ to 354 nm.
- (2) Several possible solutions to this reflector problem are suggested, including an intermediate ThF_4 (negative expansion)/metal stack between the optical coating and the substrate to obtain a near-zero single-pulse contribution to the optical distortion. The remaining substrate-limited, repeated-pulse optical distortion thresholds $(It_p)_{\text{or}}$ are $20 \text{ J/cm}^2/\text{pulse}$ for Mo and $93 \text{ J/cm}^2/\text{pulse}$ for invar. Such high values seemed quite impractical at the beginning of the program.
- (3) Other solutions include: lowering the absorptance, and possibly the damage threshold as discussed below, by considerably improving ultra-clean deposition techniques; using an invar face plate; depositing an ultralow expansion coating; and such engineering solutions as adaptive optics (possibly with an uncooled invar substrate) and heat-pipe mirrors (possibly with adaptive optics). Implementing one of these solutions possibly could increase $(It_p)_{\text{or}}$ to a value above the damage threshold, which is expected to range from 10 to possibly several hundred J/cm^2 .
- (4) A proposed damage mechanism involving clusters of microscopic imperfections appears to explain experimental damage results, including localized

Sec. B

damage sites that occur even in the absence of observable macroscopic inclusions, and indicates that the super-clean deposition techniques suggested previously to decrease the absorptance possibly may increase the damage threshold, thereby increasing the system performance if the optical threshold is increased as in (2) and (3). (5) Tetrahedral carbon (so-called diamond), recently deposited at the Aerospace Corporation, should be a superior coating material, other good candidates being ThF_4 , SiO_2 , and possibly HfO_2 . (6) The notion of a penetration depth of the irradiance into the coating is useful in explaining the coating-material absorptance, the substrate absorptance, and the optical distortion from the change in phase of the reflection coefficient. (7) Greater strength of materials in thin-film form possibly could make fracture a relatively unimportant failure mechanism. (8) Invar and molybdenum are the two leading substrate candidates, with Cu, Al, Ag, and Au having both substrate-limited repeated-pulse thresholds and single-pulse thresholds below 10 J/cm^2 , and SiC having potential reflector-fabrication problems. (9) Measurements of the expansion coefficients of coating materials, particularly ThF_4 , SiO_2 , and HfO_2 , in thin-film form are needed. (10) A figure of merit $\beta K \ln(n_H/n_L)/\alpha(1+\nu)$ is less important than technical factors in choosing candidate coating materials, the optical-coating-material requirements being substantially reduced by the use of the intermediate-thermal-layer design since the optical distortion is limited by the substrate. (11) Two-photon absorption can be tolerated in coatings (but not in windows). (12) Cooling the substrate, which is not effective for single pulses, is a major factor limiting the performance of repeated-pulse and cw reflectors. State-of-the-art water-cooled reflectors have heat-transfer coefficient $h = 10 \text{ W/cm}^2 \text{ K}$ and face-plate thickness 0.5 mm. (13) The generally difficult problems of calculating the temperature distribution

Sec. B

and stresses in layered structures with both radial and axial variation of temperature were solved with sufficient accuracy to be comparable with the assumptions, the accuracy with which the parameters are known, etc.

I. INTRODUCTION AND SUMMARY

The availability of high-power lasers has generated interest in new classes of materials problems. Numerous publications such as those in the Proceedings of the Annual Conferences on Infrared Materials, recent Boulder conferences on Laser Induced Damage in Optical Materials, and various journals afford many examples of these new problems and attest to the continued growing importance of high-power optical systems.^{1,2} Much of the recent work has been in the infrared region, but interest has been shifting to the ultraviolet and visible regions.

Theoretical analyses of optical distortion and fracture of windows for high-power systems were carried out early in the high-power infrared laser program.^{3,4} Bennett has analyzed the single-pulse optical distortion of uncoated metallic mirrors.¹ In the present paper, optical distortion, melting, and fracture of multilayer-dielectric reflectors and uncoated metallic reflectors used in single-pulse, repeated-pulse, and cw operation are analyzed. The general purpose of the investigation is to provide the theoretical study needed in anticipated programs to develop high-power reflectors. Guidelines for selecting the best candidate materials for coatings and substrates are given, and experiments needed to assist in the selection are identified. Intrinsic and extrinsic limitations of reflector performance are considered, and possible solutions to the reflector problems are suggested.

Reflectors can fail catastrophically, by melting or fracture of the coating, for example, or fail to meet their required specifications, by excessive optical distortion, for example. A general treatment of the theory of the energy density

Sec. B-1

It_p or the irradiance I at which this failure occurs in such optical components as reflectors and windows would be extremely useful, but is quite impractical to develop. Not only do the required specifications differ drastically from system to system, but the theoretical values of I or It_p for failure involve so many parameters – such as wavelength, temperature, pulse duration, pulse repetition rate, maximum irradiance, dimensions of the optics and the optical beams, pressure, and mode of operation such as single-pulse, repeated-pulse, continuous operation, or operation for a given time – that a treatment of all possible combinations of parameters is not feasible. Thus, we are forced to consider particular systems as interest arises or to make incomplete, broad analyses of general types of systems. The present study will emphasize a particular model system, but the treatment is kept as general as practical, consistent with a reasonable length and with practical usefulness, in order to be of wide interest.

The properties of the model system are as follows:

- wavelength: $\lambda = 354 \text{ nm}$ (3.50 eV); alternate: 250 nm (4.96 eV)
- laser pulse duration: $t_p = 1 \mu\text{s}$
- repetition rate: 100 Hz (100 pps), with possible increase to 10^3 pps
- total operating time: 60 s
- energy density: $It_p = 10 \text{ J/cm}^2/\text{pulse}$
- irradiance (during the pulse): $I = 10^7 \text{ W/cm}^2$
- irradiance (averaged over the 60 seconds): $I_{av} = 10^3 \text{ W/cm}^2$
- optical tolerance: $\lambda/40$ of the operating wavelength per element for thermally induced wave-front error
- pressure: two atmospheres nominal; four atmospheres during the pulse

Sec. B-1

- pulse shape: rectangular with no spikes
- laser material: not yet selected. Xenon fluoride, at 354 nm, is a prime contender. Krypton fluoride, at 250 nm, is a test system.
- environment: The optical components will be protected from the corrosives and from direct exposure to electrons and X-rays. Thus, resistance to these environmental factors is not essential, but would be desirable.
- visible transmission: sufficient for alignment.

Values of parameters. In addition to these general system parameters, the following values will be used throughout the paper in order to afford numerical examples:

- substrate thickness, $\ell_S = 0.1 \text{ cm}$
- absorptance, $A = 5 \times 10^{-3}$
- heat capacity of substrate, $C_S = [2.61 \text{ J/cm}^3 \text{ K}]$
- thermal conductivity of substrate, $K_S = [1.4 \text{ W/cm K}]$
- linear thermal expansion coefficient of substrate, $\alpha_S = [5 \times 10^{-6} \text{ K}^{-1}]$
- effective heat capacity of coating, $C_F = [3.14 \text{ J/cm}^3 \text{ K}]$
- effective thermal conductivity of coating, $K_F = [0.285 \text{ W/cm K}]$
- effective value of $\alpha(1+\nu)$ of coating, $\alpha_F(1+\nu_F) = [15.6 \times 10^{-6} \text{ K}^{-1}]$.

The numerical values in brackets above and throughout the paper are for an MgO/MgF_2 coating on a molybdenum substrate operating at 250 nm, unless specified otherwise. The effective values of C , K , and $\alpha(1+\nu)$ for the coating are derived in Appendix A. Values of C , K , and α for other materials are listed in Table I, and results for other coatings and substrates are given in Table II below. It is emphasized that the value of absorptance $A = 5 \times 10^{-3}$

Table I. Values of coating- and substrate-material parameters, and values of failure energy densities of uncoated substrates with $A = 5 \times 10^{-3}$ formally.

Substrate Material	C (J/cm ³ K)	K (W/cm K)	α (10 ⁻⁶ K ⁻¹)	ν (l)	E (10 ⁶ psi)	$C/\alpha(1+\nu)$ (10 ⁵ J/cm ³)	(t_p) _{SC} (J/cm ²)	(t_p) _{AS} (J/cm ²)	(t_p) _{SLIM} (J/cm ²)	(t_p) _{OP} at 250 nm (J/cm ²)	(t_p) _{ORTH} at 250 nm (J/cm ²)	h for (t_p) _{OP} at 250 nm (W/cm K)	h_o (W/cm K)
Invar	3.18	0.12	0.5	0.290	21	49.3	223	160	93.2	352	35.8	1.25	31.8
SiC	2.40	2.11(a)	4.3	0.3(c)	13-68(b)	4.29	25.6	323	23.7	30.7	22.2	14.2	24.0
Mo	2.61	1.4	5.0	0.279(b)	46-47(b)	4.08	22.3	187	20.0	29.2	18.0	20.2	26.1
Cu	3.45	4.0	16.8	0.364	17(b)	1.51	6.33	149	6.07	10.8	8.35	always fails	34.5
Ag	2.46	4.18	19.2	0.38	11(b)	0.928	5.39	135	5.18	6.63	5.54	always fails	—
Al	2.43	2.38	23.2	0.33	10-10.6(b)	0.788	4.63	66.0	4.32	5.63	4.20	always fails	—
Coating Material	C (J/cm ³ K)	K (W/cm K)	α (10 ⁻⁶ K ⁻¹)	ν (l)	E (10 ⁶ psi)	$C/\alpha(1+\nu)$ (10 ⁵ J/cm ³)	n	σ_t (10 ³ psi)	T _m (C)	h_f (J/cm ³)	H_f/C K ⁻¹		
MgF ₂	3.14	0.1-0.3	13.7	0.3(c)	24.5	—	1.41 [250 nm]	7.6	1221	1250	398		
MgO	3.13	0.6	10.5	0.233	36.1	—	1.74 [250 nm]	20	2642	6890	2200		
SiO ₂	1.7	0.014	0.5	0.17	10.6	—	1.477 [354 nm]	~ 10	1710	340	334		
HfO ₂	1.7(c)	0.014(c)	0.5(c)	0.17(c)	10.6(c)	—	2.14 [354 nm]	~ 10	2812	—	—		
ThF ₄	2(c)	0.1(c)	-2.5	0.3(c)	25(c)	—	1.35(c)	8(c)	1200(c)	—	—		
Coating Pairs	C _F (J/cm ³ K)	K _F (W/cm K)	$\alpha_F(1+\nu_F)$ (10 ⁻⁶ K ⁻¹)										
MgO/MgF ₂	3.14	0.285	15.6										
HfO ₂ /SiO ₂	1.7	0.014	0.585										
ThF ₄ /SiO ₂	2(c)	0.014(c)	—										

(a) Dr. W. J. Choyke, private communication.

(b) Materials Engineering 76, 13 (1972).

(c) Assumed values (for thin-film form of HfO₂).

(d) The values are calculated for $h = 10$ W/cm² K and $l_s = 0.5$ mm.

Table II. Theoretical results for threshold energy densities, temperatures, heat-transfer coefficients, lengths, and times.

Parameter	Unit	Equation Number	45 MgO/MgF ₂ at 250 nm				21 HfO ₂ /SiO ₂ at 354 nm				ThF ₄ /SiO ₂ at 354 nm on Mo
			on Invar	on SiC	on Mo	on Cu	on Invar	on SiC	on Mo	on Cu	
(<i>t_p</i>) _{op} @ <i>h</i> = ∞	J/cm ²	(5.13)	24.0	22.3	21.4	11.5	346	79.9	77.5	29.9	145
(<i>t_p</i>) _{or} @ <i>h</i> = ∞	J/cm ²	(5.15)	12.9	17.5	14.7	8.80	35.6	47.1	35.8	19.1	45.5
(<i>t_p</i>) _{or} @ <i>h</i> = 10	J/cm ²	(5.15)	11.6	7.40	6.33	always fails	29.0	13.1	11.0	3.58	15.1
(<i>t_p</i>) _{or} @ <i>h</i> = 1	J/cm ²	(5.15)	5.96	1.19	1.03	always fails	10.9	1.74	1.51	0.431	1.7
(<i>t_p</i>) _{mp} @ <i>h</i> = ∞	J/cm ²	(4.24)	238	357	339	411	52.4	55.9	55.4	56.8	57.9
(<i>t_p</i>) _{mr} @ <i>h</i> = ∞	J/cm ²	(4.24)	132	349	338	405	45.5	55.8	55.4	56.7	57.8
(<i>t_p</i>) _{mr} @ <i>h</i> = 1	J/cm ²	(4.25)	127	315	305	360	45.0	54.8	54.6	55.8	56.6
(<i>t_p</i>) _{tp} **	J/cm ²	(5.18)	12.1	18.1	17.2	20.8	85.8	92.7	92.0	94.1	1 - 7
<i>h</i> for (<i>t_p</i>) _{or} = 10	W/cm ² K	(5.16)	4.02	18.2	28.1	always fails	0.886	7.02	8.78	47.6	6.33
<i>h</i> for (<i>t_p</i>) _{fr} = 10	W/cm ² K	(5.21)	0.348	0.0929	0.0918	-0.0370 *	3.64 × 10 ⁻⁴	-0.0105 *	-0.0125 *	-0.0474 *	
<i>l_F</i>	μm	(4.1)	1.81	1.81	1.81	1.81	1.06	1.06	1.06	1.06	3.39
<i>l_{Ftp}</i>	μm	(4.2)	6.02	6.02	6.02	6.02	1.81	1.81	1.81	1.81	
<i>l_{ΔS}</i>	μm	(5.7)	1.64	7.93	6.19	9.10	1.40	6.75	5.27	7.75	
<i>τ_F</i>	10 ⁻⁸ s	(5.1)	9.02	9.02	9.02	9.02	34.1	34.1	34.1	34.1	
<i>T_{Fp0}</i>	K	(5.2)	67.1	44.8	47.2	38.9	361	338	341	333	242
<i>T_{ΔFp0}</i>	K	(5.6)	27.2	27.2	27.2	27.2	324	324	324	324	
<i>T_{FSp}</i>	K	(5.8)	40.0	17.6	20.0	11.8	41.3	14.3	16.6	9.04	
<i>T_{ΔSr0}</i>	K	(2.5)	54.1	1.18	0.179	0.625	54.1	1.18	0.179	0.625	
<i>T_{Fr0}</i> @ <i>h</i> = ∞	K	(5.2)			47.4						
<i>h_o</i>	W/cm ² K	(5.17)	2.17	17.5	19.1	36.9	22.1	44.2	49.0	67.7	
<i>h_f</i>	10 ⁻² W/cm ² K	(5.20)	7.17	7.5	6.59	-4.00 *	0.276 *	-8.71 *	-10.2 *	-39.9 *	

* Negative value of *h_f* and [*h* for (*t_p*)_{fr} = 10 J/cm²] denotes reduced stresses for repeated-pulse operation.

** The estimated fracture thresholds may be highly inaccurate, as discussed in Sec. B-IV.

Sec. B-I

listed above surely is much greater than the intrinsic limit and that solving the anticipated technical problems of obtaining lower values of absorptance would increase the values of the tolerable energy densities $I t_p$ and decrease the required cooling (value of the heat-transfer coefficient h) obtained below.

Approximations and Assumptions

- The laser pulses are approximated by square waves in time, the pulse duration being t_p .
- The irradiance has the value I at the spatial position of maximum intensity, which is at the center of the beam.
- Radial (in the plane of the substrate) heat diffusion is neglected.
- The temperature dependence of the material parameters is neglected. In accurate analyses of some particular systems, the accuracies of the calculation, the model, and the values of parameters may warrant an investigation of the effect of the temperature dependence of the parameters.
- The back side of the substrate is cooled and supported with a system that gives a heat-transfer coefficient $h(\text{W}/\text{cm}^2 \text{K})$ and holds the rear surface, at $z = \ell_F + \ell_S$, of the substrate in a plane (no bowing). Here ℓ_F is the coating thickness.
- The optical-distortion failure criterion is taken simply as

$$\ell_{\text{opd}} = \lambda/g \quad (1.1)$$

where $\ell_{\text{opd}} = 2\Delta\ell$ is the optical-path difference between rays at the center and at the edge of the reflector resulting from the laser heating, $\Delta\ell$ is the corresponding surface distortion, and g is constant.

- The thermally induced phase change ϕ_r of the reflection coefficient is neglected in the values listed in Table II. See Sec. VIII.

Sec. B-I

In order to obtain numerical values of optical-failure thresholds, the value of $g = 40$ ($\lambda/80$ surface distortion) will be used for the thermally induced optical distortion. For any particular criterion of failure, the corresponding value of g can be calculated and used to easily scale the results given for $g = 40$ to those of the particular criterion. As an example, $g = 8$ corresponds to halving the intensity in the focal plane for a single optical element under a simple set of conditions that includes a parabolic temperature distribution truncated at $1/3$.^{3,4} As another example, Winsor⁵ has considered the optical-tolerance requirements of systems containing a number of reflectors and windows, and Bennett and co-workers⁶ have derived the failure thresholds for a system containing N reflectors having physical displacement of the surface τ_f caused by initial (no heating) figuring error. Using the Maréchal criterion for allowable optical distortion, these investigators^{5,6} derived the failure criterion

$$I/I_0 = 0.8 = 1 - (2\pi/\lambda)^2 \frac{1}{2} (N\tau_f^2 + N^2 \ell_{\text{opd}}^2) .$$

Setting $\ell_{\text{opd}} = \lambda/g$, defining $\tau_f \equiv \lambda/g_f$, and solving for g gives

$$g = \frac{1}{2} 2^{1/2} N \left[\frac{1}{5(2\pi)^2} - \frac{N}{2g_f^2} \right]^{-1/2} \quad (1.2)$$

For $N = 3$ (3 mirrors) and $g_f = 25$ (that is, $\lambda/25$ initial figuring error), (1.2) gives $g = 40$. Or for $N = 4$ and $g_f \rightarrow \infty$, (1.2) gives $g = 40$. Thus, the value of $g = 40$ is not atypical. In passing, it is mentioned that in general the ray-bending angle θ is given by $\theta = -d\ell_{\text{opd}}/d\rho$, where ρ is the distance from the optical axis.

Sec. B-1

For a Gaussian beam,

$$I = I_0 e^{-a\rho^2},$$

the center ($\rho=0$) temperature T_0 and rim ($\rho=R$) temperature differ by $T_0 [1 - \exp(-aR^2)]$; thus (see Fig. 1)

$$l_{\text{opd}} \equiv 2[(\Delta l)_{\rho=0} - (\Delta l)_{\rho=R}] = 2\Delta l(1 - e^{-aR^2})$$

where $\Delta l \equiv (\Delta l)_{\rho=0}$ is the thermal expansion of the center of the mirror.⁷

Thus, the criterion (1.1) becomes

$$\Delta l = \lambda / 2 G \tag{1.3}$$

where

$$\begin{aligned} 2G &= 2g(1 - e^{-aR^2}) \\ &= 1.26 g && \text{for } 1/e \text{ truncation} \\ &= 1.73 g && \text{for } 1/e^2 \text{ truncation} \\ &= 2g && \text{for } 1/e^\infty \text{ truncation} . \end{aligned}$$

In the numerical calculations, the $1/e^2$ value with $g \cong 40$ will be used:

$$2G = 70 . \tag{1.4}$$

Reflectors considered. Invar, Mo, SiC, Cu, Ag, and Al substrates and a 45-layer MgO/MgF₂ coating⁸ and 21-layer HfO₂/SiO₂ coating⁹ are included in this report. These same two coatings are considered with each of the substrates, with no attempt to maximize the performance for the cases presented in Table II. In addition, a ThF₄/SiO₂ coating is considered in order to illustrate the potential

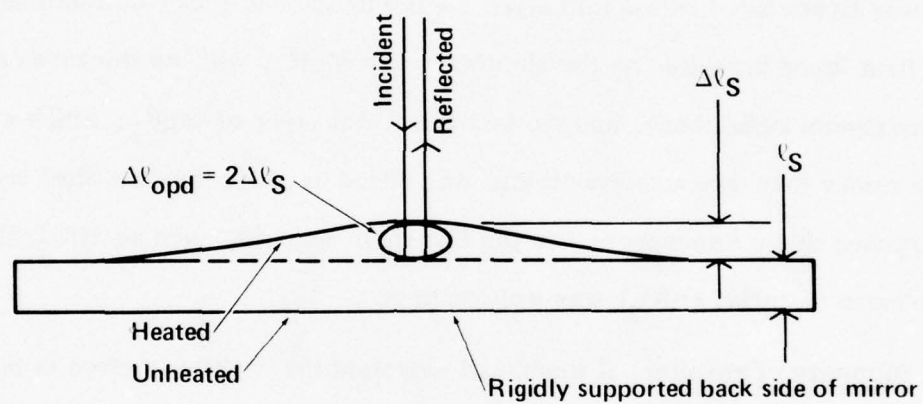


Fig. 1. Thermally distorted mirror showing that the optical-path distortion is equal to twice the physical distortion.

Sec. B-I

advantages and possible problems of using ThF_4 (with a negative thermal expansion coefficient at room temperature) in the optical coating (in addition to its use in the intermediate thermal layer discussed below). Both the $\text{HfO}_2/\text{SiO}_2$ and MgO/MgF_2 coatings were deposited on quartz substrates. For the high-power application, a substrate with a greater value of thermal conductivity will be required. An eleven-layer MgO/MgF_2 coating has been deposited on a molybdenum substrate that was first coated with a thin layer (~ 100 to 150 nm thick) of aluminum.⁸ The first layer deposited on the aluminum was MgF_2 , with its thickness adjusted for maximum reflectance, and the last (eleventh) layer of MgF_2 , which was half-wave rather than quarter-wave thick, was added in order that the MgO layer not be exposed to the atmosphere. In the film-pair notation, such as $\text{HfO}_2/\text{SiO}_2$, the high-index material (HfO_2) was written first.

Summary of results: A thumbnail sketch of the results is given in Sec. A, and a more complete summary is given here. Theoretical expressions for the temperature distributions, for the values of the laser energy density It_p at which excessive optical distortion ($\lambda/80$ surface distortion) and fracture occur, and for the required values of heat-transfer coefficients h for high-power reflectors used in single-pulse and repeated-pulse operation are derived and applied to practical systems to obtain the following results: The cardinal result is that we found no fundamental limitation on the operation of a model system with $10 \text{ J/cm}^2/\text{pulse}$, 100 pulses per second, and $\lambda/80$ thermally induced surface distortion at $\lambda = 250$ to 350 nm , but the technical problems are difficult.

Useful equations derived in this report are collected in Sec. X, and the most important equations are denoted by underscored equation numbers.

Sec. B-I

Possible solutions. Five possible theoretical solutions to the high-power reflector problem in the model system are found:

(1) Reduce the absorptance below the value $A = 5 \times 10^{-3}$ assumed for the model system. If, say, $A = 5 \times 10^{-4}$ could be attained, then the cooling requirements would not be so severe and any one of a number of coatings on molybdenum would have acceptable theoretical performance. A major difficulty is expected to be the solution of the technical problems of depositing low-absorptance coatings, as discussed previously.^{10, 11} The expected severity of this problem dictated the choice of the rather large value of absorptance, $A = 5 \times 10^{-3}$, which corresponds to an absorption coefficient $\beta_F = 200 \text{ cm}^{-1}$, very roughly. The $\text{HfO}_2/\text{SiO}_2$ coating⁹ has a measured reflectance of $R = 99.5$; thus the absorptance is at least as low as 5×10^{-3} (depending on scattering contribution to R).

(2) Develop a reflector using an intermediate layer of near-zero net thermal expansions (Sec. III). An example is a molybdenum substrate, followed by an intermediate layer consisting of ThF_4 /metal pairs, followed by a thin aluminum layer, and then the optical coating, such as ~ 10 pairs of MgO/MgF_2 . The ratio of the physical thickness of the ThF_4 layer to that of the metal layer is $\alpha_{\text{met}}(1 + \nu_{\text{met}})/|\alpha_{\text{ThF}_4}|(1 + \nu_{\text{ThF}_4})$ approximately (with a slight deviation to offset the small optical distortion of the MgO/MgF_2 coating). The intermediate layer consists of a number of pairs (rather than one pair) in order to maintain the near-zero single-pulse optical distortion through the pulse duration t_p (rather than at the end of the pulse only). The aluminum layer isolates the intermediate layer optically and reduces the required number (to seven theoretically) of MgO/MgF_2 pairs.

Sec. B-I

(3) Develop an invar-substrate reflector with values of the heat-transfer coefficient h and face-plate thickness ℓ_S approaching the state-of-the-art values $h = 10 \text{ W/cm}^2 \text{ K}$ and $\ell_S = 0.5 \text{ nm}$ (Sec. II). Such a negative-expansion-coefficient metal as the cobalt-iron-chromium alloy (Sec. VI) conceivably could be useful, but more information on such negative and ultralow expansion alloys is needed. Since invar-substrate reflectors are considerably better theoretically than those with other substrate materials, and ultralow expansion substrates are not required with invar, the feasibility of fabricating invar-substrate reflectors with cooling and initial figure approaching the state of the art should be determined early in any high-power reflector-development program.

(4) Develop a coating with a net ultralow thermal expansion. Bulk fused silica has an ultralow expansion coefficient $\alpha \cong 0.5 \times 10^{-6} \text{ K}^{-1}$, crystalline ThF_4 has $\alpha \cong -2.5 \times 10^{-6} \text{ K}^{-1}$, and it is of great importance to determine if HfO_2 , or indeed other coating materials, have ultralow expansion coefficients in thin-film form. It is possible that the $\text{HfO}_2/\text{SiO}_2$ coating of Baumeister and Arnon⁹ has an ultralow net expansion. The negative thermal expansion of ThF_4 could be especially useful if the fracture threshold is not too low, both as a coating material and as an intermediate layer between the coating and substrate.

(5) An engineering solution, such as adaptive optics or a heat-pipe mirror, possibly could solve the model-system problem. Engineering solutions are discussed below and in Sec. VI. Technical problems, in addition to those of implementing one of those solutions, are discussed below.

Possibility of reducing optical distortion to a negligible value. At the beginning of the investigation it appeared that optical distortion was a much more severe problem than that of physical damage. There is now the possibility that

Sec. B-I

the optical distortion thresholds can be reduced below the damage thresholds of reflectors, by one of the methods listed above. In addition to the obvious advantage of being able to operate at the limit set by damage, the smoke tests, as carefully controlled damage thresholds are currently called, would become more meaningful since they would correspond to the system threshold. Previously, the smoke tests were expected to establish a rather poor upper bound to the threshold value of It_p for a reflector since the values of It_p for optical distortion were believed to be lower than the values for damage. There have been no measurements of the damage thresholds for 10^{-6} s pulses for any ultraviolet wavelength, but it is anticipated that the damage threshold may be on the range of 10 to 100 J/cm^2 , probably near the lower values, at least for early coatings (Sec. III).

Promising design. The single-pulse contribution to the optical distortion usually is quite large. By using a tailored-thermal-expansion intermediate layer of ThF_4 /metal pairs mentioned above, this single-pulse contribution can be made negligible with respect to the contribution from the time-averaged-temperature rise. The resulting threshold $(It_p)_{\text{p or S}}$, which will be called the repeated-pulse substrate-limited threshold, is $(It_p)_{\text{p or S}} = 19.9 \text{ J/cm}^2$ for molybdenum and $(It_p)_{\text{p or S}} = 99.3 \text{ J/cm}^2$ for invar, both for $h = 10 \text{ W/cm}^2 \text{ K}$, and $\ell_S = 0.5 \text{ mm}$. If the damage thresholds are near 10 J/cm^2 as expected, the overall threshold will be determined by damage rather than by optical distortion. In this case, the value of h/ℓ_S could be reduced by a factor of two for molybdenum or by a factor of 9.3 for invar. The concrete example of a $2 \times 7 \text{ MgO/MgF}_2\text{:Al:ThF}_4\text{/Ag:Mo}$ reflector is considered in Sec. III. It is emphasized that the intermediate-thermal-layer design cannot compensate for the single-pulse optical distortion for pulse durations considerably shorter than a microsecond (such as picosecond or

Sec. B-I

nanosecond pulses) since the energy absorbed in the optical coatings does not have time to diffuse into the intermediate thermal layer during the pulse.

Possible explanation of single-pulse damage. There is growing concern that the macroscopic inclusion explanation of laser damage may be inadequate in many cases.^{12, 13} It is proposed that clusters of microscopic imperfections could explain the isolated damage sites that are observed almost universally, even when careful searches disclose no macroscopic imperfections. A preliminary investigation indicates that the results of the microscopic-cluster model agree well with experimental observations including the approximate magnitude of the damage energy densities It_p . An important feature of the explanation is that it now may be possible to increase the damage threshold by, say, the same ultraclean deposition techniques that were previously suggested^{10, 11} for reducing the absorptance of coatings.

Calculated failure thresholds: For a heat-transfer coefficient less than or equal to the state-of-the-art value $h = 10 \text{ W/cm}^2 \text{ K}$, the coatings considered fail by optical distortion, rather than by melting or fracture, in repeated-pulse operation. A possible exception is that ThF_4 , being in tension for single-pulse heating as a result of its negative expansion coefficient, conceivably could fail by fracture (Sec. III). The greatest practical repeated-pulse theoretical failure threshold calculated is

$$(It_p)_{\text{or}} = 93 \text{ J/cm}^2/\text{pulse}, \quad \text{for } 2 \times 7 \text{ MgO/MgF}_2:\text{Al}:\text{ThF}_4/\text{Mo}:\text{invar},$$

and other key values are

$$(It_p)_{\text{or}} = 29.0 \text{ J/cm}^2/\text{pulse}, \quad \text{for } \text{HfO}_2/\text{SiO}_2:\text{invar},$$

$$(It_p)_{\text{or}} = 15.1 \text{ J/cm}^2/\text{pulse}, \quad \text{for } \text{ThF}_4/\text{SiO}_2:\text{Mo},$$

and

$$(It_{p \text{ or}}) = 6.33 \text{ J/cm}^2/\text{pulse}, \quad \text{for MgO/MgF}_2\text{:Mo}.$$

Figures of merit and material-selection guidelines. There are no general figures of merit to determine if a substrate material or a coating material will be acceptable, other than to calculate the thresholds and temperatures as outlined herein. However, for the specific case of repeated-pulse/substrate-limited distortion attained by using the intermediate-thermal layer, (5.17a) gives (with "a" a constant of order unity)

$$(It_p) \sim \frac{1}{\alpha_S(1+\nu_S)} \left(K_S^{-1} + \frac{3}{a \ell_S h} \right)^{-1}.$$

Thus, for poor cooling, that is $h \ll h_S \equiv 3 K_S/a \ell_S$, a good figure of merit is $1/\alpha_S(1+\nu_S)$; while for good cooling, that is $h \gg h_S$, a good figure of merit is $K_S/\alpha_S(1+\nu_S)$. The single most important material parameter for substrates in general is the thermal expansion coefficient, small values of α_S being desirable. For a well designed high-power coating, the heat capacity of the substrate will not be very important (in currently envisioned reflector designs) since the single-pulse temperature rise will occur in the intermediate layer or the optical coating. Thus Bennett's¹ figure of merit, C_S/α_S , which was derived for single-pulse optical distortion of an uncoated substrate, is no longer appropriate. The value of the single-pulse optical distortion threshold $(It_{p \text{ op}})$ for the uncoated metal need not be greater than the required value of $(It_{p \text{ op}})$ (10 J/cm^2 in the examples) since the threshold for the coated reflector can be greater than for the uncoated one. An example is $\text{HfO}_2/\text{SiO}_2$ on molybdenum, for which $(It_{p \text{ op}}) = 29.2 \text{ J/cm}^2$ for uncoated molybdenum and $(It_{p \text{ op}}) = 77.5 \text{ J/cm}^2$ for $\text{HfO}_2/\text{SiO}_2\text{:Mo}$. Since the great intrinsic absorptance of metals dictates the use of dielectric coatings and a thin

Sec. B-I

intermediate layer of aluminum can often be used to reduce the required number of layers in the optical coating, the absorptance of the substrate materials is relatively less important than α and K .

For coating materials, one of the most important parameters is the absorption coefficient β . Unfortunately, values of β are not available, and reliable estimates cannot be made at present. Thus, the value of β cannot be used in selecting materials for laboratory tests. Any new developments that suggest that a pair of materials could form a low-absorptance coating would make this pair a prime candidate. For coatings to be used with the thermal compensation intermediate layer, the choice of the coating materials can be made from the technical considerations of the particular application since the thresholds are repeated-pulse, substrate-limited (independent of the coating, except for β). Nevertheless, the following figure of merit can be used in the absence of deciding technical factors. In order to ensure that the coating contribution to the optical distortion is small, the most important properties of the coatings are low values of β , high values of thermal conductivity, low thermal expansion, low values of heat capacity, and great values of the difference in the indices of refraction of the coating materials (great n_H/n_L). An appropriate figure of merit is then

$$\frac{\beta K \ln(n_H/n_L)}{\alpha(1 + \nu)}$$

The importance of an ultralow expansion coating, possibly using SiO_2 ($\alpha = 0.5 \times 10^{-6} \text{ K}^{-1}$ for fused silica) and/or ThF_4 ($\alpha = -1.4 \times 10^{-6} \text{ K}^{-1}$ average for 25 to 300 K) is discussed above and in Sec. III. The absorption edge of a coating material need not be

sufficiently great to prevent two-photon absorption (for $t_p = 10^{-6}$ s), in contrast to window materials, for which two-photon absorption must be avoided.

Candidate substrate materials. Invar and molybdenum are the two leading substrate-material candidates. The use of a very thin aluminum layer between the substrate and the cooling is discussed below. Copper, silver, gold, and aluminum substrates, with any of the three coatings, have optical-distortion thresholds that are too low for the model system considered. Theoretically, invar is considerably better than molybdenum, and silicon carbide is slightly better than molybdenum. The anticipated difficulties fabricating a silicon-carbide face plate and support/cooling structure render silicon carbide a poorer candidate than invar. Furthermore, a successful invar-substrate reflector would solve the reflector problem for the model system, while a successful silicon-carbide-substrate reflector alone would not.

Candidate coating materials, including tetrahedral carbon, SiO_2 , and ThF_4 . The most promising current design found for high-power reflectors is the intermediate-thermal-layer design. The parameters of optical coating used with this design are not critical, and the choice of the coating materials may well be dictated by technical considerations in the particular application, as discussed above. Thus, it is difficult to suggest the best candidate coating materials for laboratory study. The desirable properties of coating materials are listed above in the paragraph on figures of merit. There are a number of reviews¹⁴ that list coating materials, and several coating materials for 250 and 350 nm use are listed in Table III.

One exciting new development is the growth of tetrahedral carbon films (the so-called diamond films) with thicknesses up to several microns.¹⁵ If these films could be successfully deposited as one component of a multilayer coating stack,

Table III. Coating materials for possible use at 250 to 350 nm.

Material	Absorption edge λ_e (in nm)	Refractive index n	At Wavelength λ (in nm)	Material	Absorption edge λ_e (in nm)	Refractive index n	At Wavelength λ (in nm)
LiF	105	1.418	254	SiO ₂ (fused)	159	1.49	300
NaF	128	1.353	254	Al ₂ O ₃	141	1.80	300
BeF ₂ glass	83 (?)	1.33	300	MgO	175	1.74	250
MgF ₂	113	1.41	250	BeO	124	—	—
CaF ₂	124	1.45	300	ThO ₂	214	1.95	300
SrF ₂	129	—	—	TiO ₂	300	2.55	550
BaF ₂	136	1.50	300	ZrO ₂	270	2.1	300
PbF ₂	185	1.915	309	HfO ₂	240	2.14	350
CeF ₃	—	1.63	550	CeO ₂	—	2.05	550
LaF ₃	135	1.649 (e) 1.656 (o)	254	Y ₂ O ₃	~ 200	—	—
ThF ₄	250	1.48	300	Tetrahedral Carbon	~ 200	2.0	~ 500
Na ₃ AlF ₆	—	1.32 - 1.35	550	BN	200	—	—
NaCl	182	1.582	350	Si ₃ N ₄	—	—	—

Sec. B-I

it is likely that the coating would be superior to presently known coatings. Tetrahedral carbon/SiO₂ and tetrahedral carbon/ThF₄ are examples. The expansion coefficient may be quite low, and the band gap may be similar to that of diamond, $E_g \cong 6$ eV. The index of refraction is¹⁵ 2.0, and the hardness should far exceed that of other coating materials.

Thorium tetrafluoride, with its negative expansion coefficient, and silicon dioxide, with its ultralow expansion coefficient, should be included in the candidate materials. Most of the high index materials are oxides, with the exception of tetrahedral carbon and such heavy fluorides as PbF₂, LaF₃, and CeF₃. Magnesium oxide and magnesium fluoride should be considered since successful coatings have been used at 250 nm. Another possible combination is ThO₂/ThF₄.

Measurements of the expansion coefficient of materials in thin-film form are needed in order to make the best choice of candidate coating materials. These measurements will be especially important if the intermediate-thermal-layer design is not successful and for picosecond and nanosecond pulse durations (for which the design is not effective).

Ultralow and negative thermal expansion coatings. Crystalline thorium tetrafluoride has a small, negative expansion coefficient α for 20 C to ~ 300 C and a small positive α for ~ 300 to 600 C, the value at room temperature being $-2.5 \times 10^{-6} \text{ K}^{-1}$, and the net expansion from 25 C to 600 C being zero. The negative expansion coefficient from 20 to 300 C affords the possibility of constructing a reflector with nearly zero optical distortion. The superiority of the ThF₄/SiO₂ coating mentioned above is a result of the small negative value of α for ThF₄ and the ultralow (positive) value of $\alpha = 0.5 \times 10^{-6} \text{ K}^{-1}$ for SiO₂.

Sec. B-I

The negative thermal expansion coefficient of ThF_4 , and possibly of a metallic alloy, afford the possibility of using intermediate layers between the coating and the substrate to give a very small net thermal expansion in some cases, as mentioned above.

Thin intermediate layers have three possible uses. Adding a very thin (~ 10 nm) layer of aluminum between the substrate and coating should be useful in reducing the number of coating layers in some cases. Using an intermediate layer containing ThF_4 to partially compensate for the optical distortion of the other positive-expansion materials is a promising approach, as discussed above. Finally, adding a thin (\sim micrometer thick) molybdenum or silicon-carbide layer between an invar substrate and the coating results in poorer repeated-pulse performance of the reflector, even though the single-pulse surface temperature is reduced slightly as a result of the greater thermal conductivity because the energy density is limited by optical distortion rather than by fracture.

Greater strength of films. The estimated fracture thresholds listed in Table II probably are lower bounds, since it appears that the strengths of materials in the form of deposited thin films may be greater than in crystalline bulk form (Sec. III).^{16,17} (However, the estimates conceivably could be too low, as a result of such effects as weak bonding between layers.) Furthermore, the accuracies of the estimated values are necessarily low as a result of the lack of reliable values of and understanding of the residual stresses and the difference between the thin-film and bulk values of other material parameters. The best current estimate is that the failure thresholds are likely to be determined by optical distortion and that the damage thresholds are likely to be determined by melting, with the possible exception of ThF_4 , which could fracture before melting. The greater strength will be more important to ThF_4 coatings, since these possibly could fail by fracture otherwise.

Sec. B-I

Measurements of α are needed. Measurements of the thermal expansion coefficients α of coating materials in deposited thin-film form are needed early in any developmental program; otherwise, the selection of the best candidate coatings to study experimentally will have to be made without having access to one of the most important parameters that affects the selection. The values of α , which are much more important in high-power applications than in the previously considered (low-power) applications, may be considerably different for some materials in deposited-film form than in bulk form. It is especially important to verify the negative value of α for deposited films of ThF_4 , to determine if deposited films of HfO_2 have ultralow expansion, and to determine which deposited-film materials have the lowest values of α .

Coating and reflector absorptance. In comparing coating, it is necessarily assumed that all coatings have the same absorptance since experimental values of absorptance are not available and surely will be determined by extrinsic processes. The resulting selection of candidate coatings for experimental programs is quite reasonable (Sec. III). Nevertheless, the absorptance probably is the single most important parameter of a coating, and it is possible that a given type of coating could perform either better or worse than predicted as a result of low or high absorptance, which cannot be predicted at present.

Three contributions to the absorptance of a reflector are absorption in the in the coating, absorption in the substrate, and subsequent absorption of scattered light (possibly enhanced by entrapment¹⁸). The Kopplemann result¹⁹ for the absorptance in a thick coating

Sec. B-I

$$A_F = \frac{\frac{1}{2} (\beta_H + \beta_L) \lambda}{n_H^2 - n_L^2}$$

is explained physically in terms of an effective penetration of the irradiance to a depth of $\lambda/2 (n_H^2 - n_L^2)$, which corresponds roughly to a reduction in irradiance by a factor of $(n_L/n_H)^2$ for each pair of layers. This penetration depth is quite similar to that used below to explain the phase change on reflectance.

The theoretical expression for the coating absorptance suggests that the extinction coefficient (absorption coefficient β plus scattering coefficient) of the $\text{HfO}_2/\text{SiO}_2$ coating is 340 cm^{-1} , which is a reasonable value. A value of $A = 10^{-4}$ could be attained for $\text{HfO}_2/\text{SiO}_2:\text{Mo}$ with 30 layers (15 pairs) if the absorption coefficient can be reduced to $\beta = 7 \text{ cm}^{-1}$ (with β adjusted to include the absorption of scattered radiation). This value of $\beta = 7 \text{ cm}^{-1}$ appears to be reasonable, but the ultraclean deposition procedures discussed previously^{10,11} are expected to be required. Smaller values of β are required for smaller values of n_L/n_H since the penetration depth is greater.

Damage thresholds. Currently available coatings possibly will withstand single pulses with 10 J/cm^2 , 354 nm, and $1 \mu\text{s}$ without damage such as melting or fracture (Sec. III). If the coatings withstand single pulses, they are expected to withstand the continuously repeated pulses without melting or fracturing. This is an important result since the previously measured (single-pulse) damage thresholds can be used, and future damage measurements will not require the large laser systems necessary for repeated-pulse measurements once the insensitivity to repeated pulses is verified. In contrast to this damage result, optical distortion will be much more severe in repeated-pulse operation than in single-pulse operation unless one of the approaches discussed above is successful.

Sec. B-I

Damage threshold measurements are needed to verify the no-damage prediction for all coatings, especially those containing ThF_4 . It should be emphasized that the damage measurement will not give information on the performance thresholds (which are determined by optical distortion). Two-photon absorption is shown to be the most likely explanation of the damage thresholds of $\sim 3 \text{ J/cm}^2$ at 17 ps ($I = 159 \text{ GW/cm}^2$) of ZrO_2 , HfO_2 , and SiO_2 observed by Newnam and Gill,²⁰ but is shown to be negligible for coatings at microsecond-duration pulses.

Optical distortion and absorption change from r . For a coating with a great number of layers N , the optical distortion resulting from thermally induced change in the total reflection coefficient r of the coating is often negligible with respect to the optical distortion resulting from the thermally induced displacement of the front surface of the coating for the cases considered here. However, the r contribution can be non-negligible, especially for thermally thick coatings and for $|\alpha| \ll |n^{-1} dn/dT|$. The contributions of the thermally induced shift in the phase ϕ_r of r to the optical distortion are $(It_p)_{\phi_r} = -114 \text{ J/cm}^2$ for the MgO/MgF_2 coating and $(It_p)_{\phi_r} = -65 \text{ J/cm}^2$ for the $\text{HfO}_2/\text{SiO}_2$ coating (Sec. VIII). The negative signs are formal reminders that the optical phase distortion has the opposite sign of, and tends to cancel, the surface-displacement contribution.

The effect of the increase in absorptance (decrease in the reflectance $R = |r|^2$) is negligible, being a higher order effect than optical distortion, which is determined by the phase of r (Sec. VIII). The reason for the relatively small effect of the phase ϕ_r is explained in terms of a penetration depth for irradiance, which is considerably smaller than the coating thickness in low-absorptance high-power reflectors. Thus, the phase change of r , resulting from the expansion

Sec. B-I

and index change of the first few layers (within the penetration depth) can be small with respect to the total phase change, which includes the expansion of the whole coating and the substrate. The penetration depth for the phase change is similar in both magnitude and physical meaning to the penetration depth used above for explaining coating absorptance and to a penetration depth that explains the substrate absorptance and is consistent with a reduction in irradiance by a factor of $(n_L/n_H)^2$, roughly, for each pair of layers. Thus, the notion of a depth of penetration of the irradiance into the coating is useful and physically plausible.

Cooling. The state of the art in water-cooled metallic reflectors is a value of heat-transfer coefficient $h \cong 10 \text{ W/cm}^2$ with $\lambda_v/40 = 16 \text{ nm}$ surface distortion (where $\lambda_v = 632.8 \text{ nm}$) for 20 mil (0.51 mm)-thick molybdenum face plates. Other significant values of h are discussed in Sec. VI. Cooling is not effective for single-pulses of duration $t_p = 10^{-6} \text{ s}$ since the heat does not have time to diffuse through the substrate in such a short time. By contrast, for repeated-pulse operation, the performance of high-power reflectors is limited by the amount of cooling that can be attained. There is a limiting value $h_c = 3 K_S / a \ell_S$ of the heat-transfer coefficient such that when $h \gg h_c$ is satisfied, there is little further decrease in the substrate temperature for further increases in h . The temperature is then controlled by the heat diffusion across the substrate rather than the transfer of heat into the coolant. Currently envisioned systems are far from this limit. For example, for $K_S = 2 \text{ W/cm}^2 \text{ K}$, $a = 1$, and $\ell_S = 0.1 \text{ cm}$, the value of $h_c = 60 \text{ W/cm}^2 \text{ K}$ is considerably greater than even the state-of-the-art value of $h = 10 \text{ W/cm}^2 \text{ K}$.

Sec. B-1

Engineering solutions. An adaptive- or a corrective-optical system would have to correct for a surface distortion of $64 (\lambda/80)$ if $h = 1 \text{ W/cm}^2 \text{ K}$, or $6.4 (\lambda/80)$ if $h = 10 \text{ W/cm}^2 \text{ K}$. These values are for a molybdenum substrate with $l_S = 1 \text{ mm}$ (and are essentially independent of the coating) at 354 nm . If the state-of-the-art cooling ($h = 10 \text{ W/cm}^2 \text{ K}$ and $l_S = 0.5 \text{ mm}$) can be attained and if optical distortion of the first pulse or so (as discussed in Sec. VI) can be tolerated, then fixed (nonadaptive) corrective optics can be used. For less cooling, a greater number of the initial pulses will be optically distorted.

For a thick ($\sim 2 \text{ cm}$) uncooled invar substrate operated at 100 Hz for 60 s the value of the surface distortion that must be corrected by the adaptive optics is $50 (\lambda/80)$, which is roughly the same magnitude required for the best windows, and the required time constant is of course $\sim 60 \text{ s}$. For comparison with a cooled substrate, note that this value of $50 (\lambda/80)$ would also be required for a 1 mm -thick molybdenum substrate with $h = 1.3 \text{ W/cm}^2 \text{ K}$. The simplicity of the uncooled substrate may dictate its use in preference to cooled substrates in systems in which adaptive optics are used. A heat-pipe mirror, possibly used in conjunction with adaptive optics, is another possible engineering solution.

Optimum number of coating layers. Coatings used with an intermediate thermal layer should have the minimum number of layers consistent with the optical design. Baumeister and Arnon⁹ increased the number of layers until there was relatively little further increase in reflectance. When calorimetric measurements become available, it will often be more appropriate to increase the number of layers until there is little additional decrease in the absorptance since the absorptance leads to the troublesome heating and both absorption and

Sec. B-I

scattering give rise to a decrease in the reflectivity. For only a few layers, the absorption in the substrate will be great, and as the number of layers increases, the absorption in the coating material increases until the coating is several penetration depths thick, at which point there is essentially no further increase in the absorptance by the coating materials. In a typical case, the absorption from the substrate will still dominate at this point, and the number of layers is then increased until there is little further decrease in the absorptance (when the substrate contribution becomes negligible with respect to the contribution from the coating materials). In contrast to this absorptance-dominated case, it is possible that in some systems the scattering could become intolerably great before the absorptance begins to level off. Thus, the tolerable level of scattering conceivably could determine the thickness of some reflectors.

The optimum number of layers can be quite different for reflectors without the intermediate thermal layer. For a low-expansion coating on such normal-expansion substrates as molybdenum, the optical distortion threshold can sometimes be increased in principle by depositing more layers than are required optically. The number of layers can be increased to make the coating thickness approximately equal to the thermal diffusion distance in the coating during the pulse, thereby eliminating the great single-pulse contribution to the optical distortion from the substrate.

Protective coatings for use in such hostile environments as laser cavities containing fluorine, or in moist atmospheres, may be required in some applications. The tetrahedral-carbon films discussed above have remained intact when metallic substrates were completely etched away.¹⁵ They possibly may provide the

Sec. B-I

ultimate protection of the underlying coating or substrate. Paraffin oil provides protection and index matching to reduce scattering, and is transparent well into the ultraviolet region.^{20a, 10, 11} Polymer coatings, which have received attention for a number of years, were reviewed in the previous two Technical Reports (30 June 1976 and 31 December 1975).

Stringent optical tolerance. The severity of the system requirements is illustrated by the small magnitude of $\lambda/80 = 3.1 \text{ nm}$ (31 \AA) at $\lambda = 250 \text{ nm}$ for the thermally induced surface distortion. For comparison, small-diameter laser mirrors are routinely figured to $\lambda_v/100 = 6.33 \text{ nm}$ ⁶, which corresponds to $\lambda/40$ at 250 nm. There is a difficulty in measuring optical figures of such high perfection⁶. Optical figures of $\lambda_v/40 = 15.8 \text{ nm}$ are more readily obtainable on large optics⁶. Six-inch-diameter quartz flats good to $\lambda_v/40$ are commercially available for approximately \$1,800 apiece⁶.

Miscellaneous. It is emphasized that the results herein are for the particular system discussed above, which includes $t_p = 10^{-6} \text{ s}$, $\lambda = 250 \text{ to } 354 \text{ nm}$, $It_p = 10 \text{ J/cm}^2/\text{pulse}$, pulse-repetition rate = 100 pps, and thermally induced surface distortion $\approx \lambda/80$. Changing the parameters, such as changing the pulse duration to a few picoseconds, may drastically change the results, as illustrated in Sec. III.

Neither the value of It_p nor the value of I at which system failure occurs is very useful when quoted alone, which does not seem to be appreciated in the literature. A damage threshold of 10 J/cm^2 may be quite high for a picosecond pulse, but quite low for a one-second pulse.

Sec. B-I

The generally difficult problems of calculating the temperature distribution and stresses in layered structures with both radial and axial variation of temperature were solved with sufficient accuracy to be compatible with the assumptions, the accuracy with which the parameters are known, etc.

The windows present an even more difficult problem than do the reflectors²¹, and reflectors are expected to handle greater power than can windows. The absorptance of antireflection coatings for windows need not be as great as that of the reflector coatings since the absorptance of the window material already is great. The failure thresholds for reflectors are fundamentally different for single-pulse and repeated-pulse operation and for thermally thin and thermally thick coatings. For single-pulse irradiation of thermally thick coatings, $l_F \gg l_{Ftp}$, where l_F is the coating thickness and l_{Ftp} is the thermal diffusion distance in the coating in time t_p , the failure thresholds are independent of the substrate, depending only on the properties of the coatings. For thermally thick coatings and repeated pulses, the thresholds depend on both the coating and substrate. For thermally thin coatings, $l_F \ll l_{Ftp}$, under single- or repeated-pulse operation, the failure thresholds depend on both the coating and substrate except in the case of $l_F \ll l_{Ftp}$ extremely well satisfied, which does not occur in coatings considered to date. The three coatings considered here are thermally thin, but are well away from the extreme thin limit.

Finally, it is mentioned that the absorptance of reflectors consisting of alternate layers of dielectric and ultrathin transmitting metallic layers is too great for high-power use.

II. UNCOATED METALLIC REFLECTORS

Background. Multilayer dielectric reflectors will be required for high-power 354 nm and 250 nm systems since there are no low-absorptance metals at these wavelengths. Sodium has the lowest absorptance, $A \cong 0.06$, at 354 nm of the metals listed in the third edition of the American Institute of Physics Handbook. (The value for lithium is not listed.) Of the metals Al, Ag, Au, and Cu, the lowest absorptance for $\lambda < 385$ nm is that of aluminum, for which $A = 0.08$ on the range $124 \text{ nm} \leq \lambda \leq 500 \text{ nm}$, and the lowest absorptance for $\lambda > 385$ nm is that of silver, with A decreasing from 0.07 at $385 \text{ nm} = 0.385 \mu\text{m}$ to $A = 0.008$ at $12 \mu\text{m}$. The 354-nm values for silver and copper are $A \cong 0.2$ and ~ 0.6 , respectively. Figure 2 shows the values of absorptance of Al, Ag, Au, Cu, and Na for $\lambda = 12 \mu\text{m}$ through the vacuum-ultraviolet range, plotted from the values in the American Institute of Physics Handbook.

It might appear at first that the best reflector design would be a substrate of aluminum, having the lowest value of absorptance, with a reflection-enhancing coating to reduce the absorptance from 0.08 to an acceptably low value. However, it will be shown below that aluminum (and also silver and copper) are unacceptable as substrate materials, the thermally induced optical distortion being too great as a result of the great thermal expansion coefficient. A thin aluminum layer, $\sim 100 - 150 \text{ nm}$ thick, has been deposited on a molybdenum substrate, with the coating (MgO/MgF_2) deposited on the aluminum.⁸ Thus the advantage of reducing the required number of coating layers is gained without suffering the disadvantage of an aluminum substrate. Theoretically, the aluminum layer could be much thinner, since only approximately two skin depths are needed. Bennett and

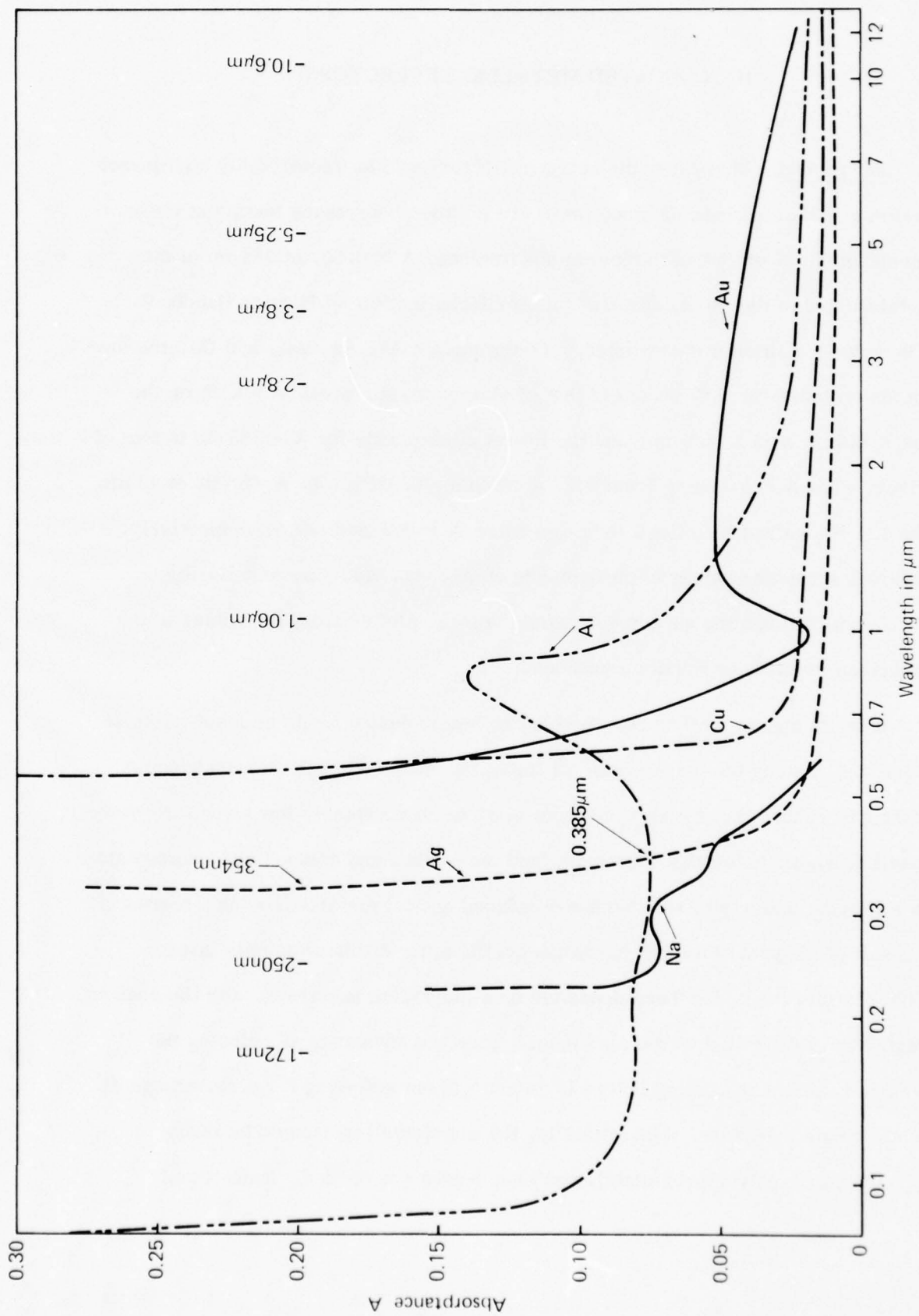


Fig. 2. Values of metallic absorbance plotted from data in the third edition of the American Institute of Physics Handbook.

Sec. B-II

co-workers⁶ pointed out that there could be difficulties with recrystallization of the aluminum layer if high temperatures were required in the coating fabricating process. For example, HfO_2 coatings baked at 400 C for four hours showed an increase in packing density.

The problems of the substrates and the coatings cannot be considered separately in general. For the case of uncoated metallic mirrors or the limit of extreme thermally thin coating, as discussed in Secs. II and V, the optical distortion is determined by the substrate. Even though this substrate model of the reflector is not valid for the model system described in Sec. I, the results are of interest in other systems, such as those in which dielectric reflectors cannot be used, and in establishing bounds from which performance limits can be estimated simply.

Bennett¹ has considered the single-pulse thermally induced optical distortion of uncoated metallic reflectors. It will be shown that the results for dielectric-coated substrates are quite different in general from the results for uncoated metals, even when the values of absorptance are formally set equal for the coated and uncoated cases. For the repeated-pulse system, the reflector must satisfy two conditions related to heat accumulation during successive pulses in addition to the single-pulse requirements, roughly speaking, as will be shown.

Single-pulse temperature. The skin depth for the absorption of the laser radiation in metals is negligibly small. Thus an accurate approximation to the temperature is attained by replacing the absorption source term in the heat-flow equation by the boundary condition of constant heat flow IA at the surface of the mirror at $z = 0$ during the pulse, where I is the incident irradiance and A is

Sec. B-II

the absorptance of the mirror. The resulting temperature distribution is well known,^{22,23} the surface temperature being²⁴

$$T_{p0} = 2 I t_p A (1/\pi t_p C_S K_S)^{1/2} = 56.4 (C_S K_S)^{-1/2} = [29.5 \text{ K}] \quad (2.1)$$

at the end of a single pulse of duration t_p .

During the pulse, the heat diffuses a distance

$$\ell_{\text{Stp}} = (4 K_S t_p / C_S)^{1/2} = [14.6 \mu\text{m}] ,$$

roughly speaking. For any reasonable mirror thickness, such as $\ell_S = 0.1 \text{ cm}$ in the example considered, $\ell_{\text{Stp}} \ll \ell_S$ is well satisfied. Thus cooling the rear surface of the mirror is not effective in reducing the value of T_p during the pulse.

A word about thermal-diffusion distances is in order. By writing the sourceless heat-flow equation

$$-K \partial^2 T / \partial z^2 + C \partial T / \partial t = 0$$

in dimensionless form, it is seen that the time τ required for heat to diffuse a distance ℓ is of the order of

$$\tau = \text{const. } C \ell^2 / K . \quad (2.2)$$

In various particular cases, the appropriate value of the constant can have such values of $1/4$, $4/\pi$, etc., depending on the geometry (linear, cylindrical, or spherical heat flow, for example) and the use to which (2.2) is put. For one-dimensional heat flow, the time τ required for heat to diffuse a distance ℓ is given by (2.2) with the constant equal to $1/4$, while the surface temperature of

Sec. B-II

a semi-infinite sample with heat flow $I t_p A$ at the surface is given by (2.1), which is equivalent to the thin-plate result

$$T = I t_p A / C \ell_{z=0}$$

if

$$t = 4 C (\ell_{z=0})^2 / \pi K ,$$

that is, if $\text{const.} = 4/\pi$ in (2.2).

Repeated-pulse temperature distribution. During the time $t_{ip} = 10^{-2}$ s between pulses, the thermal diffusion distance is $\ell_{tip} = (4 K_S 10^{-2} \text{ s} / C_S)^{1/2} = 0.15$ cm (in molybdenum) and the surface temperature returns almost to its prepulse value ($T \cong (t_p / t_{ip})^{1/2} T_{p0} \cong 10^{-2} T_{p0}$). After many pulses, in addition to the single-pulse temperature distribution, there is a quasi-steady-state temperature distribution $T_{\Delta Sr} + T_{SC}$, where T_{SC} is the temperature difference between the coolant and the back surface of the substrate and $T_{\Delta Sr}$ is the temperature drop across the substrate at the beginning of pulse, as discussed below. Quasi denotes that there are very small fluctuations in the value of $T_{\Delta Sr} + T_{SC}$ since the heat is added in pulses rather than continuously.

The value of T_{SC} is, by definition of the heat-transfer coefficient h , $T_{SC} = J/h$, where J is the average heat flow

$$J = I t_p A / t_{ip} = 5 \text{ W/cm}^2 . \quad (2.3)$$

Thus,

$$T_{SC} = I t_p A / t_{ip} h = 5/h . \quad (2.4)$$

Sec. B-II

The value of $T_{\Delta Sr}$ is determined by the average heat flow across the substrate and is different for the cases of $\ell_{tip} > \ell_S$ and $\ell_{tip} < \ell_S$. For molybdenum, $\ell_{tip} = 0.15$ cm, and $\ell_{tip} > \ell_S$ is satisfied (as is also the case for SiC, Cu, Ag, and Al); while for invar, $\ell_{tip} = 3.89 \times 10^{-2}$ cm, and $\ell_{tip} < \ell_S$ is satisfied. For $\ell_{tip} > \ell_S$, the heat diffuses across the substrate in the time between pulses; thus, the temperature distribution $T_{\Delta Sr}$ in the substrate after many pulses is approximately the same as for the steady-state case of constant heating throughout the substrate. Thus, $T_{\Delta Sr} \sim 1 - z^2 / \ell_S^2$, which is the solution to the steady-state heat-flow equation $-K_S d^2 T / dz^2 = I_t A / t_{ip} \ell_S$. For $\ell_{tip} \ll \ell_S$, the heat diffuses such a short distance between pulses that this temperature distribution $T_{\Delta Sr}$ is essentially the same as that for continuous heat input at the surface; that is, $T_{\Delta Sr} \sim 1 - z / \ell_S$, which is the solution to the source-free heat-flow equation $-K_S d^2 T / dz^2 = 0$ with constant heat flow into the surface at $z = 0$.

For the intermediate case of $\ell_{tip} < \ell_S$, but $\ell_{tip} \ll \ell_S$ not satisfied, the temperature distribution can be approximated by that for heat added uniformly in the region $0 < z < \ell_{tip} \leq \ell_S$. The simple solution to the steady-state heat-flow equation gives a parabolically decreasing temperature in the region $0 \leq z \leq \ell_{tip}$ and a linearly decreasing temperature in the region $\ell_{tip} \leq z \leq \ell_S$, with a surface temperature

$$T_{\Delta Sr0} = \frac{I_t A}{t_{ip} K_S} \left(1 - \frac{1}{2} \frac{\ell_{tip}}{\ell_S} \right), \quad \text{for } \ell_{tip} < \ell_S$$

$$= \frac{I_t A}{2 t_{ip} K_S} = \frac{2.50}{K_S} = [0.179] \quad \text{for } \ell_{tip} > \ell_S \quad (2.5)$$

Sec. B-II

The average value of $T_{\Delta Sr}$ over the substrate is

$$\langle T_{\Delta Sr} \rangle_{\ell_S} = \frac{a I_t A}{3 t_{ip} K_S} , \quad (2.6)$$

where

$$a = \frac{3}{2} \left(1 - \frac{1}{3} \frac{\ell_{tip}^2}{\ell_S^2} \right) , \quad \text{for } \ell_{tip} < \ell_S$$

and

$$a = 7 , \quad \text{for } \ell_{tip} > \ell_S .$$

For substrates of SiC, Mo, Cu, Ag, and Al, the simple forms of (2.5) and (2.6) for $\ell_{tip} > \ell_S$ apply, and for invar, $T_{\Delta Sr0}$ is increased by the factor 1.61 and $\langle T_S \rangle_{\ell_S}$ is increased by the factor $a = 1.42$ above the $\ell_{tip} > \ell_S$ limiting values.

Combining these results (2.1), (2.4), and (2.5) gives the surface ($\rho = z = 0$) temperature rise at the end of a pulse

$$T_0 = T_{p0} + \delta_r (T_{SC} + T_{\Delta Sr0}) = [29.5 \text{ K} + \delta_r (5/h + 0.179 \text{ K})] \quad (2.7)$$

where

$$\begin{aligned} \delta_r &= 1 && \text{for repeated-pulse operation} \\ &= 0 && \text{for a single pulse .} \end{aligned}$$

For repeated-pulse operation with perfect cooling (that is, $T_{SC} \ll T_{\Delta Sr}$, or $h \gg (5 \text{ W/cm}^2)/T_{\Delta Sr}$), (2.7) gives

$$T_{r0} \xrightarrow{h \rightarrow \infty} T_{p0} + T_{\Delta Sr0} = [29.7 \text{ K}] . \quad (2.8)$$

Sec. B-II

Failure mechanism. In the present section the failure of, and the optical distortion by, the coating is neglected of course, since the model is that of an uncoated substrate. The failure mechanism is then the thermally induced optical distortion resulting from the greater expansion of the hotter center of the substrate than of the cooler rim. Both the surface temperature during the pulse and the technical problems of achieving great values of the heat-transfer coefficient h while maintaining the required figure of the mirror are important. As discussed in Sec. I, the failure criterion will be taken as

$$\Delta l = \lambda/2 G = [3.57 \text{ nm}]$$

where Δl is the change in the thickness of the center ($\rho = 0$) of the structure (substrate and coating).

Single-pulse optical distortion. An accurate expression for the energy density It_p at which a given optical distortion λ/G occurs can be obtained under rather general conditions, which include the present single-pulse case, as follows: It is assumed that the system is linear (well satisfied for presently interesting cases of small temperature rise), radial diffusion is negligible, and no heat is removed from the mirror during the pulse (both well satisfied since the thermal-diffusion distance $l_{Stp} = (4K_S t_p / C_S)^{1/2} = [4(1.4) 10^{-6} / 2.61]^{1/2} = [14.6 \mu\text{m}]$ is much less than $l_S = 0.1 \text{ cm}$ and radiation is negligible). Under these conditions the energy $It_p A$ absorbed per unit area must equal the increase in the energy of the corresponding volume $l_S (1 \text{ cm})^2$ of the substrate

$$It_p A = C_S \int_0^{l_S} dz T_p, \quad (2.9)$$

Sec. B-II

where T_p is the temperature rise during the pulse. The resulting effective change in the thickness of the substrate is²⁵

$$\Delta l_S = \alpha_S (1 + \nu_S) \int_0^{l_S} dz T_p . \quad (2.10)$$

This result, which is derived in Ref. 25, can be understood as follows: To be concrete, T_p is approximated by

$$\begin{aligned} T_p &= T_0 e^{-a\rho^2} , & \text{for } z < l_{th} \\ &= 0 & \text{for } z > l_{th} . \end{aligned}$$

From Hook's law, with $\sigma_{zz} = 0$ for the thin reflector, the appropriate strain for expansion along the z axis is

$$\epsilon_{zz} = -\nu_S E^{-1} (\sigma_{\rho\rho} + \sigma_{\phi\phi}) + \alpha_S T_p , \quad (2.11)$$

and the thickness change is

$$\Delta l_S = \int_0^{l_S} dz \epsilon_{zz} = \int_0^{l_S} dz \alpha_S T_p - \int_0^{l_S} dz \nu_S (\sigma_{\rho\rho} + \sigma_{\phi\phi}) . \quad (2.12)$$

The stresses can be considered to consist of two contributions, the detached stresses σ_d being the stresses in the layer $z < l_{th}$ and the layer $z > l_{th}$ if these two layers were detached from one another, and the attachment stresses σ_a being the stresses resulting from reattaching the pieces, that is, deforming the hot ($z < l_{th}$) and cold ($z > l_{th}$) regions to bring them back together. The attachment condition is that the total attachment force on every cylinder $\rho = \text{constant}$ must be zero:

Sec. B-II

$$\int_0^{\ell_S} dz \sigma_a = 0 \quad . \quad (2.13)$$

Since the corresponding thickness change is

$$\Delta \ell_a = \int_0^{\ell_S} dz \epsilon_{zz a} = -\nu_S E_S^{-1} \int_0^{\ell_S} dz \sigma_a = 0 \quad , \quad (2.14)$$

the net contribution to the thickness change from the attachment contribution to the stress is zero for this case of an uncoated reflector. For the detached layer $z < \ell_{th}$, the sum of the two nonzero stress components from p. 290 of Ref. 26, or from Appendix A of Sec. C, this report, is

$$\sigma_{\rho\rho d} + \sigma_{\phi\phi d} = \alpha_S E [\langle T_p \rangle_R - T_p] \quad (2.15)$$

where

$$\langle T_p \rangle_R = \frac{2}{R^2} \int_0^R d\rho \rho T_p = \frac{1}{(aR)^2} (1 - e^{-aR^2}) = 0.432 T_0 \quad . \quad (2.16)$$

From (2.12) and (2.16),

$$\Delta \ell_S = \int_0^{\ell_S} dz \alpha_S T_p (1 + \nu_S) - \int_0^{\ell_S} dz \alpha_S \langle T_p \rangle_R \quad . \quad (2.17)$$

The second term does not contribute to the optical path difference since it is constant for all ρ ; thus it is not included in (2.10). The result is easily generalized to arbitrary $T_p(z)$ by considering many small detached layers; thus, (2.10) is not restricted to the square-pulse, z distribution.

Sec. B-II

Solving (2.9) and (2.10) for It_p gives

$$\begin{aligned} (It_p)_{op} &= C_S(\lambda/2G)/A\alpha_S(1+\nu_S) \\ &= 7.14 \times 10^{-5} C_S/\alpha_S(1+\nu_S) = [29.2 \text{ J/cm}^2], \quad \text{for 250 nm} \\ &= 1.01 \times 10^{-4} C_S/\alpha_S(1+\nu_S) = [41.3 \text{ J/cm}^2], \quad \text{for 354 nm} \quad (2.18) \end{aligned}$$

Apart from the factor $(1+\nu_S)^{-1}$ that accounts for the radial variation in temperature, this result is equivalent to Bennett's result,¹ as seen by setting

$$\frac{1}{g} = \left[\frac{(\lambda^2/5\pi N) - 2\tau_f^2}{2N(1+3\chi+3\chi^2)} \right]^{1/2}, \quad (2.19)$$

where N is the number of mirrors in the system, τ_f is the physical displacement of the surface resulting from nonthermal figuring error, and factors containing $\chi \equiv (1/4 \pi^{1/2})(d/\ell_S)^2$ account for bending of an unsupported plate, which is here assumed to be prevented by the support system, as already mentioned. Examples of values of g corresponding to various values of N and τ_f were given in Sec. I.

Values of $(It_p)_{op}$, along with values of the material parameters, are listed in Table I for several mirror-substrate materials. The value of absorptance $A = 5 \times 10^{-3}$ is used formally so that the values will serve as a limiting case for coated substrates. For uncoated materials having $A = A_m$, the values of $(It_p)_{od}$ in the table should be multiplied by $5 \times 10^{-3}/A_m$, which has the value $5 \times 10^{-3}/8 \times 10^{-2} = 1/16$ for aluminum at 250 to 354 nm, for example.

Continuously repeated-pulse optical distortion. The total change in the mirror thickness at the end of the m^{th} pulse, where m is sufficiently great for the steady

Sec. B-II

state to be reached ($t \approx 0.26$ for Mo with heat-transfer coefficient $h = 1 \text{ W/cm}^2 \text{ K}$, for example), is determined by the temperature contributions T_p , T_{SC} , and $T_{\Delta Sr}$. From (2.10) and (2.6)

$$\begin{aligned} \Delta \ell_S &= \alpha_S (1 + \nu_S) \int_0^{\ell_S} dz \left[T_p(z) + T_{SC} + T_{\Delta Sr} \right] \\ &= \frac{I t_p A \alpha_S (1 + \nu_S)}{C_S} \left[1 + \frac{C_S \ell_S}{t_{ip}} \left(\frac{1}{h} + \frac{a \ell_S}{3 K_S} \right) \right]. \end{aligned} \quad (2.20)$$

Setting $\Delta \ell_S = \lambda / 2 G$ in (2.20) and solving for $(I t_p)$ gives

$$(I t_p)_{or} = \frac{(I t_p)_{op}}{1 + h_o \left(\frac{1}{h} + \frac{a \ell_S}{3 K_S} \right)} \quad (2.21)$$

where $(I t_p)_{op}$ is given by (2.18), and h_o is defined as

$$\begin{aligned} h_o &= C_S \ell_S / t_{ip} \\ &= 10.0 C_S = [26.1 \text{ W/cm K}] \end{aligned} \quad (2.22)$$

For perfect cooling, that is $h \gg 3 K_S / \ell_S = [42.0 \text{ W/cm}^2 \text{ K}]$, (2.21) gives

$$(I t_p)_{or} \xrightarrow{h \rightarrow \infty} [18.0 \text{ J/cm}^2] \quad (2.23)$$

The amount of cooling, that is the value of h , required in order to avoid excessive optical distortion ($\ell_{opd} > \lambda / g$) for a given value of $(I t_p)$ is obtained by solving (2.21) for h :

$$\begin{aligned} h &= h_o \left[\frac{(I t_p)_{od}}{I t_p} - 1 - \frac{a h_o \ell_S}{3 K_S} \right]^{-1} \\ &= [20.2 \text{ W/cm}^2 \text{ K}] \end{aligned} \quad (2.24)$$

Sec. B-II

For the measured values of absorptance, the mirrors listed in Table I all fail in single-pulse operation; thus, even for $h = \infty$ they cannot survive for repeated-pulse operation. Even for the formal case of $A = 5 \times 10^{-3}$, the required values of h are extremely large, as discussed in Sec. VI.

III. DIELECTRIC COATINGS AND DISTORTION COMPENSATING LAYERS

Multilayer dielectric reflectors will be required for high-power ultraviolet and visible systems since the intrinsic absorptance of uncoated metallic reflectors is too great, as discussed in Sec. II. The problem of obtaining satisfactory dielectric coatings for the reflectors is not expected to be as severe as that of obtaining satisfactory windows.²¹ An absorptance of 5×10^{-3} or less (reflectance of 9.95 percent) has been attained at 320 nm (for a 21-layer $\text{HfO}_2/\text{SiO}_2$ coating on quartz).⁹ Single-pulse damage thresholds at 354 nm for 17 ps pulses ranging from 0.14 to 3.2 J/cm^2 have been measured¹⁵ for TiO_2 , ZrO_2 , HfO_2 , and SiO_2 films that were deposited at the University of Rochester. These results, along with general experimental results in the infrared region and theoretical results²⁷ suggest, as discussed below, that these films possibly could withstand the required value of 10 J/cm^2 for single pulses without catastrophic damage with no improvement required. Some margin of safety must of course be allowed in an operating system.

Lowering the absorptance of coatings would be one of the most useful coating improvements. It is emphasized that the cardinal difficulties in obtaining ultra-low-absorptance coatings needed in high-power systems are expected to be such technical problems of depositing the films as discussed previously.^{10, 11} The large value of $A = 5 \times 10^{-3}$ is used just for the reason that overcoming the technical problems in order to obtain lower absorptance is expected to be difficult. If the absorptance could be reduced to 10^{-4} , the reflector problem, including that of cooling the substrate, would be greatly simplified. This illustrates the

Sec. B-III

general result that the coating and substrate problems generally are closely related. The values of the absorption coefficient β_F required to give $A = 5 \times 10^{-3}$ and 10^{-4} are $\beta_F \cong A/\ell = 200 \text{ cm}^{-1}$ and 4 cm^{-1} , which are reasonable values to attain. The absorption length ℓ used in the estimate was $\ell \cong \ell_F/4 = 2.5 \times 10^{-5} \text{ cm}$.

It is also emphasized that in comparing coatings, one of the most important parameters is the absorptance A . The comparisons here, which are based on the same value of $A = 5 \times 10^{-3}$ for all coatings, therefore might at first appear to be misleading. However, the equal-absorptance comparisons, which are made of necessity, are in fact quite reasonable to use in selecting candidate coatings to study experimentally since there is no way at present of reliably predicting which coatings will have lowest value of absorptance, and it is surely the extrinsic absorptance that will reign. The intrinsic Urbach absorption edges are so steep that the values of absorptance of coatings are expected to be extrinsic. The extrinsic values of absorptance of deposited films are expected to be greater than those of high-purity bulk crystals, and the coating-absorptance values are expected to be determined by the technical problems of the deposition process.^{10, 11}

Possibility of obtaining near-zero thermally induced optical distortion. By using an intermediate layer, containing such a negative thermal expansion material as ThF_4 or perhaps the cobalt-iron-chromium alloy mentioned in Sec. II, between the optical coating and the substrate, it is theoretically possible to reduce the single-pulse contribution to the optical distortion to near zero. First consider the specific example of a seven-pair (14-layer) MgO/MgF_2 optical coating deposited on an aluminum layer, which is in turn deposited on the intermediate layer consisting of ThF_4 and silver layers, which is deposited on the substrate.

Sec. B-III

In the 10^{-6} s duration t_p of the pulse, most of the energy that is absorbed in the thin optical coating diffuses into the intermediate layer, which is just thick enough (a few micrometers thick, typically) so that little of the heat diffuses into the substrate during the pulse. The greatest contribution to the optical distortion in this case is the expansion of the intermediate layer. By choosing the thicknesses of the ThF_4 and silver in the ratio

$$\frac{\ell_{\text{TF}}}{\ell_{\text{Ag}}} = \frac{\alpha_{\text{Ag}} (1 + \nu_{\text{Ag}})}{|\alpha_{\text{TF}}| (1 + \nu_{\text{TH}})} \quad (3.1)$$

the net expansion of the intermediate layer is zero. The ratio is altered for the layers near the optical coating in order to partially compensate for the (small) optical distortion of the optical coating.

The number of ThF_4/Ag pairs in the layer is not critical. If only one pair were used, the thermally induced optical distortion at the end of the pulse, say, could be made zero theoretically. By increasing the number of pairs, the distortion can be kept small throughout the duration of the pulse. The optical properties of the ThF_4/Ag layers, such as the index of refraction, absorption coefficient, coloration, and purity, are unimportant since the intermediate layers are not exposed to the optical beam. A metallic layer over the intermediate layer could be polished.

The negative thermal expansion coefficient of ThF_4 is the key feature of the intermediate-layer concept. Other features can be changed. Silver was chosen simply because it has a great thermal conductivity and it is easily deposited. The optical coating MgO/MgF_2 could be replaced by another optical coating,

Sec. B-III

preferably a thermally thin (small physical thickness and great thermal conductivity) one. In general, the thermal conductivity of the coating, the intermediate layer, and the substrate should be great.

The limiting value of the energy density per pulse $(It_p)_{or}$ for optical failure is obtained by assuming complete correction for the single-pulse distortion. The value of $(It_p)_{or}$ is then determined by the repeated-pulse characteristics of the substrate. Setting $(It_p)_{op} = \infty$ in (5.17a) gives

$$(It_p)_{or}^{-1} = (It_p)_{SC}^{-1} + (It_p)_{\Delta S}^{-1} \quad (3.2)$$

For a molybdenum substrate with heat transfer coefficient $h = 10 \text{ W/cm}^2 \text{ K}$ and substrate thickness $\ell_S = 0.1 \text{ mm}$,

$$(It_p)_{SC} = 22.3 \text{ J/cm}^2 ; \quad (It_p)_{\Delta S} = 187 \text{ J/cm}^2$$

and (3.2) gives

$$(It_p)_{or} = 20.0 \text{ J/cm}^2 \quad (3.3)$$

This value 20.0 J/cm^2 is limited essentially by the cooling and thermal expansion of the substrate, the value of $(It_p)_{SC}$ ($= 22.3 \text{ J/cm}^2$) being proportional to h/α_S .

The value of the temperature at the surface of the optical coating at the beginning of a pulse (quasi steady-state value) is, from (2.4) and (2.5)

$$T_{SC} + T_{\Delta S r0} = 0.68 \text{ K}$$

and at the end of a pulse (assuming equal thermal conductivities $K_I = K_S$ and heat capacities $C_I = C_F$ for the optical and intermediate coatings) is

Sec. B-III

$$T_0 = 60.3 \text{ K} .$$

For an invar substrate with $h = 10 \text{ W/cm}^2 \text{ K}$ and $\ell_S = 0.5 \text{ mm}$

$$(It_p)_{SC} = 223 \text{ J/cm}^2$$

$$(It_p)_{\Delta S} = 160 \text{ J/cm}^2$$

$$(It_p)_{or} = 93.2 \text{ J/cm}^2 \quad (3.3a)$$

$$T_{SC} + T_{\Delta Sr0} = 1.54 \text{ K}$$

$$T_0 = 61.2 \text{ K}$$

The practical problems involved in reducing the single-pulse optical distortion so that the values of 20.0 J/cm^2 for molybdenum or 93.2 J/cm^2 for invar could be approached (or, alternatively, the value of h/ℓ_S increased) should be solvable without undue effort. As an illustration, assume that the intermediate layer has the same thermal properties as a 14-layer (7-pair) MgO/MgF_2 coating. The surface temperature, from (2.1) with C_S and K_S replaced by $C_F = 3.14 \text{ J/cm}^3 \text{ K}$ and $K_F = 0.285 \text{ W/cm K}$, is

$$T_0 = 59.6 \text{ K}$$

and the temperature distribution is

$$T = T_0 \operatorname{erfc} z/\ell_{th} = T_0 (1 - 2z/\ell_{th} \sqrt{\pi} + 111)$$

where

$$\ell_{th} = (4 K_F t_p / C_F)^{1/2} = 6.03 \text{ nm} .$$

Sec. B-III

The optical coating thickness, from (4.1) with $\lambda = 250$ nm,

$$\ell_F = (1.81 \mu\text{m}) (14/45) = 0.563 \mu\text{m} .$$

From (8.15) with $T = T_0 = 59.6$ K,

$$\begin{aligned} \phi_r &= -4.77 (15.6 \times 10^{-6} + 7.54 \times 10^{-6}) 59.6 \pi \\ &= -3.29 \times 10^{-3} (2 \pi) \end{aligned}$$

and from (8.16)

$$(It_p)_{\phi_r} = \frac{10 \text{ J/cm}^2}{-3.289 \times 10^{-3}} = -3.04 \times 10^3 \text{ J/cm}^2 .$$

From (8.11) with $d_{\Delta}/d_0 = \alpha_F (1 + \nu_F) \langle T \rangle_{\ell_F}$

$$\begin{aligned} \phi_s &\cong 14 \pi (15.6 \times 10^{-6}) T_0 \frac{1}{2} \left[1 + \left(1 - \frac{\ell_F^2}{\ell_{th} \sqrt{\pi}} \right) \right] \\ &\cong 14 \pi (15.6 \times 10^{-6}) T_0 (1 - \ell_F / \ell_{th} \sqrt{\pi}) \\ &\cong 6.17 \times 10^{-3} (2 \pi) \end{aligned}$$

and from (8.16)

$$(It_p)_{\phi_s} = \frac{10 \text{ J/cm}^2}{6.165 \times 10^{-3}} = 1.62 \times 10^3 \text{ J/cm}^2 .$$

The net phase shift is

$$\phi_s + \phi_r = 2.88 \times 10^{-3} (2 \pi) ,$$

Sec. B-III

and the net optical distortion is

$$(It_p)_{op} = 10 / 2.88 \times 10^{-3} = 348 \text{ J/cm}^2$$

Thus, the contribution of the optical coating to the optical distortion is extremely small, even for the case in which no cancellation of the coating distortion by the intermediate layer is assumed.

If the net thermal expansion of the intermediate layer is $\pm 0.5 \times 10^{-6} \text{ cm}^{-1}$, which is a large value for the near-zero expansion layer, the optical distortion from the intermediate layer is, from (4.7) with the small amount of heat that has not diffused into the intermediate layer neglected,

$$(It_p)_{op} = (14.0 \text{ J/cm}^2) \frac{15.6 \times 10^{-6}}{0.5 \times 10^{-6} (1.3)} = 2.49 \times 10^3 \text{ J/cm}^2$$

Thus, the contribution from the lack of perfect cancellation of the expansion of the intermediate layer also is negligibly small. The calculations suggest that if the ThF_4 /metal intermediate-layer design encounters difficulties, an invar intermediate layer would be useful.

The positive-expansion material in the intermediate layer is not critical. Magnesium fluoride, silicon carbide, or copper could be used instead of silver, for example. Other low expansion intermediate layers, such as invar or another alloy, could be investigated if difficulties develop in the ThF_4 intermediate layer.

In principle, the same technique could be used to reduce the substrate contribution to $(It_p)_{or}$. The ThF_4 /Mo structure would be extended to form the total substrate. However, the technical problems may be difficult, and the value

Sec. B-III

of (It_p) could be determined by the residual value of $(It_p)_{op}$ that cannot be cancelled entirely in a practical reflector, rather than by $(It_p)_{SC}$ and $(It_p)_{\Delta S}$. Then there would be no additional benefit from using a ThF_4 layered substrate.

The damage threshold now becomes much more important than was envisioned at the beginning of the program since it may be possible to reduce the optical distortion threshold to such an extent that the overall system failure is limited by the damage threshold rather than by optical distortion. The following new possibility of increasing the damage threshold is therefore especially important.

Clusters of microscopic imperfections. It is generally found, with only a few exceptions, that laser damage in coatings and in bulk materials occurs at small isolated spots, rather than uniformly over the high irradiance area. The macroscopic-absorbing-inclusion mechanism has been the explanation^{28, 29, 27, 10, 11} for these damage sites, but there is growing concern that the inclusion mechanism may not be a universal explanation of laser damage.^{12, 13} In some cases the macroscopic inclusion explanation is likely to be correct. Platinum inclusions in laser glass and imbedded polishing compounds in surfaces are two examples. In general, however, an alternate explanation would be welcomed since several investigators have not found inclusions in careful searches in materials known to damage at isolated spots.

Such damage could result from clusters of microscopic imperfections. A purely statistical distribution of imperfections would of course result in local areas of high imperfection density. It is probably much more significant however that imperfections often have a strong tendency to appear in clusters, for a number of reasons. There are a number of types of microscopic imperfections

Sec. B-III

and a number of damage mechanisms, including linear absorption and processes involving generated electrons, that could result from imperfection clusters as will be discussed in detail elsewhere.³⁰ For the present, consider the example of isolated point imperfections such as impurity ions, incomplete oxygen bonds, or one of the many so-called damage centers. The absorption coefficient β in the areas of great concentration of imperfections should be much greater than the spatially averaged values of absorption coefficient measured in typical calorimetry measurements.

The cluster explanation is particularly appropriate for coating damage (and also for surface damage) since coatings almost always have absorption coefficients that are much greater than the bulk-material values, which is likely to be the result of contamination of the vacuum deposited films. Thus, the imperfections are believed to be present, and they are more likely to be clustered in films than they would be in bulk samples. For a coating with $\beta = 10 \text{ cm}^{-1}$ measured calorimetrically, a value of $\beta = 200 \text{ cm}^{-1}$ for the local value corresponding to the greatest imperfection concentration seems reasonable. For a volume that is sufficiently small for thermal diffusion out of the volume during the pulse to be negligible, the temperature rise is obtained by equating the energy absorbed $IA\alpha t_p$, with absorptance $A = \beta l$, to the temperature rise times the heat capacity $TC\alpha l$ of the cluster volume αl , which gives, for $\beta = 200 \text{ cm}^{-1}$, $I t_p = 10 \text{ J/cm}^2$, and $C = 2 \text{ J/cm}^3 \text{ K}$,

$$T = \beta I t_p / C = 10^3 \text{ K}$$

Thus the numbers are quite reasonable to explain failure of local sites. As the irradiance is successively increased above the value required for the first

Sec. B-III

detectable damage, there should be successively greater numbers of damage sights corresponding to lower concentrations of imperfections in the clusters.

If the cluster explanation proves to be correct, an important consequence will be that there is now for the first time a method of possibly increasing the damage threshold. It has already been suggested that the film deposition process be cleaned up to the ultimate degree possible in order to decrease the coating absorptance. If such a program were successful in significantly reducing the overall absorption, it is possible that the value of the maximum local absorption coefficient would also be reduced, thereby reducing the damage threshold. This makes the ultraclean deposition experiments even more important than originally suggested.

Intentionally doping the best available film materials with absorbing ions and looking for simultaneous increases in the absorption coefficient and the damage threshold is perhaps the simplest test for the mechanism. It is conceivable that some type of inter-film layer contamination such as ionic diffusion across the interface, especially at the elevated temperatures of deposition, could be involved. Other considerations discussed in connection with lowering the film absorptance^{10, 11} could be important in the cluster mechanism.

Single-pulse damage threshold. For such damage as melting or fracture (but not optical distortion), if the coating survives the single pulses, it is expected to survive the continuously repeated pulses in the systems considered and in a rather wide class of systems. For inclusion damage, thermal diffusion between pulses reduces the temperature essentially to its prepulse value. The same is true for absorption in the coating as will be shown.

Sec. B-III

The damage experiments by Newnam and Gill²⁰ on TiO_2 , ZrO_2 , HfO_2 , and SiO_2 quarter-optical-wave-thick coatings on fused silica at wavelength 355 nm and pulse duration 17 ps suggest that the damage thresholds in their case result from two-photon absorption (except for TiO_2 , which has a sufficiently small band gap to allow direct absorption across the gap). Although the nature of the damage was not discussed, the following estimate suggests that the coatings may have melted.

The thermal-diffusion distance in fused silica in time $t_p = 12$ ps,

$$\ell_{th} = (4 K t_p / C)^{1/2} = [4(0.014) 17 \times 10^{-12} / 1.7]^{1/2} = 7.49 \text{ nm} ,$$

is much less than the coating thickness $\ell_F = 355/4(1.48) = 60 \text{ nm}$. Thus, the temperature rise for the observed energy density $I t_p = 2.7 \text{ J/cm}^2$ is²⁴

$$T = I t_p \beta_F / C_S = 2.38 \times 10^3 \text{ K} ,$$

which is equal to the temperature $\sim 2,000 \text{ K}$ required to melt the coating within the accuracy of the order-of-magnitude estimate. The temperature $\sim 2,000 \text{ K}$ is the sum of the melting temperature, $\sim 1690 \text{ K}$ above room temperature ($T_m = 1710 \text{ C}$), plus the temperature $H_f/C = (568 \text{ J/cm}^3) / 1.7 \text{ J/cm}^3 \text{ K} = 334 \text{ K}$ that is equivalent to the heat of fusion $H (= 568 \text{ J/cm}^3)$. Melting is expected to occur before fracture since the fracture temperature H_f/C is estimated to be somewhat greater than $2,000 \text{ K}$, even using the bulk-crystal strength. Neglecting residual stresses and assuming a compressive strength of $\sim 8 \sigma_t$, with a tensile strength of $\sigma_t \cong 10^4 \text{ psi}$, assuming the worst case (greatest stress) of no substrate heating, and using (4.15) gives

Sec. B-III

$$T = \frac{8 \sigma_t (1 - \nu)}{\alpha E} = 1.25 \times 10^{-4} \text{ K} .$$

Furthermore, the strength of the films may be greater than the corresponding bulk-crystal values, as discussed below.

The absorption coefficient was estimated by taking a typical expression^{31, 32}

$$\beta_F = \left(\frac{I}{0.1 \text{ GW/cm}^2} \right) 1 \text{ cm}^{-1}$$

which gives $\beta = 1.5 \times 10^3 \text{ cm}^{-1}$. This estimated value of β could be in error by at least an order of magnitude.

Assuming that the damage occurs by melting that results from two-photon heating, it is simple to scale from the 17 ps damage threshold to 1 μ s and a molybdenum substrate. For $t_p = 10^{-6}$ s, the thermal diffusion distance, 1.81 μ m = 1,810 nm, is much greater than the coating thickness, 60 nm. Thus the temperature is given by (2.1). With $\beta_F = 1.5 \times 10^3 (2000/2380)(I/159 \text{ GW/cm}^2) = 7.93 I \text{ cm}^{-1}/\text{GW cm}^{-2}$ and $T = 2 \times 10^3 \text{ K}$, solving for $I t_p$ gives the melting threshold

$$(I t_p)_m = 8.45 \times 10^3 \text{ J/cm}^2 .$$

This is such a great damage threshold for two-photon heating that another mechanism surely will have a lower threshold. Likely candidates are inclusion damage^{28, 29, 27, 10, 11} and clusters of microscopic inclusion, discussed under the previous paragraph heading. In the infrared region, the damage thresholds for microsecond pulses range from 10 to several hundred Joules per square centimeter.^{10, 11}

Sec. B-III

It is not difficult to show that these basic results are not changed when the additional Joule heating by the two-photon-absorption-generated electrons is included. For $\omega\tau \gg 1$, where τ is the electron relaxation frequency, the imaginary part of the dielectric constant is $\epsilon_g = 4\pi n_e e^2 / m\omega^3 \tau$ and the absorption coefficient is $\beta_g = \epsilon_g \omega / n_r e$. The density of conduction electrons n_e generated by two-photon absorption, assuming negligible recombination, is $n_e = \frac{1}{2} (It_p / \hbar\omega) \beta_2$, where β_2 is the two-photon absorption coefficient in cm^{-1} . Solving these three equations for β_g / β_2 gives

$$\frac{\beta_g}{\beta_2} = \frac{2\pi e^2 It_p}{n_r c \hbar m \omega^3 \tau} = 0.307$$

where the numerical value of 0.307 is for $It_p = 2.7 \text{ J/cm}^2$ and $\tau = 2 \times 10^{-14} \text{ s}$. Thus, the absorption at the end of the pulse is increased by a factor of 1.307, which is not sufficient to change the result that two-photon absorption (enhanced by Joule heating) is negligible at 10^{-6} s .

Two-photon absorption. An important factor in selecting coating materials is the required size of the band gap. One-photon absorption must be avoided; that is, $\hbar\omega$ must be less than the absorption edge E_a . With $\beta_F \cong 10^5 - 10^6 \text{ cm}^{-1}$ for frequencies above the absorption edge and $\ell_F \cong 10^{-4} \text{ cm}$, the absorptance A would be intolerably great since $\beta_F \ell_F = 10 - 100$. The experimental results of Newnam and Gill²⁰ just discussed support the theoretical prediction that two-photon materials (with $\frac{1}{2} E_a < \hbar\omega < E_a$) can be used for coatings, but not for windows, at $t_p = 1 \mu\text{s}$. With $\beta_F \cong 8 \text{ cm}^{-1} \text{ I/GW cm}^{-2}$ from the experiments,

Sec. B-III

assuming that the damage results from two-photon absorption, the coating absorptance at $I = 10^7 \text{ W/cm}^2$ is of the order

$$A_F \cong \beta_F \ell_F \cong [8(10^{-2}) \text{ cm}^{-1}] 2.5 \times 10^{-5} \text{ cm} = 2 \times 10^{-6}$$

which is below the absorptance level that is likely to be attained in the near future. For windows that are approximately one centimeter thick, the absorptance is $A \cong 8 \times 10^{-2}$, which is unacceptably great.

The strength of materials in thin-film form may be greater than in bulk single-crystal form, possibly to the extent that fracture of quarter-wave coatings for 250 to 354 nm use will be rare. This greater strength of thin films appears to have been largely overlooked in the literature until recently.^{16, 17} The fact that many reported values of residual stresses in films exceed the bulk-crystal strengths supports the greater-film-strength contention. For example, the reported tensile stress of 3.2×10^4 psi for MgF_2 exceeds the bulk-crystal tensile strength of 7.6×10^3 psi by a factor of 4.2. There are also theoretical reasons to believe that the strength of a given material may be greater in thin-film form than in bulk single-crystal form, just as the strengths of brittle polycrystalline materials increase as the grain size decreases. If the characteristic Griffith-microcrack size (typically 0.5 nm, but with considerable variation from case to case) associated with the bulk tensile strength is greater than the coating thickness, it is reasonable to expect that the strength will be greater in thin-film form.

Experimental values of the expansion coefficients of deposited thin films are needed in order to make the best selection of candidate coatings. An $\text{HfO}_2/\text{ThF}_4$

Sec. B-III

coating (or ThF_4 plus another high-index material) may turn out to be a good choice. If HfO_2 has the ultralow value of $\alpha = 0.5 \times 10^{-6} \text{ K}^{-1}$ and ThF_4 has $\alpha = -2.5 \times 10^{-6} \text{ K}^{-1}$, the performance of the coating will be approximately as good as that of $\text{ThF}_4/\text{SiO}_2$, and the great number of layers would not be required. If, on the other hand, $\alpha \cong 10 \times 10^{-6} \text{ K}^{-1}$ for HfO_2 , the effective expansion coefficient of the coating near room temperature is $\alpha = [10(1.35) - 2.5(2.14)] 10^{-6} / (1.35 + 2.14) = 2.3 \times 10^{-6} \text{ K}^{-1}$, which is intermediate between the ultralow value of $0.5 \times 10^{-6} \text{ K}^{-1}$ and the effective value $\alpha = 12.3 \times 10^{-6} \text{ K}^{-1}$ for MgO/MgF_2 . The number of layers required would still be small, of course. An intermediate layer of ThF_4 possibly could reduce the net expansion considerably below the value of $\alpha = 2.3 \times 10^{-6} \text{ K}^{-1}$. The compatibility of the deposition conditions of HfO_2 and ThF_4 would have to be determined, of course.

There are glasses, such as Cer-Vit (Owen-Illinois trade name for "glass ceramic"), Zerodure by Schott, and ULE by Corning that have near-zero thermal expansion over broad temperature ranges. Values as low as $\alpha = 0.1 \times 10^{-6} \text{ K}^{-1}$ over a limited temperature range have been attained (for a Corning ULE glass containing SiO_2 and TiO_2). Their principal use is mirror blanks. However, they are not useful as substrates for high-power reflectors since the thermal conductivity is too low. Such glasses usually require special manufacturing techniques, and it is not known if they can be fabricated as thin films.

The number of layers required to give a specified value of reflectance can be calculated from the expression

$$2N \cong \frac{\ln[(1-R)Z/4]}{(\ln(n_L/n_H))}, \quad \text{for } 1-R \ll 1 \quad (3.4)$$

Sec. B-III

where

$$Z \equiv n_L \frac{1 + |r_3|}{1 - |r_3|} \quad , \quad (3.5)$$

$$|r_3| = \left(\frac{(n_L - n_S')^2 + n_S''^2}{(n_L + n_S')^2 + n_S''^2} \right)^{1/2} \quad , \quad (3.6)$$

which is easily obtained from the result³³

$$R = \left(\frac{1 - (n_H/n_L)^{2N} Z}{1 + (n_H/n_L)^{2N} Z} \right)^2 \quad (3.7)$$

$$\cong 1 - 4(n_L/n_H)^{2N}/Z \quad , \quad \text{for } 1 - R \ll 1 \quad . \quad (3.8)$$

These results are for a reflector consisting of $2N$ layers, all of which are quarter wave except for the low-index layer next to the substrate. The thickness of this low-index layer is adjusted to give maximum reflectance (that is, a net quarter-wave-layer phase shift, including that of the layer itself plus the phase shift at the substrate resulting from the complex n_S).

In order to regain the correct limit of (3.7) for $2N = 0$, it is necessary to formally set $n_L = 1$ ($=n_0$) in both the expressions for Z and $|r_3|$. For $n_S'' = 0$ and $n_L > n_S$, the result (3.7) of Hass does not reduce to the result (3.13) of Lissberger below. The discrepancy is relatively unimportant for the present cases, but will be resolved in a future report. It would be useful if authors

Sec. B-III

would give key results in terms of the complex refractive indices in order to avoid ambiguities in the literature, which are not uncommon.

Other useful expressions for coatings with quarter-wave layers are as follows:
For $2N + 1$ layers (OHLHL ----- LHS)³⁴,

$$R = \left| \frac{1 - \eta^{-1}}{1 + \eta^{-1}} \right|^2, \quad (3.9)$$

where

$$\eta^{-1} = n_S / L, \quad L \equiv \frac{n_H^2}{n_0} \left(\frac{n_H}{n_L} \right)^{2N},$$

which can be written as

$$R = \frac{(L - n_S')^2 + n_S''^2}{(L + n_S')^2 + n_S''^2}, \quad (3.10)$$

with $n_S = n_S' - i n_S'' = 2.43 - i 2.97$ for Mo and $n_S = 0.34 - i 4.01$ for Al, both for λ near 354 nm. For $L^2 \gg |n_S|^2$, (3.10) gives

$$R \cong 1 - \frac{4 n_S' n_0}{n_H^2} \left(\frac{n_L}{n_H} \right)^{2N}; \quad \text{for } 1 - R \ll 1 \quad (3.11)$$

from which it follows that

$$2N \cong \frac{\ln[(1 - R) n_H^2 / 4 n_S' n_0]}{\ln[n_L / n_H]}. \quad (3.12)$$

Sec. B-III

The corresponding results for 2N layers (HLHL ----- LS) is

$$R = \frac{(n_S' - S)^2 + n_S''^2}{(n_S' + S)^2 + n_S''^2}$$

$$\cong 1 - \frac{4 n_0}{n_S'} \left(\frac{n_L}{n_H} \right)^{2N}, \quad \text{for } 1 - R \ll 1 \quad (3.13)$$

where

$$S = n_0 (n_L/n_H)^{2N},$$

and

$$2N \cong \frac{\ln[(1 - R) n_S' / 4 n_0]}{\ln(n_L/n_H)}. \quad (3.14)$$

Table IV contains calculated values of the numbers of layers required to give $1 - R = 5 \times 10^{-3}$ for various coating/substrate combinations.

Theoretical absorptance of reflectors. Three contributions to the absorptance of a reflector are absorption in the coating, absorption in the substrates, and absorption of scattered light. For a metallic or other non-transmitting substrate with no scattering and with no absorption in the coating, the absorptance is simply

$$A_S^{\bullet} = (1 - R) \beta = 0,$$

Table IV. Number of coating layers required to give $1 - R = 5 \times 10^{-3}$ for various coating/substrate combinations.

Coating	Substrate or Intermediate Layer	Wavelength (nm)	Number of Layers $2N$ or $(2N+1)$	n_H	n_L	n'_S	n''_S
$\text{ThF}_4/\text{SiO}_2$	Al	250	54.7	1.575	1.50	0.175	2.725
$\text{ThF}_4/\text{SiO}_2$	Mo	250	93.1	1.575	1.50	1.30	2.73
$\text{HfO}_2/\text{SiO}_2$	SiO_2	250	128.7 (127.7)	1.575	1.50	1.50	0
$\text{HfO}_2/\text{SiO}_2$	Al	354	7.25	2.14	1.477	0.33	3.96
$\text{HfO}_2/\text{SiO}_2$	Mo	354	12.93	2.14	1.477	2.43	2.97
$\text{HfO}_2/\text{SiO}_2$	SiO_2	354	16.93 16.02*	2.14	1.477	1.50	0
MgO/MgF_2	Al	250	12.82	1.74	1.41	0.175	2.725
MgO/MgF_2	Mo	250	21.71	1.74	1.41	1.30	2.73
MgO/MgF_2	SiO_2	250	29.86 (29.45)	1.74	1.41	1.50	0

*The corresponding experimental value⁹ is $2N = 21$.

where R is given by (3.7), (3.10), or (3.13). This contribution to the absorptance can be reduced by increasing the number of layers, which reduces the electric field at the absorbing substrate.

For an absorbing coating, in the limit in which the absorptance A is controlled by the absorption in the coating, a good approximation to the absorptance is obtained by using the model of an infinitely thick coating ($2N \rightarrow \infty$) of quarter-wave layers. For this case, Koppelman¹⁹ found that, for n_H'' and $n_L'' \ll 1$,

$$A_F = 2\pi \frac{n_H'' + n_L''}{n_H'^2 - n_L'^2} = \frac{\frac{1}{2}(\beta_H + \beta_L)\lambda}{n_H'^2 - n_L'^2} \quad (3.15)$$

where $n_H = n_H' + i n_H''$ [with $\exp(+ikz)$ for a plane wave traveling in the $+z$ direction] and $n_L = n_L' + i n_L''$. The relation between the absorption coefficient β_H and the extinction coefficient n_H'' is

$$\beta_H = 4\pi n_H''/\lambda \quad (3.16)$$

Solving (3.16) and (3.15) for β gives

$$\begin{aligned} \beta &= (n_H'^2 - n_L'^2)A/\lambda \\ &= 339 \text{ cm}^{-1}, & \text{for } n_H = 2.14, n_L = 1.477, \lambda = 354 \text{ nm} \\ &= 46.1 \text{ cm}^{-1}, & \text{for } n_H = 1.575, n_L = 1.500, \lambda = 250 \text{ nm} \end{aligned} \quad (3.17)$$

Sec. B-III

It would not be surprising if such large absorption coefficients were found in early coatings. These results show that an absorptance of 5×10^{-5} could be attained if the absorption coefficient of the $\text{HfO}_2/\text{SiO}_2$ film could be reduced to $339/100 = 3.4 \text{ cm}^{-1}$, which appears to be a reasonable typical goal for films deposited under absolute optimum conditions^{10,11}. For 24 layers (12 pairs) deposited on molybdenum at 354 nm,

$$(1 - R)_{\beta=0} = 5 \times 10^{-5} ,$$

and if the scattering contribution is negligible, the absorptance is

$$A = 10^{-4} .$$

Alternatively, 30 layers (15 pairs) could be used to reduce $(1 - R)_{\beta=0}$ to 10^{-5} , in which case the required value of the absorption coefficient is $\beta = 339/50 = 6.8 \text{ cm}^{-1}$. It is possible that an absorptance of 10^{-4} could be attained. The difficulty is expected to be that of solving the technical-deposition problems in order to obtain the relatively low value of $\beta = 6.8 \text{ cm}^{-1}$ for $\lambda = 250$ to 350 nm .

An important feature of the result (3.17) is that smaller absorption coefficients are required for coatings having smaller values of n_L/n_H ; the more coating layers required, the lower the required value of β .

The result (3.15) can be understood as follows. For simplicity, assume that $n_H'' = n_L'' = n''$. For n'' sufficiently small, the depth of penetration of incident irradiance into the coating is determined by the reflection characteristics of the coating, rather than by the absorptance. Thus, (3.15) and (3.16) can be written as

$$A \equiv \beta \ell_{\text{pen}} , \tag{3.18}$$

Sec. B-III

where

$$\begin{aligned} \ell_{\text{pen}} &= \frac{8 n_H n_L}{(n_H + n_L)^2 (n_H - n_L)} \langle d \rangle \\ &\cong \frac{2}{(n_H - n_L)} \langle d \rangle, \quad \text{for } n_H - n_L \ll n_L \end{aligned} \quad (3.19)$$

is the effective depth of penetration into the coating and

$$\langle d \rangle = \frac{1}{2} \left(\frac{\lambda}{4 n_H} + \frac{\lambda}{4 n_L} \right)$$

is the average thickness of the coating layer.

It can be seen that this result (3.19) is reasonable as follows^{34a}: The irradiance decreases by a factor of $(n_L/n_H)^2$ for each pair of layers, roughly speaking. This argument neglects such effects as the variation of the irradiance across the thickness of the given layers of the coating. The absorptance can therefore be approximated by the sum of the absorptance in each pair of layers as

$$A \cong 2 \langle d \rangle \beta [1 + (n_L/n_H)^2 + (n_L/n_H)^4 + \dots + (n_L/n_H)^{2m}] .$$

Summing the series gives, for $(n_L/n_H)^{2m} \ll 1$

$$A = \beta \ell_e$$

where

Sec. B-III

$$\begin{aligned}\ell_e &\cong \frac{2n_H^2}{n_H^2 - n_L^2} \langle d \rangle \\ &\cong \frac{n_H}{n_H - n_L} \langle d \rangle, \quad \text{for } n_H < n_L \ll 1.\end{aligned}\quad (3.20)$$

The effective depth ℓ_e from (3.20) agrees with the penetration depth ℓ_{pen} from (3.19) as well as is expected for the crude model used in obtaining (3.20)^{34a}. For $n_H = 2.14$ and $n_L = 1.477$, (3.19) and (3.20) give $\ell_{\text{pen}} = 2.916 \langle d \rangle$ and $\ell_e = 3.82 \langle d \rangle$; and for $n_H = 1.575$ and $n_L = 1.500$, the values are $\ell_{\text{pen}} = 26.6 \langle d \rangle$ and $\ell_e = 21.5 \langle d \rangle$.

Scattering is usually considered to decrease the reflectance without increasing the absorptance. However, the scattered light can be absorbed, and Winsor¹⁸ has shown that scattered light can be entrapped in the coating, thereby causing a substantial fraction of the scattered light to be absorbed. An experimental determination of the magnitude of this effect is needed.

In the limit of low absorptance, $A \ll 1$, it is expected that the three contributions add linearly

$$A = (1 - R)_{\beta=0} + \frac{\frac{1}{2}(\beta_H + \beta_L)\lambda}{n_H^2 - n_L^2} + A_{\text{sc}}. \quad (3.21)$$

Obtaining an ultralow-thermal-expansion coating would provide another of the possible solutions to the power-coating problem for the model system in Sec. I. Low thermal expansion of the coating materials results in great resistance to both thermally induced optical distortion and fracture. The theoretical superiority

Sec. B-III

of the $\text{HfO}_2/\text{SiO}_2$ coating over the MgO/MgF_2 coating is a result of the low thermal expansion assumed for both HfO_2 and SiO_2 . It may be advantageous to increase the thickness of the optical coating to a value greater than that needed optically in order to prevent excessive heat diffusion into the substrate during a pulse, which would increase the optical distortion as a result of the substrate expansion.

Bulk fused silica is known to have ultralow expansion ($\alpha = 0.5 \times 10^{-6} \text{ K}^{-1}$), and oxide coatings tend to be amorphous. Thus, the HfO_2 coating could have an ultralow thermal expansion as assumed, but this is by no means certain, especially since there are so few ultralow expansion materials. It is important to determine the expansion coefficients of thin deposited films of HfO_2 (and other candidate materials for coatings)^{34b}.

Uan Uitert and co-workers³⁵ recently found that a single crystal of thorium tetrafluoride had $|\alpha| \lesssim 2.5 \times 10^{-6} \text{ K}^{-1}$ for temperatures between 25 C and 600 C. At room temperature, $\alpha \cong -2.5 \times 10^{-6} \text{ K}^{-1}$; the average value on the range 25 C to 300 C was $\alpha = -1.4 \times 10^{-6} \text{ C}$; at $T \cong 300 \text{ C}$, $\alpha = 0$; for $T > \sim 300 \text{ C}$, α was positive; and the net expansion from $T = 25 \text{ C}$ to $T = 600 \text{ C}$ was zero. The crystal was not fractured by application of a blowtorch. One disadvantage of ThF_4 is radioactivity, but ThF_4 has been widely used in the past. Crystalline $\text{Al}_2\text{O}_3 \cdot \text{Li}_2\text{O} \cdot 2\text{SiO}_2$ has a large negative thermal expansion coefficient $\alpha = -17 \times 10^{-6} \text{ K}^{-1}$ along one axis, this value of α being constant from 20 C to 800 C.

The negative expansion coefficient of ThF_4 , or possibly other materials, at room temperature affords the possibility of a near-zero net thermal expansion

Sec. B-III

coefficient of a dielectric/metallic reflector. For example, an intermediate layer of ThF_4 of appropriate thickness ℓ_i (of the order of the coating thickness) could be deposited between the coating and the substrate, with ℓ_i chosen to give zero single-pulse optical distortion. A very thin (~ 10 nm, as discussed below) aluminum layer could be deposited over the ThF_4 in order to reduce the number of coating layers required. The coating itself could also have ThF_4 as one of the coating materials. For repeated-pulse operation, the value of ℓ_i could be chosen to maximize the overall threshold value of I_{t_p} .

Values of C , K , ν , E , σ_t , H_f , and T_m for ThF_4 were not found in the literature. In view of the potential importance of ThF_4 , reasonable values of the parameters are assumed in order to obtain a rough estimate of the performance of a coating containing ThF_4 . A $\text{ThF}_4/\text{SiO}_2$ coating is considered to be specific and to illustrate the advantages (low required value of $h = 6.33 \text{ W/cm}^2 \text{ K}$, even on Mo, for example) and disadvantages (possible low fracture threshold and, with SiO_2 , possible great number of layers required, for example) of coatings containing ThF_4 . As discussed below, the best candidate coating having ThF_4 as one of the materials can be chosen when experimental values of the expansion coefficients of deposited thin films become available. In view of the potential problems with $\text{ThF}_4/\text{SiO}_2$ that will be discussed below, this coating combination may not turn out to be the best choice.

Both SiO_2 and ThF_4 deposit well, in high-density form, at 150°C , and both materials are sufficiently transparent at 250 to 350 nm. A major problem is that a great number of layers is required. For example, at 250 nm, $n = 1.575$ for ThF_4 and $n = 1.50$ for SiO_2 , and the theoretically required number of layers, from (3.8) below, is 54 (27 pairs) on aluminum ($n_s = 0.175 + i 1.725$), or 92

Sec. B-III

(46 pairs) on molybdenum ($n_s = 1.30 + i 2.73$). This is an example of a case in which a thin aluminum layer (thickness ≈ 20 nm) is effective in reducing the required number of coating layers.

A final potential problem with coatings containing ThF_4 is that the thermal-fracture threshold could be low if the strength of the films is not greater than that of the bulk crystal of the same material. For example, for the $\text{ThF}_4/\text{SiO}_2$ coating, the value of $(It_p)_{fp}$ is only ~ 1 to 7 J/cm^2 . This great range of values is a result of the fact that the values of a number of parameters are not known for ThF_4 . Typical values are: $\sigma_{\text{tensil bulk}} \cong 6$ to $12 \times 10^3 \text{ psi}$; $\nu = 0.17$ to 0.35 ; $\alpha = -2.5 \times 10^{-6} \text{ K}$ to $-1.4 \times 10^{-6} \text{ K}$, depending on the magnitude of the temperature change; $E = 10$ to $25 \times 10^6 \text{ psi}$; and $C \cong 2$ to $3 \text{ J/cm}^3 \text{ K}$. The high temperature resulting from the low thermal conductivity and the fact that ThF_4 is in tension cause $(It_p)_{fp}$ to be small. If the strength of the film is greater than the bulk-material strength, the values of $(It_p)_{fp}$ and $(It_p)_{fr}$ may be sufficiently great that fracture will not be a problem.

If these potential difficulties do not materialize, the $\text{ThF}_4/\text{SiO}_2$ coating itself could meet the requirements of the model system. It is theoretically superior to both the MgO/MgF_2 and $\text{HfO}_2/\text{SiO}_2$ coatings, even with the assumed ultralow expansion of $0.5 \times 10^{-6} \text{ K}^{-1}$ for HfO_2 . For example, the values of $(It_p)_{op}$ are 145 J/cm^2 for $\text{ThF}_4/\text{SiO}_2$, 77.5 J/cm^2 for $\text{HfO}_2/\text{SiO}_2$, and 21.4 J/cm^2 for MgO/MgF_2 , all on molybdenum substrates at $\lambda = 250 \text{ nm}$. For the $\text{ThF}_4/\text{SiO}_2$ coating, the value $2N+1 = 55$ was used formally, which requires a thin aluminum intermediate layer. This layer can be as thin as a few skin depths (of the order of 10 nm).

A cursory investigation indicates that optimizing a coating containing ThF_4 by selecting the other coating material (or materials for a $3N$ layer coating)

Sec. B-III

would reduce the value of $(It_p)_{\text{p or}} = 15.1 \text{ J/cm}^2$ for $\text{ThF}_4/\text{SiO}_2:\text{Mo}$ with $h = 10 \text{ W/cm}^2 \text{ K}$ to the value $(It_p)_{\text{p or}} \approx 19 \text{ J/cm}^2$ that is determined by the substrate (with a slight improvement for a net negative expansion coefficient of the coating).

Coating failure modes. Under laser irradiation, absorption in and on the surface of a multilayer reflection coating generates heat, which flows through the coating into the metallic (or other heat conducting) substrate. The resulting temperature rise possibly could cause melting or fracture of the coating, in addition to optical distortion. For pulsed irradiation, as the pulse duration t_p becomes shorter with respect to the thermal diffusion time τ in the coating, the absorption-generated heat in the coating cannot diffuse out of the heat-generation region in time t_p . Thus, for a given amount of energy absorbed in the coating, the temperature rise will be greater for the case of $t_p \lesssim \tau$ than for the case of $t_p \gg \tau$. Also, cooling the substrate from the rear surface is not effective for a single microsecond pulse.

Nonlinear effects, such as two-photon absorption, nonlinear-index defocusing, etc., that arise as the irradiance I increases (for decreasing t_p at fixed It_p) have been considered previously^{36,37} and were discussed above in the treatment of the picosecond damage thresholds. In addition to melting, fracture, and optical distortion, the thermally induced thickness and refractive index changes in the coating layers change the reflectance of the coatings. This effect is shown in Sec. VIII to be negligible. Scattering is important at the high ultraviolet frequencies, and Winsor has shown that entrapped scattered radiation can cause increased absorption¹⁸. However, in high-power systems, scattering that does not lead to increased absorptance tends to be less important than absorption since the optical distortion

Sec. B-III

and fracture resulting from the temperature increase caused by absorption usually limits the system performance.

The temperature distribution in the coating and substrate and the resulting stresses and optical distortion are difficult to calculate accurately in general. Estimates will be made for the two limiting cases of thermally thick and thermally thin coatings. The single-pulse and repeated-pulse damage and optical distortion will be treated together. In general, the problem of calculating thermally induced stresses is complicated, even in systems having cylindrical geometry, when the temperature is a function of both ρ and z (cylindrical coordinates) as it is in the present case. However, for the case of thin coatings (thickness $\ell_F \ll$ substrate thickness ℓ_S) on thin substrates ($\ell_S \ll$ diameter D_S), the stresses in the layers of the coating can be estimated fairly simply²⁵.

Material properties. Such materials as fluorides and oxides that transmit well into the ultraviolet region generally have superior physical and chemical properties such as great strength, great thermal conductivity, and high melting points. The values of the index of refraction tend to be fairly low; thus, many layers may be required in multilayer coatings, as discussed above.

IV. THERMALLY THICK DIELECTRIC REFLECTORS

In multilayer coatings, the absorption usually is greatest near the coating-air interface since the irradiance must drop to near zero at the substrate and each pair of layers reduces the incident intensity, roughly speaking. Thus, most of the heat is generated near the surface of the coating. A coating will be called thermally thick if a negligible amount of this heat diffuses out of the coating into the substrate in the duration t_p of a single pulse. That is, $l_{Ftp} \approx l_F$, where²⁴

$$l_F = (N/2) (\lambda/4) (n_1^{-1} + n_2^{-1}) = [1.81 \mu\text{m}] \quad (4.1)$$

(with F for film) is the coating thickness and

$$l_{Ftp} = (4 K_F t_p / C_F)^{1/2} = (K_F / C_F)^{1/2} 20 \mu\text{m} = [6.02 \mu\text{m}] \quad (4.2)$$

is the thermal diffusion distance in the coating in time t_p . Here $(N/2)$ is the number of pairs of quarter-optical-wavelength layers having refractive indices n_1 and n_2 , λ is the operating wavelength, and

$$K_F = [0.285 \text{ W/cm K}] \quad (4.3)$$

and

$$C_F = [3.14 \text{ J/cm}^3 \text{ K}] \quad (4.4)$$

are the effective values of the thermal conductivity and heat capacity per unit volume for the many-layer coating, which are obtained in the Appendix. The MgO/MgF_2 and $\text{HfO}_2/\text{SiO}_2$ coatings are not thermally thick, while the $\text{ThF}_4/\text{SiO}_2$ coating is.

The temperature distribution in the thermally thick coating and substrate can be estimated as follows: At the end of a single pulse, negligible heat has diffused

AD-A040 596

XONICS INC SANTA MONICA CALIF
THEORETICAL STUDIES OF HIGH-POWER ULTRAVIOLET AND INFRARED MATE--ETC(U)
DEC 76 M SPARKS, C J DUTHLER

F/G 20/5

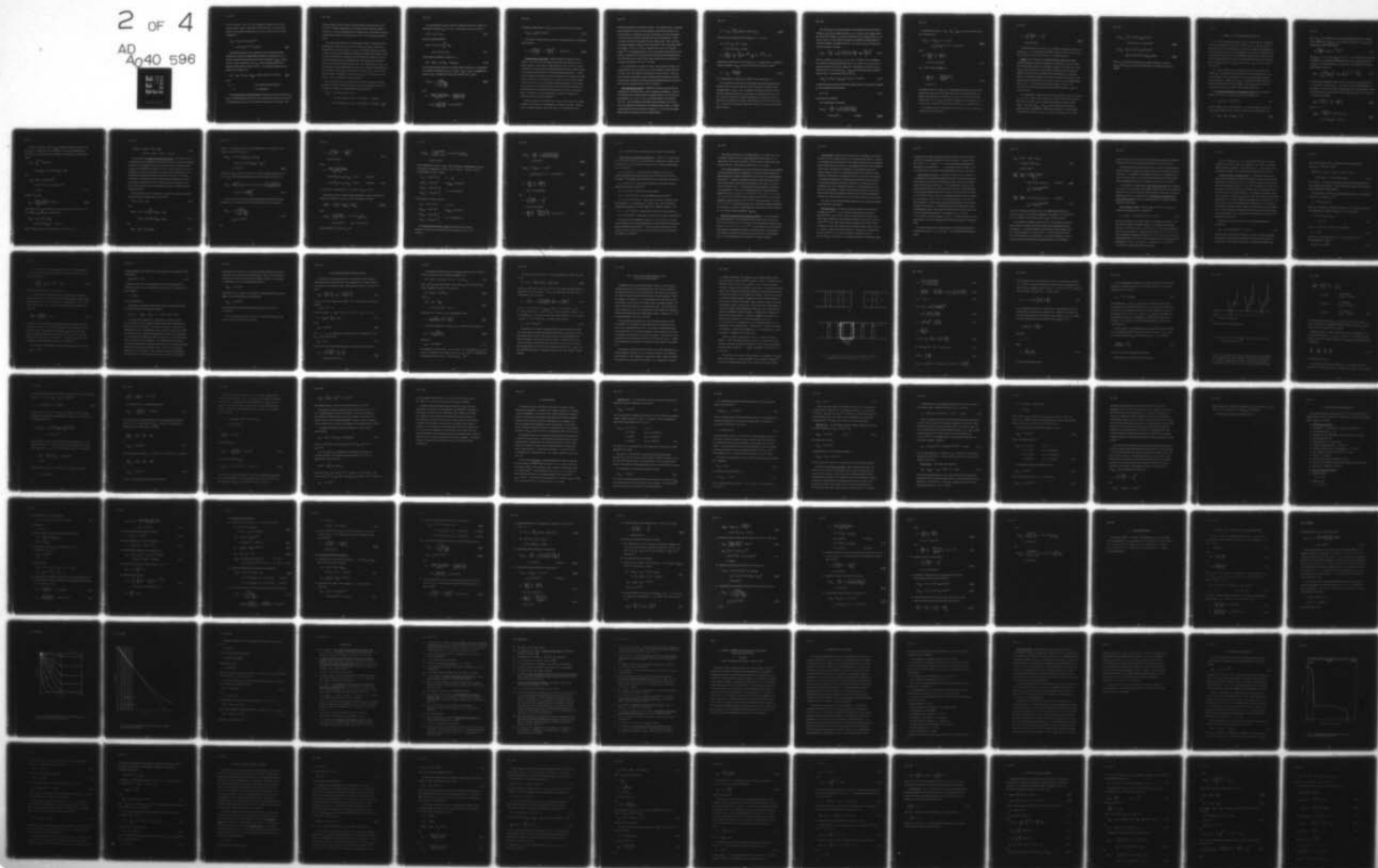
DAHC15-73-C-0127

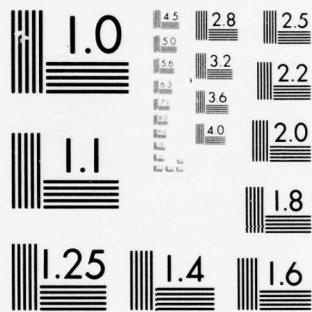
NL

UNCLASSIFIED

2 OF 4

AD
A040 596





MICROCOPY RESOLUTION TEST CHART
NATIONAL BUREAU OF STANDARDS-1963-A

Sec. B-IV

into the substrate. Thus, all of the temperature increase occurs in the coating, and the surface temperature is given by (2.1), with C_S and K_S replaced by the effective coating values C_F and K_F from (A.5) and (A.6) in Appendix A:

$$\begin{aligned} T_{Fp0} &= 2 I t_p A (1/\pi t_p C_F K_F)^{1/2} \\ &= 56.4 (C_F K_F)^{-1/2} = [59.6 \text{ K}] \end{aligned} \quad (4.5)$$

The additional increase in the temperature in the coating and substrate resulting from continuous repeated-pulse operation was calculated in Sec. II. The quasi-steady-state temperature drop across the substrate $T_{\Delta Sr0}$ is given by (2.5), and the temperature drop T_{SC} across the boundary layer of the substrate-coolant interface is given by (2.4). The resulting temperature of the surface of the coating is then

$$T_{F0} = T_{Fp0} + \delta_r (T_{SC} + T_{\Delta Sr0}) = [59.6 + \delta_r (5/h + 0.179 \text{ K})] \quad (4.6)$$

where

$$\begin{aligned} \delta_r &= 1 && \text{for continuously repeated pulses,} \\ &= 0 && \text{for a single pulse.} \end{aligned}$$

The thermally induced optical-distortion calculation is somewhat involved, even when the simplifying approximations for thin coatings and thin substrates are made.²⁵

The demonstration in Sec. II that the attachment stresses do not contribute to the

Sec. B-IV

thickness change fails for the case of a coated substrate because the factor νE^{-1} in (2.15) is no longer independent of z and cannot be taken outside the integral. Thus there is a nonzero attachment-stress contribution $\Delta \ell_a$ to the thickness change resulting from the difference in the values of νE^{-1} of the coating layers and substrate.

The results of the analysis of that problem given in Ref. 25 should be used for thermally thick substrates for the case in which the temperature is peaked in the coating (that is, when $\ell_S \langle T \rangle_{\ell_S} \gg \ell_F \langle T \rangle_{\ell_F}$ is not satisfied) when great accuracy is required. In the present treatment, in which the thermally thick-substrate results are only used formally for comparison with the thermally thin results of primary interest, the attachment-stress contribution to the optical distortion is neglected in favor of the clarity and simplicity of the results. The resulting values of (It_{p0}) are often accurate to within approximately five percent for temperature distributions that are peaked in the coating and are quite accurate (to order ℓ_F/ℓ_S) for nearly constant temperature distributions. In the worst case, the error is of the order of 30 percent, which is tolerable for the present estimates.

When the attachment-stress contribution to the thickness change is neglected, the analysis of Sec. II is valid for the present case of a thermally thick substrate if the substrate variables S are replaced by the coating variables F :

$$\begin{aligned} (It_{p0}) &= C_F (\lambda/2G) / A\alpha_F (1 + \nu_F) \\ &= 7.14 \times 10^{-5} C_F / \alpha_F (1 + \nu_F) = [14.0 \text{ J/cm}^2], \quad \text{for 250 nm} \\ &= 1.01 \times 10^{-4} C_F / \alpha_F (1 + \nu_F) = [19.8 \text{ J/cm}^2], \quad \text{for 354 nm . (4.7)} \end{aligned}$$

Sec. B-IV

For repeated-pulse operation, both the coating and substrate are heated. The same failure criterion, $\ell_{\text{opd}} = \lambda/G$ at $\rho = 0$, and analysis used in Sec. II gives

$$\lambda/2G = \Delta \ell_F + \Delta \ell_S \quad (4.8)$$

where the coating expansion is

$$\begin{aligned} \Delta \ell_F &\cong \alpha_F (1 + \nu_F) \int_0^{\ell_F} dz T_{Fp} \\ &= \alpha_F (1 + \nu_F) I t_p A / C_F \end{aligned} \quad (4.9)$$

and the substrate expansion, from Sec. II, is

$$\Delta \ell_S = \alpha_S \ell_S (1 + \nu_S) (T_{SC} + \langle T_{\Delta Sr} \rangle_{\ell_S}) . \quad (4.10)$$

It was assumed that the coating is much thinner than the substrate, as is usually the case; then the contribution $\alpha_F \ell_F (1 + \nu_F) (T_{SC} + T_{\Delta Sr})$ to $\Delta \ell_F$ is negligible with respect to $\Delta \ell_S$. Solving (4.8)-(4.10), (4.4), and (4.5) for $I t_p$ gives

$$(I t_p)_{\text{or}} = \frac{(I t_p)_{\text{op}}}{1 + h_o \left(\frac{1}{h} + \frac{\alpha \ell_S}{3K_S} \right)} \quad (4.11)$$

where

$$\begin{aligned} h_o &= \frac{\ell_S \alpha_S (1 + \nu_S) A (I t_p)_{\text{op}}}{t_{ip} (\lambda/2G)} = \frac{C_F \ell_S \alpha_S (1 + \nu_S)}{t_{ip} \alpha_F (1 + \nu_F)} \\ &= 10.0 C_F \frac{\alpha_S (1 + \nu_S)}{\alpha_F (1 + \nu_F)} = [12.8 \text{ W/cm}^2 \text{ K}] . \end{aligned}$$

Sec. B-IV

For perfect cooling, that is $h \gg 3 K_S / \ell_S = [42.0 \text{ W/cm}^2 \text{ K}]$, (4.11) gives

$$(I t_p)_{\text{or}} \xrightarrow{h \rightarrow \infty} [10.7 \text{ J/cm}^2] \quad . \quad (4.12)$$

The amount of cooling required to prevent the optical distortion, as discussed above (2.24), is

$$h = h_o \left[\frac{(I t_p)_{\text{op}}}{(I t_p)} - 1 - \frac{a h_o \ell_S}{3 K_S} \right]^{-1} = 134 \text{ W/cm}^2 \text{ K} \quad . \quad (4.13)$$

Coating stresses and strength. Finally consider the coating stress and fracture. The cases of thermally thick and thermally thin coatings will be considered together. Unfortunately, reliable estimates of the stresses in, and the strengths of, the coatings and the resulting irradiance limitations cannot be made, and the failure thresholds will have to be determined experimentally. The difficulties in making the estimates are that the strengths of the materials in thin-film form are not known, as discussed in Sec. III, and that the values of the residual stresses (the stresses in the coating after deposition and aging, in other words, the stresses in the coating before the laser is turned on) and the strengths of the bonds between layers and between the coating and the substrate are not usually known. Furthermore, the other properties of a deposited material can be different from those of the bulk material.¹⁴

Residual stresses are discussed in Ref. 10 (pp. 90-100), which also contains excerpts, with comments, of several papers on stresses in coatings. Reported values of residual stresses, which can be great, vary considerably with the

Sec. B-IV

deposition temperature and substrate material. The residual stress in a deposited film is believed to consist of three components, one from the mismatch of the thermal expansion coefficients of the film and substrate, one from contaminants in the film, and one intrinsic contribution that is not well understood. Of the materials considered in the application below, MgF_2 , MgO , ThO_2 , and HfO_2 , the residual stresses in MgF_2 have been measured.¹⁴ Most of the MgF_2 values are between $+10^4$ and $+7 \times 10^4$ psi (tensile) but one value of $+10^3$ psi was reported.²⁴ In the application below, where the thermally induced stress is compressive, including a large residual tensile stress increases the damage resistance of the MgF_2 layers, and the MgF_2 layers should not fail for any value of residual stress between $+10^4$ and $+7 \times 10^4$ psi.

In the calculations of the numerical values of the thresholds for failure, the residual stresses are set equal to zero, and the strengths of the bulk materials are used. Thus, the results are not expected to be very accurate. They may tend to be lower bounds since the film strengths could be greater than the bulk-crystal values, but this is not certain since the bond between layers may fail and the increase in strength of films, if any, is not known.

Thermally induced stresses are difficult to calculate in general when the temperature is a function of both z and ρ (cylindrical coordinates). However, in the present case a reliable estimate is possible because: (1) The total structure thickness, $l_F + l_S \cong 0.1$ cm, is small with respect to the diameter $D \cong 5$ cm. (2) The coating is much thinner than the substrate ($l_F \ll l_S$). Thus, the expansion of the substrate is not affected by the coating. A straightforward analysis in Ref. 25 yields the stresses at $z = \rho = 0$ (where the magnitudes usually are maximum, as in the example herein):

Sec. B-IV

$$\sigma_1 = \sigma_{1\text{res}} - \frac{E_1}{1 - \nu_1} \left(\alpha_1 T_{F0} - \alpha_S B_S \langle T_S \rangle_{\ell_S} \right) \quad (4.14)$$

where T_{F0} is the temperature of the coating at $z = \rho = 0$, and

$$B_S = \frac{1}{2} (1 + \nu_S) + \frac{1}{2} (1 - \nu_S) r_R$$

$$= 0.716 + 0.284 \nu_S = [0.801]$$

$$r_R = \frac{\langle T \rangle_R}{\langle T \rangle_{\rho=0}} = \frac{2}{R^2} \int_0^R d\rho \rho e^{-a\rho^2} = \frac{1}{aR^2} \left(1 - e^{-aR^2} \right) = 0.432 \quad .$$

Replacing the 1 subscripts by 2 in (4.14) gives σ_2 . For single pulses, the substrate heating is negligible, $\langle T_S \rangle_{\ell_S} \cong 0$, and (4.14) gives the well known result²⁶

$$\sigma_1 = \sigma_{\text{res}} - \frac{\alpha_1 E_1 T_{F0}}{1 - \nu_1} \quad (4.15)$$

for T independent of ρ , which is also valid for $T(\rho)$ in the limit $\rho \rightarrow 0$.

The result (4.14) for the stress in the coating can be understood by again considering a model in which the stress is a sum of two terms. A thin layer of the coating between z_1 and $z_1 + \Delta z$ is considered as detached from the rest of the structure, and the thermal stresses in the layer are calculated as the first term. The second term is the stress required to bring the layer back to the same configuration (same displacement along the radial direction ρ) as the rest of the structure. This scheme was discussed briefly above and in Sec. II, and is considered in detail in Ref. 25.

Sec. B-IV

The limit $(It_p)_f$ on It_p set by fracture is easily obtained from (4.14) by first setting $\sigma_1 = \sigma_{1t}/f_s$ if σ_1 is positive (tensile), or $\sigma_1 = -|\sigma_{1c}|f_s$ if σ_2 is negative (compressive), and solving for It_p . Here the safety factor f_s is usually chosen as $f_s = 4$, and σ_{1t} and σ_{1c} are the tensile and compressive strengths of coating material 1. The same procedure is repeated for layer 2. The value of $(It_p)_f$ is then the lower of these two values. This gives

$$(It_p)_f = - \left(\frac{\sigma_f}{f_s} - \sigma_{res} \right) \left(\frac{1 - \nu_i}{E_i} \right) \left(\alpha_i \frac{T_{F0}}{It_p} - \alpha_S B_S \frac{\langle T_S \rangle_{\ell_S}}{It_p} \right)^{-1} \quad (4.16)$$

where σ_f is either σ_{1t} , σ_{2t} , σ_{1c} , or σ_{2c} and i is either 1 or 2, according to the selection procedure described above (4.16). The signs of σ_i and σ_F must be observed (positive for tension or negative for compression). The value of T_{F0} is given by (4.6) (or by (5.6) with $T_{\Delta Fp} = T_{\Delta Fp0}$ for the thermally thin coatings discussed in Sec. V), and from the δ_r term in (2.7),

$$\langle T_S \rangle_{\ell_S} \cong \delta_r \left(T_{SC} + \langle T_{\Delta Sr} \rangle_{\ell_S} \right) = [\delta_r (5/h + 0.119 K)] \quad (4.17)$$

for both thermally thin and thermally thick coatings. When the compressive strengths σ_c are not known, the rule of thumb

$$\sigma_c \cong 8 \sigma_t \quad (4.18)$$

can be used as an estimate.

For a single pulse, (4.16) gives

$$\begin{aligned} (It_p)_{fp} &= - \left(\frac{\sigma_F}{f_s} - \sigma_{res} \right) \left(\frac{1 - \nu_i}{\alpha_i E_i} \right) \left(\frac{It_p}{T_{Fp0}} \right) \\ &= [12.4 \text{ J/cm}^3] , \quad \text{for MgO} . \end{aligned} \quad (4.19)$$

Sec. B-IV

By using (4.19) and $T_{F0} = T_{Fp0} + T_{SC} + T_{\Delta Sr0}$, (4.16) can be written in the more convenient form

$$(It_p)_{fr} = "(It_p)_{fp}" (1 + \epsilon + h_f/h)^{-1} \quad (4.20)$$

$$\xrightarrow{h \rightarrow \infty} "(It_p)_{fp}" (1 + \epsilon)^{-1} = [12.4 \text{ J/cm}^2]$$

where

$$h_f \equiv \frac{(T_{SC} h)}{T_{Fp0}} \left(1 - \frac{\alpha_S B_S}{\alpha_i} \right)$$

$$= [5.19 \times 10^{-2} \text{ W/cm}^2 \text{ K}] \quad (4.21)$$

and ϵ , which is often negligible, is

$$\epsilon \equiv \frac{T_{\Delta Sr}}{T_{Fp0}} \left(1 - \frac{\langle T_{\Delta Sr} \rangle_{\ell_S} \alpha_S}{T_{\Delta Sr0} \alpha_i} \right) \quad (4.22)$$

$$= [2.24 \times 10^{-3}]$$

The quotation marks on $"(It_p)_{fp}"$ are a reminder that a different layer can fail in repeated-pulse operation than in single-pulse operation and that the failure can change from compressive in single-pulse to tensile in repeated-pulse operation. Then the sign of σ_F in $(It_p)_{fp}$ in (4.19) can change and i can change from 1 to 2 or vice versa. An example is encountered for the $\text{HfO}_2/\text{SiO}_2$ coating in Sec. IX.

The cooling required to prevent fracture (that is, to keep It_p less than $(It_p)_f$) is obtained by solving (4.20) for h :

Sec. B-IV

$$h = h_f \left[\frac{''(It_p)''_{fp}}{It_p} - 1 - \epsilon \right]^{-1} \quad (4.23)$$

$$= [0.216 \text{ W/cm}^2 \text{ K}] \quad .$$

As discussed above, the values of $\sigma_{i \text{ res}}$ usually are not known. In such cases, setting $\sigma_{i \text{ res}} = 0$ in (4.20) and (4.23) affords an estimate of the values of $(It_p)_f$ and h , but the accuracies of the estimates are expected to be poor.

Melting. In Sec. III under the paragraph heading of single-pulse damage threshold, failure by melting of a coating layer was discussed. Since the details of the melting damage process are not known in general, the estimate of the value $(It_p)_m$ of the energy density at which failure by melting occurs is necessarily imprecise, which may not be important in the cases considered, as discussed below. It is assumed that failure occurs when the temperature of any layer of the coating formally reaches the value $T_m + H_f/C$, where T_m is the melting temperature, H_f and C are the heat of fusion and heat capacity of a layer, and $H_f/C \equiv T_f$ is an effective temperature rise that makes the energy CT_f equal to the heat of fusion.

For an MgO/MgF_2 coating, the value of the temperature rise to failure of MgF_2 is $T_m + H_f/C = (1221^\circ\text{C} - 20^\circ\text{C}) + 1250 \text{ K}/3.14 = 1600 \text{ K}$, which is less than that of MgO ; thus, the failure occurs by melting of the MgF_2 layer near the coating surface. The values $(It_p)_{mp}$ or $(It_p)_{mr}$ of the energy density at which this failure occurs for single-pulse or repeated-pulse operation are easily obtained by scaling from 10 J/cm^2 at T_{Fp0} or T_{Fr0} to the value of It_p at $T_m + H_f/C$:

Sec. B-IV

$$\begin{aligned} (It_p)_{mp} &= \left[(T_m + H_f/C) / T_{Fp0} \right] 10 \text{ J/cm}^2 \\ &= (1.60 \times 10^3 / 47.2) = (339 \text{ J/cm}^2) \end{aligned} \quad (4.24)$$

$$\begin{aligned} (It_p)_{mr} &= \left[(T_m + H_f/C) / T_{Fr0} \right] 10 \text{ J/cm}^2 \\ &= \left[1.60 \times 10^3 / (47.2 + 5/h) \right] \xrightarrow{h=1} 305 \text{ K} \end{aligned} \quad (4.25)$$

where T_m is measured with respect to the initial temperature. Values of $(It_p)_{mp}$ and $(It_p)_{mr}$ for various coating-substrate combinations are listed in Table II.

V. THERMALLY THIN DIELECTRIC REFLECTORS

The case of thermally thin coatings, $\ell_F \lesssim \ell_{Ftp}$, is somewhat more complicated than that of thermally thick ones. For the extreme case of $\ell_F \ll \ell_{Ftp}$ very well satisfied, the analysis is simple since the coating can be neglected. In particular, the temperature drop across the coating is negligible with respect to the temperature at the coating-substrate interface. The following results from Sec. II, which are summarized in Sec. X(c) and X(c), are then valid: T_{F0} from (2.7); T_{Fp0} from (2.1); T_{SC} from (2.4); $T_{\Delta Sr0}$ from (2.5); $(It_p)_{op}$ from (2.18); $(It_p)_{or}$ from (2.21); and h from (2.24).

These extreme values are not very accurate for the cases considered since $\ell_F \ll \ell_{Ftp}$ is not sufficiently well satisfied. Thus, improved approximations will now be developed. First, notice that the value of the energy density for optical-distortion failure in a single pulse, $(It_p)_{op}$, lies between the value (2.18) for the substrate and the value (4.7) for the coating. In the examples below, this determines the value of $(It_p)_p$ to within a factor of approximately two.

The temperature distribution in a thermally thin coating can be estimated as follows: For this case of $\ell_F \ll \ell_{Ftp}$, the thermal diffusion time

$$\tau_F = C_F \ell_F^2 / 4 K_F = [9.02 \times 10^{-8} \text{ s}] \quad (5.1)$$

for heat to diffuse across the film thickness ℓ_F is much less than t_p . Thus, the temperature distribution in the coating has reached its quasi-steady-state value

$$T_F = T_{\Delta Fp} + T_{FSp} + \delta_r (T_{\Delta Sr0} + T_{SC}) \quad (5.2)$$

Sec. B-V

where T_{FSp} is the temperature rise of the coating-substrate interface resulting from a single pulse, $\delta_r (T_{\Delta Sr0} + T_{SC})$ is defined in (2.4)-(2.7), and $T_{\Delta Fp}$ is the solution to the steady-state problem

$$-K_F \frac{d^2 T_{\Delta Fp}}{dz^2} = I A k \left(1 - e^{-k\ell_F} \right)^{-1} e^{-kz} \quad (5.3)$$

with $T_{\Delta Fp} = 0$ at $z = \ell_F$ and $dT_{\Delta Sp}/dz = 0$ at $z = 0$. The source term on the right-hand side of (5.3) corresponds to absorption that decreases exponentially into the coating (as a result of the decrease in irradiance I). The solution to (5.3) with the given boundary conditions is

$$T_{\Delta Fp} = \frac{I A \ell_F}{K_F (1 - e^{-k\ell_F})} \left[1 - \frac{z}{\ell_F} + \frac{1}{k\ell_F} \left(e^{-k\ell_F} - e^{-kz} \right) \right]. \quad (5.4)$$

The value of the exponential prefactor in (5.4) was chosen to make the heat flow, $J = I A$, equal to $-K_F dT/dz$ at $z = \ell_F$; that is, to give overall absorptance A in the coating. In a low-loss reflector, the absorptance by the substrate must be small, which implies that $\exp(-k\ell_F)$ must be small. Setting $\exp(-k\ell_F) = 10^{-3}$ gives $k\ell_F = 6.91$, and (5.4) becomes

$$T_{\Delta Fp} \cong \frac{I A \ell_F}{K_F} \left(1 - \frac{z}{\ell_F} - \frac{e^{-kz}}{6.91} \right), \quad (5.5)$$

and at $z = 0$,

$$\begin{aligned} T_{\Delta Fp0} &= \frac{0.855 I A \ell_F}{K_F} = 4.28 \times 10^4 \ell_F / K_F \\ &= 4.28 \times 10^4 \ell_F / K_F = [27.2 \text{ K}] . \end{aligned} \quad (5.6)$$

Sec. B

In order to estimate the value of T_{FSp} , equating the absorbed energy per unit area $I t_p A$ in a single pulse to the energy increase in the corresponding volume gives (for t_p short with respect to the diffusion time $C_S \ell_S^2 / 4 K_S$ across the substrate)

$$I t_p A = \int_0^{\ell_S + \ell_F} dz C(z) T(z)$$

$$\cong C_S T_{FS} \ell_{S\Delta} + C_F \ell_F (0.415 T_{\Delta Fp0} + T_{FS}) ,$$

where

$$\ell_{S\Delta} = [\pi(t_p - \tau_F) K_S / 4 C_S]^{1/2}$$

$$= 8.86 \times 10^{-4} [(1 - \tau_F / t_p) K_S / C_S]^{1/2}$$

$$= [6.19 \mu m] . \quad (5.7)$$

Solving for T_{FS} gives

$$T_{FSp} = \frac{I A (t_p - 1.42 \tau_F)}{C_S \ell_{S\Delta} + C_F \ell_F} = [20.0 K] . \quad (5.8)$$

In the limit $\ell_F \ll \ell_{Ftp}$, the factors $1.42 \tau_F$ and $C_F \ell_F$ in (5.8) and τ_F in (5.7) are negligible, $T_{\Delta Fp} \ll T_{FSp}$, and (5.2) gives

$$T_{Fp0} \cong T_{FSp} \cong I A t_p / C_S \ell_{\Delta S}$$

$$= 5.00 \times 10^{-2} (C_S \ell_{\Delta S})^{-1} = [29.5 K]$$

which is equal to T_{Fp0} in (2.1), giving the correct limit. For $h = \infty$,

Sec. B-V

$$\begin{aligned} (T_{F0r})_{h=\infty} &= T_{\Delta Fp0} + T_{FSp} + T_{\Delta Sr0} \\ &= [27.2 \text{ K} + 20.0 \text{ K} + 0.20 \text{ K}] = [47.4 \text{ K}] \end{aligned} \quad (5.9)$$

Next consider the thermally induced optical distortion. As discussed in Sec. IV, the attachment-stress contribution to the thickness change of the coating and substrate is neglected. The resulting error in the single-pulse optical-distortion threshold $(It_p)_{op}$ for the $\text{MgO/MgF}_2\text{:Mo}$ reflectors is only 3.7 percent, and the error for repeated-pulse operation is even smaller. The expected overall disagreement of the theoretical and experimental results is greater than this value of 3.7 percent. Nevertheless, the correction for the attachment-stress contribution to the thickness change is calculated in Ref. 25, and the correction can be applied to new cases to insure that the error is not anomalously great and to obtain the greatest theoretical accuracy.

When the attachment-stress contribution is neglected, the single-pulse optical-distortion threshold is obtained from the expression

$$\lambda/2G = \Delta l_{Fp} + \Delta l_S \quad (5.10)$$

where

$$\begin{aligned} \Delta l_{Fp} &= \alpha_F (1 + \nu_F) \int_0^{\ell_F} dx (T_{\Delta Fp} + T_{FSp}) \\ &= \alpha_F \ell_F (1 + \nu_F) (0.415 T_{\Delta Fp0} + T_{FSp}) \end{aligned} \quad (5.11)$$

and

$$\Delta l_{Sp} = \alpha_S (1 + \nu_S) T_{FSp} \ell_{S\Delta} \quad (5.12)$$

Sec. B-V

Using $T = (T/It_p)It_p$, where T/It_p is independent of I , for the three T 's and solving (5.10)-(5.12) for It_p gives

$$\begin{aligned} (It_p)_{op} &= (\lambda/2G) It_p \left[\alpha_S \ell_{S\Delta} (1 + \nu_S) T_{FSp} \right. \\ &\quad \left. + \alpha_F \ell_F (1 + \nu_F) (0.415 T_{\Delta Fp0} + T_{FSp}) \right]^{-1} \\ &= [21.4 \text{ J/cm}^2] \quad . \end{aligned} \quad (5.13)$$

This form of $(It_p)_p$ is preferred since the T 's will be calculated separately; however, $(It_p)_p$ can be expressed explicitly in terms of the material parameters as

$$\begin{aligned} (It_p)_{op} &= \frac{\lambda/G}{2A} \left\{ \left[\alpha_S \ell_{S\Delta} (1 + \nu_S) + \alpha_F \ell_F (1 + \nu_F) \right] \left[\frac{1 - 1.42 \tau_F/t_p}{C_S \ell_{S\Delta} + C_F \ell_F} \right] \right. \\ &\quad \left. + \alpha_F \ell_F (1 + \nu_F) \frac{0.355}{K_F t_p} \right\}^{-1} \quad . \end{aligned} \quad (5.14)$$

The analysis of the continuously repeated-pulse optical distortion for the thermally thin case is similar to that for the thermally thick case. The results are:

$$\begin{aligned} (It_p)_{or} &= \frac{(It_p)_{op}}{1 + h_o \left(\frac{1}{h} + \frac{a \ell_S}{3 K_S} \right)} \\ &\xrightarrow{h \rightarrow \infty} [14.7 \text{ J/cm}^2] \end{aligned} \quad (5.15)$$

and

Sec. B-V

$$h = h_o \left[\frac{(It_p)_{od}}{It_p} - 1 - \frac{\ell_S h_o}{3K_S} \right]^{-1} \quad (5.16)$$

$$= [28.1 \text{ W/cm}^2 \text{ K}]$$

where

$$h_o = \frac{\ell_S \alpha_S (1 + \nu_S) A (It_p)_{od}}{t_{ip} (\lambda / 2G)}$$

$$= 1.40 \times 10^5 \alpha_S (1 + \nu_S) (It_p)_{op} = [19.1] \quad \text{for 250 nm}$$

$$= 9.89 \times 10^4 \alpha_S (1 + \nu_S) (It_p)_{op} = [19.1] \quad \text{for 354 nm} \quad (5.17)$$

The value of h_o is independent of $(\lambda / 2G)$ (since $(It_p)_{op} \sim \lambda / 2G$).

Equation (5.15) can be rewritten in the following form, which is useful in calculating one contribution to It_p when the other contributions are known,

$$\frac{1}{(It_p)_{or}} = \frac{1}{(It_p)_{op}} + \frac{1}{(It_p)_{SC}} + \frac{1}{(It_p)_{\Delta S}} \quad (5.17a)$$

where

$$(It_p)_{SC} = \frac{h t_{ip} (\lambda / 2G)}{\alpha_S \ell_S (1 + \nu_S) A} = 7.14 \times 10^{-6} \frac{h}{\alpha_S (1 + \nu_S)}$$

$$= [31.4 \text{ J/cm}^2] \quad \text{for } h = 28.1 \text{ W/cm}^2 \text{ K}$$

is the contribution to It_p from T_{SC} and

Sec. B-V

$$(It_p)_{\Delta S} = \frac{3 t_{ip} K_S (\lambda/2G)}{a \alpha_S \ell_S^2 (1 + \nu_S) A} = 2.14 \times 10^{-4} \frac{K_S}{a \alpha_S (1 + \nu_S)}$$

$$= [46.9 \text{ J/cm}^2]$$

is the contribution to It_p from $T_{\Delta S}$. For the example of $\text{MgO/MgF}_2\text{:Mo}$ at 250 nm, the numbers corresponding to (5.17a) are $(10)^{-1} = (21.4)^{-1} + (31.4)^{-1} + (46.9)^{-1}$.

For MgO/MgF_2 on invar at 250 nm,

$$\ell_{tip} = 3.89 \times 10^{-2} \text{ cm}, \quad a = 1.42$$

$$(It_p)_{op} = 24.0 \text{ J/cm}^2, \quad (It_p)_{\Delta S} = 28.0 \text{ J/cm}^2$$

$$\left. \begin{aligned} (It_p)_{SC} &= 44.5 \text{ J/cm}^2 \\ (It_p)_{or} &= 10.0 \text{ J/cm}^2 \end{aligned} \right\} \quad \text{at } h = 4.02 \text{ W/cm}^2 \text{K}.$$

For $\text{HfO}_2/\text{SiO}_2$ on invar at 354 nm,

$$\ell_{tip} = 3.89 \times 10^{-2} \text{ cm}, \quad a = 1.42$$

$$(It_p)_{op} = 346 \text{ J/cm}^2, \quad (It_p)_{\Delta S} = 39.7 \text{ J/cm}^2$$

$$\left. \begin{aligned} (It_p)_{SC} &= 13.9 \text{ J/cm}^2 \\ (It_p)_{or} &= 10.0 \text{ J/cm}^2 \end{aligned} \right\} \quad \text{at } h = 0.886 \text{ W/cm}^2 \text{K}$$

The coating stress and fracture analysis for thermally thin coatings is formally the same as the thermally thick coating analysis of Sec. IV. The results are:

Sec. B-V

$$\begin{aligned} (I_{tp})_{fp} &= - \left(\frac{\sigma_F}{f_S} - \sigma_{res} \right) \left(\frac{1 - \nu_i}{\alpha_i E_i} \right) \left(\frac{I_{tp}}{T_{Fp0}} \right) \\ &= [17.2 \text{ J/cm}^2] , \end{aligned} \quad (5.18)$$

$$\begin{aligned} (I_{tp})_{fr} &= "(I_{tp})_{fp}" (1 + \epsilon + h_f/h)^{-1} \\ \xrightarrow{h \rightarrow \infty} "(I_{tp})_{fp}" (1 + \epsilon)^{-1} &= [17.2 \text{ J/cm}^2] , \end{aligned} \quad (5.19)$$

$$\begin{aligned} h_f &= \frac{T_{SC} h}{T_{Fp0}} \left(1 - \frac{\alpha_S B_S}{\alpha_i} \right) \\ &= [6.59 \times 10^{-2} \text{ W/cm}^2 \text{ K}] , \end{aligned} \quad (5.20)$$

and

$$\begin{aligned} h &= h_f \left[\frac{(I_{tp})_{fp}}{I_{tp}} - 1 - \epsilon \right]^{-1} \\ &= [9.18 \times 10^{-2} \text{ W/cm}^2 \text{ K}] \end{aligned} \quad (5.21)$$

$$\epsilon = \frac{T_{\Delta Sr}}{T_{Fp0}} \left(1 - \frac{\langle T_{\Delta Sr} \rangle \alpha_S}{T_{\Delta Sr0} \alpha_i} \right) = [2.83 \times 10^{-3}] . \quad (5.22)$$

VI. ADAPTIVE OPTICS AND SUBSTRATE MATERIALS AND COOLING

Typical values of heat-transfer coefficients h . Values of h at least as great as several hundred $\text{W}/\text{cm}^2 \text{K}$ are desirable in some applications. However, such great values of h are well beyond the state of the art. Typical attainable values of h are as follows:

- $h = 40 \text{ W}/\text{cm}^2 \text{K}$. This greatest value of which we are aware was attained by using a high-temperature liquid metal coolant and state-of-the-art techniques.³⁸ Maintaining optical tolerance was not a requirement of the system.
- $h \cong 10 \text{ W}/\text{cm}^2 \text{K}$. State of the art for reflectors with water cooling at high pressure and great turbulence.³⁹
- $h \cong 1 \text{ W}/\text{cm}^2 \text{K}$. Good value for liquid coolants.
- $h = 6 \times 10^{-2} \text{ W}/\text{cm}^2 \text{K}$. Best value obtained with gas coolant.⁴⁰
- $h = 6.12 \times 10^{-4} \text{ W}/\text{cm}^2 \text{K}$. Formal value for radiative cooling of a body with emissivity $\epsilon = 1$ and temperature $T = 300 \text{ K} + \Delta T$, where $\Delta T \ll 300 \text{ K}$, radiating into temperature $T = 300 \text{ K}$: $\sigma[(300 + T)^4 - (300)^4] \cong 4(300)^3 \sigma T \equiv hT$.
- $h = 3 \times 10^{-4} \text{ W}/\text{cm}^2 \text{K}$. Convection in a still room for plate geometry.
- $h \cong 10^{-4} \text{ W}/\text{cm}^2 \text{K}$. Convection in a still room for a small-rod geometry.⁴¹

The state of the art in high-power mirrors is $h \cong 10 \text{ W}/\text{cm}^2 \text{K}$ for a water-cooled, 20 mill (0.51 mm) -thick molybdenum face plate polished under operating pressure (400 psi pressure drop).³⁹ The lowest surface distortion was 16 nm ($\lambda_v/40$, where $\lambda_v = 632.8 \text{ nm}$), and the greatest value of the heat transferred to the coolant was $\sim 2 \text{ kW}/\text{cm}^2$.

Sec. B-VI

The current requirements are somewhat different. The value $\lambda/40 = 6 \text{ nm}$ at $\lambda/250 \text{ nm}$ requires a factor of approximately three improvement over the state of the art, but the heat removed, 5 W/cm^2 is a factor of 400 smaller than the state of the art. The maximum possible value of h is needed.

Work on invar reflectors at the Garrett AiResearch Corporation was abandoned several years ago in favor of molybdenum as a result of technical difficulties in fabricating the invar structure (connection of the face plate to the cooling/support structure).³⁹ It would be worthwhile to determine if these difficulties could be overcome since invar is far superior theoretically to SiC, Mo, C, Ag, and Au, as seen in Table II of Sec. I. The properties of invar reported in the literature vary considerably. In Ref. 33 the following values of the thermal expansion coefficient for invar were given: $\alpha = 1.98 \times 10^{-6} \text{ K}^{-1}$ for $-129 \text{ C} < T < -18 \text{ C}$; $\alpha = 1.26 \times 10^{-6} \text{ K}^{-1}$ for $-18 \text{ C} < T < 93 \text{ C}$; and $\alpha = 2.70 \times 10^{-6} \text{ K}^{-1}$ for $93 \text{ C} < T < 204 \text{ C}$. Apparently, values as low as $\alpha = 0.3 \times 10^{-6} \text{ K}^{-1}$ have been attained. The value $\alpha = 0.5 \times 10^{-6} \text{ K}^{-1}$ is used in the present study, in which the maximum temperature rise of the invar is 75 K for a small region near the surface at the end of a pulse, or 19.7 K for the average temperature $\langle T_{\Delta \text{Sr}} \rangle_{\text{LS}}$.

Cobalt-iron-chromium negative-expansion substrate. The second edition of the American Institute of Physics Handbook reports that cobalt-iron-chromium (53.0 to 55.5 Co; 35.0 to 37.5 Fe; 9.0 to 10.5 Cr) has expansion coefficients ranging from $-1.1 \times 10^{-6} \text{ K}^{-1}$ to $+1.7 \times 10^{-6} \text{ K}^{-1}$ on the temperature range 20 to 60 C. This suggests the possibility of partially compensating for the coating expansion if the expansion coefficient of this alloy can be tailored to give a small negative value. No other information has been obtained on the alloy at present.

Sec. B-VI

Silicon carbide is slightly better theoretically than molybdenum, and scattering may be less of a problem since SiC can be polished better than Mo. However, it is anticipated that the fabrication of SiC reflectors would be much more difficult than the fabrication of Mo reflectors. Even though sintered SiC can be machined before firing, such problems as attaching a 0.5 mm-thick face plate to the support/cooling structure (or avoiding this problem by such a method as using single-piece construction) and attaining $10 \text{ W/cm}^2 \text{ K}$ heat transfer are expected to be sufficiently difficult that the slight gain in performance would not warrant the increased complication in general. Furthermore, the advantage of lower scattering of SiC than of molybdenum will not be a major consideration if invar also can be well polished. Finally, a successful invar substrate would have far greater impact than a successful SiC substrate since the former would afford a solution to the reflector problem for the model system, while the latter would not.

The severity of the reflector problem suggests that such engineering solutions as the following be investigated:

Heat-pipe mirrors. An attractive concept for high-power mirrors is the heat-pipe mirror.⁴²⁻⁴⁴ In a five-centimeter-diameter heat-pipe mirror, 350 W/cm^2 with a total of 729 W of heat was removed from the center of the mirror while maintaining a total temperature difference of less than 1 K over the mirror.^{42, 44} In the model system under consideration only 5 W/cm^2 will be removed at the center of the reflector, but the diameter will be greater, say, up to ~ 15-20 cm, and the temperature difference corresponding to a thickness difference of $\lambda/80$ for a 0.1 cm-thick molybdenum substrate is less than $\Delta T \cong \lambda/80 \cdot \ell_S \alpha_S = [0.625 \text{ K}]$ by an amount that depends on the thickness change

Sec. B-VI

resulting from the single-pulse heating of the thin surface layer of the reflector and from the temperature distribution across the substrate. A typical value is $\Delta T = 0.25 \text{ K}$. D. L. Jacobson⁴⁵ believes that the likelihood of attaining these specifications is sufficiently great to warrant experimental investigation. Use of a heat-pipe mirror in conjunction with adaptive optics could prove interesting.

Adaptive optics for lower h . In principle, corrective optics could be used to compensate for thermally induced optical distortion, thereby allowing the substrate temperature to increase and allowing successful operation with available values of heat-transfer coefficient h . In some applications, fixed corrective optics possibly could be used. When the laser is turned on, the distortion would be great until the thermal steady state is reached. For state-of-the-art cooling ($h = 10 \text{ W/cm}^2 \text{ K}$ and $l_S = 0.5 \text{ nm}$) of a molybdenum substrate, the time constant τ_C is quite small, $\tau_C = 1.3 \times 10^{-2} \text{ s}$, as will be shown below. Thus, only the first few pulses of a 100 Hz system would be optically distorted, which should be tolerable in many systems. The initial distortion could in principle be reduced by using adaptive optics, which would be especially useful in systems where state-of-the-art cooling is not practical. For example, for $l_S = 1 \text{ mm}$ and $h = 0.1 \text{ W/cm}^2 \text{ K}$, the time constant is $\tau_C = 2.61 \text{ s}$. Another example of the use of adaptive optics is the use in conjunction with an uncooled substrate, as discussed below.

For large corrections by the adaptive optics, the optical path difference is controlled by the value of $T_{SC} = I A t_p / t_{ip} h$. The coating-independent distortion is then

$$\begin{aligned}
\ell_{\text{opd}} &= 2 \Delta \ell_S = 2 \alpha_S (1 + \nu_S) T_{\text{SC}} \\
&= 2 I A t_p \alpha_S (1 + \nu_S) / t_{\text{ip}} h_{\text{ao}} \\
&= 10 \alpha_S (1 + \nu_S) / h ,
\end{aligned} \tag{6.1}$$

$$\begin{aligned}
\frac{\Delta \ell_S}{\lambda/2G} &= \frac{\ell_{\text{opd}}}{\lambda/G} = \frac{I A t_p \alpha_S (1 + \nu_S) 2G}{\lambda t_{\text{ip}} h_{\text{ao}}} \\
&= 1.40 \times 10^7 \alpha_S (1 + \nu_S) / h_{\text{ao}} , \quad \text{for 250 nm} \quad \underline{(6.2)} \\
&\xrightarrow{h_{\text{ao}} = 10 \text{ W/cm}^2 \text{ K}} [9.10] ,
\end{aligned}$$

$$\begin{aligned}
\frac{\Delta \ell_S}{\lambda/2G} &= \frac{\ell_{\text{opd}}}{\lambda/G} = 9.89 \times 10^6 \alpha_S (1 + \nu_S) / h_{\text{ao}} , \quad \text{for 354 nm} \\
&\xrightarrow{h_{\text{ao}} = 10 \text{ W/cm}^2 \text{ K}} [6.43] . \quad (6.3)
\end{aligned}$$

Thus, for a molybdenum coating at 250 nm, the adaptive optics would have to correct for $\ell_{\text{opd}} = 9.1(\lambda/G)$ while maintaining λ/G tolerance at $h = 10 \text{ W/cm}^2 \text{ K}$. For $h = 1 \text{ W/cm}^2 \text{ K}$, the correction would be $\ell_{\text{opd}} = 91(\lambda/G)$ at 250 nm.

The feasibility of an adaptive optics system, or even nonadaptive corrective optics, should be carefully studied theoretically before undertaking laboratory investigations. The technical problems of correcting for several hundred times λ/G while maintaining λ/G could be severe. The time constant would range from a small fraction of a second to 260 s in the systems considered. Even in the absence of thermal distortion, obtaining (and indeed even measuring) the

Sec. B-VI

required low figure-error tolerance for the large optics will require considerable improvement over the best results obtained to date, as discussed in Sec. I.

Since adaptive optics will be required in order to reduce the optical distortion from the windows,²¹ a single system should suffice for both the window and mirror corrections. The possibility of improving the performance of an adaptive-optics system by programming in an expected correction (theoretical value that is fine-tuned experimentally) plus an active feedback correction could be considered.

As an alternative to adaptive optics, rapid interpulse cooling, that is operating for, say, one or two seconds and then rapidly cooling the optics has been discussed.³ However, even in cases in which this type of operation is acceptable, the technical difficulties are great. In principle, the radial temperature distribution of the coolant could be tailored to reduce the optical distortion, but again the technical difficulties would be great.

Time constant for cooling. The above value of 1.3×10^{-2} s for the time constant can be obtained from the expression²³

$$\tau_C = C_S l_S / h = (2.61) (0.05) / 10 = 1.3 \times 10^{-2} \text{ s} \quad (6.4)$$

for the time constant for the surface cooling of a thermally thin substrate. The thermally thin-substrate condition $l_S \ll K_S / h$ is sufficiently well satisfied since $l_S = 5 \times 10^{-2}$ cm and $K_S / h = 1.4 / 10 = 0.14$ cm. The numerical values are for the case of molybdenum. A rough check of this value of $\tau_C = 1.3 \times 10^{-2}$ from (6.4) is obtained by equating the energy per area $\epsilon / A = \Delta T C_S l_S = (1/h) C_S l_S = (5/10) (2.61) (0.05) = 6.53 \times 10^{-2} \text{ J/cm}^2$ in the steady state to the energy per area added in time t ; that is, $I t_p A(t/t_{ip}) = 5t$, which gives $t = 6.53 \times 10^{-2} / 5 = 1.31 \times 10^{-2}$ s, in agreement with the value in (6.4).

Sec. B-VI

The total cooling time $\tau_{\text{tot}} = \tau_C + \tau_S$ is approximately equal to the surface cooling time τ_C because the time $\tau_S = C_S \ell_S^2 / 4 K_S = 1.17 \times 10^{-3}$ s for thermal diffusion through the substrate is much smaller than τ_C . This condition $\tau_S \ll \tau_C$ is essentially equivalent to the substrate being thermally thin ($\ell_S \ll K_S / h$).

Uncooled substrate with adaptive optics. If a satisfactory adaptive optical system could be developed, a thick uncooled reflector substrate could be used for operation for a limited time such as 60 s. However, it will now be shown that if the great heat-transfer coefficient $h = 10 \text{ W/cm}^2 \text{ K}$ is attained in the model system, the amount of correction required by the adaptive optics is considerably less for the cooled than for the uncooled substrate. An uncooled invar substrate operated for 60 s requires a correction $\ell_{\text{opd}} / (\lambda / 2 G) \cong 100$, which is the same correction required for a 0.1 cm-thick molybdenum face plate with $h = 0.64 \text{ W/cm}^2 \text{ K}$. This value of 100 is an order of magnitude greater than the value of 9.1 from (6.2). The simplicity of the uncooled invar substrate may dictate its use in some applications. The time constant of the adaptive optical system would be much longer for the uncooled substrate (~ 60 s) than for the cooled substrate (as small as 10^{-2} s, depending on the value of h).

During the 60 seconds of operation, the thermal diffusion distance in molybdenum is

$$\ell_{S60} = [4(1.4)60/2.61]^{1/2} = 11.35 \text{ cm} \quad . \quad (6.5)$$

Since this value is greater than the distance over which the irradiance changes substantially, the radial diffusion will decrease the severity of the problem. As an upper bound to the thickness change $\Delta \ell_S$, neglecting radial diffusion and

Sec. B-VI

using (2.10) and (2.9), with $I t_p$ replaced by the total energy density $I t_p (t/t_{ip}) = 6 \times 10^4 \text{ J/cm}^2$, gives

$$\Delta \ell_S \lesssim \alpha_S (1 + \nu_S) I t_p A t / t_{ip} C_S = 300 \alpha_S (1 + \nu_S) / C_S$$

$$\lesssim [7.35 \mu\text{m}] = [1.45 \times 10^3 (\lambda/2G)] , \quad (6.6)$$

for $\lambda = 354 \text{ nm}$. The amount by which $\Delta \ell_S$ is below this bound depends on the size and shape of the substrate. Several models afford estimates of the reduction in $\Delta \ell_S$ resulting from radial diffusion.

The temperature at the center of a Gaussian beam incident on a semi-infinite medium for cw irradiance I_{cw} is¹³

$$T_\infty = \pi^{1/2} I_{cw} A D_e / 8 K_S$$

where D_e is the diameter at which the irradiance is e^{-1} times the center value I . For the present case, formally setting $I_{cw} = \langle I \rangle_t = I t_p / t_{ip}$ gives

$$T_\infty = \pi^{1/2} I A D_e t_p / 8 t_{ip} K_S$$

$$= 1.11 D_e / K_S . \quad (6.7)$$

For $D_e = 5 \text{ cm}$ and $K_S = 1.4 \text{ W/cm K}$ for molybdenum,

$$T_\infty = 3.96 \text{ K} \quad (6.8)$$

which is a very small temperature rise. A very crude estimate of the corresponding value of $\Delta \ell_S$ is

$$\Delta \ell_S / (\lambda/2G) \cong [400] . \quad (6.9)$$

For a two-centimeter-thick molybdenum substrate, 10 cm in diameter with a Gaussian beam that is down by $\exp(-aR^2) = \exp(-2)$ at the rim ($\rho = 5$ cm), the average temperature is

$$T = \frac{I A_t t_p}{C_S \ell_S t_{ip}} \frac{1}{aR^2} (1 - e^{-aR^2}) \approx 24.9 \text{ K} \quad (6.10)$$

and again the temperature rise is not excessive.

As a simple order-of-magnitude estimate, the difference in temperature between the center ($\rho = 0$) and rim ($\rho = R = 5$ cm) of the mirror is approximately equal to the value of T at $\rho = 0$ at the end of $t = (C_S R^2 / 4 K_S)^{1/2} = 11.7$ s, which is $\Delta T \sim 20$ K for $\ell_S = 2$ cm. Thus, the adaptive optical system would have to correct for

$$\frac{\ell_{\text{opd}}}{\lambda/G} \cong \frac{\alpha_S \ell_S \Delta T}{2(\lambda/2G)} \cong [280] \quad (6.11)$$

The factor of $1/2$ accounts for the equal expansion of the front and rear surface, in contrast to a factor of 1 for a thin face plate, which is supported with its rear surface in a plane. These estimates indicate that $\ell_{\text{opd}}/(\lambda/G) \cong 300$ to 400 , which is considerably greater than the value of 6.4 from Eq. (6.3) for molybdenum with the great value of $h = 10 \text{ W/cm}^2 \text{ K}$. The value of $\ell_{\text{opd}}/(\lambda/G) \cong 350$ corresponds to the cooled-substrate case of $h = 0.19 \text{ W/cm}^2 \text{ K}$.

For an uncooled invar substrate, (6.9) and (6.5) give $\Delta \ell_S / (\lambda/2G) = 120$ and

$$\ell_{S60} = 3.01 \text{ cm}$$

Sec. B-VI

A simple estimate of the reduction in the value $\Delta\ell_S/(\lambda/2 G)$ resulting from radial diffusion gives

$$\Delta\ell_S/(\lambda/2 G) \cong 100 \quad (6.12)$$

The surface temperature corresponding to (6.12) for a two-centimeter thick substrate is, from (2.1) with t_p replaced by $t_p t/t_{ip}$ and with a reduction by the factor 100/120,

$$T = 59.0 \text{ K} ,$$

which is not excessive.

The substrate temperature could be decreased by increasing the thickness.

The ultimate reduction in temperature would give

$$(T)_{z=\rho=0} = T_{\Delta F0p} + T_{FSp} + T_{\infty} = 46.9 + 3.96 = 50.9 \text{ K}$$

For a single-pulse operation, the small thermal conductivity of invar ($K_S = 0.12 \text{ W/cm K}$) causes a greater increase in the surface temperature than for the case of say an Mo ($K_S = 1.4 \text{ W/cm K}$) or SiC ($K_S = 2.11 \text{ W/cm K}$). By depositing a thin layer of molybdenum or silicon carbide (typically a few micrometers thick) on the invar substrate and depositing the coating on the molybdenum or silicon carbide, the temperature would be decreased as a result of the greater thermal conductivity of the molybdenum. The contribution to the optical distortion from the temperature distribution that extends across the substrate during repeated-pulse operation still would be small as a result of the low thermal expansion of the invar substrate. Thus it might at first appear that adding the intermediate Mo or SiC layer would improve the performance of the reflector.

Sec. B-VI

Unfortunately this is not the case in presently considered reflectors because the performance is not limited by the high temperature. That is, the performance is limited by optical distortion rather than by melting or fracture. As an example, for MgO/MfG_2 on invar, the limiting energy density is

$$(It_p)_{\text{or}} = 11.6 \text{ J/cm}^2$$

if the state-of-the-art cooling, $h = 10 \text{ W/cm}^2 \text{ K}$, is attained (and lower It_p if not). Adding a Mo layer would decrease the threshold to

$$(It_p)_{\text{or}} = 10.9 \text{ J/cm}^2 .$$

(The formal fracture threshold would be increased from $\sim 12.1 \text{ J/cm}^2$ to $\sim 17.2 \text{ J/cm}^2$.)

The use of an intermediate layer of near-zero thermal expansion (Sec. III) could be effective for the uncooled substrates.

VII. CONTINUOUS-OPERATION REFLECTORS

The analysis of cw-operated reflectors is considerably simpler than that of continuously repeated-pulse operation. The temperature of the coating, measured with respect to the temperature of the coating-substrate interface, is given by (5.5), that is

$$T_{\Delta F} \cong \frac{IA \ell_F}{K_F} \left(1 - \frac{z}{\ell_F} - \frac{e^{-6.91z/\ell_F}}{6.91} \right) \quad (7.1)$$

for $k\ell_F = 6.91$. In the substrate, the solution to the steady-state thermal-diffusion equation

$$-K_S d^2 T / dz^2 = 0$$

that gives heat flow $J = -K_S dT/dz$ with $J = IA$ and $T = T_{SC}$ at $z = \ell_S$, is

$$T_S = T_{\Delta S} \left(1 - \frac{z'}{\ell_S} \right) + T_{SC} \quad (7.2)$$

where

$$T_{\Delta S} = IA \ell_S / K_S \quad (7.3)$$

and $z' = z - \ell_F$. The temperature of the back surface of the substrate is, from

$T_{SC} = J/h$ (see above (2.3)),

$$T_{SC} = IA/h \quad (7.4)$$

From (7.1)-(7.4), the maximum temperature at the surface of the coating, is

$$\begin{aligned} T_{F0} &= IA \left(\frac{0.855 \ell_F}{K_F} + \frac{\ell_S}{K_S} + \frac{1}{h} \right) \\ &= [IA(7.20 \times 10^{-2} + 1/h)] \quad (7.5) \end{aligned}$$

Sec. B-VII

In calculating the optical distortion, the change in thickness of the reflector is (with the attachment-stress contribution negligible here)

$$\Delta l = \alpha_S l_S (1 + \nu_S) \langle T_S \rangle_{l_S} + \alpha_F l_F (1 + \nu_F) \langle T_F \rangle_{l_F} . \quad (7.6)$$

Since $l_F \ll l_S$ and the other factors in the two terms in (7.6) are of the same order of magnitude in general, (7.6) reduces to

$$\Delta l \cong \alpha_S l_S (1 + \nu_S) \langle T_S \rangle_{l_S} . \quad (7.7)$$

From (7.2)

$$\begin{aligned} \langle T_S \rangle_z &= T_{SC} + \frac{1}{2} T_{\Delta S} \\ &= [IA (3.57 \times 10^{-2} + 1/h)] . \end{aligned} \quad (7.8)$$

Setting Δl in (7.7) equal to $\lambda/2G$ and solving for I gives

$$I_o = \frac{\lambda/2G}{A \alpha_S l_S (1 + \nu_S)} \left(\frac{1}{h} + \frac{l_S}{2K_S} \right)^{-1} \quad (7.9)$$

For perfect cooling, that is, $h \gg 2K_S/l_S = 28 \text{ W/cm}^2 \text{ K}$, (7.9) reduces to

$$I_{oh\infty} = \frac{\lambda K_S}{A G \alpha_S l_S^2 (1 + \nu_S)} \quad (7.10)$$

which gives

$$I_{oh\infty} = 4.36 \text{ kW/cm}^2 \quad (7.11)$$

for molybdenum at 354 nm with $l_S = 0.1 \text{ cm}$ and $G = 35$. This value of $I_{oh\infty} = 4.36 \text{ kW/cm}^2$ is comparable to the average intensity $I t_p / t_{ip} = 10/10^{-2} = 1 \text{ kW/cm}^2$ in the repeated-pulse system with $I t_p = 10 \text{ J/cm}^2$ and $t_{ip} = 10^{-2} \text{ s}$.

Sec. B-VII

The stresses at the center ($\rho = z = 0$) in the coating layers 1 and 2 are, from (4.14)

$$\sigma_1 = \sigma_{1\text{res}} - \frac{E_1}{1 - \nu_1} \left(\alpha_1 T_{F0} - \alpha_S B_S \langle T_S \rangle_z \right) \quad (7.12)$$

where T_{F0} is given by (7.5) and $\langle T_S \rangle_z$ by (7.8). The fracture-limited irradiance is obtained from (7.11) by setting $\sigma_1 = \sigma_F / f_s$ and setting other subscripts 1 by i , as defined under (4.16). This gives

$$I_f = - \left(\frac{\sigma_F}{f_s} - \sigma_{i\text{res}} \right) \left(\frac{1 - \nu_i}{A E_i} \right) \left(\alpha_i \frac{T_{F0}}{A I} - \alpha_S B_S \frac{\langle T_S \rangle_z}{A I} \right)^{-1}. \quad (7.13)$$

For $\sigma_F = -8(2 \times 10^4)$ psi, $f_s = 4$, $\sigma_{i\text{res}} = 0$, $E_i = 3.61 \times 10^7$ psi, $\nu_i = 0.3$, $\alpha_i = 10.5 \times 10^{-6} \text{ K}^{-1}$, $\alpha_S = 5 \times 10^{-6} \text{ K}^{-1}$, $B_S = 0.716 + 0.284(0.3) = 0.801$, $h = \infty$, $\ell_F / K_F \ll \ell_S / K_S = 0.1/1.4$, the values of the temperatures in (7.12) are $T_{F0}/A I = \ell_S / K_S = 7.14 \times 10^{-2}$ and $\langle T_S \rangle_z = \ell_S / 2 K_S$, and (7.12) gives

$$I_f = 2.53 \times 10^5 \text{ W/cm}^2. \quad (7.14)$$

Comparison of (7.11) and (7.14) shows that cw-operated reflectors are much more prone to failure by optical distortion than by fracture. For the case of continuous repeated-pulse operation, the difference between the optical-distortion and failure thresholds is not as great as for cw operation. This is because the great surface temperature at the end of a pulse in the former case increases the stress in the coating much more than it does in the total expansion $\Delta \ell = \Delta \ell_F + \Delta \ell_S$, since the single-pulse temperature is great at the surface but does not extend far into the substrate.

VIII. THERMALLY INDUCED CHANGES IN THE REFLECTION COEFFICIENT

In addition to the thermally induced change in thickness of the coating and substrate considered in the preceding calculations, the reflection coefficient r (measured with respect to the final position of the front surface of the coating) of the reflector changes because the optical thickness of the coating layers changes. The change ϕ_r in the phase of r , is proportional to the small change ℓ_Δ in the optical thickness of the layers of the coating, while the magnitude squared $|r|^2$, which is equal to the reflectance, is proportional to ℓ_Δ^2 . Thus the optical distortion resulting from ϕ_r is more important than is the change in the reflectance. It will be shown below that the thermally induced change in reflectance $R = |r|^2$ is entirely negligible in the cases of interest.

The approximation of neglecting ϕ_r in the preceding calculations is often well satisfied. The calculations to follow illustrate this result and also show how ϕ_r can be included when necessary. The results of a detailed treatment of ϕ_r and of absorption in the coating and substrate, which is expected to yield accurate analytical approximations to ϕ_r and the absorptance, will be used in a future report to obtain improved approximations to the various values of It_p . A simplified treatment below should suffice to illustrate the salient features of the effects of ϕ_r .

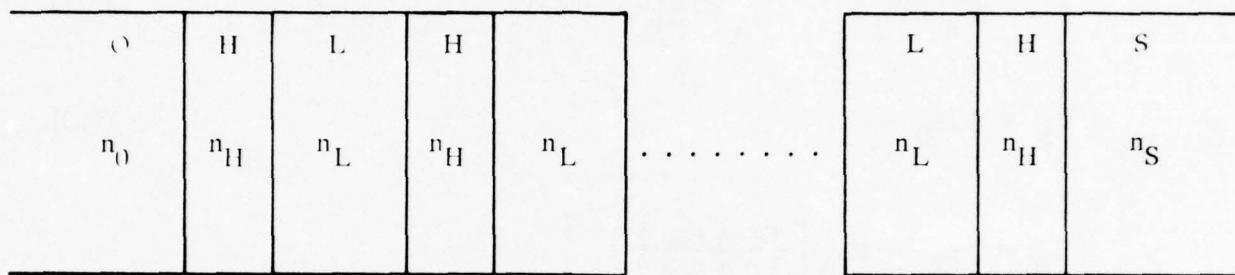
The following simple physical interpretation of the results illustrates why ϕ_r is often negligible and indicates when ϕ_r should be included in the calculation of optical distortion. The irradiance in a coating drops rather rapidly as a function of the distance from the surface of the coating. For a coating that is optimized

Sec. B-VIII

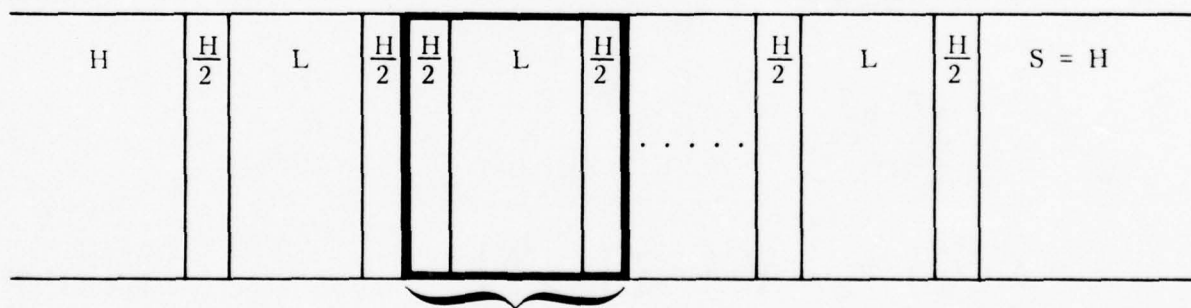
for minimum absorptance, the irradiance at the absorbing substrate must be extremely small. It will be shown^{35a} that when $1 - R \ll 1$ is satisfied, the irradiance decreases by a factor of $(n_L/n_H)^2$ for each pair of layers; thus the irradiance is large only in the top layers of the coating. The effective penetration depths of the irradiance into the coating range from 0.756 pairs (1.51 layers) to 6.65 pairs (13.3 layers) in the examples in (8.13) below. The total phase change ϕ_r is equal to the phase change of a single pair of layers times the number of pairs of layers in the penetration depth. Since the number of layers in the penetration depth is smaller, sometimes by a great factor, than the total number of layers in the coating, while the expansion of all layers in the coating and of the substrate contributes to the phase change ϕ_s resulting from the change in the position of the coating surface, ϕ_r tends to be negligible with respect to ϕ_s . However, the contribution of ϕ_r can be non-negligible in the case of $\alpha_F \ll n_F^{-1} dn_F/dT$ in a coating used with an intermediate thermal layer or a coating that is rather thick thermally. Notice that both α and dn/dT contribute to the change ϕ_r , while only α contributes to ϕ_s . The contribution to ϕ_r from the substrate is negligible in all normal cases.

Consider a reflector consisting of a set of $2N - 1$ quarter-wave layers, OHLHL -----HS, with refractive indices n_H and n_L , as shown in Fig. 3(a). In order to determine the reflection coefficient r of this system, first consider the model reflector $H \frac{H}{2} \text{LHL} \text{-----} \text{HL} \frac{H}{2} H$, consisting of N units $\frac{H}{2} L \frac{H}{2}$, as in Fig. 3(b).

The symmetry of the model structure makes the calculation of the reflectance rather simple, as shown by Herpin⁴⁶ and reviewed by Lissberger³⁴, who gives the following expression for the reflectance of the model reflector



(a)



one unit
(b)

Fig. 3. (a) Reflector of interest, and (b) a model reflector used in calculating the reflection coefficient of the reflector in (a).

Sec. B-VIII

$$r_m = \frac{r' [1 - \exp(i 2N \delta_E)]}{1 - r'^2 \exp(i 2N \delta_E)} \quad (8.1)$$

$$r' = \frac{Z_E - Z_S}{Z_E + Z_S} \rightarrow - \frac{Z_S - i Z_E''}{Z_S + i Z_E''} \cong i \exp \left[-i \frac{n_H + n_L}{n_H - n_L} \frac{\pi}{2} \frac{d_\Delta}{d_0} \right] \quad (8.2)$$

$$Z_S = 1/n_S = 1 \quad (8.3)$$

$$\begin{aligned} Z_E \rightarrow i Z_E'' &= i Z_A \left[\frac{1 + A \cos \delta}{1 - A \cos \delta} \right]^{1/2} \\ &\cong i \left(1 - \frac{n_H + n_L}{n_H - n_L} \frac{\pi}{2} \frac{d_\Delta}{d_0} \right) \end{aligned} \quad (8.4)$$

$$A = + \left(\frac{Y+1}{Y-1} \right)^{1/2} = \frac{n_H + n_L}{n_H - n_L} \quad (8.5)$$

$$Y = \frac{n_H^2 + n_L^2}{2 n_H n_L}$$

$$\delta = \delta_b = 2\delta_a = \frac{2\pi}{\lambda} n d = \frac{\pi}{2} \left(1 + \frac{d_\Delta}{d_0} \right) \quad (8.6)$$

$$d = d_0 + d_\Delta; \quad d_0 = \lambda/4n; \quad n_H d_H = n_L d_L \quad (8.7)$$

$$\cos \delta \cong - \frac{\pi}{2} \frac{d_\Delta}{d_0} \quad (8.8)$$

$$\delta_E = \pi + i \cosh^{-1} [Y - (Y+1) \cos \delta] \cong \pi + i \cosh^{-1} Y - i A \left(\frac{\pi}{2} \frac{d_\Delta}{d_0} \right)^2.$$

Sec. B-VIII

The arrows denote that the expressions are valid in the region of high reflectance.

For $1 - R \ll 1$ it is easy to show that the two terms in (8.1) containing the factor $\exp(i 2N\delta_E)$ are negligible. (Notice that $\cosh^{-1} Y = \ln[Y + (Y^2 - 1)^{1/2}] = \ln(n_H/n_L)$ and $\exp(-2N\delta_E) = (n_L/n_H)^{2N} \ll 1$.) Thus (8.1) gives

$$r_m \cong r' \cong i \exp\left(i \frac{n_H + n_L}{n_H - n_L} \frac{\pi}{2} \frac{d\Delta}{d_0}\right) \quad (8.9)$$

For the Lissberger convention $E \sim \exp(-i\omega t)$, the exponential factor in (8.10) corresponds to a retardation of the reflected field. Adding an $H/2$ (eight-wave) layer to the model reflector in Fig. 3(b) gives the reflector in Fig. 3(a). Adding this layer retards the phase by an additional $(\pi/2)(1 \pm d\Delta/d_0)$; that is

$$r \cong \exp\left(i \frac{\pi}{2} + i \frac{\pi}{2} \frac{d\Delta}{d_0}\right) r'$$

which gives

$$r \cong -e^{i\phi_r}$$

where

$$\phi_r = \pi \frac{d\Delta}{d_0} \frac{n_0}{n_H - n_L} \quad (8.10)$$

is the phase of the reflected wave.

Sec. B-VIII

The corresponding phase change for the change in position of the front surface when the rear (substrate) surface of the coating is held fixed as the coating expands is (for $2N + 1$ layers)

$$\phi_{Fs} = - (2N + 1) \pi \Delta / d_0 \quad (8.11)$$

Two contributions ϕ_r and ϕ_{Fs} to the total phase change have opposite signs, as suggested by the schematic illustration in Fig. 4. Thus, the two contributions tend to cancel, which reduces the severity of the optical distortion. However, it is possible that $|\phi_r| - |\phi_s| > |\phi_s|$, where $\phi_s = \phi_{Fs}$ plus the contribution from the substrate expression, so that including ϕ_r would result in greater optical distortion. This is unlikely in currently envisioned high-power reflectors for repeated-pulse use.

The phase change ϕ_{Fs} normally has the same magnitude as the phase change of a ray traveling from the front to the rear surface and return. Thus, an effective ray-penetration depth $\ell_{pen\phi}$ for the phase change ϕ_r can be defined as

$$\frac{\ell_{pen\phi}}{(2N + 1) \langle d \rangle} \equiv \frac{\phi_r}{\phi_{Fs}} \quad (8.12)$$

where $(2N + 1) \langle d \rangle$ is the thickness of the coating.

With (8.10) and (8.11), this expression (8.12) gives

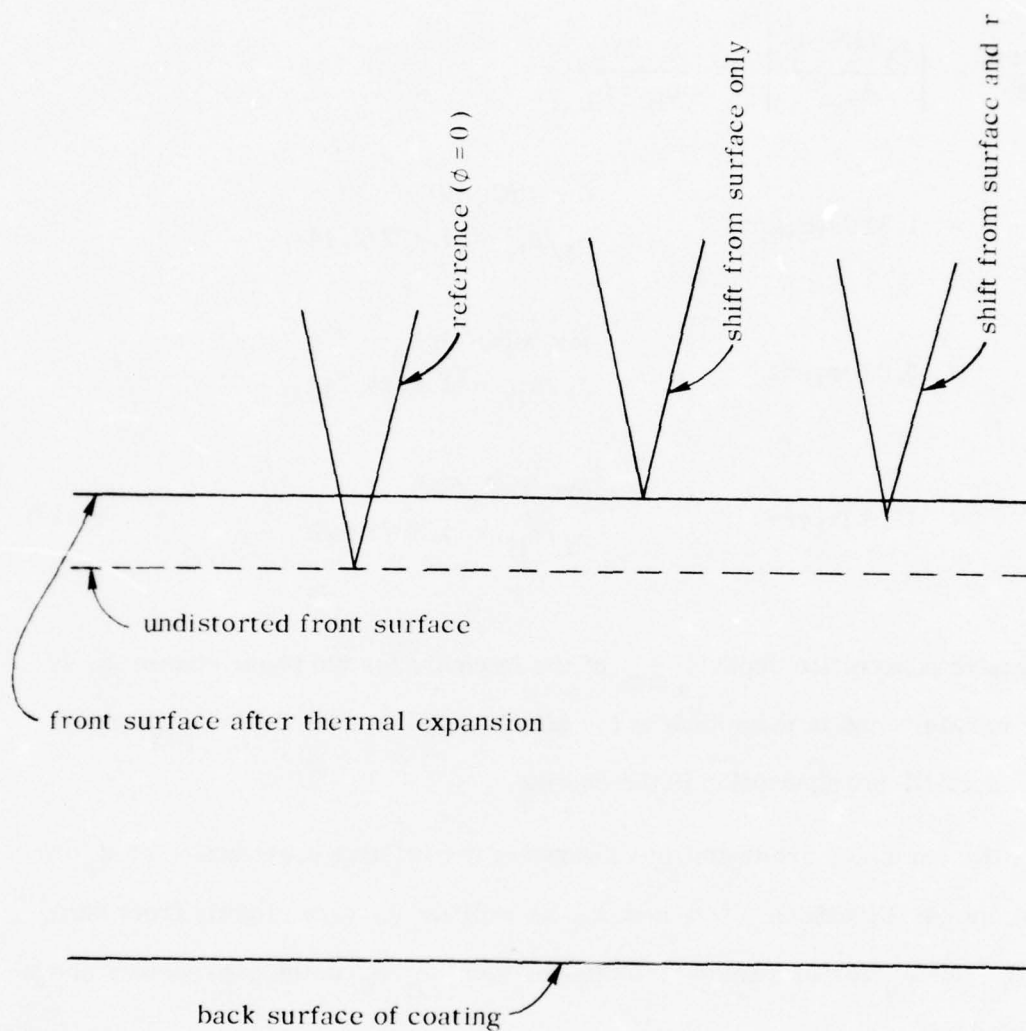


Fig. 4. Schematic illustration showing the advance in phase of the reflected wave resulting from the change in position of the surface of the coating, and the retardation resulting from the phase ϕ_r of the reflector coefficient r (resulting from deeper penetration into the thermally expanded coating).

Sec. B-VIII

$$\begin{aligned}
 \frac{\ell_{\text{pen}\phi}}{\langle d \rangle} &= \left| \frac{\phi_r (2N+1)}{\phi_{Fs}} \right| = \frac{n_0}{n_H - n_L} \\
 &= 1.51 \text{ layers} && \text{for HfO}_2/\text{SiO}_2 \\
 & && n_L/n_H = 1.477/2.14 \\
 &= 3.03 \text{ layers} && \text{for MgO/MgF}_2 \\
 & && n_L/n_H = 1.41/1.74 \\
 &= 13.3 \text{ layers} && \text{for ThF}_4/\text{SiO}_2 \\
 & && n_L/n_H = 1.50/1.575 \quad (8.13)
 \end{aligned}$$

The effective penetration depth $\ell_{\text{pen}\phi}$ of the intensity for the phase change ϕ_r is similar in nature and in magnitude to the effective penetration depth ℓ_{pen} introduced in Sec. III for absorption in the coating.

Specific examples are useful in illustrating the relative contribution of ϕ_r to the total optical distortion. If n and λ , as well as d , vary slightly from their values n_0 and λ_0 for maximum reflectance, then d_{Δ}/d_0 in the expressions above is replaced by

$$\frac{d_{\Delta}}{d_0} \rightarrow \frac{d_{\Delta}}{d_0} + \frac{n_{\Delta}}{n_0} - \frac{\lambda_{\Delta}}{\lambda_0} \quad (8.14)$$

In the present case, $\lambda_{\Delta} = 0$.

It will now be shown that the contribution of ϕ_r to the optical distortion of the 45-layer MgO/MgF_2 :Mo reflector is negligible with respect to the uncertainties

Sec. B-VIII

in the theoretical and experimental results. From (8.10), (8.13), and (8.14), with $d_{\Delta}/d_0 = \alpha(1+\nu)T$ and $n_{\Delta}/n_0 \equiv n_{\Delta}/n = n^{-1}(dn/dT)T$,

$$\phi_r = -3.03 \pi [\alpha(1+\nu) + n^{-1} dn/dT] T \quad (8.15)$$

With $n^{-1} dn/dT = 1.5 \times 10^{-6}$ for MgF_2 and $n^{-1} dn/dT = 15 \times 10^{-6}$ for MgO (approximate values obtained by extrapolation to 250 nm), the average value of $n^{-1} dn/dT$ for the film is

$$\begin{aligned} (n^{-1} dn/dT)_F &= \frac{15 \times 10^{-6}(1.41) + 1.5 \times 10^{-6}(1.74)}{1.41 + 1.74} \\ &= 7.54 \times 10^{-6} K^{-1} . \end{aligned}$$

Since the top layers of the coating make the greatest contribution to ϕ_r , the appropriate value of T in (8.15) is an average over the surface layers. With surface temperature $T_{Fr0} = 47.9 K$ from Table II, and for $h = 10 W/cm^2 K$,

$$\begin{aligned} T &= \frac{1}{2} \left[1 + \frac{45 - 4.77}{45} \right] T_{Fr0} = (0.947)(47.9) \\ &= 45.4 K . \end{aligned}$$

With (8.15) and $\alpha_F(1+\nu_F) = 15.6 \times 10^{-6} K^{-1}$ from Table I, this gives

$$\phi_r = -1.59 \times 10^{-3} (2\pi) ,$$

or

Sec. B-VIII

$$\frac{\phi_r}{(2\pi/G)} = \frac{\phi_r}{(2\pi/35)} = -5.57 \times 10^{-2}.$$

The contribution of ϕ_r to the optical distortion is

$$(It_p)_{\phi_r} = - \frac{10 \text{ J/cm}^2}{5.57 \times 10^{-2}} = -180 \text{ J/cm}^2 \quad (8.16)$$

The minus sign is a reminder that the phase ϕ_r has the opposite sign from the phase of ϕ_s . The previous value of $(It_p)_{\text{op}} = 21.4 \text{ J/cm}^2$ is replaced by the following value as a result of the ϕ_r correction

$$\frac{1}{(It_p)_{\text{op}}} = \frac{1}{21.4} - \frac{1}{180} = \frac{1}{24.3}$$

or

$$(It_p)_{\text{op}} = 24.3 \text{ J/cm}^2 \quad (8.17)$$

and the previous value of $(It_p)_{\text{or}} = 6.33 \text{ J/cm}^2$ for $h = 10 \text{ W/cm}^2 \text{ K}$ is corrected to

$$\frac{1}{(It_p)_{\text{or}}} = \frac{1}{6.33} - \frac{1}{180} = \frac{1}{6.56}$$

or

$$(It_p)_{\text{or}} = 6.56 \text{ J/cm}^2 \quad (8.18)$$

which is 3.7 percent greater than the uncorrected value.

Next it will be shown that for the 21-layer $\text{HfO}_2/\text{SiO}_2$ coating with the assumed ultralow expansion of HfO_2 , the single-pulse threshold is considerably greater when ϕ_r is included, but the repeated-pulse value is only 17 percent greater even for the state-of-the-art values of the surface heat-transfer coefficient $h = 10 \text{ W/cm}^2 \text{ K}$ and face-plate thickness $\ell_S = 0.5 \text{ mm}$. From (8.10), (8.13), and (8.14),

$$\begin{aligned}\phi_r &= -1.51 \pi [0.585 \times 10^{-6} + 9.55 \times 10^{-6}] 319 \\ &= -2.44 \times 10^{-3} (2\pi)\end{aligned}$$

or

$$\frac{\phi_r}{(2\pi/35)} = 8.52 \times 10^{-2}$$

The value of $(It)_{p\phi_r}$ is

$$(It)_{p\phi_r} = - \frac{10 \text{ J/cm}^2}{8.52 \times 10^{-2}} = -117 \text{ J/cm}^2 \quad (8.19)$$

The corrected value of $(It)_{p_{op}}$ is

$$(It)_{p_{op}} = | 77.5^{-1} - 117^{-1} |^{-1} = 228 \text{ J/cm}^2 \quad (8.20)$$

The accuracy of this value of 228 J/cm^2 is low since the approximate expression for ϕ_r was used and there is near cancellation of the two terms in (8.20). The corrected value of $(It)_{p_{or}}$ for $h = 10 \text{ W/cm}^2 \text{ K}$ and $\ell_S = 0.5 \text{ mm}$ is

Sec. B-VIII

$$(It_p)_{\text{or}} = \left[\frac{1}{11.0} - \frac{1}{117} \right]^{-1} = 12.1 \text{ J/cm}^2 ,$$

which differs by 10 percent from the uncorrected value of 11.0 J/cm^2 .

Next consider the thermally induced change in the reflectance $R = |r|^2$. For a coating designed for maximum reflectance at a specific wavelength λ_0 , the reflectance normally decreases as $|\lambda - \lambda_0|$ increases. The value of λ_0 usually is chosen as the operating wavelength λ . However, as the temperature of the coating increases, the value of λ_0 changes, thus reducing the value of $R(\lambda_L)$.

The measured reflectance change of the Baumeister-Arnon coating⁹ is approximated by

$$R_{\Delta} \equiv R(\lambda_0) - R(\lambda_0 - \lambda_{\Delta}) = 1.64 (\lambda_{\Delta}/\lambda_0)^2 , \quad (8.21)$$

which is a parabolic fit to the maximum and the point $R_{\Delta} = 1.60 \times 10^{-3}$ at $\lambda_{\Delta} = 10 \text{ nm}$.

The value of $\lambda_{\Delta}/\lambda_0$ corresponding to a temperature change T_{Δ} can be estimated as follows. The change in the optical thickness $n\ell$ of a layer is, neglecting the stress optic terms,

$$\Delta(n\ell) = \ell \frac{dn}{dT} T_{\Delta} + n\ell \alpha T_{\Delta} .$$

Both dn/dT and $n\alpha$ are of order 10^{-5} K^{-1} , typically. Thus, $\Delta(n\ell)/n\ell \approx \alpha \Delta T$ is of the order 10^{-3} for $T_{\Delta} = 100 \text{ K}$. With $\lambda_{\Delta}/\lambda_0 \approx \Delta(n\ell)/n\ell \approx 10^{-3}$, (8.21) gives

$$R_{\Delta} = 1.64 \times 10^{-6} ,$$

Sec. B-VIII

which is negligibly small (compare $A = 5 \times 10^{-3}$) even for the large value of $\Delta T = 100$ K. It is also easy to show from (8.9) that R_{Δ} is negligible.

It should be mentioned that sufficient temperature increases could cause such effects as interlayer or coating-substrate mass diffusion³¹ and changes in the porosity of the coating, which could change $R(\lambda)$, probably irreversibly. The absorptance of the coating materials themselves increases in general as the temperature increases, but this increase usually cannot be estimated since the source of the absorptance in the ultraviolet and visible regions usually is not known. In well designed, ultralow-absorptance ultraviolet and visible reflectors, the temperature dependence of the absorptance of the substrate does not affect the absorptance of the reflector because the coating must contain a sufficient number of layers to make the absorption in the substrate negligible. An exception would be a coating in which the number of layers is restricted by technical considerations.

IX. APPLICATIONS

Two coatings, one for use at 354 nm and one for use at 250 nm, and six substrates are considered. In addition, some results are given for a $\text{ThF}_4/\text{SiO}_2$ coating on molybdenum. It was shown in Sec. III that it should not be difficult in practice to make the thermally induced single-pulse optical distortion negligible by using a near-zero thermal expansion intermediate layer containing ThF_4 (which has negative thermal expansion at room temperature). The optical distortion is then determined by the long-time average temperature of the substrate, the values of $(It)_{\text{p or}}$ being 19.9 J/cm^2 for molybdenum and 99.3 J/cm^2 for invar.

The following results are for reflectors not employing the intermediate layer. The values of the temperatures, optical-distortion-limited and fracture-limited energy densities for single-pulse and repeated-pulse operation, and the cooling (values of h) required to prevent excessive optical distortion and fracture are listed in Table II of Sec. I. Three values of cooling $h = 1, 10$ and $\infty \text{ W/cm}^2 \text{ K}$ are included for the repeated-pulse case. The results to follow are summarized in Sec. B-I.

For the 45-layer MgO/MgF_2 coating developed by the Northrop Corporation for use at 250 nm, the values of the parameters n_F , K , C , and α for bulk crystals, listed in Table I, will be used since MgF_2 and MgO are believed to deposit as crystalline films.¹⁴ The film thickness, from (4.1), is $\ell_F = 1.81 \mu\text{m}$, and the thermal diffusion distance in the coating during the pulse, from (4.2), is $\ell_{Ftp} = 6.02 \mu\text{m}$. Thus the thin-film approximation $\ell_F = 1.81 \mu\text{m} \ll \ell_{Ftp} = 6.02 \mu\text{m}$ is not well satisfied, and the corrections of Sec. IV are needed.

Sec. B-IX

MgO/MgF₂:Mo. For a single pulse, the optical-distortion threshold for the MgO/MgF₂ coating on molybdenum is, from (5.13)

$$(It_{p_{op}}) = 21.4 \text{ J/cm}^2 \quad (9.1)$$

which is between the thermally-thick-coating value of 14.0 J/cm^2 and the uncoated-metallic-reflector value of 28.7 J/cm^2 , as it must be. Several repeated-pulse optical-distortion thresholds, from (5.15), are

$$\begin{aligned} (It_{p_{or}}) &= 14.7 \text{ J/cm}^2, & \text{for } h = \infty \\ &= 10.0 \text{ J/cm}^2, & \text{for } h = 28.1 \text{ W/cm}^2 \text{ K} \\ &= 6.33 \text{ J/cm}^2, & \text{for } h = 10 \text{ W/cm}^2 \text{ K} \\ &= 1.03 \text{ J/cm}^2, & \text{for } h = 1 \text{ W/cm}^2 \text{ K} \end{aligned} \quad (9.2)$$

The value for $h = \infty$ lies between 10.7 J/cm^2 (thick, from (4.11)) and 17.7 J/cm^2 (uncoated, from (2.14)).

The value of $h = 28.1 \text{ W/cm}^2 \text{ K}$ required to prevent excessive optical distortion ($It_p = 10 \text{ J/cm}^2$) is between the values $20.9 \text{ W/cm}^2 \text{ K}$ (uncoated, (2.17)) and $134 \text{ J/cm}^2 \text{ K}$ (thick, (4.13)). As discussed in Sec. VI, this extremely large value of $\sim 30 \text{ W/cm}^2 \text{ K}$ is well beyond the state of the art ($\sim 10 \text{ W/cm}^2 \text{ K}$) for mirrors.

For single pulses, the fracture threshold, from (5.18),

$$(It_{p_{fp}}) = 17.2 \text{ J/cm}^2 \quad (9.3)$$

is less than the optical distortion threshold, but the accuracy of estimate of $(It_{p_{fp}})$ is not sufficiently great to afford confidence in this conclusion. Also recall that a safety factor of four in the strength was used in obtaining (9.3).

Sec. B-IX

For repeated-pulse operation with perfect cooling, the fracture-threshold value of It_p from (5.19) is

$$[(It_p)_{fr}]_{h=\infty} = 17.2 \text{ J/cm}^2, \quad (9.4)$$

which is essentially equal to the optical-distortion value of 14.7 J/cm^2 from (9.2) to within the accuracy of the estimate of the fracture value. The value of h required to prevent fracture, from (5.21)

$$h = 0.0918 \text{ W/cm}^2 \text{ K} \quad (9.5)$$

is much less than the value $h = 28.1 \text{ W/cm}^2 \text{ K}$ for optical distortion from (9.4). The reason is that the temperature increase, above the single-pulse temperature, for repeated-pulse operation is not confined to a small region near the coating surface. The optical distortion from the small temperature rise is great because l_S is great with respect to the thermal diffusion distances in time $t_p = 10^{-6} \text{ s}$, but the additional stress is small because the temperature increase is small.

The values of the temperature rise at the surface of the coating are reasonable: for a single pulse,

$$T_{Fp0} = 47.2 \text{ K}; \quad (9.6)$$

for repeated-pulse operation with $h = \infty$,

$$[T_{Fr0}]_{h=\infty} = 47.4 \text{ K}; \quad (9.7)$$

and for repeated-pulse operation with $h = 28.1 \text{ W/cm}^2 \text{ K}$ by (9.3), the value of T from (5.2) is

Sec. B-IX

$$T_{Fr0} = 47.6 \text{ K} . \quad (9.8)$$

For the fracture thresholds in (9.5) and (9.6), the failure is by compression in MgO with the residual stress σ_{res} formally set equal to zero since its value is not known. Both MgO and MgF_2 are in compression, and the thermal stresses are approximately equal. Since MgF_2 films are believed to have large tensile residual stresses,¹⁴ the failure was assumed to occur in an MgO layer.

MgO/MgF₂:Cu. The MgO/MgF₂ coating on a copper substrate will not meet the system requirement $(It)_{por} > 10 \text{ J/cm}^2$ since

$$(It)_{por} = 8.80 \text{ J/cm}^2 , \quad \text{for } h = \infty . \quad (9.9)$$

The single-pulse threshold

$$(It)_{pop} = 11.5 \text{ J/cm}^2$$

is sufficiently great, as is the fracture threshold

$$(It)_{pfp} \cong (It)_{pf} = 20.8 \text{ J/cm}^2 .$$

The corresponding thresholds are even lower for silver and aluminum substrates.

Next consider the 21-layer HfO₂/SiO₂ coating developed by Baumeister and Arnon⁹ for use at 320 nm. In the analysis of this coating, it is assumed that the same materials and number of layers are used in a coating designed for 354 nm. Unfortunately the properties of the coating materials are not sufficiently well known to allow even reliable predictions about catastrophic failure to be made. Since the damage resistance of this coating is great, if the assumed properties are correct, experimental studies to determine the coating properties are important.

Sec. B-IX

The thickness can be calculated with sufficient accuracy since the values of the refractive indices should not be greatly in error. From (4.1)

$$\ell_F = (21/2)(3.54 \times 10^{-5}/4)(2.14^{-1} + 1.48^{-1}) = 1.06 \mu\text{m} . \quad (9.10)$$

Only a very rough estimate of the value of the thermal diffusion distance can be made since the properties of the deposited materials are not known. Oxide films tend to deposit in an almost amorphous form,¹⁴ for which the values of α and K could differ from those of the crystals by factors of ~ 10 . Thus, the best estimate seems to be to use typical values of $K = 0.014 \text{ W/cm}^2 \text{ K}$ and $\alpha = 0.5 \times 10^{-6} \text{ K}^{-1}$ for amorphous oxides, assuming that the HfO_2 films are essentially amorphous, which gives

$$\ell_{Ftp} = (4K_F t_p / C_F)^{1/2} \cong (4(0.014) 10^{-6} / 1.7)^{1/2} = 1.81 \mu\text{m} . \quad (9.11)$$

Thus, the approximation $\ell_F = 1.06 \mu\text{m} \ll \ell_{Ftp} = 1.81 \mu\text{m}$ is not well satisfied, and again the results of Sec. V, rather than the extreme limit of thermally thin coatings, must be used.

$\text{HfO}_2/\text{SiO}_2:\text{Mo}$. From (5.5), (5.6), and (5.8)

$$T_{Fp0} = T_{\Delta Fp0} + T_{FSp} = 324 \text{ K} + 17 \text{ K} = 341 \text{ K} . \quad (9.12)$$

This rather large temperature of 341 K results chiefly from the temperature differential of 324 K across the coating, which is a result of the low thermal conductivity $K_F = 0.014 \text{ W/cm}^2 \text{ K}$. If the HfO_2 coating had a value of K much greater than that of SiO_2 , then (A.6) gives

Sec. B-IX

$$K_F \approx K_{\text{SiO}_2} (n_{\text{SiO}_2} + n_{\text{HfO}_2}) / n_{\text{HfO}_2}$$

$$\approx 1.69 K_{\text{SiO}_2}$$

and the value of $T_{\Delta Fp0}$ would be decreased to $T_{Fp0} \cong 324/1.69 = 192$ K. The value of 341 K in (9.12) is between the uncoated-metallic-reflector value of 29.5 K and the thermally-thick-substrate value of 366 K from (4.3).

The single-pulse optical distortion threshold from (5.13) is

$$(It_p)_{op} = 77.5 \text{ J/cm}^2 \quad (9.13)$$

and the repeated-pulse values are:

$$\begin{aligned} (It_p)_{or} &= 35.8 \text{ J/cm}^2, & \text{for } h = \infty, \\ &= 11.0 \text{ J/cm}^2, & \text{for } h = 10 \text{ W/cm}^2 \text{ K}, \\ &= 10.1 \text{ J/cm}^2, & \text{for } h = 8.78 \text{ W/cm}^2 \text{ K}, \\ &= 1.51 \text{ J/cm}^2, & \text{for } h = 1 \text{ W/cm}^2 \text{ K}. \end{aligned} \quad (9.14)$$

The single-pulse fracture threshold from (5.18) is

$$(It_p)_{fp} = 92.0 \text{ J/cm}^2 \quad (9.15)$$

and the repeated-pulse value for $h = \infty$ is, from (5.19)

$$(It_p)_{pfr} \xrightarrow{h = \infty} 92.2 \text{ J/cm}^2. \quad (9.16)$$

Sec. B-IX

The difference between these two values of 92.0 J/cm^2 and 92.2 J/cm^2 is insignificant, but the fact that the repeated-pulse value is greater than the single-pulse value illustrates an interesting point. The coating is in compression, as always, for a single pulse. But the additional temperature rise resulting from repeated-pulse operation gives rise to tensile stresses in the film, which partially cancel the single-pulse compressive stresses. The additional stresses are tensile in both layers of the coating in the present case because the thermal expansion coefficients of the coating layers ($0.5 \times 10^{-6} \text{ K}^{-1}$) are sufficiently smaller than the thermal expansion coefficient of the substrate ($5 \times 10^{-6} \text{ K}^{-1}$). The substrate consequently expands more (radially) than does the coating, thus putting the coating in tension.

This result, that the coating will not fracture under repeated-pulse operation if it does not fracture under single-pulse operation (within limits discussed below) is reflected mathematically by the fact that h_f from (5.20) is negative, and (5.21) gives a negative value of h required to prevent fracture. If the cooling is sufficiently small, the temperature of the substrate eventually becomes so great that the tensile stress becomes greater than the compressive stress by an amount sufficient to cause failure of a coating layer in tension. Then the value of $''(It_p)''$ in the two equations (5.21) and (5.22)

$$h = h_f \left[\frac{''(It_p)''}{It_p} - 1 - \epsilon \right]^{-1}$$

and

$$(It_p)_{fr} = ''(It_p)'' (1 + \epsilon + h_f/h)^{-1}$$

Sec. B-IX

becomes negative as a result of the sign change of σ_F in (5.18) (with σ_{res} still zero). Then h becomes positive, and $(It)_{pfr}$ remains positive.

The ThF_4/SiO_2 coating was discussed in Sec. III.

X. TABULATION OF DERIVED RESULTS

The results derived herein and the values of the system parameters used are tabulated for the convenience of the reader. Subscripts F, S, and C denote coating (film), substrate, and coolant.

(a) Model-System Parameters

- wavelength: $\lambda = 354 \text{ nm}$ (3.50 eV); alternate: 250 nm (4.96 eV)
- laser pulse duration: $t_p = 1 \mu\text{s}$
- repetition rate: 100 Hz (100 pps), with possible increase to 10^3 pps
- total operating time: 60 s
- energy density: $It_p = 10 \text{ J/cm}^2/\text{pulse}$
- irradiance (during the pulse): $I = 10^7 \text{ W/cm}^2$
- irradiance (averaged over the 60 seconds): $I_{av} = 10^3 \text{ W/cm}^2$
- area of window or mirror: up to 300 cm^2 ($15 \times 20 \text{ cm}$)
- energy: $E = 10^3 \text{ J/pulse}$
- optical tolerance: 1/40 wavelength per element
- pressure: two atmospheres nominal; four atmospheres during the pulse
- pulse shape: rectangular with no spikes

(b) Material-Component Parameters

- substrate thickness

$$\ell_S = 0.1 \text{ cm}$$
- substrate radius

$$R = 2.5\text{-}10 \text{ cm}$$

Sec. B-X

- coating thickness for N-layer coating

$$\ell_F = (N/2)(\lambda/4)(n_1^{-1} + n_2^{-1}) = [1.81 \mu\text{m}] \quad (4.1)$$

- absorptance

$$A = 5 \times 10^{-3}$$

- optical path difference between center and rim of reflector

$$\ell_{\text{opd}} = 2 \left[\Delta \ell_S - (\Delta \ell_S)_{\rho=R} \right]$$

$$\Delta \ell_S \equiv (\Delta \ell_S)_{\rho=0}$$

- beam profile: square in time, with duration $t_p = 10^{-6} \text{ s}$,
interpulse time $t_{ip} = 10^{-2} \text{ s}$

$$I(\rho) = I \exp(-a\rho^2)$$

$$aR^2 = 1/c^2$$

- optical tolerance

$$\Delta \ell_S = \lambda/2G = \lambda/70; (\ell_{\text{opd}} = \lambda/g = \lambda/40)$$

$$2G = 2g \left(1 - e^{-aR^2} \right) = 1.73g \cong 70$$

- effective values for coating of heat capacity per unit volume, thermal conductivity (along z) and thermal expansion coefficient (along z) for thickness $\ell_1 \sim 1/n_1$ and $\ell_2 \sim 1/n_2$

$$C_F = \frac{C_1 n_2 + C_2 n_1}{n_1 + n_2} = [3.14 \text{ J/cm}^3 \text{ K}] \quad (A.5)$$

$$K_F = \frac{K_1 K_2 (n_1 + n_2)}{K_1 n_1 + K_2 n_2} = [0.285 \text{ W/cm K}] \quad (A.6)$$

$$\alpha_F(1 + \nu_F) = \frac{\alpha_1(1 + \nu_1)n_2 + \alpha_2(1 + \nu_2)n_1}{n_1 + n_2}$$

$$= [15.9 \times 10^{-6} \text{ K}^{-1}] \quad (\text{A.7})$$

- time-averaged heat flow through the substrate

$$J = I A t_p / t_{ip} = 5 \text{ W/cm}^2 \quad (2.3)$$

- thermal-diffusion time through coating (along z)

$$\tau_F = C_F \ell_F^2 / 4 K_F = [9.02 \times 10^{-8} \text{ s}] \quad (5.1)$$

- thermal-diffusion distance in the coating during t_p

$$\ell_{Ftp} = (4 K_F t_p / C_F)^{1/2} = (K_F / C_F)^{1/2} 20.0 \mu\text{m}$$

$$= (K_F / C_F)^{1/2} 20.0 \mu\text{m} = [6.02 \mu\text{m}] \quad (4.2)$$

- average temperature across substrate thickness at $\rho = 0$

$$\langle T_S \rangle_z = \ell_S^{-1} \int_0^{\ell_S} dz T_S$$

- radial-average temperature

$$\langle T \rangle_\rho = \frac{2}{R^2} \int_0^R d\rho \rho T = T_0 \frac{1}{aR^2} \left(1 - e^{-aR^2} \right) \quad (2.16)$$

$$= 0.432 T_0, \text{ for } 1/e^2 \text{ truncation } (aR^2 = 2)$$

$$r_\rho \equiv \frac{\langle T \rangle_\rho}{T_0} = 0.432$$

(c) Uncoated Metallic Reflectors

- temperature at the surface ($\rho = z = 0$) at the end of a pulse

$$\begin{aligned} T_0 &= T_{p0} + \delta_r (T_{SC} + T_{\Delta Sr0}) \\ &= [29.5 \text{ K} + \delta_r (5/h + 0.179 \text{ K})] \end{aligned} \quad (2.7)$$

$$\begin{aligned} T_{p0} &= 2 I t_p A (1/\pi t_p C_S K_S)^{1/2} \\ &= 56.4 (C_S K_S)^{-1/2} = [29.5 \text{ K}] \end{aligned} \quad (2.1)$$

$$T_{r0} = \xrightarrow{h \rightarrow \infty} T_{p0} + T_{\Delta Sr0} = [29.7 \text{ K}] \quad (2.8)$$

$$T_{SC} = I t_p A / t_{ip} h = 5/h \quad (2.4)$$

$$\begin{aligned} T_{\Delta Sr0} &= (I t_p A / t_{ip} K_S) (1 - \ell_{tip} / 2 \ell_S) \quad , \quad \text{for } \ell_{tip} < \ell_S \\ &= I t_p A \ell_S / 2 t_{ip} K_S = (4 K_S)^{-1} = [0.179] \quad , \quad \text{for } \ell_{tip} > \ell_S \end{aligned} \quad (2.5)$$

- single-pulse optical-distortion limit to the energy density

$$(I t_p)_{op} = C_S (\lambda / 2 G) / A \alpha_S (1 + \nu_S) \quad (2.18)$$

$$= 7.14 \times 10^{-5} C_S / \alpha_S (1 + \nu_S) = [29.2 \text{ J/cm}^2] \quad , \quad \text{for } 250 \text{ nm}$$

$$= 1.01 \times 10^{-4} C_S / \alpha_S (1 + \nu_S) = [41.3 \text{ J/cm}^2] \quad , \quad \text{for } 354 \text{ nm}$$

- repeated-pulse optical-distortion limit to the energy density (per pulse)

$$(I t_p)_{or} = \frac{(I t_p)_{op}}{1 + h_o \left(\frac{1}{h} + \frac{a \ell_S}{3 K_S} \right)} \quad (2.21)$$

$$\xrightarrow{h \rightarrow \infty} \frac{(I t_p)_{op}}{1 + C_S \ell_S^2 / 3 t_{ip} K_S} = \frac{(I t_p)_{op}}{1 + a C_S / 3 K_S} = [18.0 \text{ J/cm}^2]$$

Sec. B-X

$$\begin{aligned} h_o &= C_S \ell_S / t_{ip} \\ &= 10.0 C_S = [26.1 \text{ W/cm K}] \end{aligned} \quad (2.22)$$

- required cooling (value of surface heat-transfer coefficient h) to prevent excessive ($\ell_{opd} > \lambda/40$) optical distortion during continuous repeated-pulse operation

$$\begin{aligned} h &= h_o \left[\frac{(It_p)_{od}}{It_p} - 1 - \frac{ah_o \ell_S}{3 K_S} \right]^{-1} \\ &= [20.2 \text{ W/cm}^2 \text{ K}] \end{aligned} \quad (2.24)$$

(d) Thermally Thick Dielectric Reflectors

- temperature of the surface of the coating ($\rho = z = 0$), with T_{SC} and $T_{\Delta Sr}$ given by (2.4) and (2.6) in (c) above

$$\begin{aligned} T_{F0} &= T_{Fp0} + \delta_r (T_{SC} + T_{\Delta Sr0}) \\ &= [59.6 \text{ K} + \delta_r (5/h + 0.179 \text{ K})] \end{aligned} \quad (4.6)$$

$$T_{F0} \xrightarrow{h \rightarrow \infty} T_{Fp0} + T_{\Delta Sr0} = [59.8 \text{ K}]$$

- temperature at the surface of the coating ($\rho = z = 0$) at the end of a single pulse

$$\begin{aligned} T_{Fp0} &= 2 It_p A (1/\pi t_p C_F K_F)^{1/2} \\ &= 56.4 (C_F K_F)^{-1/2} = [59.6 \text{ K}] \end{aligned} \quad (4.5)$$

- single-pulse optical-distortion limit to the energy density

$$(It_p)_{op} = C_F (\lambda / 2 G) / A \alpha_F (1 + \nu_F) \quad (4.7)$$

$$= 7.14 \times 10^{-5} C_F / \alpha_F (1 + \nu_F) = [14.0 \text{ J/cm}^2] , \quad \text{for 250 nm}$$

$$= 1.01 \times 10^{-4} C_F / \alpha_F (1 + \nu_F) = [19.8 \text{ J/cm}^2] , \quad \text{for 354 nm}$$

- repeated-pulse optical-distortion limit to the energy density (per pulse)

$$(It_p)_{or} = \frac{(It_p)_{op}}{1 + h_o \left(\frac{1}{h} + \frac{a \ell_S}{3 K_S} \right)} \quad (4.11)$$

$$(It_p)_{or} \xrightarrow{h \rightarrow \infty} [10.7 \text{ J/cm}^2] \quad (4.12)$$

where

$$h_o = \frac{\ell_S \alpha_S (1 + \nu_S) A (It_p)_{op}}{t_{ip} (\lambda / 2 G)} = \frac{C_F \ell_S \alpha_S (1 + \nu_S)}{t_{ip} \alpha_F (1 + \nu_F)}$$

$$= 10 C_F \frac{\alpha_S (1 + \nu_S)}{\alpha_F (1 + \nu_F)} = [12.8 \text{ W/cm}^2 \text{ K}]$$

- required cooling (value of surface heat-transfer coefficient h) to prevent excessive ($\ell_{opd} > \lambda/40$) optical distortion during continuous repeated-pulse operation

$$h = h_o \left[\frac{(It_p)_{op}}{It_p} - 1 - \frac{a h_o \ell_S}{3 K_S} \right]^{-1} = [134 \text{ W/cm}^2 \text{ K}] \quad (4.13)$$

Sec. B-X

- thermally induced stress in coating layer 1 (replace 1 by 2 for layer 2)
at $\rho = z = 0$

$$\sigma_1 = \sigma_{1 \text{ res}} - \frac{E_1}{1 - \nu_1} \left(\alpha_1 T_{F0} - \alpha_S B_S \langle T_S \rangle_z \right) \quad (4.14)$$

$$\begin{aligned} B_S &= \frac{1}{2} (1 + \nu_S) + \frac{1}{2} (1 - \nu_S) r_\rho \\ &= 0.716 + 0.284 \nu_S = [0.801] \end{aligned}$$

- single-pulse fracture limit to the energy density

$$\begin{aligned} (It_p)_{fp} &= - \left(\frac{\sigma_F}{f_s} - \sigma_{\text{res}} \right) \left(\frac{1 - \nu_i}{\alpha_i E_i} \right) \left(\frac{It_p}{T_{Fp0}} \right) \\ &= [12.4 \text{ J/cm}^2] \quad , \quad \text{for MgO, } f_s = 4 \quad (4.19) \end{aligned}$$

- repeated-pulse fracture limit to the energy density

$$\begin{aligned} (It_p)_{fp} &= "(It_p)_{fp} (1 + \epsilon + h_f/h)^{-1} \\ &\xrightarrow{h \rightarrow \infty} [12.4 \text{ J/cm}^2] \quad \text{for MgO, } f_s = 4 \quad (4.20) \end{aligned}$$

$$\begin{aligned} h_f &\equiv \frac{(T_{SC} h)}{T_{Fp0}} \left(1 - \frac{\alpha_S B_S}{\alpha_i} \right) \\ &= [5.19 \times 10^{-2} \text{ W/cm}^2 \text{ K}] \quad (4.21) \end{aligned}$$

$$\begin{aligned} \epsilon &\equiv \frac{T_{\Delta Sr}}{T_{Fp0}} \left(1 - \frac{\langle T_{\Delta Sr} \rangle_{\ell_S} \alpha_S}{T_{\Delta Sr0} \alpha_i} \right) \\ &= [2.24 \times 10^{-3}] \quad (4.22) \end{aligned}$$

Sec. B-X

- cooling required to prevent fracture (that is, to keep $I_{t_p} < (I_{t_p})_f$)

$$h = h_f \left[\frac{(I_{t_p})_f}{I_{t_p}} - 1 - e \right]^{-1} \quad (4.23)$$

$$= [0.216 \text{ W/cm}^2 \text{ K}]$$

(e) Extreme Thermally Thin Dielectric Reflectors

- The results for the case of $\ell_F \ll \ell_{Ftp}$ extremely well satisfied are the same as for uncoated metallic reflectors directly above, with $T_0 \cong T_{F0}$ in (2.7) and $T_{p0} \cong T_{Fp0}$ in (2.1). (The subscripts S are not to be replaced by F's.)

(f) Thermally Thin Dielectric Reflectors

- temperature at the surface of the coating ($\rho = z = 0$), with T_{SC} and $T_{\Delta Sr0}$ given by (2.4) and (2.5) in (c) above

$$T_{F0} = T_{\Delta Fp0} + T_{FSp} + \delta_r (T_{SC} + T_{\Delta Sr0}) \quad (5.2)$$

$$= [27.2 \text{ K} + 20.0 \text{ K} + \delta_r (5/h + 0.20 \text{ K})]$$

$$T_{Fp0} = T_{\Delta Fp0} + T_{FSp} = [47.2 \text{ K}]$$

$$T_{Fr0} \xrightarrow{h \rightarrow \infty} [47.4 \text{ K}]$$

- temperature difference across the coating ($T_{\Delta Fp} = 0$ at $z = \ell_F$) at the end of a single pulse for absorption at $z = \ell_F$ equal to 10^{-2} times the value of $z = 0$

$$T_{\Delta Fp} \cong \frac{IA \ell_F}{K_F} \left(1 - \frac{z}{\ell_F} - \frac{e^{-kz}}{6.91} \right) \quad (5.5)$$

Sec. B-X

$$T_{\Delta Fp0} \equiv (T_{\Delta Fp})_{z=0} = \frac{0.855 I A \ell_F}{K_F} \quad (5.6)$$

$$= 4.28 \times 10^4 \ell_F / K_F = [27.2 \text{ K}]$$

- temperature of the coating-substrate interface at the end of a single pulse

$$T_{FSp} = \frac{I A (t_p - 1.42 \tau_F)}{C_S \ell_{S\Delta} + C_F \ell_F} = [20.0 \text{ K}] \quad (5.8)$$

$$\ell_{S\Delta} \equiv \left[\pi (t_p - \tau_F) K_S / 4 C_S \right]^{1/2}$$

$$= 8.86 \times 10^{-4} \left[(1 - \tau_F / t_p) K_S / C_S \right]^{1/2} \quad (5.7)$$

$$= [6.19 \mu\text{m}]$$

- single-pulse optical-distortion limit to the energy density

$$(It_p)_{op} = (\lambda / 2 G) I t_p \left[\alpha_S (1 + \nu_S) \ell_{S\Delta} T_{FSp} \right. \\ \left. + \alpha_F (1 + \nu_F) \ell_F (0.415 T_{\Delta Fp0} + T_{FSp}) \right]^{-1} \quad (5.13)$$

$$= [21.4 \text{ J/cm}^2]$$

- repeated-pulse optical-distortion limit to the energy density (per pulse)

$$(It_p)_{or} = \frac{(It_p)_{op}}{1 + h_o \left(\frac{1}{h} + \frac{a \ell_S}{3 K_S} \right)}$$

$$\xrightarrow{h \rightarrow \infty} [14.7 \text{ J/cm}^2] \quad (5.15)$$

where

$$\begin{aligned}
 h_o &= \frac{\ell_S \alpha_S (1 + \nu_S) A (It_p)_{op}}{t_{ip} (\lambda / 2 G)} \\
 &= 1.40 \times 10^5 \alpha_S (1 + \nu_S) (It_p)_{op} \\
 &= [19.1 \text{ W/cm}^2 \text{ K}] \quad \text{for 250 nm} \\
 &= 9.89 \times 10^4 \alpha_S (1 + \nu_S) (It_p)_{op} \quad (5.17) \\
 &= [19.1 \text{ W/cm}^2 \text{ K}] \quad \text{for 354 nm}
 \end{aligned}$$

- required cooling (value of surface heat-transfer coefficient h) to prevent excessive ($\ell_{opd} > \lambda / 40$) optical distortion during continuous repeated-pulse operation

$$\begin{aligned}
 h &= h_o \left[\frac{(It_p)_{od}}{It_p} - 1 - \frac{h_o \ell_S}{3 K_S} \right]^{-1} \\
 &= [28.1 \text{ W/cm}^2 \text{ K}] \quad (5.16)
 \end{aligned}$$

- single-pulse fracture limit to the energy density

$$\begin{aligned}
 (It_p)_{fp} &= - \left(\frac{\sigma_F}{f_S} - \sigma_{res} \right) \left(\frac{1 - \nu_i}{\alpha_i E_i} \right) \left(\frac{It_p}{T_{Fp0}} \right) \\
 &= [17.2 \text{ J/cm}^2] \quad (5.18)
 \end{aligned}$$

- repeated-pulse fracture limit to the energy density

$$\begin{aligned}
 (It_p)_{fr} &= (It_p)_{fp} (1 + \epsilon + h_f/h)^{-1} \\
 &\xrightarrow{h \rightarrow \infty} (It_p)_{fp} (1 + \epsilon)^{-1} = [17.2 \text{ J/cm}^2] \quad (5.19)
 \end{aligned}$$

where

$$h_f = \frac{T_{SC} h}{T_{Fp0}} \left(1 - \frac{\alpha_S B_S}{\alpha_i} \right) \quad (5.20)$$

$$= [6.59 \times 10^{-2} \text{ W/cm}^2 \text{ K}]$$

and

$$\epsilon = \frac{T_{\Delta Sr}}{T_{Fp0}} \left(1 - \frac{\langle T_{\Delta Sr} \rangle_{\ell_S} \alpha_S}{T_{\Delta Sr0} \alpha_i} \right) = [2.83 \times 10^{-3}] \quad (5.22)$$

- cooling required to prevent fracture

$$h = h_f \left[\frac{(It_p)_{fp}}{It_p} - 1 - \epsilon \right]^{-1} \quad (5.21)$$

$$= [1.26 \times 10^{-2} \text{ W/cm}^2 \text{ K}]$$

- single-pulse melting limit to the energy density (valid for both thermally thin and thermally thick coatings)

$$(It_p)_{mp} = [(T_m + H_f/C)/T_{Fp0}] 10 \text{ J/cm}^2 \quad (4.24)$$

$$(It_p)_{mr} = [(T_m + H_f/C)/T_{Fr0}] 10 \text{ J/cm}^2 \quad (4.25)$$

- convenient relation between values of optical distortion thresholds (valid for both thermally thin and thermally thick coatings)

$$\frac{1}{(It_p)_{or}} = \frac{1}{(It_p)_{op}} + \frac{1}{(It_p)_{SC}} + \frac{1}{(It_p)_{\Delta S}} \quad (5.17a)$$

Sec. B-X

where

$$\begin{aligned} (It_p)_{SC} &= \frac{h t_{ip} (\lambda/2 G)}{\alpha_S \ell_S (1 + \nu_S) A} = 7.14 \times 10^{-6} \frac{h}{\alpha_S (1 + \nu_S)} \\ &= [31.4 \text{ J/cm}^2] \end{aligned}$$

and

$$\begin{aligned} (It_p)_{\Delta S} &= \frac{3 t_{ip} K_S (\lambda/2 G)}{a \alpha_S \ell_S^2 (1 + \nu_S) A} = 2.14 \times 10^{-4} \frac{K_S}{a \alpha_S (1 + \nu_S)} \\ &= [46.9 \text{ J/cm}^2] \end{aligned}$$

Sec. B-XI

XI. ACKNOWLEDGEMENTS

Conversations with Dr. A. D. Baer, Dr. Phil Baumeister, Dr. H. E. Bennett, Mr. Oscar Buchmann, Dr. D. L. Decker, Mr. M. R. Flannery, Dr. R. W. Hoffman, Dr. S. J. Holmes, Dr. R. S. Hughes, Dr. D. L. Jacobson, Dr. D. A. Pinnow, Dr. J. O. Porteus, Dr. V. L. Rehn, Dr. W. Reichelt, and Capt. H. V. Winsor are greatly appreciated.

APPENDIX. HEAT FLOW IN MANY-LAYERED STRUCTURES

The time required for heat to diffuse a distance $d \gg \ell_1 + \ell_2$ along z in a semi-infinite medium consisting of repeated pairs of layers of thickness $z = \ell_1$ and $z = \ell_2$ is

$$t = C_F d^2 / 4 K_F \quad (A.1)$$

where

$$C_F = \frac{C_1 \ell_1 + C_2 \ell_2}{\ell_1 + \ell_2} \quad (A.2)$$

and

$$K_F = \frac{K_1 K_2 (\ell_1 + \ell_2)}{K_1 \ell_2 + K_2 \ell_1} \quad (A.3)$$

For $C_1 = C_2 \equiv C$, (A.2) gives $C_F = C$; and for $C_1 \equiv C_g \gg C_2$ with $\ell_1 = \ell_2$, $C_F = \frac{1}{2} C_g$. For $K_1 = K_2 = K$, (A.3) gives $K_F = K$; and for $K_2 \gg K_1 \equiv K_\ell$ with $\ell_1 = \ell_2$, $K_F = 2 K_\ell$.

If $c \equiv C \ell$ and $k \equiv K \ell$, (A.2) and (A.3) can be written as

$$c_F = c_1 + c_2 \quad ; \quad k_F^{-1} = k_1^{-1} + k_2^{-1} \quad (A.4)$$

For the case of optical coatings with all layers of one-quarter wavelength optical thickness (that is, $\ell_1 = (\lambda/4)/n_1$, etc.), (A.2) and (A.3) give

$$C_F = \frac{C_1 n_2 + C_2 n_1}{n_1 + n_2} = [3.14 \text{ J/cm}^3 \text{ K}] \quad (A.5)$$

$$K_F = \frac{K_1 K_2 (n_1 + n_2)}{K_1 n_1 + K_2 n_2} = [0.28 \text{ W/cm K}] \quad (A.6)$$

Sec. B-Appendix

The effective value of $\alpha(1 + \nu)$ for the coating is

$$\begin{aligned}\alpha_F(1 + \nu_F) &= \frac{\alpha_1(1 + \nu_1)n_2 + \alpha_2(1 + \nu_2)n_1}{n_1 + n_2} \\ &= [16.0 \times 10^6 \text{ K}^{-1}] \quad .\end{aligned}\tag{A.7}$$

A formal explanation of these results is useful in developing intuition. First consider a two-layer structure with $T = 0$ at time $t = 0$ and $T = T_0$ at $x = 0$ at all times with no heat flow ($dT/dx = 0$) at $x = \ell_1 + \ell_2$ at all times. A schematic illustration of the temperature distribution at various times for the case of $K_1 \ll K_2$ and $C_1 = C_2$ is given in Fig. A.1. If this two-layer structure were replaced by the semi-infinite structure in which the structure of Fig. A.1 is repeated over and over, the values of T at $x = \ell_1 + \ell_2$ would be lower than the values in Fig. A.1 as a result of the heat flow across the surface $x = \ell_1 + \ell_2$ into the next layer (the third layer, which has $K = K_1$).

At a later time, after the heat has diffused through many pairs of layers, the temperature distribution is as shown schematically in Fig. A.2. In the first few layers starting from $x = 0$ in Fig. A.2, the dashed curve corresponds to the known steady-state heat flow results

$$\begin{aligned}J &= K_F(\Delta T_1 + \Delta T_2)/(\ell_1 + \ell_2) \\ &= K_1 \Delta T_1 / \ell_1 = K_2 \Delta T_2 / \ell_2\end{aligned}$$

whose solution gives (A.3).

Sec. B-Appendix

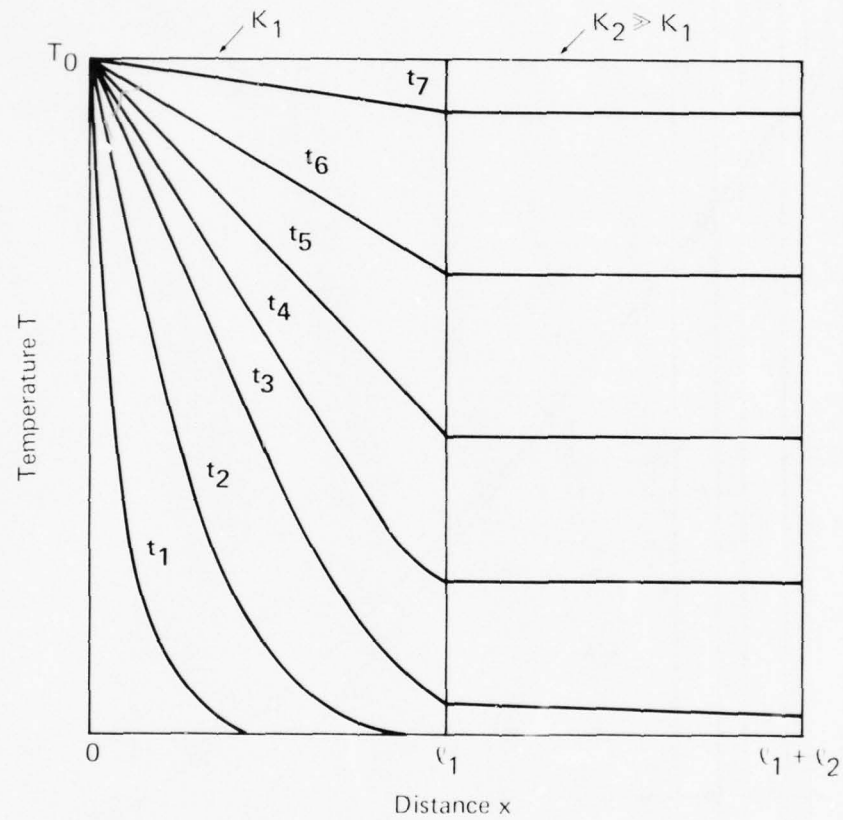


Fig. A.1. Schematic illustration of the temperature distribution in a two-layer structure at various times.

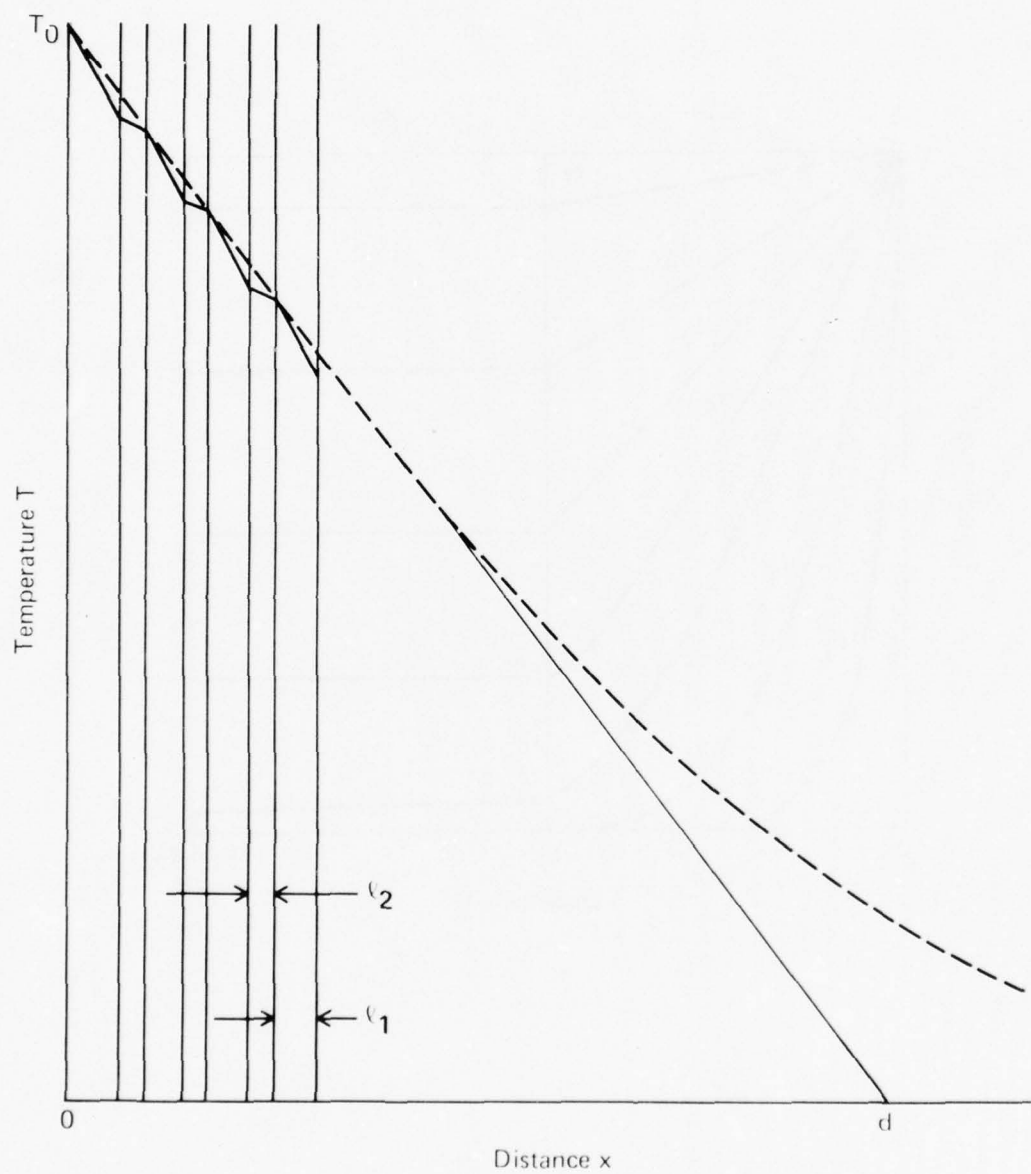


Fig. A.2. Schematic illustration of the temperature distribution in a many-layered structure.

Sec. B-Appendix

Equating the product of rate of energy added to the sample per unit times the time t

$$\sim K_F (T_0/d) t$$

to the increase in energy of the sample

$$\sim (C_1 \ell_1 + C_2 \ell_2) \frac{d}{\ell_1 + \ell_2}$$

and solving for t gives

$$t = 4 K_F d^2 / C_F^2 \quad (\text{A. 8})$$

where C_F is given by (A. 2) and the constant 4 in (A. 4) was chosen to give $t = 4 K d^2 / C$ for the case of $K_1 = K_2 \equiv K$ and $C_1 = C_2 \equiv C$.

The effective value of $\alpha(1 + \nu)$ that determines the normal (along z) expansion of the coating is easily obtained as follows:

$$\Delta \ell_F = N(\Delta \ell_1 + \Delta \ell_2) \quad (\text{A. 9})$$

where

$$N = \ell_F (\ell_1 + \ell_2)^{-1}$$

is the number of pairs of layers in the coating. With $\ell_1 \sim 1/n_1$ and $\ell_2 \sim 1/n_2$

$$\Delta \ell_1 = \ell_1 \alpha_1 (1 + \nu_1) \langle T \rangle_{\ell_F}$$

and the corresponding expression with subscripts 1 replaced by 2's, (A. 9) reduces to

$$\Delta \ell_F = \ell_F \alpha_F (1 + \nu_F) \langle T \rangle_{\ell_F} \quad (\text{A. 10})$$

with $\alpha_F (1 + \nu_F)$ given by (A. 7).

Sec. B-References

REFERENCES

1. H. E. Bennett, in Laser Induced Damage in Optical Materials: 1976, A. J. Glass and A. H. Guenther, eds., NBS Special Publication 462, Proceedings of a Symposium at Boulder, Colo., July 13-15, 1976, 11.
2. Proceedings of the Fifth Annual Conference on Infrared Laser Window Materials, sponsored by DARPA, Las Vegas, Nevada, Dec. 1-4, 1975. Laser Induced Damage in Optical Materials: 1975, A. J. Glass and A. H. Guenther, eds., NBS Special Publication 435, Proceedings of a Symposium at Boulder, Colo., July 29-31, 1975.
3. M. Sparks, J. Appl. Phys. 42, 5029 (1971).
4. M. Sparks and H. C. Chow, AFCRL Conference on High Power Infrared Laser Window Materials, Hyannis, Mass., Nov. 1973; M. Sparks and H. C. Chow, J. Appl. Phys. 45, 1510 (1974).
5. H. V. Winsor, in Proceedings of the Third Conference on High-Power Infrared Laser Window Materials, Nov. 12-14, 1973, Hyannis, Mass., C. A. Pitha and B. Bendow, eds. (Air Force Cambridge Research Laboratories AFCRL-TR-74-0085, Special Report 174, 1974), 1069.
6. H. E. Bennett, V. L. Rehn, A. D. Baer, R. S. Hughes, and J. L. Stanford, Naval Weapons Center, China Lake, Ca., unpublished.
7. There is a contribution to the expansion (the attachment-stress contribution) that does not have the same ρ dependence as does I, but this contribution is often negligible and is neglected in the present paper, as discussed in Sec. II.
8. S. J. Holmes, Northrop Corporation, private communication.
9. Phil Baumeister and Aded Arnon, Applied Optics, in press.
10. M. S. Sparks, in Laser Induced Damage in Optical Materials: 1976, A. J. Glass and A. H. Guenther, eds., NBS Special Publication 462, Proceedings of a Symposium at Boulder, Colo., July 13-15, 1976, 203.

Sec. B-References

11. M. Sparks and C. J. Duthler, Theoretical Studies of High-Power Ultraviolet and Infrared Materials, Xonics, Inc. Seventh Technical Report, 30 June 1976, under Contract No. DAHIC 15-73-C-0127. A number of experimental and theoretical references, some of which are abstracted, are given.
12. D. W. Fradin, Lawrence Livermore Laboratories, Livermore, Ca., private communication.
13. N. L. Boling, private communication.
14. E. Ritter, in Physics of Thin Films, Vol. 8, 1 (1975).
15. Dr. Gerald Comisar, Aerospace Corporation, El Segundo, Ca., private communication.
16. J. W. Matthews and F. Klokholm, Mat. Res. Bull. 7, 213 (1972).
17. R. W. Hoffmann, in Physics of Nonmetallic Thin Films Series, NATO Advanced Study Institute B14, 273, Plenum Press (1976).
18. Harry V. Winsor, Conference on High-Power Infrared Laser Window Materials, Charles S. Sahagian and Carl A. Pitha, eds., Bedford, Mass., Oct. 27-28, 1971.
19. G. Koppelman, Ann. Phys. 5, 388 (1960), in German.
20. B. E. Newnam and D. H. Gill, in Laser Induced Damage in Optical Materials: 1976, A. J. Glass and A. H. Guenther, eds., NBS Special Publication 462, Proceedings of a Symposium at Boulder, Colo., July 13-15, 1976, 292.
- 20a. A. J. Sievers and R. O. Pohl, Technical Progress Report of Contract No. F19628-75-C-0177, July 1 - Dec. 31, 1976, Cornell University.
21. Sec. D of this report.
22. H. S. Carslaw and J. C. Jaeger, in Conduction of Heat in Solids, 2nd Edition, (Oxford-Clarendon Press, 1959).
23. M. Sparks, J. Appl. Phys. 47, 837 (1976)
24. The numerical values in the equations, such as 56.4 in (2.1), are for the values of the system parameters listed in Sec. I, and the numerical values in brackets, such as [29.5 K] in (2.1), are for an MgO/MgF₂:Mo reflector at 250 nm.

Sec. B-References

25. M. Sparks, Sec. C of this report.
26. B. A. Boley and J. H. Weiner, Theory of Thermal Stress, John Wiley & Sons Inc., New York, 1960.
27. M. Sparks and C. J. Duthler, J. Appl. Phys. 44, 3038 (1973).
28. L. I. Van Torne, Phys. Stat. Sol. 16, 171 (1966).
29. R. W. Hooper and D. R. Uhlmann, J. Appl. Phys. 41, 4023 (1970).
30. M. Sparks, Xonics, Incorporated, Santa Monica, Ca., to be published.
31. R. Braunstein, Phys. Rev. 125, 475 (1962).
32. M. Sparks, Theoretical Studies of High-Power Ultraviolet and Infrared Materials, Xonics, Inc. Third Technical Report, 30 June 1974, under Contract No. DAHC 15-73-C-0127, Sec. C.
33. American Institute of Physics Handbook, Third Edition, McGraw-Hill Book Co., Inc., New York, N. Y., 1972.
34. P. H. Lissberger, Rep. Prog. Phys. 33, 197 (1970).
- 34a. After the manuscript was completed, the first results of a study of the phase ϕ_r of the coating reflection coefficient and the absorption in the coating material were obtained. A slight modification of the argument used to obtain ℓ_e in (3.20) gives $\ell_e = \ell_{pen}$ exactly, and in fact gives all the coating results needed here, including the phase of the reflection coefficient discussed in Sec. VIII, almost by inspection. A key result is use of the zeroth-order electric field, which is reduced by a factor n_0/n_H at the surface of the coating and by a factor n_L/n_H at every low-to-high interface (one factor n_L/n_H for each pair of layers).
- 34b. After the manuscript was completed, we learned of the tetrahedral carbon (so-called diamond) films deposited at the Aerospace Corporation. These films may have low expansion coefficients in addition to other superior qualities. See Sec. I and Ref. 15.
35. L. Van Uitert, H. J. Guggenheim, H. M. O'Bryan, A. W. Warner, Jr., D. Brownlow, J. L. Bernstein, G. A. Pasteur, and L. F. Johnson, Mat. Res. Bull. 11, 669 (1976).

Sec. B-References

36. M. Sparks and C. J. Duthler, Theoretical Studies of High-Power Ultraviolet and Infrared Materials, Xonics, Inc. Seventh Technical Report, 30 June 1976, under Contract No. DAHC 15-73-C-0127, Sec. B.
37. M. Sparks and C. J. Duthler, Proceedings of the Fourth Annual Conference on Infrared Laser Window Materials, Tucson, Arizona, November 18-20, 1974.
38. Dr. Walter Reichelt, Los Alamos Scientific Laboratories, Los Alamos, New Mexico, private communication.
39. Dr. O. Buchmann, Garrett AiResearch Corp., Los Angeles, Ca., private communication.
40. It is of interest that the values of effective-boundary-layer thickness ~~$b = K_C / h$ are close for the "good liquid" and "best gas" values.~~ For air, with $K = 2.4 \times 10^{-4} \text{ W/cm}^2$ and $h = 6 \times 10^{-2} \text{ W/cm K}$, the value of b is $40 \mu\text{m}$; and for water, with $K = 6.0 \times 10^{-3} \text{ W/cm K}$ and $h = 1 \text{ W/cm}^2 \text{ K}$, the value of b is $60 \mu\text{m}$.
41. D. A. Pinnow, T. C. Rich, F. W. Ostermayer, Jr., and M. Di Domenico, Jr., Appl. Phys. Lett. 22, 527 (1973).
42. D. L. Jacobson, W. Bickford, J. Kidd, R. Barthelemy, R. H. Bloomer, Analysis and Testing of a Heat Pipe Mirror for Lasers, AIAA Thermophysics Conference, Denver, May 1975.
43. D. L. Jacobson, Performance of a Laser Mirror Heat Pipe, ASME 74-WA/HT-61, New York, Nov. 17-22, 1974.
44. D. Jacobson, R. Barthelemy, and D. Rabe, in Proceedings of the Infrared Laser Window Materials Meeting, 12 July 1976, Boulder, Colorado.
45. Dr. D. L. Jacobson, Arizona State University, Tempe, Arizona, private communication.
46. A. Herpin, C. R. Acad. Sci. Paris 225, 182 (1947).
47. D. L. Decker, in Laser Induced Damage in Optical Materials: 1975, A. J. Glass and A. H. Guenther, eds., NBS Special Publication 435, Proceedings of a Symposium at Boulder, Colo., July 29-31, 1975, 230.

Sec. C

C. THERMAL STRESSES AND EXPANSION IN MULTILAYER DIELECTRIC REFLECTORS

M. Sparks

Xonics, Incorporated, Santa Monica, California 90401

Expressions, needed in analyzing fracture and optical distortion of high-power reflectors, are derived for the thermal stress and expansion in thin multilayer coatings (total thickness ℓ_F) on thick heat-conducting substrates (thickness ℓ_S and diameter D). Simple closed-form results are obtained, even though the temperature varies axially and radially, by considering the usual case of $\ell_F \ll \ell_S \ll D$ and by considering the stress as the sum of two terms. The detached-stress term is that of a reflector divided into many thin layers, and the attachment-stress term is the stress required to bring the layers back to their actual positions. The general results for the stress simplifies considerably for $\rho \approx 0$ (axis of the cylinder), where fracture often occurs. Thickness changes, which cause optical distortion, tend to be more affected by detachment stresses than by attachment stresses. Neglecting the latter greatly simplifies the analysis and results and gives quite accurate results (five percent for the worst temperature distribution and of order $\sim \ell_F/4 \ell_S$ for the best case of a currently used reflector) for many, but not all, reflectors.

I. INTRODUCTION AND SUMMARY

The availability of high-power lasers has generated interest in new classes of materials problems¹⁻⁵, as discussed in Ref. 5. A theoretical analysis of problems of windows for high-power systems was carried out some time ago³. In a recent analysis^{4,5} of high-power reflectors, it was found that dielectric reflectors were required because the intrinsic absorptance A of metals is too great, the value A being 0.08 for aluminum for $124 \text{ nm} \leq \lambda \leq 500 \text{ nm}$. The high-power reflectors considered here consist of metallic substrates or other high-thermal-conductivity substrates. Low-absorptance reflectors must have a sufficient number of dielectric layers to reduce the irradiance to a very low value at the substrate in order to prevent excessive absorption by the substrate. Two typical ultraviolet reflectors^{6,7} deposited on fused silica have 21 and 45 layers. The number of layers can be reduced by depositing the optical coating on a thin aluminum intermediate layer. The substrate serves to conduct heat out of the coating and to provide the mechanical stability necessary to maintain the required optical figure.

Two problems are of interest in laser-heated reflectors. The first is the calculation of stresses⁸ in the layers of the coating and fracture resulting from excessive stresses. The second is calculation of the thickness change from thermal expansion and the resulting optical distortion. In considering these problems, the needed thermal-stress analyses were not found in the standard references. Difficulties arise because the temperature varies in two directions (axially and radially). In the present study, the stresses will be estimated and several simple problems will be solved and related to well known results in order to provide sufficient background and intuition to understand the results. It is found that reliable estimates

Sec. C-I

can be made for the usual case in which the substrate is thin and the coating is much thinner than the substrate.

In the calculations, the following assumptions will be made:

- The problems of calculating the deviations from the idealized results that occur near the rim (within a distance of the order of the thickness) of thin disks and near the ends (within a distance of the order of the diameter) of a long rod are not considered.

- The substrates are thin (thickness $\ell_S \ll \text{diameter } D_S$).
- The coatings are thin (thickness $\ell_F \ll \ell_S$).
- The system has cylindrical symmetry (all variables independent of the azimuthal angle ϕ) and is linear.

- The support system for the reflector does not allow the reflector to bow.

Specifically, the rear surface (at $z = \ell_S + \ell_F$) remains in a plane.

In order to afford numerical examples of the results derived, the following parameters will be used:

- pulse duration: $t_p = 10^{-6} \text{ s}$
- pulse repetition rate: 100 pulses per second ($t_{ip} = 10^{-2} \text{ s}$)
- energy density: $10 \text{ J/cm}^2/\text{pulse}$
- absorptance of the reflector: $A = 5 \times 10^{-3}$
- heat-transfer coefficient:⁹ $h = 0.1 \text{ W/cm}^2 \text{ K}$
- substrate (Mo) heat capacity: $C_S = 2.61 \text{ J/cm}^3 \text{ K}$
- substrate (Mo) thermal conductivity: $K_S = 1.4 \text{ W/cm K}$
- substrate thickness:⁹ $\ell_S = 0.1 \text{ cm}$
- total coating thickness: $1.81 \mu\text{m}$

Numerical values in brackets in the results below are for these values of parameters.

Sec. C-I

Summary of Results. In analyzing the failure of high-power reflectors, the thermal-stress components and the thickness change are needed. In general, when the temperature is a function of two variables such as ρ and z , calculating the stress components is difficult. However, a sufficiently accurate estimate is made for thin coatings (thickness ℓ_F) on thin substrates (thickness ℓ_S and diameter D), that is, for $\ell_F \ll \ell_S \ll D$. In the estimate, the stress is considered to be the sum of two terms. The detached-stress term is the stress that would arise if the reflector were divided into many thin layers that are detached from one another, and the attachment stress is the stress resulting from reattaching the layers, that is, from returning the layers to their proper positions.

The general results for the stress components are given in (4.1), (4.2), (4.14-4.17). In most practical cases, the center of the coating ($\rho = 0$) is expected to fracture first. In this case, the general results simplify considerably to the result (4.19). The stress components for the limiting case of ρ approaching R also are given, in (4.20) through (4.23).

The detached stresses tend to cause greater thickness changes than do the attachment stresses. The analysis and results are greatly simplified by neglecting the attachment stresses. The resulting expression for the thickness change is quite accurate for the following cases: (1) For an uncoated reflector, the result is exact (to within the limitations of the model, of course.) (2) For a temperature distribution that is not peaked in the coating the errors are very small, of order ℓ_F/ℓ_S . (3) For a thermally thin coating (thickness $\ell_F \ll$ thermal diffusion distance ℓ_{th}), the errors are small since most of the expansion occurs in the substrate, which does not contribute to the error. (4) For elastically similar coating and substrate materials, that is, for a small magnitude of $\nu_i/E_i - \nu_S/E_S$, the error is small,

Sec. C-1

being zero when $\nu_i/E_i - \nu_S/E_S = 0$ for both layers $i = 1$ and 2 . The greatest error, which could be approximately 30 percent, is likely to occur in a thermally thick coating ($l_{th} \gtrsim l_F$) with $T_{SC} \ll T_p$, where T_{SC} is the average temperature (over many pulses in the repeated-pulse system) of the substrate and coating and T_p is the temperature resulting from a single pulse (see (2.1)), and elastically dissimilar materials (great magnitudes of $(\nu_i/E_i - \nu_S/E_S)$). The general expression for the thickness change, including the attachment-stress effects, is given in (5.12) and (5.13), and the simple approximation obtained by neglecting the attachment-stress components is given by (5.13).

The general results for the stresses and thickness change are applied to practical reflectors. Several well known results, which are useful in the present context, are given in the Appendix.

II. TEMPERATURE DISTRIBUTION

The general results derived herein will be illustrated with the following specific temperature distributions. The radial distribution will be taken as Gaussian

$$T(\rho, z) = T(0, z)e^{-a\rho^2}, \quad (2.1)$$

truncated at $1/c^2$, that is, at $R^2=2$, where R is the radius of the reflector and ρ and z are circular-cylindrical coordinates. All variables are assumed to be independent of the angle coordinate ϕ ; that is, the system is invariant under all rotations around the z axis. The temperature distribution (2.1) could result from a Gaussian laser profile with negligible radial heat diffusion, for example.

A typical z dependence of the temperature is that of a repeated-pulse system, which is shown schematically in Fig. 1. The energy absorption from the incident optical beam occurs near the surface of the coating (near $z=0$). During the pulse, of duration t_p , the heat diffuses into the structure a distance ℓ_{th} . Thus the temperature is great in the region $0 < z \lesssim \ell_{th}$ as shown. The temperature distribution in the region $\ell_{th} \lesssim z < \ell_F + \ell_S$ results from the diffusion across the substrate during the interpulse time and the cooling at the back surface of the substrate (at $z = \ell_F + \ell_S$).

A good approximation to the z dependence of the temperature for the purpose of illustration and indeed for important practical systems is

$$T(\rho, z) = T_p(\rho, z) + T_{SC}(\rho) \quad (2.2)$$

where T_p , the temperature resulting from a single pulse, is large only in the region $0 < z \lesssim \ell_{th}$ in Fig. 1. The long-time average temperature $T_{SC}(\rho)$ is

Sec. C-II

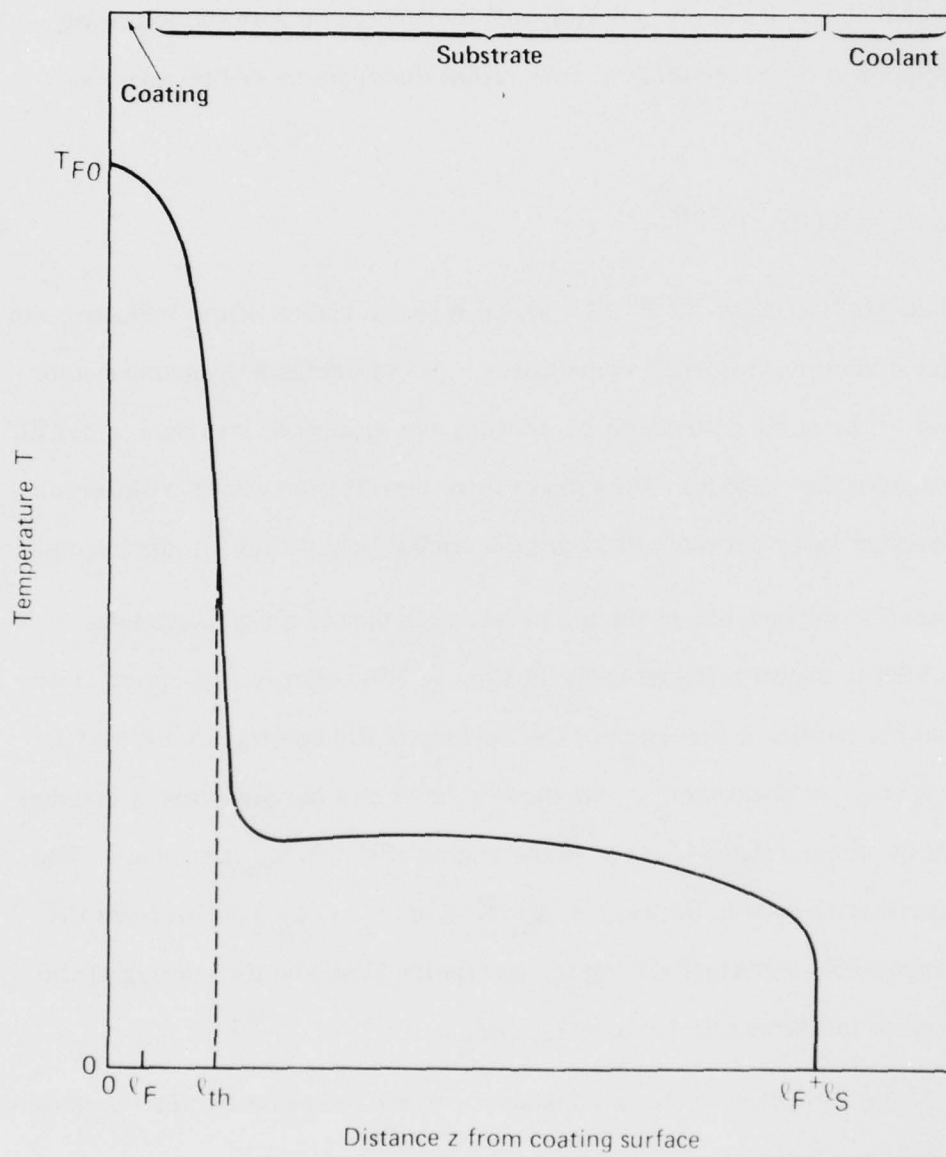


Fig. 1. Typical temperature distribution at the end of a pulse during repeated-pulse operation.

essentially the temperature at the beginning of a pulse in the repeated-pulse system. For a single pulse, (2.2) is replaced by

$$T(\rho, z) = T_p(\rho, z), \quad (2.3)$$

and for cw operation (2.2) is replaced by

$$T(\rho, z) = T_{SC}(\rho). \quad (2.4)$$

The thermal-diffusion distance in the substrate in time $t_p = 10^{-6}$ s is⁵

$$\ell_{th} = (4K_S t_p / C_S)^{1/2} = 14.6 \text{ } \mu\text{m}, \quad (2.5)$$

which is two orders of magnitude smaller than the substrate thickness $\ell_S = 0.1$ cm.

Thus, the approximation $\ell_{th} \ll \ell_S$ is well satisfied.

The temperature T_{SC} of the back surface (at $z = \ell_F + \ell_S$) of the substrate is determined by the magnitude of the heat flow $IA t_p / t_{ip}$, where I is the irradiance, t_{ip} is the time between pulses, and A is the absorptance of the reflector into the coolant and the heat-transfer coefficient $h(\text{W}/\text{cm}^2\text{K})$:⁵

$$T_{SC} = I t_p A / t_{ip} h = [50 \text{ K}]. \quad (2.6)$$

The value of T_{SC} is measured with respect to the coolant temperature. (For this temperature of 50 K, the optical distortion is excessive. Methods of reducing the optical distortion are considered in Ref. 5.)

That the temperature drop across the substrate is small, as assumed in (2.2), can be seen as follows: Since the thermal-diffusion distance $\ell_{tip} = 0.146$ cm during the time $t_{ip} = 10^{-2}$ s between pulses is greater than the substrate thickness,

Sec. C-II

the temperature distribution in the substrate is approximately the same as if the absorption occurred uniformly throughout the substrate. The steady-state heat-flow equation is then

$$-K_S d^2 T/dz^2 = I t_p A/t_{ip} \ell_S.$$

The solution for the boundary conditions $\partial T/\partial z = 0$ at $z = 0$ (no heat flow at the surface) and $T = T_{SC}$ at $z = \ell_F + \ell_S \cong \ell_S$ is

$$T = T_{\Delta S} (1 - z^2/\ell_S^2)$$

where

$$T_{\Delta S} = I t_p A \ell_S / 2 t_{ip} K_S = [0.179 \text{ K}]. \quad (2.7)$$

Since $T_{\Delta S} \ll T_{SC}$ according to (2.6) and (2.7), the constant-substrate-temperature approximation in (2.2) is well satisfied.

For the Gaussian radial-temperature distribution (2.1), the radial-average temperature is, for $aR^2 = 2$,

$$\langle T \rangle_R = \frac{1}{aR^2} (1 - e^{-aR^2}) T(0, z) = 0.432 T(0, z), \quad (2.8)$$

and the rim ($\rho = R$) temperature is

$$T(R, z) = 0.135 T(0, z). \quad (2.9)$$

For the z dependence in (2.2) and for the typical case of $\ell_{th} T_p \ll T_{SC} \ell_S$ satisfied, the z -averaged temperature is

$$\langle T \rangle_{\ell_S} \cong T_{SC}. \quad (2.10)$$

III. SIMPLE CASES OF THERMAL STRESSES

Several simple cases of thermal stresses will be considered, as discussed in Sec. I, before considering the most general case of interest. As the first case, consider a long, thin composite rod consisting of a core having thermal expansion coefficient α_S , thermal conductivity K_S , heat capacity C_S , and diameter D_S . A thin outside coating of thickness ℓ_F has α_F , C_F , and K_F . The temperature of the core and coating is increased uniformly from the temperature at which the stresses are zero (defined as the zero of temperature) to temperature T . Since the rod is long (length $L \gg D_S$), the slight deformations of the ends of the rod are negligible, and the rod maintains its cylindrical shape. In particular, the assumption that the ends remain flat is well satisfied when considering the stresses away (distance $\gtrsim D_S$) from the ends of the rod. For simplicity of the illustration, only the expansion along the length of the rod is considered.

An important conceptual device in the calculations herein is to consider the reflector to be divided into many thin layers that are first considered to be detached from the other layer and then exposed to stresses, called attachment stresses, that bring the layers back to their proper positions. The total stresses are then the sums of the stresses, called detached stresses, in the detached layers and attachment stresses. In the present example the coating is considered to be detached from the core. The detached coating expands (assuming that α_F is positive), the displacement being

$$w_F = \alpha_F Tz ,$$

and the detached-core displacement is

Sec. C-III

$$w_S = \alpha_S Tz .$$

The detached stresses are zero

$$\sigma_{Sd} = \sigma_{Fd} = 0 \quad (3.1)$$

since the expansion is unconstrained.

Now suppose that the coating and core are brought back to their proper positions at temperature T by applying the attachment stresses. In this simple case, forces can be applied to the ends of the coating and core. In general, for temperature variations along the length of the structure, for example, the attachment stresses σ_a would be functions of z . To be concrete, suppose that $\alpha_F > \alpha_S$. Then the film must be compressed (compressive stress) and the core must be lengthened (tensile stress). The attachment condition is that the sum of the forces at the ends of the rod must be zero. That is, the total tensile force on the core, $(\pi D_S^2/4)\sigma_{zz Sa}$, must equal the magnitude of the total compressive force on the coating, $\sim(\pi D_S \ell_F)\sigma_{zz Fa}$:

$$D_S \sigma_{zz Sa} + 4 \ell_F \sigma_{zz Fa} = 0 . \quad (3.2)$$

Here $\sigma_{zz Sa}$ is positive (tensile), and $\sigma_{zz Fa}$ is negative (compressive).

Since $\ell_F \ll D_S$, (3.2) indicates that $\sigma_{zz Fa}$ has a much greater magnitude than that of $\sigma_{zz Sa}$. Thus the length change of the core resulting from the attachment stress is negligible, assuming no anomalies in the values of Young's modulus. Physically, the coating is too small to affect the large core. The stress $\sigma_{zz Fa}$ is therefore the value required to compress the coating until its length is equal to that of the core $(L + \alpha_S TL)$; that is, to compress the coating by $\alpha_F TL - \alpha_S TL$:

Sec. C-III

$$\sigma_{zz Fa} = -(\alpha_F - \alpha_S) E_F T \quad (3.3)$$

where E_F is the Young's modulus of the film.

The total stress in the coating is the sum of the detached value, which is zero from (3.1), and the attachment value, from (3.3):

$$\sigma_{zz F} = -(\alpha_F - \alpha_S) E_F T. \quad (3.4)$$

This result is independent of the heat capacities C and thermal conductivities K of the coating and core for this case of a constant temperature rise. If heat were applied to the surface for a given time, for example, the stresses would depend on the values of C and K in general.

If $l_F \ll D_S$ is not well satisfied, the second condition in addition to (3.2) required to find the values of the stresses is that the lengths of the coating and core must be equal. Then (3.2), (3.1), and

$$\begin{aligned} \sigma_{zz Fa} &= E_F \Delta l_{Fa} \\ \sigma_{zz Sa} &= E_S \Delta l_{Sa} \\ -\Delta l_{Fa} + \Delta l_{Sa} &= (\alpha_F - \alpha_S) TL \end{aligned}$$

give

$$\sigma_{zz F} = - \frac{D_S E_S E_F (\alpha_F - \alpha_S) TL}{D_S E_S + 4 l_F E_F} \quad (3.5)$$

and

$$\sigma_{zz S} = \frac{4 l_F E_S E_F (\alpha_F - \alpha_S) TL}{D_S E_S + 4 l_F E_F} \quad (3.6)$$

Sec. C-III

As the second case, consider a thin circular substrate (thickness $\ell_S \ll \text{diameter } D_S$) coated with a much thinner coating (thickness $\ell_F \ll \ell_S$). The temperature is increased uniformly to T above the temperature, defined as zero, at which the stresses are zero. The detached stresses are zero

$$\sigma_{\rho\rho Fd} = \sigma_{\phi\phi Fd} = \sigma_{\rho\rho Sd} = \sigma_{\phi\phi Sd} = 0 \quad (3.7)$$

since the temperature is uniform. Here ρ , ϕ , and z are the circular-cylindrical coordinates. The radial displacement of the coating relative to the substrate is

$$u_{Fd} - u_{Sd} = (\alpha_F - \alpha_S) T \rho. \quad (3.8)$$

As in the previous example, for $\ell_F \ll \ell_S$, the change in the radial displacement of the substrate on attachment is negligible. Thus the attachment stresses in the coating must change the coating displacement by the amount

$$u_{Fa} = -(u_{Fd} - u_{Sd}) = -(\alpha_F - \alpha_S) T \rho. \quad (3.9)$$

From (3.7), (3.9), and $\sigma_{\rho\rho F} = \sigma_{\rho\rho Fd} + \sigma_{\rho\rho Fa}$ and the corresponding $\phi\phi$ result,

$$\sigma_{\rho\rho F} = \sigma_{\phi\phi} = -\frac{E_F T}{1 - \nu_F} (\alpha_F - \alpha_S) \quad (3.10)$$

where ν_F is the Poisson ratio of the coating and $E_F / (1 - \nu_F)$ is the appropriate elastic stiffness constant for the circular cylindrical geometry and displacement proportional to ρ , just as E_F is the elastic stiffness constant for the linear geometry of the previous geometry.

Both of these stress-strain relations follow from the general relations for rectilinear coordinates⁸

Sec. C-III

$$\sigma_{ij} = \lambda \delta_{ij} \epsilon + 2\mu \epsilon_{ij} - (3\lambda + 2\mu) \delta_{ij} T \quad (3.11)$$

where δ_{ij} is the Kronecker delta,

$$\epsilon = \sum_{i=1}^3 \epsilon_{ii} ,$$

$$\lambda = \frac{\nu E}{(1+\nu)(1-2\nu)} ,$$

$$\mu = E/2(1+\nu) ,$$

$$3\lambda + 2\mu = E/(1-2\nu) ,$$

and

$$\lambda + 2\mu = \frac{E(1-\nu)}{(1+\nu)(1-2\nu)} .$$

For the linear geometry, $\epsilon_{xx} = \epsilon_{yy} = -\nu \epsilon_{zz}$ by the definition of the Poisson ratio ν . Then (3.11) with $T = 0$ gives

$$\sigma_{zz} = (-2\lambda\nu + \lambda + 2\mu) \epsilon_{zz} = E\epsilon_{zz} \quad (3.12)$$

which is the result used above.

For circular-cylindrical geometry, setting $\sigma_{zz} = 0$ (plane-stress, for thin disks) in (3.11) gives

$$\epsilon_{zz} = -\frac{\nu}{1-\nu} (\epsilon_{\rho\rho} + \epsilon_{\phi\phi}) . \quad (3.13)$$

From (3.11) and (3.13),

$$\sigma_{\rho\rho} = \frac{E(\epsilon_{\rho\rho} + \nu\epsilon_{\phi\phi})}{1-\nu^2} \quad (3.14)$$

and

Sec. C-III

$$\sigma_{\phi\phi} = \frac{E(\epsilon_{\phi\phi} + \nu\epsilon_{\rho\rho})}{1 - \nu^2} \quad (3.15)$$

For the present case of u proportional to ρ , the strains $\epsilon_{\rho\rho} = \partial u / \partial \rho$ and $\epsilon_{\phi\phi} = u/\rho$ are equal, and (3.14) and (3.15) give

$$\sigma_{\rho\rho} = \sigma_{\phi\phi} = \frac{E\epsilon_{\rho\rho}}{1 - \nu} \quad (3.16)$$

which is the result above.

As the third case, the result (3.10) is easily extended to the case of a thin multilayer dielectric coating, where thin means that the total thickness ℓ_F of all layers in the coating satisfies $\ell_F \ll \ell_S$. Each layer of the coating is considered as detached, and each of the detached layers acts just as the single detached layer in the previous case. Thus the detached stresses are zero, as in (3.7). Since $\ell_F \ll \ell_S$, the attachment stresses do not change the substrate diameter appreciably; thus, (3.8) is satisfied for each layer, and the remaining analysis is the same as in the previous case. The result (3.10) is therefore valid for each layer i :

$$\sigma_i = - \frac{E_i T}{1 - \nu_i} (\alpha_i - \alpha_S) \quad (3.17)$$

where $\sigma_i \equiv \sigma_{\rho\rho i} = \sigma_{\phi\phi i}$.

The fourth case is the same as the third, except that the temperature is a function of z . The displacements of the detached coating layers are

$$u_{id} = \alpha_i T_F \rho. \quad (3.18)$$

The temperature T_F in the coating typically varies smoothly with z , as shown in Appendix A of Ref. 5. The displacement of the detached substrate is

$$u_{Sd} = \alpha_S \langle T \rangle_{\ell_S} \rho \quad (3.19)$$

where

$$\langle T \rangle_{\ell_S} = \frac{1}{\ell_S} \int_{\ell_F}^{\ell_F + \ell_S} dz T_S \quad (3.20)$$

is the average substrate temperature. As before, the attachment displacement of the substrate is negligible since $\ell_F \ll \ell_S$. The attachment displacements of the layers are therefore

$$u_{ia} = -(u_{id} - u_{Sd}) = -(\alpha_i T_F - \alpha_S \langle T \rangle_{\ell_S}) \rho, \quad (3.21)$$

and the attachment stresses required to give the displacement (3.21), which are the total stresses since the detached stresses are zero, are

$$\sigma_{\rho\rho i} = \sigma_{\phi\phi i} = -\frac{E_i}{1-\nu_i} (\alpha_i T_F - \alpha_S \langle T \rangle_{\ell_S}). \quad (3.22)$$

For constant temperature, (3.22) reduces correctly to (3.10).

Setting $E_i = E_S \equiv E$, $\alpha_i = \alpha_S \equiv \alpha$, and $\nu_i = \nu_S \equiv \nu$ in (3.22) gives the result (with $\ell = \ell_S \cong \ell_S + \ell_F$)

$$\sigma_{\rho\rho} = \sigma_{\phi\phi} = \frac{E\alpha}{1-\nu} (-T + \langle T \rangle_{\ell}). \quad (3.23)$$

The well known result for a thin, unsupported (bowing not prevented) plate is⁸

$$\sigma_{\rho\rho} = \sigma_{\phi\phi} = \frac{E\alpha}{1-\nu} \left(-T + \langle T \rangle_{\ell} + \frac{12z'}{\ell^2} \langle Tz' \rangle \right) \quad (3.24)$$

where

$$z' \equiv z - \frac{1}{2}\ell$$

and

Sec. C-III

$$\langle T z' \rangle_{\ell} \equiv \frac{1}{\ell} \int_0^{\ell} dz \left(z - \frac{1}{2} \ell \right) T = \frac{1}{2h} \int_{-h}^h dz' z' T$$

with $h = \frac{1}{2} \ell$, determine the bowing of the plate. For $\langle T z' \rangle_{\ell} = 0$ there is no bowing, and (3.24) agrees with (3.23), which was derived for no bending.

The bending factor $12 z' \langle T z' \rangle E \alpha / (1 - \nu) \ell^2$ in (3.24) can be obtained by the detachment method. For the cases considered, the attachment stresses exert torques on the plate, the torques being necessary to prevent bowing. If the bowing is not prevented, the torque must be zero:

$$\frac{1}{2h} \int_{-h}^h dz' z' \sigma = 0. \quad (3.25)$$

The torque, normalized as in (3.25), from the stress $\sigma_{\rho\rho}$ in (3.23) is

$$- \frac{E \alpha}{1 - \nu} \langle T z' \rangle_{\ell}.$$

Adding the stress (const.) z' to (3.23) and solving for the value of the constant (const.) required to satisfy (3.25) gives (3.24).

IV. GENERAL CASE OF STRESSES

Having demonstrated the general features of the method in the preceding cases, the general case in which the temperature is a function of ρ and z will now be considered. The method is simple, but the algebra is slightly involved. The stresses in the detached coating layers are, from (A. 32)

$$\sigma_{\rho\rho id} = \frac{1}{2} \alpha_i E_i \left(\langle T \rangle_R - \langle T \rangle_\rho \right) , \quad (4.1)$$

$$\sigma_{\phi\phi id} = \frac{1}{2} \alpha_i E_i \left[\langle T \rangle_R + \langle T \rangle_\rho - 2T(\rho, z) \right] \quad (4.2)$$

and from (A. 35) the detached coating layer and substrate displacements are

$$u_{id} = B_{\rho i} \alpha_i \langle T \rangle_\rho \rho , \quad (4.3)$$

and

$$u_{Sd} = B_{\rho S} \alpha_S \langle \langle T \rangle_\rho \rangle_{\ell_S} \rho , \quad (4.4)$$

where

$$\langle \langle T \rangle_\rho \rangle_{\ell_S} = \frac{2}{\rho^2 \ell_S} \int_{\ell_F}^{\ell_F + \ell_S} dz \int_0^\rho d\rho \rho T , \quad (4.5)$$

$$\langle T \rangle_\rho \equiv \frac{2}{\rho^2} \int_0^\rho d\rho \rho T(\rho, z) , \quad (4.6)$$

$$\langle T \rangle_R \equiv \frac{2}{R^2} \int_0^R d\rho \rho T(\rho, z) , \quad (4.7)$$

$$B_{\rho i} \equiv \frac{1}{2} (1 + \nu_i) + \frac{1}{2} (1 - \nu_i) \langle T \rangle_R / \langle T \rangle_\rho , \quad (4.8)$$

and

$$B_{\rho S} \equiv \frac{1}{2} (1 + \nu_S) + \frac{1}{2} (1 - \nu_S) \langle \langle T \rangle_R \rangle_{\ell_S} / \langle \langle T \rangle_\rho \rangle_{\ell_S} . \quad (4.9)$$

Sec. C-IV

For $\ell_F \ll \ell_S$, the change in u_S on attachment is negligible, and the attachment displacements of the layers are

$$u_{ia} = -(u_{id} - u_{Sd}) = -B_{\rho i} \alpha_i \langle T_0 \rangle_\rho - B_{\rho S} \alpha_S \langle \langle T \rangle_\rho \rangle_{\ell_S} \rho \quad (4.10)$$

Next consider the strains, which are needed in the expression (3.14) and (3.15) for the stresses. The general expressions are

$$\epsilon_{\rho\rho ia} = \frac{\partial u_{ia}}{\partial \rho} ; \quad \epsilon_{\phi\phi ia} = \frac{u_{ia}}{\rho} . \quad (4.11)$$

From (4.10), (4.11), and

$$\frac{\partial B_{\rho}}{\partial \rho} = B_{\rho} + \rho B'_{\rho}$$

with the prime denoting $\partial/\partial \rho$, the strains are

$$\epsilon_{\rho\rho ia} = -[(B_{\rho i} + \rho B'_{\rho i}) \alpha_i \langle T_0 \rangle_\rho - (B_{\rho S} + \rho B'_{\rho S}) \alpha_S \langle \langle T \rangle_\rho \rangle_{\ell_S}] \quad (4.12)$$

and

$$\epsilon_{\phi\phi ia} = -\left(B_{\rho i} \alpha_i \langle T_0 \rangle_\rho - B_{\rho S} \alpha_S \langle \langle T \rangle_\rho \rangle_{\ell_S} \right) . \quad (4.13)$$

Substituting (4.12) and (4.3) into (3.14) and (3.15) gives

$$\begin{aligned} \sigma_{\rho\rho ia} = & - \frac{E_i}{1 - \nu_i^2} \left\{ [B_{\rho i} (1 + \nu_i) + \rho B'_{\rho i}] \alpha_i \langle T \rangle_\rho \right. \\ & \left. - [B_{\rho S} (1 + \nu_i) + \rho B'_{\rho S}] \alpha_S \langle \langle T \rangle_\rho \rangle_{\ell_S} \right\} \end{aligned} \quad (4.14)$$

and

$$\begin{aligned} \sigma_{\phi\phi ia} = & - \frac{E_i}{1 - \nu_i^2} \left\{ [B_{\rho i} (1 + \nu_i) + \nu_i \rho B'_{\rho i}] \alpha_i \langle T \rangle_\rho \right. \\ & \left. - [B_{\rho S} (1 + \nu_i) + \nu_i \rho B'_{\rho S}] \alpha_S \langle \langle T \rangle_\rho \rangle_{\ell_S} \right\} \end{aligned} \quad (4.15)$$

Sec. C-IV

where

$$\rho B'_{\rho i} = - \frac{(1 - \nu_i) \langle T \rangle_R}{\langle T \rangle_\rho^2} (T - \langle T \rangle_\rho)$$

The general results for the coating-layer stress are

$$\sigma_{\rho\rho i} = \sigma_{\rho\rho id} + \sigma_{\rho\rho ia} \quad (4.16)$$

and

$$\sigma_{\phi\phi i} = \sigma_{\phi\phi id} + \sigma_{\phi\phi ia} \quad (4.17)$$

where $\sigma_{\rho\rho id}$, $\sigma_{\phi\phi id}$, $\sigma_{\rho\rho ia}$, and $\sigma_{\phi\phi ia}$ are given by (4.1), (4.2), (4.14), and (4.15).

For the limiting case of $\rho \rightarrow 0$, we have

$$\lim_{\rho \rightarrow 0} B'_\rho = 0, \quad (4.18)$$

$$\lim_{\rho \rightarrow 0} \langle T_0 \rangle_\rho = T(0, 0),$$

and

$$\lim_{\rho \rightarrow 0} \langle \langle T \rangle \rangle_{\rho \ell_S} = \frac{1}{\ell_S} \int_{\ell_F}^{\ell_F + \ell_S} dz T(0, z) \equiv \langle T_0 \rangle_{\ell_S},$$

and the rather involved general results (4.1), (4.2), (4.12) – (4.15), reduce to the simple result

$$\lim_{\rho \rightarrow 0} \sigma_{\rho\rho i} = \lim_{\rho \rightarrow 0} \sigma_{\phi\phi i} = - \frac{E_i \alpha_i}{1 - \nu_i} \left[T(0, z) - \frac{B_{0S} \alpha_S}{\alpha_i} \langle T \rangle_{\ell_S} \right] \quad (4.19)$$

where

Sec. C-IV

$$B_{0S} = \frac{1}{2} (1 + \nu_S) + \frac{1}{2} (1 - \nu_S) \langle \langle T \rangle_R \rangle_{\ell_S} / \langle T_0 \rangle_{\ell_S} .$$

In (4.18) it was assumed that $\partial T / \partial \rho = 0$ at $\rho = 0$.

This result (4.19) has a number of interesting limiting values:

$$\sigma_{00i} \equiv \lim_{\rho \rightarrow 0} \sigma_{\rho\rho i} = \lim_{\rho \rightarrow 0} \sigma_{\phi\phi i} ,$$

$$\xrightarrow{T = T_0 = \text{const.}} - \frac{\alpha_i E_i T_0}{1 - \nu_i} (\alpha_i - \alpha_S) , \quad (4.19a)$$

$$\xrightarrow{T(\rho)} - \frac{\alpha_i E_i}{1 - \nu_i} \left(T_0 - \frac{\alpha_S}{\alpha_i} B_{0S} \right) , \quad (4.19b)$$

$$\xrightarrow{T(\rho), \alpha_i = \alpha_S, \nu_i = \nu_S} - \frac{1}{2} \alpha_i E_i (T - \langle T \rangle_R) , \quad (4.19c)$$

$$\xrightarrow{T(z)} - \frac{\alpha_i E_i}{1 - \nu_i} \left(T_0 - \frac{\alpha_S}{\alpha_i} \langle T \rangle_{\ell_S} \right) , \quad (4.19d)$$

$$\xrightarrow{T(z), \alpha_i = \alpha_S} - \frac{\alpha_i E_i}{1 - \nu_i} (T_0 - \langle T \rangle_{\ell_S}) , \quad (4.19e)$$

$$\xrightarrow{\text{pulse } (\langle T \rangle_S \cong 0)} - \frac{\alpha_i E_i T_0}{1 - \nu_i} . \quad (4.19f)$$

For the limiting case of $\rho \rightarrow R$, we have

$$\lim_{\rho \rightarrow 0} \frac{\partial \langle T \rangle}{\partial \rho} = - \frac{2}{R} [\langle T \rangle_R - T(R, z)] ,$$

$$\lim_{\rho \rightarrow 0} \rho B' = (1 - \nu) (1 - T(R, z) / \langle T \rangle_R) ,$$

AD-A040 596

XONICS INC SANTA MONICA CALIF
THEORETICAL STUDIES OF HIGH-POWER ULTRAVIOLET AND INFRARED MATE--ETC(U)
DEC 76 M SPARKS, C J DUTHLER

F/G 20/5

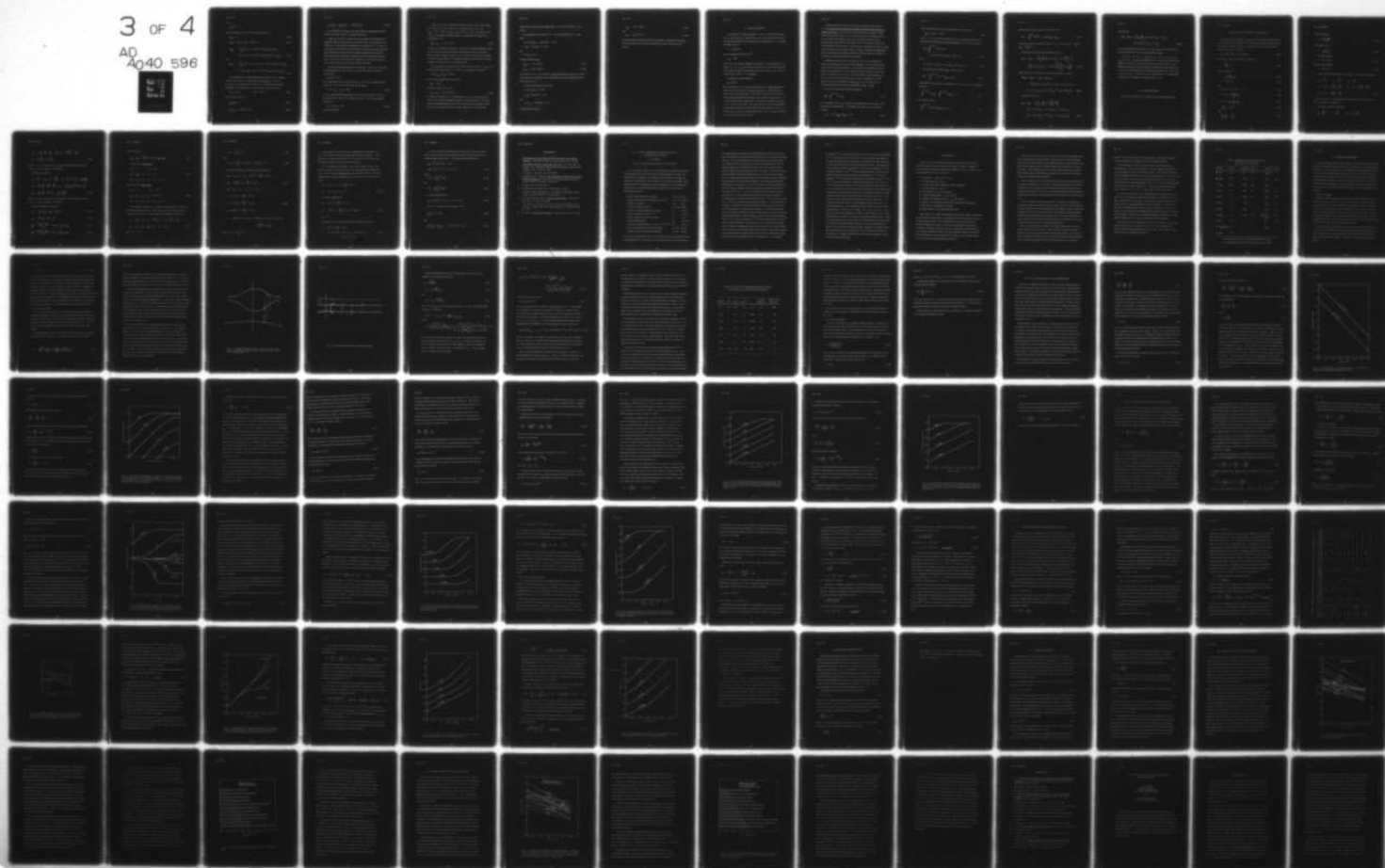
DAHC15-73-C-0127

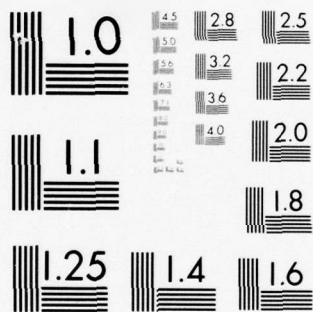
NL

UNCLASSIFIED

3 OF 4

AD
A040 596





Sec. C-IV

and

$$\lim_{\rho \rightarrow R} B = 1 ,$$

and the results (4.1), (4.2), (4.14), and (4.15) become

$$\sigma_{\rho\rho id} = 0 , \quad (4.20)$$

$$\sigma_{\phi\phi id} = \alpha_i E_i [\langle T_0 \rangle_R - T(R, 0)] , \quad (4.21)$$

$$\sigma_{\rho\rho ia} = - \frac{E_i}{1 - \nu_i^2} \left\{ [2 - (1 - \nu_i) T(R, 0) / \langle T_0 \rangle_R] \alpha_i \langle T_0 \rangle_R \right. \\ \left. - [2 + \nu_i - \nu_S - (1 - \nu_S) T(R, 0) / \langle T_0 \rangle_R] \alpha_S \langle \langle T \rangle_R \rangle_{\ell_S} \right\} , \quad (4.22)$$

and

$$\sigma_{\phi\phi ia} = - \frac{E_i}{1 - \nu_i^2} \left\{ [(1 + \nu_i) + \nu_i (1 - \nu_i) (1 - T(R, 0) / \langle T_0 \rangle_R)] \alpha_i \langle T_0 \rangle_R \right. \\ \left. - [(1 + \nu_i) + \nu_i (1 - \nu_S) (1 - T(R, 0) / \langle T_0 \rangle_R)] \alpha_S \langle \langle T \rangle_R \rangle_{\ell_S} \right\} . \quad (4.23)$$

It is possible that the coating could fracture near the rim of the reflector rather than at the center. For example, if $\alpha_i = \alpha_S$ and $\nu_i = \nu_S$, and $T \neq f(z)$, the attachment stresses are zero. For a Gaussian temperature distribution (2.1) truncated at $1/e^2$, the values of $\langle T \rangle_R$ and $T(R)$ are

$$\langle T \rangle_R = 0.432 \quad T(R) = 0.135 , \quad (4.24)$$

and (4.1) and (4.2) give

$$\lim_{\rho \rightarrow R} \sigma_{\rho\rho i} = 0 \quad (4.25)$$

$$\lim_{\rho \rightarrow R} \sigma_{\phi\phi i} = 0.297 \alpha_i E_i T_0 \quad (4.26)$$

Sec. C-IV

$$\lim_{\rho \rightarrow 0} \sigma_{\rho\rho i} = \lim_{\rho \rightarrow 0} \sigma_{\phi\phi i} = -0.284 \alpha_i E_i T_0 . \quad (4.27)$$

The magnitudes of the $\sigma_{\phi\phi i}$ at the center and rim are approximately equal, but the rim, being in tension, is expected to fail first.

In general, however, the properties of the coating layers and substrate are sufficiently different that the failure occurs in the center of the coating ($\rho = 0$). Furthermore, the temperature distribution that is peaked near $z = 0$ at the end of single pulse causes failure at the center of the coating, and in typical repeated-pulse systems the requirement for small optical distortion dictates that the peaked single-pulse temperature essentially determines the fracture threshold. Thus, in most cases, the center of the coating ($\rho = 0$) is expected to fracture first, and the stresses are given by the simple result (4.19).

Consider the following application⁵ as an example. The 45-layer MgO/MgF₂ coating designed⁷ for use at 250 nm has a theoretical surface-temperature increase of⁵

$$T_{\rho}(0, 0) = 47 \text{ K}$$

for a single pulse with $I t_p > 10 \text{ J/cm}^2$ and $t_p = 10^{-6} \text{ s}$ and a molybdenum substrate. For $h = 0.1 \text{ W/cm}^2/\text{K}$, (2.6) and (2.10) give

$$\langle T(0, z) \rangle_{\ell_S} = T_{SC} = 50 \text{ K} \quad (4.28)$$

for the average substrate temperature in repeated-pulse operation. Thus, the temperature of the center of the coating surface ($\rho = z = 0$) in repeated-pulse operation is

$$T_0 \equiv T(0, 0) = 97 \text{ K} \quad (4.29)$$

at the end of a pulse.

Sec. C-IV

For the first case of a single pulse, the stresses at the center of the coating in an MgO layer near the surface are, from (4.19) with $\nu_i = \nu_S = 0.3$, $E_{\text{MgO}} = 36.1 \times 10^6$ psi, $\alpha_{\text{MgO}} = 10.5 \times 10^{-6} \text{ K}^{-1}$, $T(0, 0) = T_\rho(0, 0) = 47 \text{ K}$, $\langle T_0 \rangle_{\ell_S} = 0$ (negligible substrate heating for a single pulse since $\ell_{\text{th}} \ll \ell_S$ according to (2.5)),

$$\sigma_{\rho\rho} = \sigma_{\phi\phi} = -2.55 \times 10^4 \text{ psi} . \quad (4.29)$$

The negative sign denotes compression. Physically, the unheated substrate, which does not expand, constrains the coating, thus causing compressive stresses. Since the tensile strength of MgO is $\sigma_t \cong 2 \times 10^4$ psi and compressive strength of a brittle material typically is approximately eight times greater than the tensile strength, the MgO layers are not expected to fail.

For repeated-pulse operation, with $T(0, 0) = 97 \text{ K}$ from (4.29), $\langle T_0 \rangle_{\ell_S} = 50 \text{ K}$ from (2.6) and (2.10), and $\alpha_S = 5 \times 10^{-6} \text{ K}$ for molybdenum, (2.8) gives

$$\langle \langle T \rangle_R \rangle_{\ell_S} / \langle T \rangle_{\ell_S} = 0.432 ,$$

and the value of B_{0S} defined under (4.19) is

$$B_{0S} = 0.801 .$$

With these results, (4.19) gives

$$\sigma_{\rho\rho} = \sigma_{\phi\phi} = -4.22 \times 10^4 \text{ psi} . \quad (4.30)$$

The surface temperature 97 K is approximately twice as great as single-pulse value of 47 K, but the magnitude of stresses is not twice as great. The reason is that the additional temperature of 50 K extends across the substrate, and the expansion of the substrate makes the relative expansions of the coating and

Sec. C-IV

substrate less than that of the single pulse, for which the substrate is not neutral.

Next consider the stresses at $\rho = R$. From (2.8) and (2.9), for a single pulse

$$T(R, 0)/\langle T_0 \rangle_R = 0.135/0.432 = 0.313 ,$$

$$\langle T_0 \rangle_R = 0.432 (47) = 20.3 K ,$$

and

$$\langle \langle T \rangle_R \rangle_{\ell_S} = 0 ,$$

and (4.22) and (4.23) give

$$\sigma_{\rho\rho ia} = -1.51 \times 10^4 \text{ psi} , \quad (4.31)$$

$$\sigma_{\phi\phi ia} = -1.22 \times 10^4 \text{ psi} . \quad (4.32)$$

The stresses at $\rho = R$ are smaller in magnitude than those at the center, and all four stresses are compressive, thus illustrating the fact that coatings tend to fail at the center ($\rho = 0$).

For the repeated-pulse case, we have

$$T(R, 0)/\langle T_0 \rangle_R = 0.313 ,$$

$$\langle T_0 \rangle_R = 0.432 (97) = 41.9 ,$$

and

$$\langle \langle T \rangle_R \rangle_{\ell_S} = 0.432 (50) = 21.6 ,$$

and (4.22) and (4.23) give

Sec. C-IV

$$\sigma_{\rho\rho} = -2.35 \times 10^4 \text{ psi} \quad (4.33)$$

and

$$\sigma_{\phi\phi} = -1.90 \times 10^4 \text{ psi} . \quad (4.34)$$

The stress values in (4.33) and (4.34), being smaller in magnitude and having the same signs as those of (4.30), again illustrate the failure at the center of the coating.

V. THERMAL EXPANSION

The expansion of a reflector along the z axis, in particular the change in this z -axis expansion as a function of ρ , gives rise to optical distortion that can become greater than the tolerable limit of a practical system. The angular bending of a ray is³

$$\theta = -d\ell_{\text{opd}}/d\rho$$

where the optical-path difference is⁵

$$\ell_{\text{opd}} = 2\Delta\ell$$

where $\Delta\ell$ is the thickness change of the reflector. It is assumed that the rear surface ($z = \ell_F + \ell_S$) of the reflector remains in a plane so that all the thickness change $\Delta\ell$ appears at the front surface of the reflector. The reflector is operated in air; thus, $n - 1$ is negligible.

In addition to the usual expansion

$$\Delta\ell = \int dz \alpha T$$

for the stress-free case, stresses generally give rise to additional expansion (which can be either positive or negative in general). A simple example is a cube of material having volume L^3 that has its temperature increased by T . For unconstrained expansion, the change in the length of an edge is αTL . If the cube is not allowed to expand in the x direction, the expansions along the y and z axes are $\alpha(1 + \nu)TL$. The extra factor of νTL can be understood by considering the compression of the unconstrained cube along the x axis by a distance αTL , which increases the lengths along y and z by $\nu\alpha TL$ according to the definition of the Poisson ratio ν .

Sec. C-V

An important point to be made concerning the expansion of thin reflectors is that the detached stresses tend to cause greater thickness changes than do the attachment stresses. For an uncoated metallic reflector, the thickness change from the attachment stresses is zero. For a thin ($\ell_F \ll \ell_S$) multilayer dielectric coating on a thin substrate ($\ell_S \ll D_S$), the attachment stresses in the substrate can be eliminated from the expression for the thickness change, and the contributions from the layers i of the coating are proportional to $(\nu_i/E_i - \nu_S/E_S)$, which is small for similar materials ($\nu_i/E_i \cong \nu_S/E_S$). Neglecting the attachment-stress contribution to the thickness change $\Delta\ell$ greatly simplifies the calculation and affords an approximation that is often adequate.

Unfortunately, there are cases in which the errors in $\Delta\ell$ resulting from neglecting the attachment stress can be non-negligible, an error in $\Delta\ell$ of approximately thirty percent being possible. For a temperature distribution that is not peaked in the coating, the errors are small since most of $\Delta\ell$ arises in the substrate, for which the error is zero. For a thermally thin coating ($\ell_F \ll \ell_{th}$ in Fig. 1) the errors are small for the same reason. The greatest errors are likely to occur in a thermally thick coating ($\ell_{th} \gtrsim \ell_F$) with $T_{SC} \ll T_p$ in (2.2) and dissimilar materials (great magnitudes of $\nu_i/E_i - \nu_S/E_S$).

The stress in the detached reflector contributes

$$\Delta\ell_d = \int_{\nu}^{\ell_F + \ell_S} dz \epsilon_{zzd} \quad (5.1)$$

to the expansion, where ϵ_{zz} is the strain component for expansion along z , and d denotes the detached system. From Hooke's law, with $\sigma_{zz} = 0$ for the thin reflector,

$$\epsilon_{zzd} = -\nu E^{-1} (\sigma_{\rho\rho d} + \sigma_{\phi\phi d}) + \alpha T. \quad (5.2)$$

Sec. C-V

From (4.1) and (4.2) the sum of the detached stress components is

$$\sigma_{\rho\rho id} + \sigma_{\phi\phi id} = -\alpha_i E_i T \quad (5.3)$$

where $i = 1, 2$, or S , and a constant $\alpha_i E_i \langle T \rangle_R$ was dropped since it does not contribute to optical distortion, being independent of ρ . From (5.1) to (5.3)

$$\begin{aligned} \Delta l_d &= \int_0^{\ell_F + \ell_S} dz \alpha(1+\nu) T \\ &= (1+\nu_F) \alpha_F \ell_F \langle T \rangle_{\ell_F} + \alpha_S (1+\nu_S) \ell_S \langle T \rangle_{\ell_S} , \end{aligned} \quad (5.4)$$

where

$$(1+\nu_F) \alpha_F \equiv [\ell_1 \alpha_1 (1+\nu_1) + \ell_2 \alpha_2 (1+\nu_2)] / (\ell_1 + \ell_2) . \quad (5.5)$$

The attachment contribution Δl_a to Δl is given by

$$\Delta l_a = - \int_0^{\ell_F + \ell_S} dz \nu E^{-1} (\sigma_{\rho\rho a} + \sigma_{\phi\phi a}) , \quad (5.6)$$

which follows from (5.2) with d replaced by a and T by zero. The attachment condition is

$$\int_0^{\ell_F + \ell_S} dz \sigma_{\rho\rho a} = \int_0^{\ell_F + \ell_S} dz \rho_{\phi\phi a} = 0 , \quad (5.7)$$

from which it follows

$$\int_0^{\ell_F + \ell_S} dz \nu_S E_S^{-1} (\sigma_{\rho\rho a} + \sigma_{\phi\phi a}) = 0 . \quad (5.8)$$

Subtracting (5.8) from (5.6) gives the general result

$$\Delta \ell_a = - \int_0^{\ell_F} dz (\nu E^{-1} - \nu_S E_S^{-1}) (\sigma_{\rho\rho a} + \sigma_{\phi\phi a}) . \quad (5.9)$$

The integral vanishes on the interval $\ell_F < z < \ell_F + \ell_S$ since $\nu E^{-1} - \nu_S E_S^{-1} = \nu_S E_S^{-1} - \nu_S E_S^{-1} = 0$.

From (4.14) and (4.15), the ρ dependent terms are

$$\begin{aligned} \sigma_{\rho\rho ia} + \sigma_{\phi\phi ia} = & - \frac{E_i}{1 - \nu_i} \left\{ \alpha_i \left[(1 + \nu_i) \langle T \rangle_\rho - (1 - \nu_i) \frac{\langle T \rangle_R}{\langle T \rangle_\rho} T \right] \right. \\ & \left. - \alpha_S \left[(1 + \nu_S) \langle \langle T \rangle \rangle_{\rho \ell_S} - (1 - \nu_S) \frac{\langle \langle T \rangle_R \rangle_{\ell_S}}{\langle \langle T \rangle_\rho \rangle_{\ell_S}} \langle T \rangle_{\ell_S} \right] \right\} . \end{aligned} \quad (5.10)$$

Subtracting the value of (5.10) at $\rho = R$ from the value at $\rho = 0$ gives

$$\begin{aligned} (\sigma_{\rho\rho ia} + \sigma_{\phi\phi ia})_0 - (\sigma_{\rho\rho ia} + \sigma_{\phi\phi ia})_R = \\ = - \frac{E_i}{1 - \nu_i} \left\{ \alpha_i [(1 + \nu_i) T(0, z) - 2 \langle T \rangle_R + (1 - \nu_i) T(R, z)] \right. \\ \left. - \alpha_S [(1 + \nu_S) \langle T_0 \rangle_{\ell_S} - 2 \langle \langle T \rangle_R \rangle_{\ell_S} + (1 - \nu_S) \langle T(R) \rangle_{\ell_S}] \right\} . \end{aligned} \quad (5.11)$$

From (5.9) and (5.11)

$$\begin{aligned} \Delta \ell_{a0} - \Delta \ell_{aR} = & \frac{\ell_F}{\ell_1 + \ell_2} \sum_{i=1}^2 \left(1 - \frac{\nu_S E_i}{\nu_i E_S} \right) \frac{\nu_i \ell_i}{1 - \nu_i} \\ & \times \left\{ \alpha_i [(1 + \nu_i) \langle T_0 \rangle_{\ell_F} - 2 \langle \langle T \rangle_R \rangle_{\ell_F} + (1 - \nu_i) \langle T_R \rangle_{\ell_F}] \right. \\ & \left. - \alpha_S [(1 + \nu_S) \langle T_0 \rangle_{\ell_S} - 2 \langle \langle T \rangle_R \rangle_{\ell_S} + (1 - \nu_S) \langle T_R \rangle_{\ell_S}] \right\} , \end{aligned} \quad (5.12)$$

Sec. C-V

and from (5.4)

$$\begin{aligned} \Delta \ell_{d0} - \Delta \ell_{dR} = & \frac{\ell_F}{\ell_1 + \ell_2} \sum_{i=1}^2 (1 + \nu_i) \alpha_i (\langle T_0 \rangle_{\ell_F} - \langle T_R \rangle_{\ell_F}) \\ & + \alpha_S (1 + \nu_S) \ell_S (\langle T_0 \rangle_{\ell_S} - \langle T_R \rangle_{\ell_S}). \end{aligned} \quad (5.13)$$

These expressions (5.12) and (5.13) are the general results for the difference between the center and rim values of the thickness change.

For $\nu_1 = \nu_2 = \nu_S = 0.3$, $1 - \nu_S E_i / \nu_i E_S = 0.5$, $\ell_1 \cong \ell_2$, $\alpha_1 \cong \alpha_2 \cong \alpha_3$, $\langle T \rangle_{\ell_S} \ll \langle T \rangle_{\ell_F}$, and equal contributions of the F and S terms to (5.13), the attachment term (5.12) is five percent of the detached term (5.13). For the single-pulse expansion of the MgO/MgF₂: Mo reflector, the attachment term is 3.7 percent of the detached term, according to (5.12) and (5.13). For $\langle T \rangle_{\ell_S}$ of the order of $\langle T \rangle_{\ell_F}$, as for the case of T independent of z for example, the attachment term is negligible, being of the order ℓ_F / ℓ_S .

VI. ACKNOWLEDGMENTS

Several conversations with M. Flannery are gratefully acknowledged.

APPENDIX. USEFUL THERMAL-STRESS RESULTS

The books by Boley and Weiner⁸ and by Johns⁹ on the theory of thermal stress are useful. Most of the results below are from Boley and Weiner. First consider some general results for rectilinear coordinate systems. The linear thermo-electric stress-strain relations are

$$\sigma_{ij} = \lambda \delta_{ij} \epsilon + 2 \mu \epsilon_{ij} - (3\lambda + 2\mu) \delta_{ij} \alpha T \quad , \quad (\text{A.1})$$

where δ_{ij} is the Kronecker delta, the dilatation is

$$\epsilon = \sum_{i=1}^3 \epsilon_{ii} \quad , \quad (\text{A.2})$$

Lamé's constants are

$$\lambda = \frac{\nu E}{(1+\nu)(1-2\nu)} \quad , \quad (\text{A.3})$$

$$\mu = E/2 (1+\nu) \quad , \quad (\text{A.4})$$

and

$$3\lambda + 2\mu = E/(1-2\nu) = 3R \quad , \quad (\text{A.5})$$

$$\lambda + 2\mu = \frac{E(1-\nu)}{(1+\nu)(1-2\nu)} \quad , \quad (\text{A.6})$$

$$\lambda + \mu = \frac{E}{2(1+\nu)(1-2\nu)} \quad , \quad (\text{A.7})$$

$$\frac{\lambda}{\lambda + 2\mu} = \frac{\nu}{1-\nu} \quad , \quad (\text{A.8})$$

and

$$\frac{3\lambda + 2\mu}{\lambda + 2\mu} = \frac{1+\nu}{1-\nu} \quad . \quad (\text{A.9})$$

Sec. C-Appendix

Young's modulus is

$$E = \frac{(3\lambda + 2\mu)\mu}{\lambda + \mu} . \quad (\text{A. 10})$$

The Poisson ratio is

$$\nu = \frac{\lambda}{2(\lambda + \mu)} . \quad (\text{A. 11})$$

The bulk modulus is

$$k = E/3 (1 - 2\nu) , \quad (\text{A. 12})$$

and the shear modulus is

$$G = E/2 (1 + \nu) . \quad (\text{A. 13})$$

The strain-displacement relations are as follows: In Cartesian coordinates,

$$\begin{aligned} \epsilon_{xx} &= \frac{\partial u}{\partial x} , & \epsilon_{yy} &= \frac{\partial v}{\partial y} , & \epsilon_{zz} &= \frac{\partial w}{\partial z} , \\ \epsilon_{xy} &= \frac{1}{2} \gamma_{xy} = \frac{1}{2} \left(\frac{\partial u}{\partial y} + \frac{\partial v}{\partial x} \right) , & \epsilon_{yz} &= \frac{1}{2} \gamma_{yz} = \frac{1}{2} \left(\frac{\partial v}{\partial z} + \frac{\partial w}{\partial y} \right) , \\ \epsilon_{zx} &= \frac{1}{2} \gamma_{zx} = \frac{1}{2} \left(\frac{\partial w}{\partial x} + \frac{\partial u}{\partial z} \right) , \end{aligned} \quad (\text{A. 14})$$

where u , v , and w are the components of the displacement vector in the x , y , and z directions, respectively.

In circular-cylindrical coordinates,

$$\epsilon_{\rho\rho} = \frac{\partial u}{\partial \rho} , \quad \epsilon_{zz} = \frac{\partial w}{\partial z} , \quad \epsilon_{\phi\phi} = \frac{u}{\rho} + \frac{1}{\rho} \frac{\partial v}{\partial \phi} ,$$

Sec. C-Appendix

$$\begin{aligned}\epsilon_{\rho\phi} &= \frac{1}{2} \left(\frac{1}{\rho} \frac{\partial u}{\partial \phi} + \frac{\partial v}{\partial \rho} - \frac{v}{\rho} \right), \quad \epsilon_{\rho z} = \frac{1}{2} \left(\frac{\partial u}{\partial z} + \frac{\partial w}{\partial \rho} \right), \\ \epsilon_{z\phi} &= \frac{1}{2} \left(\frac{\partial v}{\partial z} + \frac{1}{\rho} \frac{\partial w}{\partial \phi} \right),\end{aligned}\quad (\text{A. 15})$$

where u , v , and w represent here the components of the displacement vector in the ρ , ϕ , and z directions, respectively.

In spherical coordinates

$$\begin{aligned}\epsilon_{rr} &= \frac{\partial u}{\partial r}, \quad \epsilon_{\theta\theta} = \frac{u}{r} + \frac{1}{r} \frac{\partial v}{\partial \theta}, \quad \epsilon_{\phi\phi} = \frac{u}{r} + \frac{v}{r} \cot \theta + \frac{1}{r \sin \theta} \frac{\partial w}{\partial \phi}, \\ \epsilon_{r\theta} &= \frac{1}{2} \left(\frac{1}{r} \frac{\partial u}{\partial \theta} + \frac{\partial v}{\partial r} - \frac{v}{r} \right), \quad \epsilon_{r\phi} = \frac{1}{2} \left(\frac{1}{r \sin \theta} \frac{\partial u}{\partial \phi} + \frac{\partial w}{\partial r} - \frac{w}{r} \right), \\ \epsilon_{\theta\phi} &= \frac{1}{2} \left(\frac{1}{r} \frac{\partial w}{\partial \theta} - \frac{\cot \theta}{r} w + \frac{1}{r \sin \theta} \frac{\partial v}{\partial \phi} \right),\end{aligned}\quad (\text{A. 16})$$

where u , v , and w represent here the components of the displacement vector in the r , θ , and ϕ directions, respectively.

In circular cylindrical coordinates,

$$\epsilon_{zz} = -\frac{\nu}{1-\nu} (\epsilon_{\rho\rho} + \epsilon_{\phi\phi}) + \frac{1+\nu}{1-\nu} \alpha T, \quad (\text{A. 17})$$

$$\epsilon_{zz} = -\frac{\nu}{E} (\sigma_{\rho\rho} + \sigma_{\phi\phi}) + \alpha T, \quad (\text{A. 18})$$

$$\sigma_{\rho\rho} = \frac{E(\epsilon_{\rho\rho} + \nu\epsilon_{\phi\phi})}{1-\nu^2} + E\alpha T \frac{\nu}{(1-\nu)(1-2\nu)}, \quad (\text{A. 19})$$

$$\sigma_{\phi\phi} = \frac{E(\epsilon_{\phi\phi} + \nu\epsilon_{\rho\rho})}{1-\nu^2} + E\alpha T \frac{\nu}{(1-\nu)(1-2\nu)}, \quad (\text{A. 20})$$

Sec. C- Appendix

and for $\epsilon_{\rho\rho} = \epsilon_{\phi\phi}$,

$$\sigma_{\rho\rho} = \sigma_{\phi\phi} = \frac{E\epsilon_{\rho\rho}}{1-\nu} + E\alpha T \frac{\nu}{(1-\nu)(1-2\nu)} \quad . \quad (A.21)$$

For the case of plane stress:

$$\begin{aligned} \sigma_{zz} &= 0 , & \epsilon_{zz} &= \alpha T , \\ \epsilon_{\rho\rho} &= \epsilon_{\phi\phi} = \epsilon_{xx} = \epsilon_{yy} = \alpha T , & (A.22) \\ \epsilon_{\rho\phi} &= \epsilon_{\rho z} = \epsilon_{\phi z} = \epsilon_{xy} = \epsilon_{xz} = \epsilon_{yz} = 0 . \end{aligned}$$

and for the case of plane strain:

$$\begin{aligned} \epsilon_{zz} &= 0 , & \sigma_{zz} &= -\alpha E T , \\ \epsilon_{\rho\rho} &= \epsilon_{\phi\phi} = \epsilon_{xx} = \epsilon_{yy} = (1+\nu)\alpha T , & (A.23) \\ \epsilon_{\rho\phi} &= \epsilon_{\rho z} = \epsilon_{\phi z} = \epsilon_{xy} = \epsilon_{xz} = \epsilon_{yz} = 0 . \end{aligned}$$

For a thin plate (thickness $\ell \equiv 2h$ along z much less than L , where L is the shortest dimension in the x - y plane) with no surface traction and with the temperature a function of z only, the plane-stress conditions apply, and

$$\begin{aligned} \sigma_{\rho\rho} &= \sigma_{\phi\phi} = \sigma_{xx} = \sigma_{yy} = \frac{\alpha E}{1-\nu} \left[-T + \langle T \rangle_{\ell} + \frac{12z'}{\ell^2} \langle Tz' \rangle_{\ell} \right] , \\ \sigma_{zz} &= \sigma_{\phi z} = \sigma_{\rho z} = \sigma_{\phi\rho} = \sigma_{xy} = \sigma_{yz} = \sigma_{zx} = 0 , & (A.24) \end{aligned}$$

where $z' \equiv z - \frac{1}{2}\ell$,

Sec. C-Appendix

$$\langle T \rangle_{\ell} \equiv \frac{1}{\ell} \int_0^{\ell} dz T \quad , \quad (\text{A.25})$$

and

$$\langle Tz' \rangle_{\ell} \equiv \frac{1}{\ell} \int_0^{\ell} dz \left(z - \frac{1}{2}\ell \right) T = 2h \int_{-h}^h dz' z' T \quad . \quad (\text{A.26})$$

The strain components and displacement components are

$$\begin{aligned} \epsilon_{\rho\rho} = \epsilon_{\phi\phi} = \epsilon_{xx} = \epsilon_{yy} &= \alpha \left(\langle T \rangle_{\ell} + \frac{12z'}{\ell^2} \langle Tz' \rangle_{\ell} \right) \quad , \\ \epsilon_{zz} &= -\frac{2\nu\alpha}{1-\nu} \left(\langle T \rangle_{\ell} + \frac{12z'}{\ell^2} \langle Tz' \rangle_{\ell} \right) \quad , \end{aligned} \quad (\text{A.27})$$

$$\epsilon_{\rho\phi} = \epsilon_{\rho z} = \epsilon_{\phi z} = \epsilon_{xy} = \epsilon_{yz} = \epsilon_{zx} = 0 \quad ,$$

$$\begin{aligned} u_x &= \alpha x \left(\langle T \rangle_{\ell} + \frac{12z'}{\ell^2} \langle Tz' \rangle_{\ell} \right) \quad , \\ v_y &= \alpha y \left(\langle T \rangle_{\ell} + \frac{12z'}{\ell^2} \langle Tz' \rangle_{\ell} \right) \quad , \\ u_{\rho} &= \alpha \rho \left(\langle T \rangle_{\ell} + \frac{12z'}{\ell^2} \langle Tz' \rangle_{\ell} \right) \quad , \end{aligned} \quad (\text{A.28})$$

$$\begin{aligned} w &= -6\alpha\rho^2\ell^{-2} \langle Tz' \rangle_{\ell} + \alpha(1-\nu)^{-1} \left[(1+\nu)z' \langle T \rangle_{z'} - 2\nu z' \langle T \rangle_{\ell} \right. \\ &\quad \left. - \frac{12\nu z'^2}{\ell^2} \langle Tz' \rangle_{\ell} \right] \quad , \end{aligned}$$

$$\text{where} \quad \langle T \rangle_{z'} \equiv \int_0^{z'} dz' T \quad .$$

Sec. C-Appendix

It was shown in Sec. III that the stress-component form containing $\langle Tz' \rangle_\ell$ in (A.24) is related to torques on the plate and to bowing of the plate. In particular, if the bowing is prevented, the $\langle Tz' \rangle_\ell$ term in (A.24) is absent, and the torque resulting from the attachment stress is zero.

For a rectangular beam of depth $\ell \equiv 2h$ (z axis), width b (y axis), and length L (x axis), with $b \ll L$ and $2h \ll L$, and temperature varying along z only, the plane-stress conditions apply (since the beam is thick). The stress components are, with all coordinates (x, y, z) measured from the center of the beam,

$$\begin{aligned}\sigma_{xx} &= \alpha E \left(-T + \langle T \rangle_\ell + \frac{12z'}{\ell^2} \langle Tz' \rangle_\ell \right), \\ \sigma_{yy} &= \sigma_{zz} = \sigma_{xy} = \sigma_{zy} = 0.\end{aligned}\quad (\text{A.29})$$

The strain components are

$$\begin{aligned}\epsilon_{xx} &= \alpha \left(\langle T \rangle_\ell + \frac{12z'}{\ell^2} \langle Tz' \rangle_\ell \right), \\ \epsilon_{zz} &= -\alpha \nu \left(\langle T \rangle_\ell + \frac{12z'}{\ell^2} \langle Tz' \rangle_\ell \right) + \frac{1+\nu}{E} \alpha T, \\ \epsilon_{xz} &= 0.\end{aligned}\quad (\text{A.30})$$

The displacement components are (aside from rigid-body motions)

$$\begin{aligned}u_x &= x \left(\langle T \rangle_\ell + \frac{12z'}{\ell^2} \langle Tz' \rangle_\ell \right), \\ w &= -6 \langle Tz' \rangle_\ell (x/\ell)^2 - \alpha \nu \left(z' \langle T \rangle_\ell + 6(z'/\ell)^2 \langle Tz' \rangle_\ell \right) \\ &\quad + \alpha E^{-1} (1+\nu) \langle T \rangle_z.\end{aligned}\quad (\text{A.31})$$

Sec. C-Appendix

For a thin circular disc with thickness l much less than radius R , with no surface traction and with the temperature a function of ρ only, the plane-stress conditions apply (since $l \ll R$). The nonzero stress components are

$$\begin{aligned}\sigma_{\rho\rho} &= \frac{1}{2} \alpha E (\langle T \rangle_R - \langle T \rangle_\rho) , \\ \sigma_{\phi\phi} &= \frac{1}{2} \alpha E (\langle T \rangle_R + \langle T \rangle_\rho - 2T) ,\end{aligned}\tag{A.32}$$

where

$$\langle T \rangle_R \equiv \frac{2}{R^2} \int_0^R d\rho \rho T \tag{A.33}$$

and

$$\langle T \rangle_\rho \equiv \frac{2}{\rho^2} \int_0^\rho d\rho \rho T . \tag{A.34}$$

The radial displacement is

$$u_\rho = \frac{1}{2} \alpha \rho \left[(1 - \nu) \langle T \rangle_\rho + (1 + \nu) \langle T \rangle_R \right] . \tag{A.35}$$

For $\rho \rightarrow 0$, if there is no heat source at $\rho = 0$,

$$\lim_{\rho \rightarrow 0} \langle T \rangle_\rho = T(0) \tag{A.36}$$

and

$$\lim_{\rho \rightarrow 0} \sigma_{\rho\rho} = \lim_{\rho \rightarrow 0} \sigma_{\phi\phi} = -\frac{1}{2} \alpha E [T(0) - \langle T \rangle_R] . \tag{A.37}$$

Sec. C-References

REFERENCES

1. Proceedings of the Fifth Annual Conference on Infrared Laser Window Materials, sponsored by DARPA, Las Vegas, Nevada, Dec. 1-4, 1975.
2. Laser Induced Damage in Optical Materials: 1975, A. J. Glass and A. H. Guenther, eds., NBS Special Publication 435, Proceedings of a Symposium at Boulder, Colo., July 29-31, 1975.
3. M. Sparks, J. Appl. Phys. 42, 5029 (1971).
4. M. Sparks and C. J. Duthler, Theoretical Studies of High-Power Ultraviolet and Infrared Materials, Xonics, Inc. Fifth Technical Report, under Contract No. DAHC 15-73-C-0127, 30 June 1975.
5. M. Sparks, Sec. A of this report.
6. Phil Baumeister and Aded Arnon, Applied Optics, in press.
7. S. Holmes, private communication. Dr. Holmes' coating and the coating of Ref. 6 are discussed in Sec. A of this report.
8. B. A. Boley and J. H. Weiner, Theory of Thermal Stress, John Wiley & Sons, Inc., New York, N. Y., 1960.
9. The values of $h = 0.1 \text{ W/cm}^2 \text{ K}$ and $\ell_S = 1 \text{ mm}$ are not difficult to achieve in practice. Compare the state-of-the-art values of $h = 10 \text{ W/cm}^2 \text{ K}$ and $\ell_S = 0.5$.⁵
10. D. J. Johns, Thermal Stress Analysis, Pergamon Press, New York, 1965.

D. FAILURE THRESHOLDS OF NEAR-ULTRAVIOLET TRANSPARENT MATERIALS

C. J. Duthler

Xonics, Incorporated, Santa Monica, California 90401

(1) Various failure mechanisms have been studied for repetitively pulsed and for singly pulsed lasers operating in the near-ultraviolet spectral region. The following failure thresholds, in $\text{J}/\text{cm}^2/\text{pulse}$ (or MW/cm^2 during the pulse), are calculated for one-centimeter-thick windows for use at 350 nm wavelength, 1 μsec pulse duration, 10^3 Hz repetition rate, 60 sec operating time, and allowed optical distortion $\lambda/40$ in the optical path difference (values in parentheses are for single-pulse operation):

Thermal optical distortion, two-photon	2.4×10^{-2}	(2.9)*
Thermal optical distortion, extrinsic $\beta = 10^{-4} \text{ cm}^{-1}$	3.3×10^{-2}	$(2 \times 10^3)^*$
Fracture, two-photon	0.22	(14)
Fracture, inclusion or clusters	~ 2 to ~ 500	(same)
Free-carrier optical distortion, two-photon	2.2	(same)
Fracture, extrinsic $\beta = 10^{-4} \text{ cm}^{-1}$	3.3	(2×10^5)
Thermal optical distortion, three-photon	28	$(440)^*$
Fracture, three-photon	89	(1.4×10^3)
Free-carrier optical distortion, extrinsic $\beta = 10^{-4} \text{ cm}^{-1}$	140	(same)
Free-carrier optical distortion, three-photon	1.8×10^3	(same)
Nonlinear refractive index optical distortion	3.1×10^3	(same)

In view of the approximations made in the calculations, failure thresholds for 250 nm wavelength operation are expected to be essentially the same as those listed above.

Sec. D

The major difference between the two wavelength regions is that many materials that are limited by three-photon absorption at 350 nm become two-photon absorbing at 250 nm. (2) It is conceivable that an adaptive optical system [with a typical time constant of 10^{-4} sec for low-power reflectors extrapolated to 10^{-3} sec for high-power (greater mass) reflectors] could be used in the repetitive pulse to attain the single-pulse optical distortion values, as marked * above. In this case, by using materials out of the two-photon region, the overall (lowest) thresholds are ~ 2 to ~ 500 J/cm²/pulse for inclusion or cluster damage, and 3.3 J/cm²/pulse for thermal fracture from extrinsic absorption. The limiting threshold without adaptive optics is much lower, 3.3×10^{-2} J/cm²/pulse, for thermal optical distortion from extrinsic absorption (even assuming that the absorption coefficient can be reduced to 10^{-4} cm⁻¹). (3) For the repetitively pulsed system, at a fixed repetition rate, the thermal-distortion and thermal-fracture pulse-intensity thresholds increase with decreasing pulse durations as t^{-1} for extrinsic absorption and as $t^{-1/2}$ for two-photon and three-photon absorption. The average-intensity threshold is independent of the pulse duration for extrinsic absorption and varies as $t^{1/2}$ for two-photon and three-photon absorption. At a fixed pulse duration, the pulse-intensity thresholds for thermal distortion and thermal fracture increase with decreasing numbers of pulses (product of repetition rate and total operating time) as q^{-1} for extrinsic absorption, $q^{-1/2}$ for two-photon absorption, and $q^{-1/4}$ for three-photon absorption. If the repetition rate is constant and the operating period is changed, the dependence of the average intensity on the number of pulses is the same as the above dependence of the pulse-intensity on the number of pulses. If the operating period is constant and the repetition rate is changed, the average intensity varies with the number of pulses as independent of q for extrinsic

Sec. D

absorption, $q^{1/2}$ for two-photon absorption, and $q^{3/4}$ for three-photon absorption.

(4) For single-pulse operation, the nonlinear index threshold is independent of the pulse duration and becomes relatively more important with shorter durations. The other thresholds increase with decreasing pulse durations, with free-carrier optical distortion having the dependences t^{-1} for extrinsic absorption, $t^{-1/2}$ for two-photon absorption, and $t^{-1/3}$ for three-photon absorption. The thermal distortion and thermal fracture thresholds are proportional to t^{-1} for extrinsic absorption, $t^{-2/3}$ for two-photon absorption at pulse durations less than 10^{-8} sec, $t^{-1/2}$ for two-photon absorption at pulse durations greater than 10^{-8} sec, and $t^{-1/2}$ for three-photon absorption. The inclusion threshold is proportional to t^{-1} .

(5) In a comparison of our previous theoretical estimates of the two-photon absorption coefficient with eight experimental values, the absorption coefficient in alkali iodides and alkali bromides is typically underestimated by a factor of two. This agreement is better than that previously predicted for the crude estimate. The absorption coefficient for ZnO is overestimated by a factor of 20, which is the greatest disagreement. (6) Reasonable materials that do not suffer two-photon absorption for use at 350 nm are LiF, MgF_2 , CaF_2 , BeO, NaF, SrF_2 , BaF_2 , Al_2O_3 , SiO_2 (fused and crystalline), and MgO. Of these materials, LiF, MgF_2 , and perhaps CaF_2 and BeO, do not suffer two-photon absorption at 250 nm. Technical considerations, such as the positions of F-bands and other factors that limit the achievable extrinsic absorption coefficients, are more important than are figures of merit in choosing candidate materials. Sapphire is noteworthy because the fracture temperature is estimated to be a factor of 10 greater than that for other materials. Alkaline-earth fluorides tend to be less susceptible to thermal distortion than other materials.

I. INTRODUCTION

Recently, interest has focused on high-power lasers operating in the near-ultraviolet spectral region, particularly near 350 nm wavelength. Although the laser system has not yet been selected, xenon fluoride is a prime candidate. Some desired properties of the laser system are:

- wavelength: $\lambda = 350 \text{ nm}$ ($\hbar\omega = 3.5 \text{ eV}$).
- laser pulse duration: $1 \mu\text{sec}$.
- repetition rate: 100 Hz (100 pps) to 1000 Hz (1000 pps).
- total operating time: 60 sec.
- energy density: $I_p t_p = 10 \text{ J/cm}^2\text{-pulse}$.
- irradiance (during pulse): $I_p = 10^7 \text{ W/cm}^2$.
- irradiance (averaged over 60 sec): $I_{av} = 10^3 \text{ W/cm}^2$.
- pressure: two atmospheres nominal; four atmospheres during pulse.
- pulse shape: rectangular with no spikes.
- optical tolerance: $1/40$ wavelength per element.

In this report, the irradiance thresholds of various failure modes of transparent optical elements are examined for a repetitively pulsed laser operating in the near-ultraviolet spectral region. The wavelength of 350 nm is used for calculation purposes throughout this report. In view of the approximations required in the calculations, thresholds for 250 nm operation are expected to be essentially the same as those calculated for 350 nm. The major difference between materials for these wavelengths is that some materials that are limited by three-photon absorption at 350 nm suffer two-photon absorption at 250 nm.

Sec. D-I

Transparent materials used as laser windows must survive each individual pulse and overall heating from repeated pulses. Important failure mechanisms during a single pulse are localized fracture from absorbing inclusions, optical distortion from mobile electrons liberated by the absorbed radiation, thermal distortion, and thermal fracture. With repeated pulses the thermally-induced effects become relatively more important since cooling during the operating period is generally not effective and heating by individual pulses integrates.

The two mechanisms of free-carrier optical distortion and thermal distortion are not completely independent. Free-carrier optical distortion results from radiation scattering by mobile conduction-band electrons and valence-band holes that were created by the absorption. These excited electrons contribute to the heating both by contributing directly to the absorption and by converting their excitation energy into heat.

Another mechanism, that initially appears to be independent of absorption, is optical distortion from the nonlinear refractive index. However, this mechanism is intimately related to two-photon absorption with the nonlinear refractive index being associated with the real part of the third-order susceptibility and with two-photon absorption being associated with the imaginary part. It has been shown that a resonance enhancement of the nonlinear index may occur at frequencies near one-half the band gap, but outside the two-photon absorption region.¹

There are other nonlinear mechanisms for optical distortion that are not considered explicitly in this report since, with the long pulse durations of current interest, they occur at greater intensities than those given above. One such mechanism is enhanced, stimulated Raman scattering which results in optical distortion since the radiation frequency is shifted, and heating because it is an inelastic

Sec. D-1

process.² Other unusual types of "optical distortion" are frequency doubling or frequency tripling, where allowed by symmetry and index matching.

Several candidate materials are listed in Table I along with their optical absorption edge. This list is not exhaustive, and some listed materials may not be viable candidates except in thin-film applications. Three-photon absorption of 350 nm wavelength radiation will not occur if the absorption edge is less than 117 nm (greater than 10.6 eV). Materials satisfying this condition are LiF and MgF₂. Materials having an absorption edge greater than 7.1 eV, so that two-photon absorption does not occur, but less than 10.6 eV, so that three-photon absorption does occur, include NaF, CaF₂, SrF₂, Al₂O₃, SiO₂, BeO and perhaps MgO.

For 250 nm wavelength operation, materials having an absorption edge greater than 9.9 eV are required to avoid two-photon absorption. Such materials are LiF, MgF₂, and perhaps CaF₂ and BeO. The glass BeF₂ is under consideration as a window material. Its absorption edge is at small wavelength. (A value of 83 nm appearing in unpublished works surely is incorrect; compare 105 nm for LiF.) However, BeF₂ is hygroscopic, and difficulties have been encountered in manufacturing good glass. Solutions to the manufacturing problems and protective coating problems should render BeF₂ glass a good window-material candidate.

Besides having large absorption edges, fluoride materials may have desirable chemical properties for use with lasers, such as XeF, that contain fluorine. Oxides tend to have good mechanical properties, but may suffer excessive absorption and may not be compatible with fluorine.

Table I. Candidate transparent materials for use with a 350 nm wavelength laser.

Material	E_a (eV)	Material	E_a (eV)	Material	E_a (eV)
●● LiF	11.8	KF	9.0	Na_3AlF_6	
●● MgF_2	11.0	LiCl	7.4	ThF_4	4.96
● CaF_2	10.0	NaCl	6.8	Si_2O_3	
● BeO	10	KCl	6.9	ThO_2	5.8
● NaF	9.7	PbF_2	6.7	ZrO_2	4.6
● SrF_2	9.6	AlF_3		HfO_2	5.2
● BaF_2	9.1	CeF_3		Y_2O_3	~ 6
● Al_2O_3	8.8	● LaF_3	9.2	●● BeF_2	14.9
● SiO_2	8.4			glass	
● SiO_2 (fused)	7.8			BN	6.2
● MgO	7.1			Si_3N_4	

●● reasonable material with no 3-photon absorption at 350 nm

● reasonable material with no 2-photon absorption at 350 nm

II. ABSORPTION COEFFICIENTS

In the near-ultraviolet and vacuum-ultraviolet spectral regions, the optical transmission of transparent materials is limited by either intrinsic or extrinsic electronic transitions. Two-photon absorption is the dominant intrinsic absorption mechanism in materials having an absorption-edge energy greater than the photon energy, but less than twice the photon energy. Three or more photons are required for band-to-band transitions in materials having an absorption-edge energy two or more times greater than the photon energy. Extrinsic absorption is expected to be dominant at low intensities in materials whose intrinsic absorption is limited by multiphoton absorption.

1. Extrinsic Absorption.

Currently, many uv transparent materials have absorption coefficients in the range from 10^{-1} cm^{-1} to 10 cm^{-1} . These large absorption coefficients are thought to arise from donor levels in the band gap with the absorption of a photon exciting the electron to the conduction band. Other possibilities are transitions between donor levels in the gap or transitions from the valence band to acceptor levels. It may be expected that materials improvement programs will result in much lower extrinsic absorption coefficients, perhaps to the current state-of-the-art level of approximately 10^{-4} cm^{-1} that is being achieved with infrared materials.

At high intensities the absorption may be dominated by intrinsic multiphoton absorption, since the multiphoton absorption increases with increasing intensity. Also at high intensities or with long irradiation times, the donor levels may become depleted (or the acceptor levels filled). The extrinsic absorption coefficient can be written

$$\beta = \sum_i N_i \sigma_i, \quad (2.1)$$

where N_i and σ_i are the concentration and absorption cross section, respectively, of the i^{th} absorbing species. Depletion of strongly absorbing species will be most likely because of both the larger cross section and smaller number for a given absorption coefficient. An overall absorption coefficient of 10^{-4} cm^{-1} requires a concentration of 10^{12} cm^{-3} strongly absorbing impurities having a cross section of 10^{-16} cm^2 , or 10^{16} cm^{-3} weakly absorbing impurities with a cross section of 10^{-20} cm^{-1} . Upon depletion of the donor levels, the absorption coefficient will either increase or decrease, depending on the relative magnitudes of the impurity cross section and the free-carrier cross section. This is discussed further in the following section.

2. Two-Photon Absorption.

There have been no measurements of multiphoton absorption coefficients in ultraviolet-transmitting materials. Theoretical estimates are difficult to make for nearly all materials because of incomplete knowledge in most materials of the band structure, oscillator strengths, importance of many-body effects, etc. The origin of the linear absorption edge in a material as simple as LiF is still being debated.

Using perturbation theory, the two-photon absorption coefficient for transitions from an initial state denoted by i to a final state denoted by f can be written^{3,4}

$$\beta_2 = \frac{4\pi\epsilon^{1/2}}{\hbar c n_L} \sum_i \sum_f \delta(\tilde{E}) \left| \sum_h \frac{\mathcal{H}_{fh} \mathcal{H}_{hi}}{E_f - E_h - \hbar\omega} \right|^2, \quad (2.2)$$

Sec. D-II

where ϵ is the dielectric constant, n_L is the density of laser photons, ω is the laser frequency, $\delta(\tilde{E})$ is an energy-conserving delta function with $\tilde{E} = E_f - E_i - 2\hbar\omega$, \mathcal{K}_{fh} and \mathcal{K}_{fi} are transition matrix elements between the subscripted states. The transition matrix elements are summed over all possible intermediate states denoted by h .

It is expected that transitions involving one particular intermediate state will be dominant. For simplicity, the three-level band structure shown in Fig. 1 is used. This model system, which may apply to alkali halides, has a filled valence band denoted by v , an unfilled conduction band denoted by c_1 , and an upper unfilled conduction band denoted by c_2 . The minimum band gap occurs at the zone center and has a magnitude greater than the photon energy. An energy difference between the conduction and valence bands equal to twice the photon energy occurs at a nonzero k value. In the terminology of perturbation theory, virtual transitions take place between the valence band on the upper conduction band, and between the upper conduction band and the lower conduction band.

Some other possibilities for the intermediate state are shown in Fig. 2, where the dashed line below the conduction band denotes exciton levels. In the diagram labeled 1, the exciton level is the intermediate state. In the second diagram, an electron from a lower valence band is first excited to the conduction band, and then the hole in the lower conduction band is filled by an electron from the upper conduction band. In the third diagram, an electron is first excited to the conduction band, and then an intraconduction band transition, with the simultaneous creation of a phonon, takes place. Other transitions are possible, and in materials with large band gaps, the exciton level may be the final state. Present theoretical knowledge is insufficient to predict which is dominant.

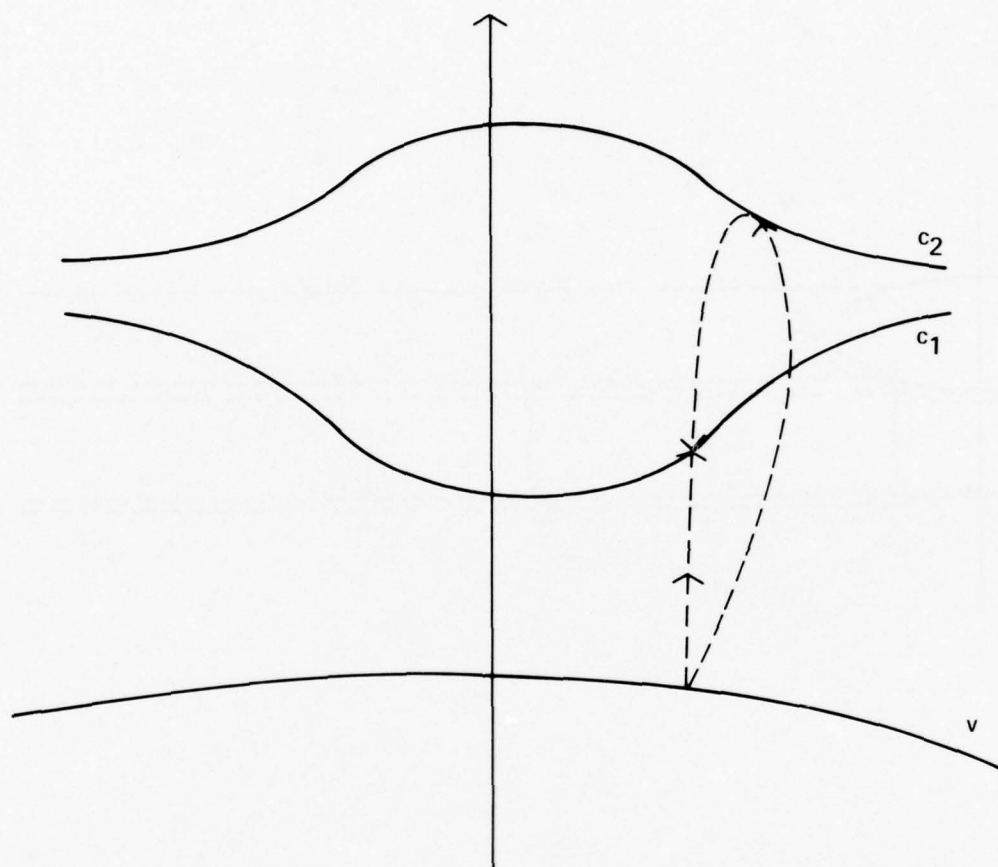


Fig. 1. Two-photon absorption exciting an electron from the valence band to the conduction band with an upper-conduction band serving as the intermediate state.

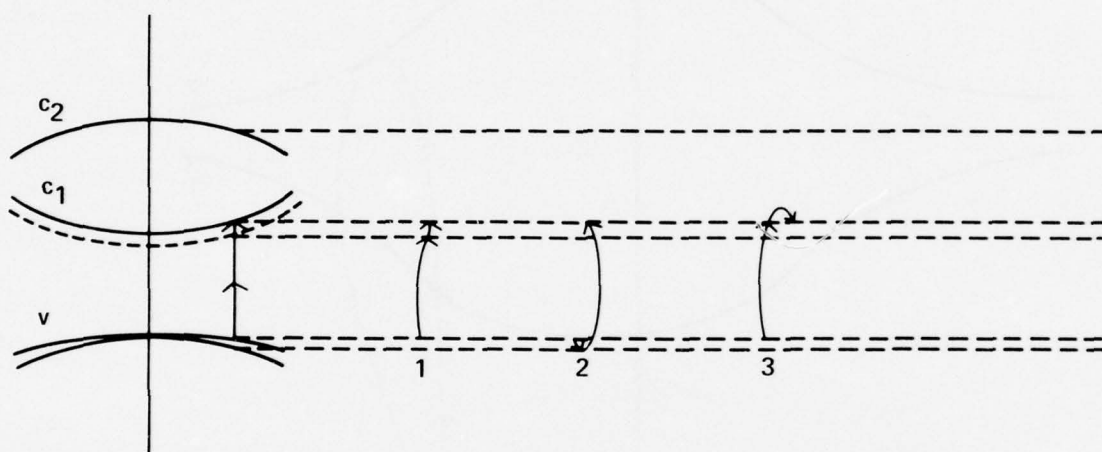


Fig. 2. Other intermediate states for two-photon absorption.

Sec. D-II

Using the band structure in Fig. 1, the band energies as a function of k are assumed to be parabolic and are written:

$$E_v = \frac{\hbar^2 k^2}{2m} \alpha_v, \quad (2.3)$$

$$E_{c_1} = E_g + \frac{\hbar^2 k^2}{2m} \alpha_{c_1}, \quad (2.4)$$

and

$$E_{c_2} = E_{c_2 v} + \frac{\hbar^2 k^2}{2m} \alpha_{c_2}, \quad (2.5)$$

where the α 's are the inverse effective mass ratios, $\alpha = m/m^* = (\hbar^2/d^2E/dk^2)$.

Using $n_L = I\epsilon^{1/2}/c\hbar\omega$ and

$$|\mathcal{H}_{fh}|^2 = |\mathcal{H}_{c_1 c_2}|^2 = \frac{3\pi e^2}{m\omega V} E_{c_1 c_2} f_{c_1 c_2} \quad (2.6)$$

yields

$$\beta_2 = \frac{18\sqrt{2} \pi e^4 f_{c_2 v} f_{c_2 c_1}}{c^2 m^{1/2} (\alpha_v + \alpha_c)^{3/2} (\hbar\omega)^3} \frac{(2\hbar\omega - E_g)^{1/2} E_{c_2 v} E_{c_2 c_1} I}{\left[E_{c_2 v} - \left(\frac{\alpha_{c_2} - \alpha_v}{\alpha_v + \alpha_{c_1}} \right) (2\hbar\omega - E_g) - \hbar\omega \right]^2}. \quad (2.7)$$

In view of the crudeness of the model, it is further approximated that the two conduction bands have the same mass $\alpha = \alpha_{c_1} = \alpha_{c_2}$. The inverse effective mass of the valence bands is less than the error in the effective masses of the conduction bands, and hence, is taken to be zero. Approximating, $E_{c_2 v} = 2E_g$, and evaluating the constants in Eq. (2.7) yields

Sec. D-II

$$\beta_2 = (1.6 \times 10^{-43} \text{ erg}^{3/2} \text{ sec cm}) \frac{f_{c_2 v} f_{c_2 c_1}}{(\alpha)^{3/2}} \frac{1}{(\hbar \omega)^3} \times \frac{(2\hbar \omega - E_g)^{1/2} E_{c_2 v} E_{c_2 c_1} I}{\left[2 E_g - (2\hbar \omega - E_g) - \hbar \omega\right]^2} \quad (2.8)$$

We wish to write β_2 in the form

$$\beta_2 = (I/I_0) (1 \text{ cm}^{-1}), \quad (2.9)$$

where I_0 is the characteristic intensity at which β_2 equals 1 cm^{-1} . The expression for I_0 obtained from Eq. (2.8) is not convenient. Rather, it is useful to have an expression in which explicit dependence of I_0 on each of the parameters is clear. To derive such an expression, Eq. (2.8) was evaluated for $\hbar \omega = 3.54 \text{ eV}$, $E_g = 1.9\hbar \omega$, $\alpha = 1$, $f_{c_2 c_1} = 1$, and $f_{c_2 v} = 1$. Each of these parameters was then varied independently, and the dependence of I_0 on each parameter was fit to a power law:

$$I_0 = (0.174) (f_{c_2 v} f_{c_2 c_1})^{-1} (\hbar \omega / 3.5 \text{ eV})^{2.5} (\alpha)^{1.5} (\gamma / 0.1)^{-0.5} \text{ GW/cm}^2, \quad (2.10)$$

where γ is a measure of the distance of the final state above the band gap, obtained from $E_g = (2 - \gamma)\hbar \omega$. It was noticed from graphical plots that the power-law dependence was a good fit to I_0 from Eq. (2.8), even when the parameters were varied by a factor of ten and when two parameters were varied at the same time.

Subject to all the limitations of the model, Eq. (2.10) predicts an explicit 2.5-power dependence of I_0 on the frequency ω . That is, if two different frequencies and two different materials are used such that the f-numbers, effective masses and

Sec. D-II

densities of states are constant, the ratio of the I_0 's will equal the ratio of the frequencies raised to the 2.5 power. With large frequency changes, such as going from the infrared to the ultraviolet, one generally expects materials suffering two-photon absorption in the ultraviolet to have a larger characteristic intensity I_0 than infrared materials.

With small frequency changes in a given material, implicit frequency dependences of I_0 in the density-of-states, in the effective masses, and in the f -numbers are equally as important as the explicit 2.5-power dependence on frequency. For frequencies very near the two-photon absorption edge, the density-of-states term $\gamma^{-0.5}$ is dominant, neglecting possible rapid changes in the f -numbers. Exciton effects, which have been neglected in the above analysis, may be important near the two-photon absorption edge, depending on the particular crystal under study.

In the following sections, Eq. (2.10) is used as an order-of-magnitude estimate for I_0 with f -numbers equal to unity, the effective mass equal to unity, and $\gamma = 0.1$. The resulting 174 MW/cm^2 characteristic intensity can be considerably in error for materials suffering two-photon absorption at $\hbar\omega = 3.5 \text{ eV}$. Each of the f -numbers could be in error by a factor of 10. Smaller variations are expected from the effective mass and from the density of states through γ . Most of the changes anticipated in these parameters are expected to yield larger values for I_0 , hence less efficient two-photon absorption.

Values of I_0 from Eq. 2.10 are compared with experimental values⁵⁻¹⁰ in Table II. In the experimental references, two-photon absorption spectra were obtained by the simultaneous absorption of an ultraviolet photon from a broad-band uv source plus a photon from a ruby laser. The characteristic intensity values are compared at a single frequency value (at $\hbar\omega = E_a$) on a smooth portion of the experimental curve above the band gap (E_g) where the value of γ was approximately 0.05. The experimental I_0 is the ruby laser intensity divided by the two-photon absorption

Table II. Comparison of experimental and theoretical values of the characteristic two-photon absorption intensity.

Material	Ref.	E_a (eV)	E_g (eV)	ϵ	$I_0(\text{exp})$ (MW/cm ²)	I_0 (Eq. (2.10)) (MW/cm ²)
KI	5,6	6.5	6.0	0.15	130	120
RbI	7	6.2	6.1	0.048	94	190
KBr	7	7.6	7.3	0.092	94	230
RbBr	7	7.4	7.2	0.057	190	260
CsI	8	6.2	6.0	0.077	47	150
CsBr	8	7.3	7.2	0.027	94	370
ZnO	9,10	3.45	3.43	0.011	950	50

Sec. D-II

coefficient at the chosen frequency value. Values from Eq. (2.10) were obtained using values for γ and $\hbar\omega = E_a/2$ from the chosen point on the curve along with the assumed values of $f = 1$ and $\alpha = 1$. The values for alkali halides are in good agreement with the value for I_0 from Eq. (2.10), being approximately a factor of two greater than the experimental values. With ZnO, the experimental spectrum is complicated by nearby exciton lines, and the agreement is less good, with the experimental I_0 value being approximately 20 times greater than the theoretical value. This less efficient two-photon absorption could be due to smaller f -numbers than the values of unity used in Eq. (2.10).

In each alkali halide, the frequency dependence of the two-photon absorption coefficient was in good qualitative agreement with the predicted dependence from γ in Eq. (2.10).

3. Three-Photon Absorption.

Three-photon absorption is the dominant, intrinsic absorption mechanism in materials having an absorption edge greater than twice the photon energy but less than three times the photon energy. The perturbation-theory expression for the three-photon absorption coefficient is similar to that for the two-photon absorption coefficient except that the two-photon Eq. (2.7) is multiplied by an additional factor⁴

$$F = \frac{3\pi f_{ij} e^2 E_{ij} I}{mc \omega^2 E_{den}^2}, \quad (2.11)$$

where f_{ij} is the f -number for the additional intermediate state transition, E_{ij} is the energy difference between intermediate states, and E_{den} is an additional energy denominator. This factor can be written in the form

$$F = I/I_F, \quad (2.12)$$

Sec. D-II

where $I_F = 8 \times 10^{14} \text{ W/cm}^2$ for $f_{ij} = 1$, $\hbar\omega = 3.5 \text{ eV}$, and $E_{ij}/E_{\text{den}}^2 = 1/13.6 \text{ eV}$.

Combining this result with the estimate for two-photon absorption yields the three-photon absorption coefficient

$$\beta_3 = \frac{I^2}{I_{03}^2} (\text{cm}^{-1}), \quad (2.13)$$

where $I_{03} = 370 \text{ GW/cm}^2$. The numerical value for the characteristic intensity I_{03} is subject to the same uncertainties as the characteristic intensity I_0 for two-photon absorption and should be regarded as an order-of-magnitude estimate.

With four-photon or greater absorption, one can estimate the absorption coefficient by the inclusion of additional F-factors.

III. FREE CARRIER CREATION AND RECOMBINATION

Both intrinsic multiphoton absorption and extrinsic impurity absorption generally result in the creation of mobile carriers such as electrons in the conduction band and holes in the valence band. With intrinsic band-to-band absorption, equal numbers of electrons in the conduction band and holes in the valence band are created. If the final state for the electron is an exciton state rather than the conduction band, the electron and hole are bound together and will not respond independently to an applied electric field. In this case, the dc conductivity may be zero, but the optical susceptibility of the pair will be nonzero although different from unbound pairs. With donor impurities, only mobile electrons in the conduction band are created. Acceptor impurities yield mobile holes in the valence band. Transitions between two bound impurity levels do not yield free carriers.

Most insulating, transparent solids have valence bands that are flat compared to the conduction bands. Hence, the hole-effective masses are greater than those of the electrons. Consequently, optical effects from the electrons are dominant over those from the holes because of the lesser mobilities of the holes which are inversely proportional to the effective masses. When the term free electron is used in the following discussion of intrinsic absorption, it is understood to be an electron-hole pair. (The effective mass of a conduction-band electron is approximately equal to the free-electron mass, and the effective mass of the valence-band hole is approximately infinite.) With impurity absorption, the effects of donor impurities that yield electrons are dominant over acceptor impurities that yield holes.

First consider the creation of conduction-band electrons from donor impurities. The rate-of-change in the concentration N_F of free electrons is given by

Sec. D-III

$$\frac{dN_F}{dt} = \frac{\beta I}{\hbar \omega} - \frac{N_F}{\tau_R}, \quad (3.1)$$

where β is the instantaneous absorption coefficient which may decrease with time due to depletion of the donor levels and τ_R is the time constant for the loss of free electrons from the conduction band. In writing the first term in Eq. (3.1) for the rate of creation of free electrons, it has been assumed that each photon absorbed creates an electron. For simplicity, τ_R is assumed to be the time constant for the recombination of the electrons with the impurities, although other processes that trap, or immobilize, the electrons may shorten this time. It is further assumed for simplicity that the instantaneous, extrinsic absorption coefficient can be written

$$\beta = N_b \sigma_b, \quad (3.2)$$

where N_b is the instantaneous concentration of bound electrons at impurity sites and σ_b is absorption cross section of an impurity. Actually, a sum over different types of impurities is needed in Eq. (3.2). The additional creation of conduction electrons by electrons already in the conduction band has been neglected in Eq. (3.1). The neglect of the electron avalanche process is justified by the fact that we are primarily interested in the lower threshold processes of optical distortion and thermal fracture, rather than intense local heating.

Setting the concentration N_0 of impurity sites equal to the sum of the concentrations of bound and free electrons

$$N_0 = N_b + N_F, \quad (3.3)$$

Sec. D-III

Eq. (3.1) can be written in the form

$$\frac{dN_F}{dt} = \frac{N_0 \sigma_b I}{\hbar \omega} - N_F \left(\frac{1}{\tau_R} + \frac{\sigma_b I}{\hbar \omega} \right). \quad (3.4)$$

The second term in Eq. (3.4) suggests the definition of an effective time constant τ_R' for recombination:

$$\frac{1}{\tau_R'} = \frac{1}{\tau_R} + \frac{1}{\tau_R''}, \quad (3.5)$$

where

$$\tau_R'' = \frac{\hbar \omega}{\sigma_b I}. \quad (3.6)$$

The time constant τ_R'' is a manifestation of depletion of the impurity levels with decreasing values of τ_R'' at high intensities and with large absorption cross sections being indicative of more rapid depletion under these conditions. Values of τ_R'' as a function of intensity are plotted in Fig. 3 for the two impurity absorption cross sections 10^{-16} cm^2 (strongly absorbing) and 10^{-20} cm^2 (weakly absorbing). Significant depletion of the impurity levels occurs at times greater than τ_R' when the intensity is great enough that $\tau_R'' < \tau_R$. Accurate values of the intrinsic recombination time τ_R in materials of interest at room temperature are not known. Values of τ_R in the range from 10^{-2} sec to 10^{-4} sec have been observed in room temperature samples of germanium.¹¹ If such large values of τ_R occur in materials of interest, the effective time constant τ_R'' will be dominant for intensities greater than approximately 10^4 W/cm^2 , depending on σ_b , and depletion will occur if the laser pulse duration is greater than τ_R' .

Sec. D-III

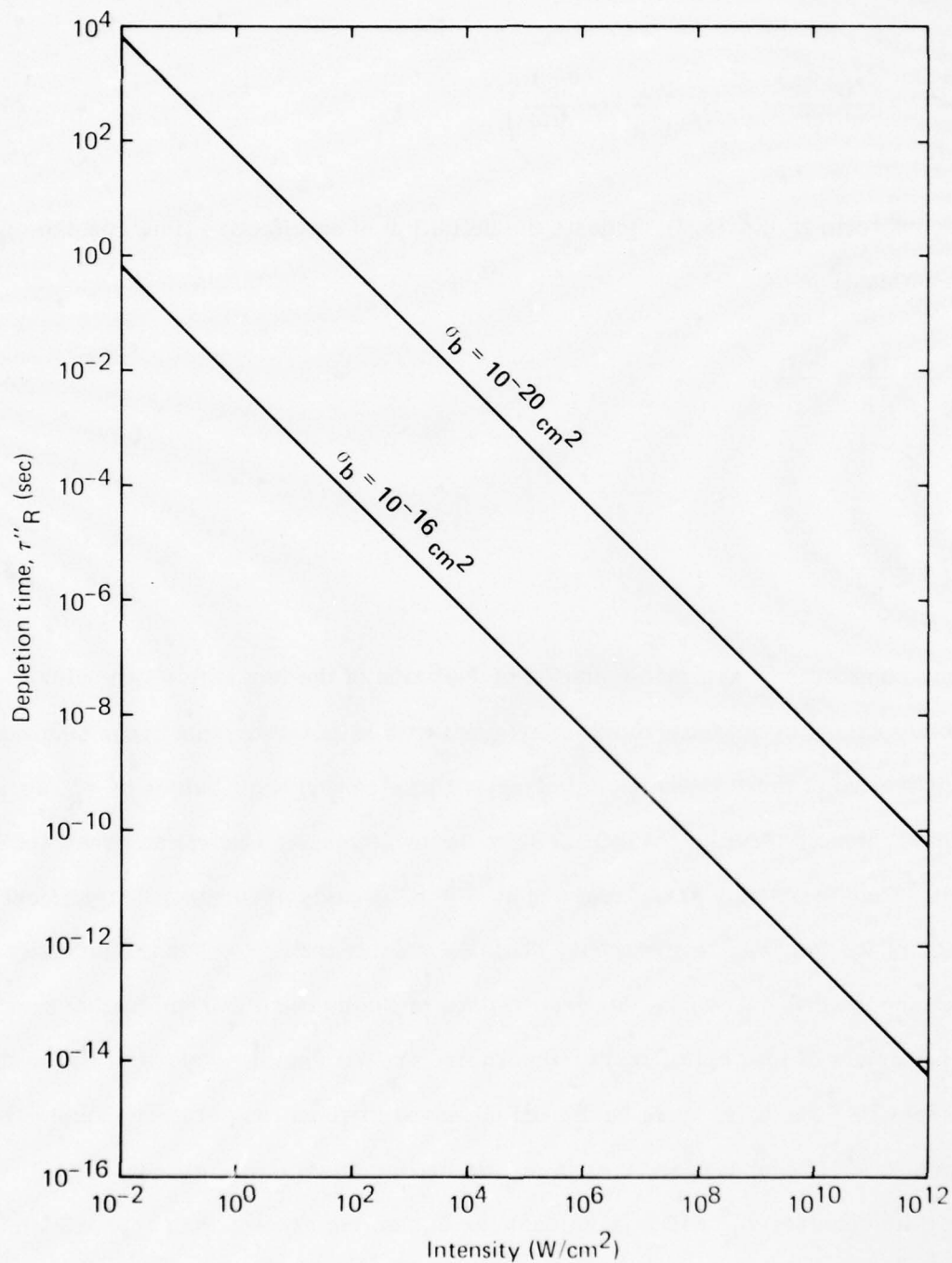


Fig. 3. Time constant τ_R'' for impurity depletion as a function of laser intensity for two impurity-absorption cross sections.

Sec. D-III

Using the fact that the initial, low-intensity extrinsic absorption coefficient is given by

$$\beta_0 = N_0 \sigma_b \quad (3.7)$$

and using Eq. (3.5), Eq. (3.4) can be written

$$\frac{dN_F}{dt} = \frac{\beta_0 I}{\hbar \omega} - \frac{N_F}{\tau_R'} \quad (3.8)$$

For zero concentration of free electrons at zero time, Eq. (3.8) has the solution

$$N_F = \frac{\beta_0 I}{\hbar \omega} \tau_R' \left(1 - e^{-t/\tau_R'} \right) \quad (3.9)$$

Concentrations N_F of free electrons are plotted as a function of time in Fig. 4 for five laser intensities. The laser intensities are expressed in units of a characteristic intensity I_c where τ_R'' equals τ_R' :

$$I_c = \frac{\hbar \omega}{\sigma_b \tau_R'} \quad (3.10)$$

At short times $t \ll \tau_R'$, Eq. (3.9) becomes

$$N_F = \frac{\beta_0 I t}{\hbar \omega}, \quad t \ll \tau_R' \quad (3.11)$$

In the short-time limit, no depletion or recombination occurs, and according to Eq. (3.11), one free electron is created for each photon absorbed. The concentration of free electrons is linear in I and in β_0 in this limit.

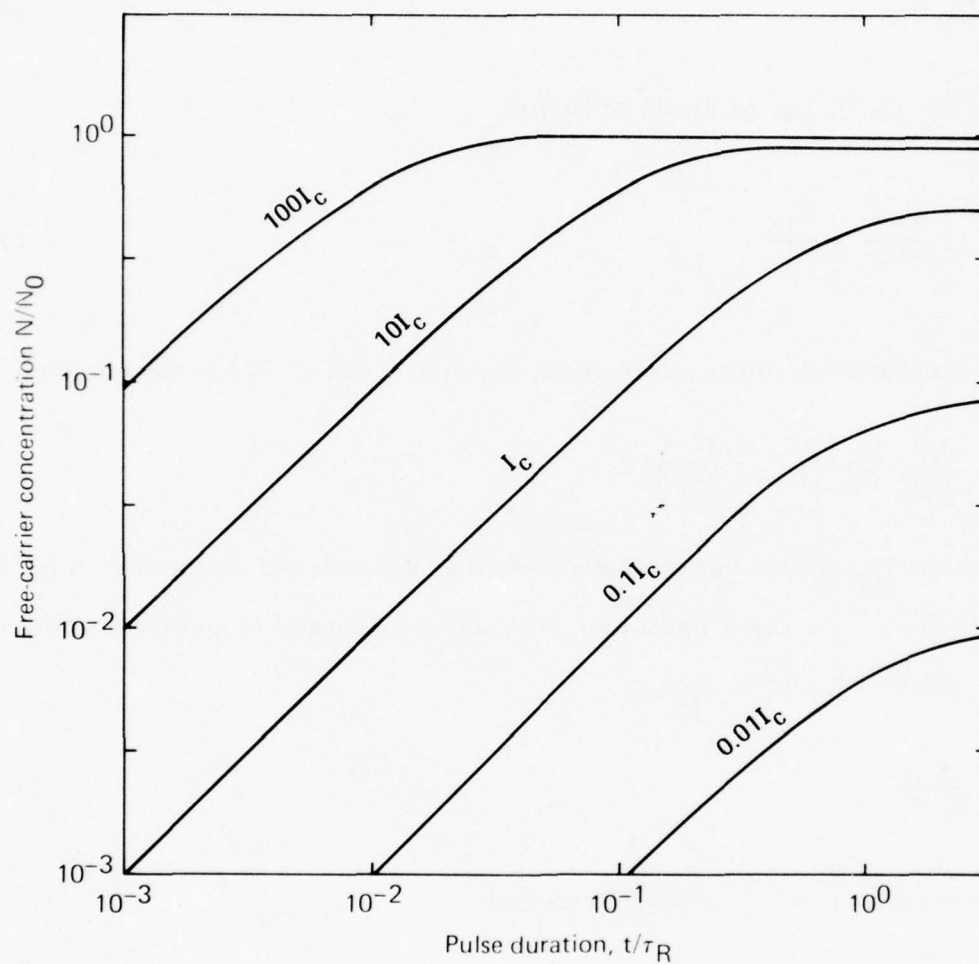


Fig. 4. Free-carrier concentration as a function of time at five intensities for materials limited by donor-impurity absorption. N_0 is the concentration of donor impurities, τ_R is the intrinsic recombination time, and I_C is the characteristic intensity for depletion.

Equilibrium is attained in the long-time limit where $t \gg \tau_R'$. In this limit Eq. (3.9) becomes

$$N_F = \frac{\beta_0 I}{\hbar \omega} \tau_R', \quad t \gg \tau_R'. \quad (3.12)$$

This equation, effectively, states that one free electron is created by each photon absorbed for an initial period of time τ_R' , with subsequent absorption maintaining the equilibrium concentration. Out of necessity, the equilibrium concentration of free electrons in Eq. (3.12) must be less than the initial concentration of bound electrons N_0 . At low intensities $I \ll I_c$, the time constant τ_R' is equal to the recombination time τ_R , and the equilibrium number is less than N_0 and proportional to I . At high intensities $I \gg I_c$, the equilibrium number of free electrons in Eq. (3.12) is prevented from exceeding N_0 by decreasing values of τ_R' with increasing intensity. In this limit, the time constant τ_R' is approximately equal to τ_R'' and substitution of Eq. (3.6) into (3.12) yields $N_F \cong N_0$. At the characteristic intensity I_c , extrapolation of the short-time slope of N_F from Eq. (3.11) to a time τ_R yields $N_F = N_0$. However, at this intensity, $\tau_R' = \tau_R/2$ and the equilibrium concentration from Eq. (3.12) is $N_F = N_0/2$.

The above analysis shows that saturation occurs when the intensity is greater than the characteristic intensity I_c and when the time is greater than the time constant τ_R' . In practical situations, the recombination time τ_R may be much greater than the laser pulse duration, and hence, intensities that are large compared to I_c are required for depletion to occur while the laser is on. For a recombination time τ_R of 10^{-2} sec and an impurity cross section of 10^{-16} cm^2 , the value of I_c is approximately 1 W/cm^2 .

Sec. D-III

In order for depletion to occur during the laser pulse duration of 10^{-6} sec or less, it is necessary that the intensity be greater than $10^4 I_c$ or 10^4 W/cm^2 . This is still a small intensity, and depletion will occur in many practical situations unless the impurity cross section is very small or the laser pulse duration is very short.

The creation of electron-hole pairs by intrinsic multiphonon absorption can be analyzed in a similar manner, subject to certain modifications and approximations. Analogous to Eq. (3.1), the rate of change of the concentration of electron-hole pairs N_F due to two-photon absorption is written

$$\frac{dN_F}{dt} = \frac{\beta_2 I}{2\hbar\omega} - \frac{N_F}{\tau_R}, \quad (3.13)$$

where the factor of two in the denominator arises from the fact that the absorption of two photons is required to create a pair. The absorption coefficient for two-photon absorption β_2 is proportional to the intensity and is written in Eq. (2.9) as

$$\beta_2 = (I/I_0) (1\text{cm}^{-1}). \quad (3.14)$$

At very high intensities, depletion of the intrinsic valance electrons may occur, and to analyze this effect, it is useful to define a two-photon absorption cross section σ_2 per unit cell of the crystal:

$$\sigma_2 = I/I_0 N_0, \quad (3.15)$$

where N_0 is the number of unit cells per unit volume. The definition of a two-photon cross section is used in a loose sense because, besides being intensity dependent,

Sec. D-III

In order for depletion to occur during the laser pulse duration of 10^{-6} sec or less, it is necessary that the intensity be greater than $10^4 I_c$ or 10^4 W/cm^2 . This is still a small intensity, and depletion will occur in many practical situations unless the impurity cross section is very small or the laser pulse duration is very short.

The creation of electron-hole pairs by intrinsic multiphonon absorption can be analyzed in a similar manner, subject to certain modifications and approximations. Analogous to Eq. (3.1), the rate of change of the concentration of electron-hole pairs N_F due to two-photon absorption is written

$$\frac{dN_F}{dt} = \frac{\beta_2 I}{2\hbar\omega} - \frac{N_F}{\tau_R}, \quad (3.13)$$

where the factor of two in the denominator arises from the fact that the absorption of two photons is required to create a pair. The absorption coefficient for two-photon absorption β_2 is proportional to the intensity and is written in Eq. (2.9) as

$$\beta_2 = (I/I_0) (1\text{cm}^{-1}). \quad (3.14)$$

At very high intensities, depletion of the intrinsic valance electrons may occur, and to analyze this effect, it is useful to define a two-photon absorption cross section σ_2 per unit cell of the crystal:

$$\sigma_2 = I/I_0 N_0, \quad (3.15)$$

where N_0 is the number of unit cells per unit volume. The definition of a two-photon cross section is used in a loose sense because, besides being intensity dependent,

Sec. D-III

the cross section per unit cell may change if significant depletion occurs. The changes in the cross section upon depletion may involve such many-body effects as a change in the crystal band gap when sufficient numbers of valence band electrons are excited to the conduction band.

Using Eq. (3.15) in Eq. (3.13), an equation for the rate of change of the pair concentration similar to Eq. (3.4) is obtained:

$$\frac{dN_F}{dt} = \frac{N_0 \sigma_2 I}{2\hbar\omega} - N_F \left(\frac{1}{\tau_R} + \frac{\sigma_2 I}{2\hbar\omega} \right), \quad (3.16)$$

where now the second term in the effective time constant is inversely proportional to the square of the intensity:

$$\tau_R'' = \frac{2\hbar\omega}{\sigma_2 I} = \frac{2N_0 I_0 \hbar\omega}{I^2}. \quad (3.17)$$

Assuming that Eq. (3.15) is valid, the solution of Eq. (3.16) is

$$N_F = \frac{I^2}{2I_0 \hbar\omega} \tau_R' \left(1 - e^{-t/\tau_R'} \right), \quad (3.18)$$

where $\tau_R'^{-1} = \tau_R^{-1} + \tau_R''^{-1}$.

As before, one can define a characteristic intensity I_c for depletion as the intensity where the time constant τ_R'' equals the intrinsic recombination time τ_R . Setting τ_R'' in Eq. (3.17) equal to τ_R and solving for the intensity yields

$$I_c = (2N_0 I_0 \hbar\omega / \tau_R)^{1/2}. \quad (3.19)$$

Sec. D-III

Using $I_0 = 1.7 \times 10^8 \text{ W/cm}^2$ from Eq. (2.10) as a typical value at 350nm wavelength and using $N_0 = 10^{22} \text{ cm}^{-3}$ and $\tau_R = 10^{-2} \text{ sec}$, the value of I_c from Eq. (3.19) is $1.4 \times 10^7 \text{ W/cm}^2$. This value will increase if the intrinsic recombination time in materials of interest is shorter than 10^{-2} sec . For an intensity equal to I_c , the two-photon absorption coefficient is equal to 0.08 cm^{-1} .

In many practical situations, the laser pulse duration is much less than the intrinsic recombination time. Hence, intensities greater than I_c (consequently, larger two-photon absorption coefficients) are required for depletion to occur. The concentration N_F of electron-hole pairs is plotted as a function of time in Fig. 5 for several laser intensities. For pulse durations less than 10^{-6} sec , laser intensities greater than the characteristic two-photon absorption intensity I_0 are required to approach saturation. With an intensity $10 I_0$, one percent of the valence electrons are excited after an irradiation time of 10^{-8} seconds . This time decreases to 10^{-10} seconds for an intensity equal to $100 I_0$. Although Fig. 5 is plotted in terms of the characteristic intensity I_0 , the times at which saturation takes place will vary due to the dependence of π_R'' on I_0 . In materials with small values of I_0 (strong two-photon absorbers), the times for saturation will decrease from those in Fig. 5.

Besides neglecting many-body effects which may change the two-photon cross section, the possibility of the additional creation of free carriers at high intensities by the electron-avalanche process has also been neglected. In spite of the difficulties near saturation, many failure thresholds occur in the low-intensity, short-time regime where estimates of the pair concentration are thought to be reliable. The limiting form for Eq. (3.18) in this region is

$$N_F = \frac{I_t^2}{2 I_0 \hbar \omega} , \quad N_F \ll N_0 . \quad (3.20)$$

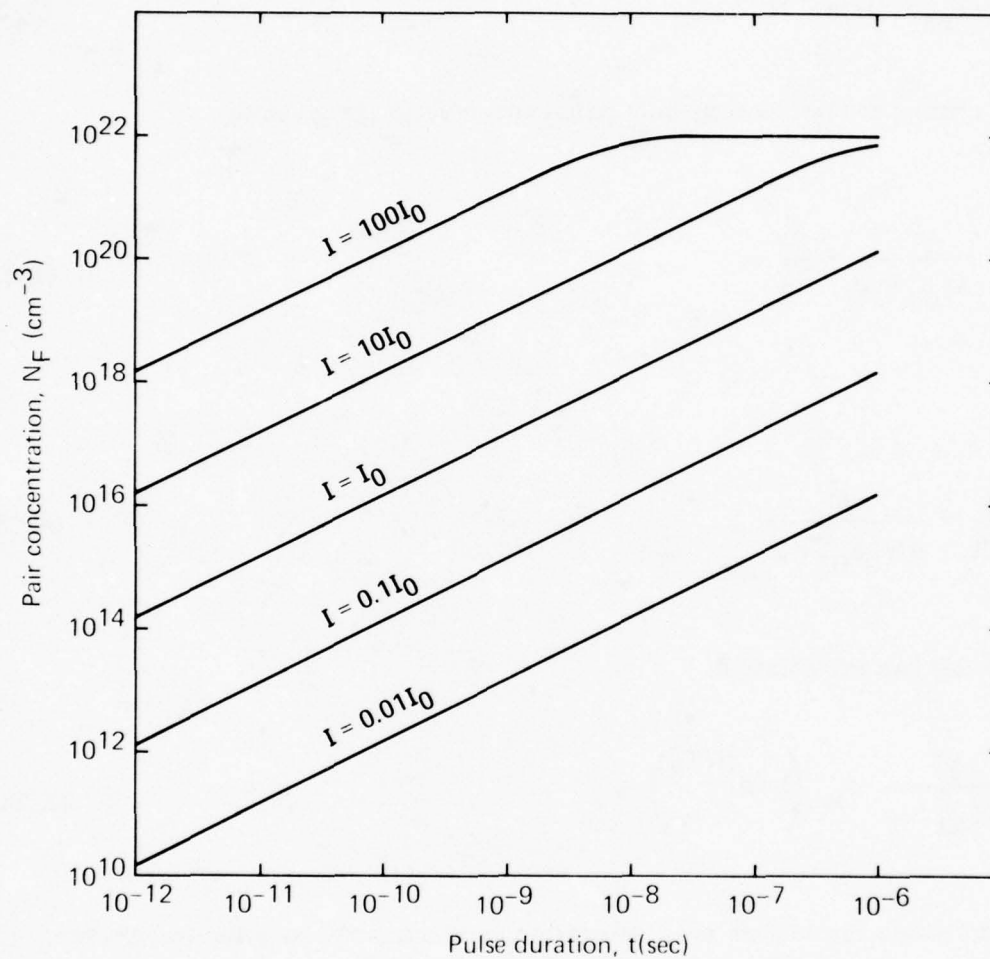


Fig. 5. Electron-hole pair concentration as a function of time at five laser intensities for materials limited by intrinsic two-photon absorption. I_0 is the characteristic intensity where the two-photon absorption coefficient equals 1 cm^{-1} .

Sec. D-III

Similarly, for materials suffering three-photon absorption at the laser frequency and having an absorption coefficient

$$\beta = (I^2/I_{03}^2) \text{ (1cm}^{-1}\text{)}, \quad (3.21)$$

the rate of change of the electron-hole pair concentration is given by

$$\frac{dN_F}{dt} = \frac{I^3}{3I_{03}^2 \hbar \omega} - \frac{N_F}{\tau_R}, \quad (3.22)$$

where

$$\frac{1}{\tau_R} = \frac{1}{\tau_R} + \frac{I^3}{3N_0 I_{03}^2 \hbar \omega}. \quad (3.23)$$

Equation (3.22) has the solution

$$N_F = \frac{I^3}{3I_{03}^2 \hbar \omega} \tau_R' \left(1 - e^{-t/\tau_R'} \right), \quad (3.24)$$

subject to the same limitations near saturation as discussed above for two-photon absorption. Additionally near the characteristic intensity I_{03} for three-photon absorption, the value of the intensity is sufficiently large that electron avalanche will occur. A typical value of I_{03} equal to $3.7 \times 10^{11} \text{ W/cm}^2$ was derived in the previous section.

Neglecting electron avalanche, values of N_F as a function of time are plotted in Fig. 6 using $N_0 = 10^{22} \text{ cm}^{-3}$ and $I_{03} = 3.7 \times 10^{11} \text{ W/cm}^2$ at $\hbar \omega = 3.5 \text{ eV}$. The

Sec. D-III

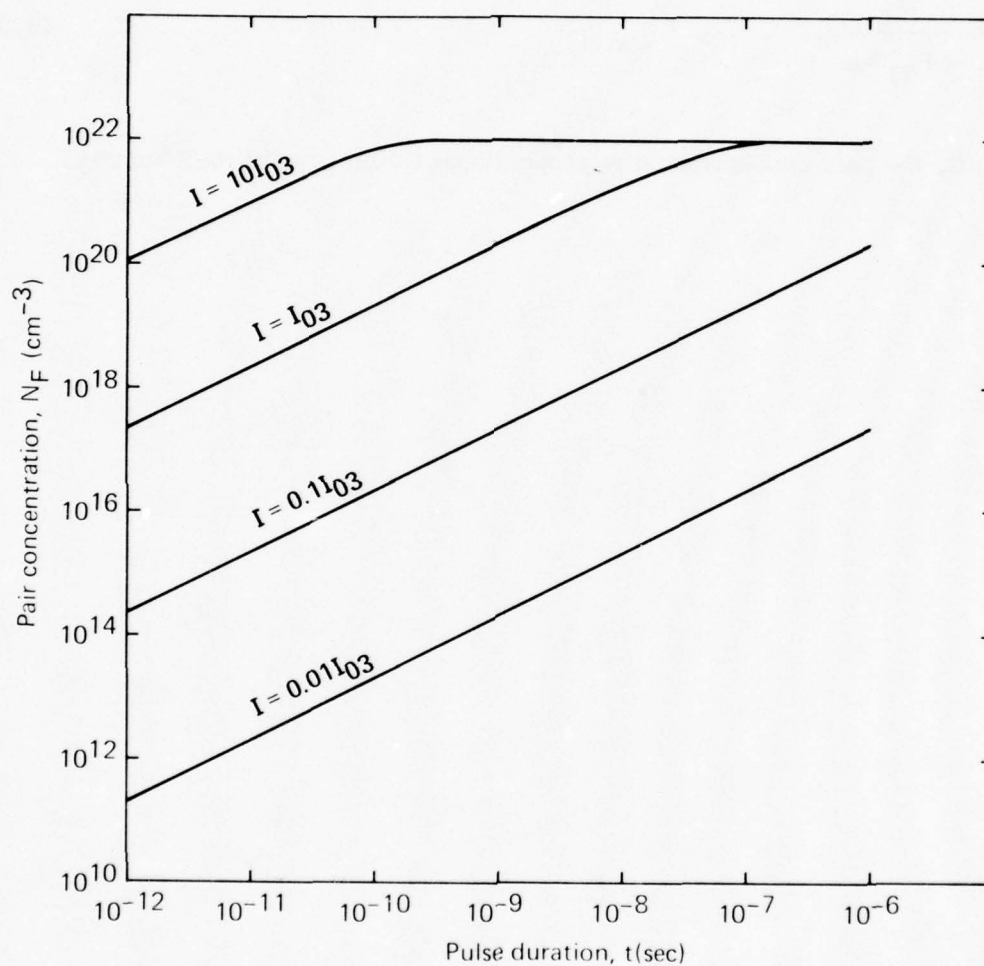


Fig. 6. Electron-hole pair concentration as a function of time at four laser intensities for materials limited by intrinsic three-photon absorption. I_{03} is the characteristic intensity where the three-photon absorption coefficient equals 1 cm^{-1} .

Sec. D-III

second term in the effective time constant decreases with increasing intensity as I^3 and results in rapidly decreasing saturation times for intensities greater than I_{03} . In the short-time, low-intensity limit, the pair concentration is given by

$$N_F = \frac{I_t^3}{3I_{03}^2 \hbar \omega} , \quad N_F \ll N_0 . \quad (3.25)$$

In this limit, the pair concentration is proportional to the cube of the intensity.

IV. FREE CARRIER OPTICAL DISTORTION AND ABSORPTION

Free carriers created by either intrinsic multiphoton absorption or extrinsic absorption can both absorb subsequent radiation and result in a change of the refractive index with resulting optical distortion. Both of these effects are connected by the complex dielectric constant. If we assume that the effects of depletion of the bound electrons and the effects of free carriers on the optical properties are additive, the complex dielectric constant of a crystal containing a density N_F of free carriers can be written

$$\epsilon = \epsilon_0 - \frac{N_F}{N_0} (\epsilon_0 - 1) - \frac{\omega_p^2}{\omega^2 + i\omega/\tau_c}, \quad (4.1)$$

with

$$\omega_p^2 = 4\pi N_F e^2/m, \quad (4.2)$$

where ϵ_0 is the unperturbed dielectric constant, N_0 is the initial density of bound electrons, τ_c is the collisional relaxation time of the free carriers, ω_p is the plasma frequency of the free carriers, e is the electronic charge, and m is the effective mass of the free carriers. With donor impurities, m is the effective mass of a conduction electron m_e which typically is approximately equal to the free electron mass. With acceptor impurities, m is the effective mass m_h of a hole which typically is much larger than the free electron mass. With intrinsic absorption, m is equal to the reduced effective mass of an electron and a hole which is approximately equal to the electron mass because of the large effective mass of the hole. Optical effects of holes are negligible in comparison to electrons because of their large effective mass, hence, small mobility. Such effects are neglected in the following, and the mass m is always taken to be equal to the free electron mass.

Sec. D-IV

The second term in Eq. (4.1) is the decrease in the dielectric constant due to a decrease in the number of bound electrons. In writing this term it has been assumed that each bound electron contributes equally to the dielectric constant and that the change in the dielectric constant is linear in the number of liberated electrons. This assumption should be valid for small changes in the number of intrinsic, bound electrons. With impurity electrons, there is an additional difficulty that the polarizability of the impurities are generally not known. The use of the unperturbed dielectric constant ϵ_0 in the second term of Eq. (4.1) assumes that the polarizability of a bound, impurity electron is the same as a bound, intrinsic electron.

The third term in Eq. (4.1) gives the contribution of the free carriers to the dielectric constant as derived from the Drude theory of the free electron gas.¹² This term is negative, as is the second term, avoiding the possible analytical difficulty of a cancellation between the second and third terms. Hence, the net effect is a decrease in the dielectric constant.

In the frequency range of interest, the conditions $\omega \gg \omega_p$ and $\omega > \tau_c^{-1}$ are satisfied. These conditions allow the dielectric constant to be written in the form

$$\epsilon = \epsilon_0 - \frac{N_F}{N_0} (\epsilon_0 - 1) - \frac{\omega_p^2}{\omega^2} + i \frac{\omega_p^2}{\omega^3 \tau_c} . \quad (4.3)$$

To obtain the real part of the refractive index n , the relation $n = \epsilon^{1/2}$ is used to obtain

$$n = n_0 - \frac{N_F}{2n_0 N_0} (n_0^2 - 1) - \frac{\omega_p^2}{2n_0 \omega^2} , \quad (4.4)$$

where we have also used $n_0^2 = \epsilon_0$ and $(\epsilon_0 - \Delta\epsilon)^{1/2} \cong \epsilon_0^{1/2} - \Delta\epsilon/2\epsilon_0^{1/2}$.

Sec. D-IV

The assumption that each bound electron contributes equally to the dielectric constant is only approximate in view of the Clausius-Mossotti relation. Hence, one can make a similar approximation for the refractive index yielding a simpler form for Eq. (4.4):

$$n = n_0 - \frac{N_F}{N_0} (n_0 - 1) - \frac{\omega_p^2}{2n_0\omega^2}. \quad (4.5)$$

a. Free Carrier Absorption

The effect of the creation of free carriers on the absorption coefficient is obtained using $\beta = \epsilon'' \omega / n_0 c$, where ϵ'' is the imaginary part of ϵ and c is the velocity of light. Assuming that the absorption by the bound electrons is proportional to the density of bound electrons, we obtain

$$\beta = \frac{N_F}{N_0} \beta_0 + \frac{\omega_p^2}{n_0 c \omega^2 \tau_c}. \quad (4.6)$$

It is useful to define an absorption cross section σ_F for the free carriers. Substituting Eq. (4.2) into the second term of Eq. (4.6) yields

$$\beta_F = N_F \frac{4\pi e^2}{n_0 m c \omega^2 \tau_c}, \quad (4.7)$$

and using $\beta_F = N_F \sigma_F$ yields

$$\sigma_F = \frac{4\pi e^2}{n_0 m c \omega^2 \tau_c}. \quad (4.8)$$

Using $\omega = 5.4 \times 10^{15} \text{ sec}^{-1}$ ($\lambda = 350 \text{ nm}$), m equal to the free electron mass, and $\tau_c = 10^{-14} \text{ sec}$, yields $\sigma_F = 2.4 \times 10^{-18} \text{ cm}^2$.

Sec. D-IV

In the case of a material limited by donor impurity absorption, the overall absorption coefficient of the material is written

$$\beta = N_b \sigma_b + N_F \sigma_F, \quad (4.9)$$

where N_b and N_F are the concentrations of bound and free electrons, respectively.

Using $N_0 = N_b + N_F$ yields

$$\beta = \beta_0 + N_F (\sigma_F - \sigma_b), \quad (4.10)$$

where $\beta_0 = N_0 \sigma_b$ is the initial, unperturbed absorption coefficient. The density N_F of free electrons under various conditions was derived in the previous section with the results presented in Eq. (3.9) and in Fig. 4. As the concentration of bound electrons becomes depleted, the overall absorption coefficient in Eq. (4.10) will either increase or decrease, depending on the relative magnitudes of σ_b and σ_F . The value $2.4 \times 10^{-18} \text{ cm}^2$ for σ_F derived above falls midway in the range of expected impurity absorption cross sections.

Assuming an initial, unperturbed absorption coefficient of 10^{-4} cm^{-1} , the overall absorption coefficient is plotted as a function of time under various conditions in Fig. 7. For $\sigma_b = \sigma_F$, the absorption coefficient is constant for all times and all intensities, neglecting the temperature dependence of β . For weakly absorbing impurities with $\sigma_b = 10^{-2} \sigma_F$, the overall absorption coefficient increases with time as is shown for three different intensities in the upper portion of the figure. These intensities are expressed in units of the characteristic intensity for depletion defined in Eq. (3.10). Similarly, decreasing absorption coefficients are shown in the lower portion of the figure for three different intensities incident on a material containing

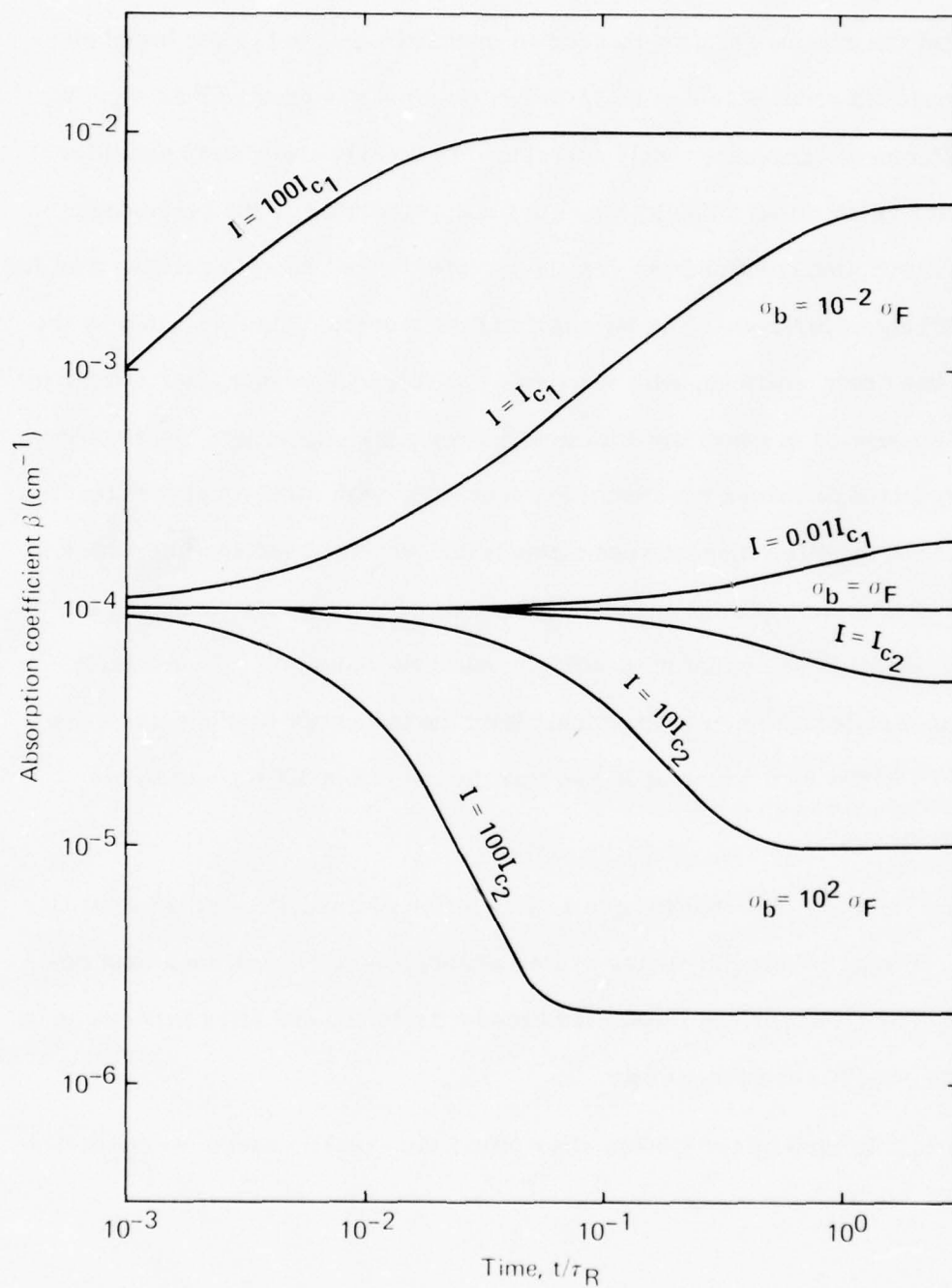


Fig. 7. Overall absorption coefficient as a function of time for materials containing donor impurities of various absorption cross sections, all having an initial absorption coefficient of 10^{-4} cm⁻¹.

Sec. D-IV

strongly absorbing impurities with $\sigma_b = 10^2 \sigma_F$.

Recall from the previous section that for an intensity equal to I_c , the bound electron concentration is reduced to half its initial value for times greater than τ_R . We notice two differences between strongly absorbing and weakly absorbing impurities from the figure. First at an intensity equal to the appropriate I_c , the percentage change in the absorption coefficient is greater for weakly absorbing impurities than for strongly absorbing impurities. This follows from the fact that β is dominated by the larger of the two cross sections, with relatively few free electrons being required to dominate the absorption in materials with weakly absorbing impurities; but significant depletion is required to change the absorption coefficient with strongly absorbing impurities. The second difference between strongly and weakly absorbing impurities is that it is easier to deplete strongly absorbing impurities than weakly absorbing impurities. The figure is somewhat misleading because the value of I_c is inversely proportional to the absorption cross section. With the two cross sections used, the two values of I_c differ by a factor of 10^4 so that the two cases $100I_{c2}$ and $0.01I_{c1}$ have the same intensity.

Actual materials are expected to have a distribution of impurities cross sections. When such a material is irradiated, the overall absorption coefficient may first decrease as the strongly absorbing impurities become depleted, and later increase upon depletion of the weakly absorbing levels.

For materials limited by two-photon absorption, the overall absorption coefficient can be written

$$\beta = (I/I_0) (1\text{cm}^{-1}) + N_F (\sigma_F - \sigma_2), \quad (4.11)$$

Sec. D-IV

where the first term is the intrinsic two-photon absorption from Eq. (2.9) and the second term is the contribution from electron-hole pairs. As discussed above, the electron-hole-pair cross section is approximately equal to the free-electron cross section σ_F used for donor impurities. The two-photon absorption cross section $\sigma_2 = I/N_0 I_0$, defined in Eq. (3.15), is proportional to the intensity and is generally much smaller than σ_F unless the intensity is very large. For $N_0 = 10^{22} \text{cm}^{-3}$, the two-photon cross section is approximately equal to $10^{-4} \sigma_F$ for an intensity equal to I_0 . A very large intensity $10^4 I_0$ is required for σ_2 to equal σ_F . Hence, for all practical cases, the overall absorption coefficient will increase with time as free pairs are generated.

Using the results from Eq. (3.18) and Fig. 5 for the pair concentration, the overall absorption coefficient is plotted as a function of time in Fig. 8 for five different laser intensities. At times less than the effective recombination time τ_R' when saturation has not yet occurred, Eq. (3.20) can be used for the pair concentration, yielding

$$\beta = (I/I_0) (1 \text{cm}^{-1}) + \frac{I^2 t}{2I_0 \hbar \omega} (\sigma_F - \sigma_2), \quad t \ll \tau_R'. \quad (4.12)$$

At short times in the figure, the second term in Eq. (4.12) is negligible compared to the intrinsic absorption in the first term. In this region the absorption coefficient is time-independent and proportional to the intensity. At later times as the free-carrier term becomes dominant, the absorption increases linearly with time and is proportional to the square of the intensity. Saturation occurs at long times in the figure for the two large intensities $10 I_0$ and $100 I_0$.

Similarly, with a material limited by three-photon absorption, the overall absorption coefficient is

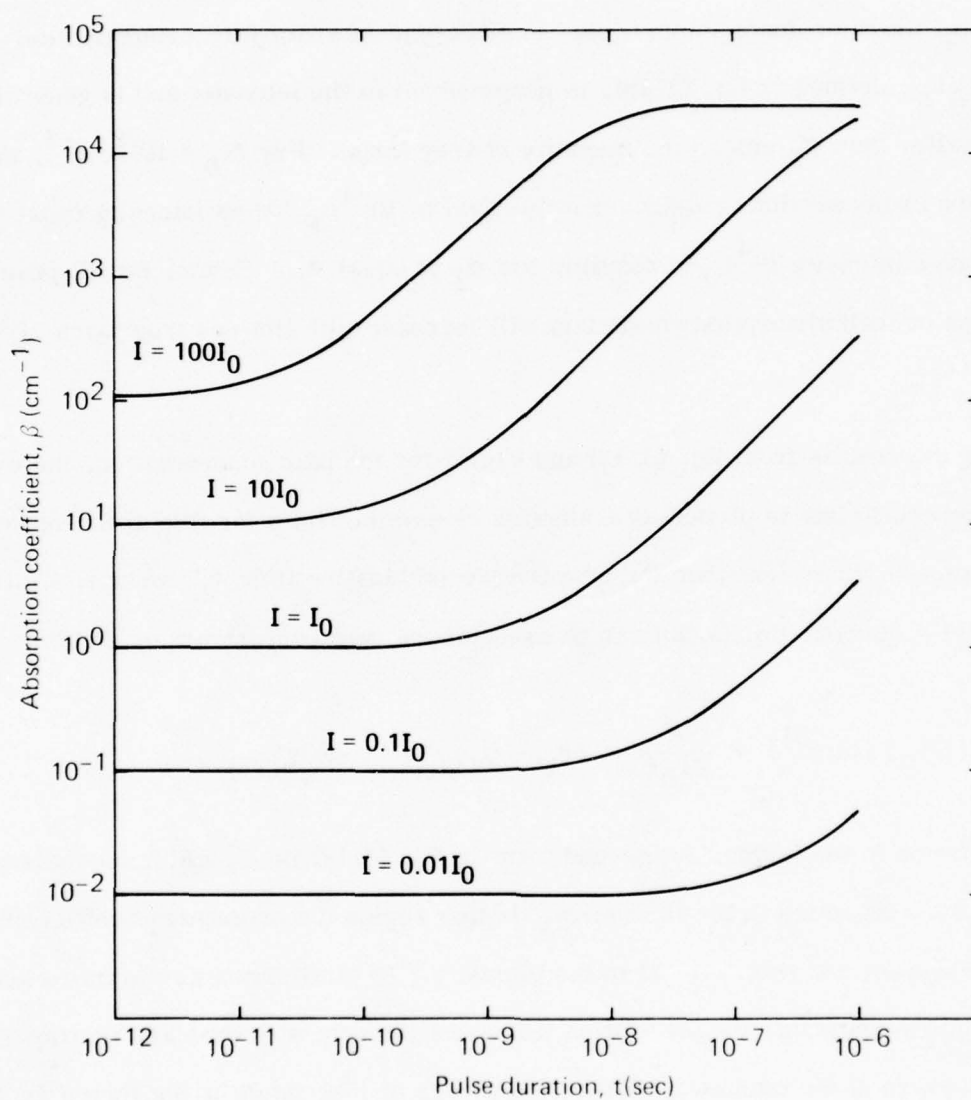


Fig. 8. Overall absorption coefficient, including free-carrier absorption, as a function of time at five intensities for a material limited by intrinsic two-photon absorption.

$$\beta = (I^2/I_{03}^2) (1\text{cm}^{-1}) + N_F (\sigma_F - \sigma_3), \quad (4.13)$$

where the first term is the intrinsic three-photon absorption coefficient and the second term is the electron-hole pair contribution. The pair concentration is given in Eq. (3.24), and in the short-time limit, the absorption coefficient becomes

$$\beta = (I^2/I_{03}^2) (1\text{cm}^{-1}) + \frac{I^3 t}{3I_{03}^2 \hbar \omega} (\sigma_F - \sigma_3), \quad t \ll \tau_R'. \quad (4.14)$$

Results similar to those for two-photon absorption are plotted in Fig. 9 for three-photon absorption. At short times in the figure, the overall absorption coefficients approach the intrinsic three-photon values which are time-independent and proportional to the square of the intensity. As the pair contribution becomes dominant, the overall absorption coefficient increases linearly with time and is proportional to the cube of the intensity. Saturation occurs on the time scale of the figure at intensities greater than I_{03} .

b. Free Carrier Optical Distortion.

Free carrier optical distortion is primarily a single pulse effect since the free carriers liberated during the pulse tend to recombine between pulses. Significant recombination occurs if the repetition rate is less than the inverse of the intrinsic recombination time τ_R . In the following, it is assumed that this is true, although for recombination times of 10^{-2} sec the repetition rate is limited to 100 Hz or less.

Optical distortion results from the fact that the laser intensity, hence the free carrier concentration, is nonuniform in going from the center to the edge of the optical element being irradiated. With intrinsic multiphonon absorption, the carrier concentration is more nonuniform than the intensity, since the density of free carriers

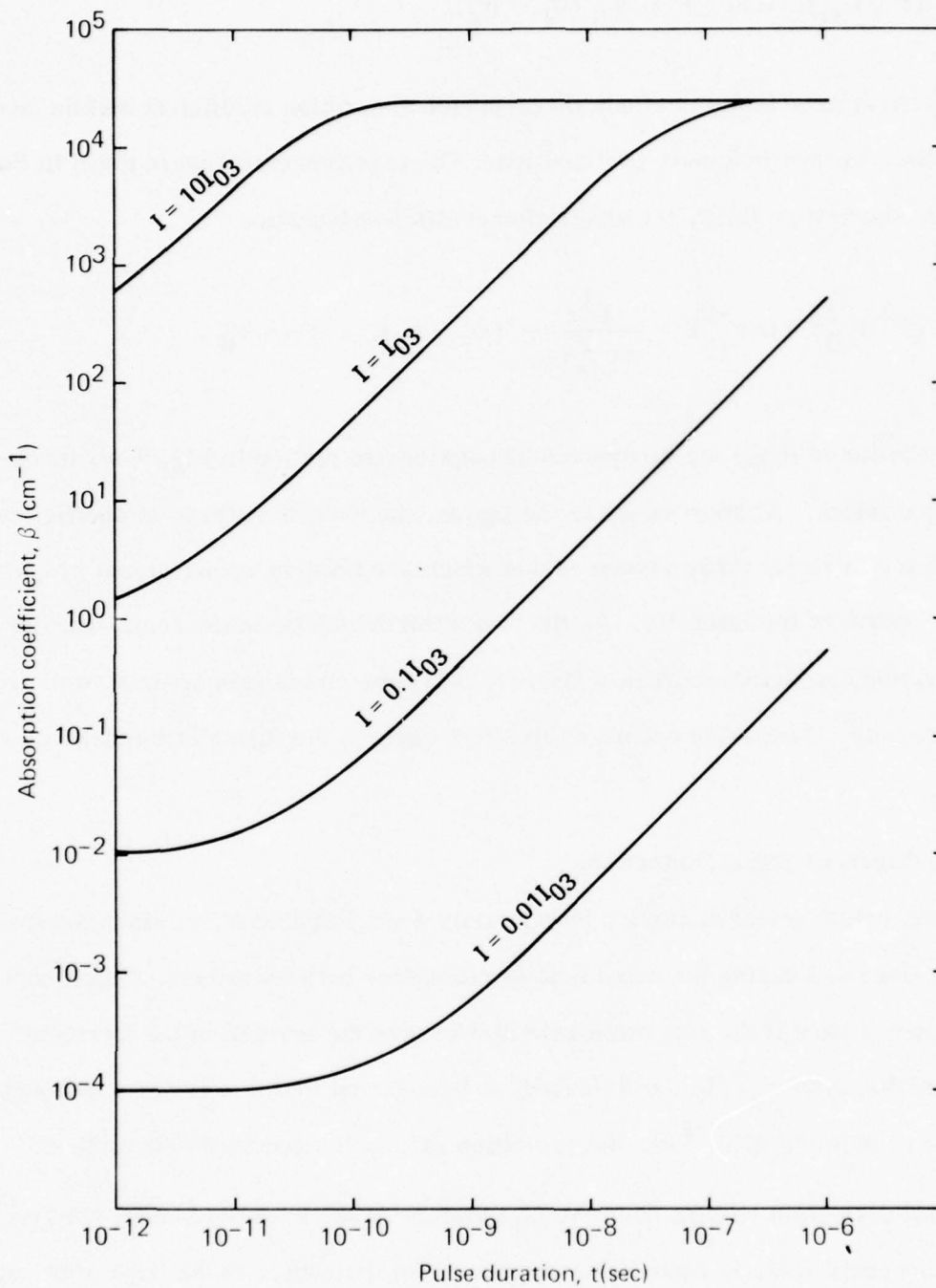


Fig. 9. Overall absorption coefficient, including free-carrier absorption, as a function of time at four intensities for a material limited by intrinsic three-photon absorption.

Sec. D-IV

is proportional to the square of the intensity for two-photon absorption and to the cube of the intensity for three-photon absorption. Neglecting edge effects, the limit on the change in the optical path through the center of the optical element can be expressed in fractions of a wavelength:

$$\delta n \cdot \ell = \lambda / \gamma, \quad (4.15)$$

where δn is the change in the refractive index, ℓ is the thickness of the element and γ is an integer typically in the range from 10 to 100. Since the change in the optical path is linear in the thickness, only a thickness of 1cm will be considered in the following threshold calculations.

Substituting the change $n - n_0$ from Eq. (4.5) into (4.15) and using Eq. (4.2), we obtain

$$\delta n = \frac{-N_F}{N_0} (n_0 - 1) - \frac{2\pi N_F e^2}{N_0 m \omega^2} \cong \frac{-\lambda}{\gamma}. \quad (4.16)$$

Notice that the change in the refractive index is negative, implying that the distortion effect will be a defocusing of the beam. Equation (4.16) is linear in the free carrier concentration, so that a limit on N_F can easily be obtained:

$$N_F \cong 2.4 \times 10^{16} \text{ cm}^{-3}, \quad (4.17)$$

for $\lambda = 350 \text{ nm}$, $\gamma = 40$, and $n_0 = 1.5$.

Intensity thresholds for distortion are readily obtained from Eq. (4.17) using the results of Sec. III for the free carrier concentration. In materials limited by donor impurities, there may not be enough donor electrons available to cause distortion.

Sec. D-IV

For an extrinsic absorption coefficient of 10^{-4} cm^{-1} , the concentration of donor impurities ranges from 10^{12} cm^{-3} to 10^{16} cm^{-3} for absorption cross sections ranging from 10^{-16} cm^2 to 10^{-20} cm^2 . For comparison to the thresholds obtained for intrinsic multiphonon absorption, it is assumed that the cross section is sufficiently small that there are ample donor electrons available for distortion. It is further assumed that the short-time limit $t < \tau_R'$ applies so that the concentration of free electrons can be written

$$N_F = \frac{I \beta_0 t}{\hbar \omega}, \quad t < \tau_R' \quad (4.18)$$

The validity of the short-time limit can readily be checked by reference to Fig. 3. Hence, the distortion threshold becomes

$$I \cong \frac{N_F \hbar \omega}{\beta_0 t}, \quad (4.19)$$

$$I = 1.4 \times 10^2 t^{-1} \text{ W/cm}^2, \quad \text{impurity } (\beta = 10^{-4} \text{ cm}^{-1}) \quad (4.20)$$

for t expressed in seconds.

With intrinsic, multiphoton absorption, the short-time limit always applies since the value of N_F in Eq. (4.17) is much less than the concentration of valence electrons. Using Eq. (3.20) for N_F in materials limited by two-photon absorption, the threshold for optical distortion is obtained:

$$I \cong \left(\frac{2 N_F I_0 \hbar \omega}{t} \right)^{1/2} \quad (4.21)$$

or using Eq. (4.17) for N_F and Eq. (2.10) for I_0 ,

$$I \cong 2.2 \times 10^3 t^{-1/2}, \quad \text{two-photon} \quad (4.22)$$

Sec. D-IV

for t expressed in seconds. Similarly, for three-photon absorption, the threshold is obtained using Eq. (3.25) for N_F :

$$I \cong \left(\frac{3 N_F I_{03}^2 \hbar \omega}{t} \right)^{1/3}, \quad (4.23)$$

or using $I_{03} = 3.7 \times 10^{11} \text{ W/cm}^2$,

$$I \cong 1.8 \times 10^7 t^{-1/3} \text{ W/cm}^2. \quad \text{three-photon} \quad (4.24)$$

The thresholds for distortion in Eqs. (4.19) - (4.24) have different dependences of the absorption coefficients on intensity. The threshold for donor impurities decreases with decreasing t as t^{-1} , while the intrinsic two-photon and three-photon thresholds decrease as $t^{-1/2}$ and $t^{-1/3}$, respectively. Hence, optical distortion from impurity absorption is relatively more important, compared to the intrinsic absorption, with long pulse durations. With the parameters used above, the impurity threshold intensity equals the two-photon threshold intensity for a pulse duration of 4×10^{-3} sec. The impurity and three-photon thresholds are equal with a pulse duration of 2×10^{-8} sec.

Similarly, the various thresholds have different dependences on other parameters. If the optical tolerance in Eq. (4.15) is relaxed by decreasing the value of γ , the impurity threshold increases by the same factor that γ decreases, while the two-photon and three-photon thresholds have the lesser dependences $\gamma^{-1/2}$ and $\gamma^{-1/3}$, respectively. The two-photon threshold intensity in Eq. (4.21) is proportional to $I_0^{1/2}$. Hence, if the value of I_0 is only known to within a factor of 10, the threshold intensity can still be calculated within a factor of approximately three.

V. THERMAL DISTORTION AND THERMAL FRACTURE

The failure modes of thermal distortion and thermal fracture occur primarily in repeated-pulse systems. Besides having greater single-pulse-intensity thresholds than other failure modes such as free-carrier optical distortion, thermal distortion may not occur during the pulse and fracture may not occur until after the pulse has been transmitted. In the absorption process, the energy absorbed during the first part of the pulse goes primarily into creating free carriers. This energy is not converted into heat until the free carriers recombine in a time as long as 10^{-4} to 10^{-2} sec. The energy absorbed by the free carriers degrades rapidly into heat in a time comparable to the electron-collision time of approximately 10^{-14} sec. Even after the absorbed energy is degraded into heat, thermal distortion and thermal fracture do not occur immediately. In order for these effects to take place, it is necessary for the material to expand, which takes a time comparable to the time for sound to traverse the sample, i. e., of the order of 10^{-5} sec/cm.

Cooling window materials is generally not effective in reducing thermal effects, since for reasonably large windows, the thermal time constant is greater than the total operating time of the laser. With edge cooling, the thermal time constant is

$$\tau_E = C (1/2 D)^2 / 4 K \quad , \quad (5.1)$$

where C is heat capacity, K is the thermal conductivity, and D is the window diameter. Using the typical values of $C = 2 \text{ J/cm}^3 \text{ K}$ and $K = 0.1 \text{ W/cm}^2 \text{ K}$ τ_E is equal to 125 sec for a 10 cm window diameter. With face cooling, the thermal time constant is

$$\tau_F = \frac{C \ell}{h} \left(1 + \frac{h \ell}{3K} \right) \quad , \quad (5.2)$$

Sec. D-V

where ℓ is the window thickness and h is the surface heat-transfer coefficient. Using $h = 10^{-2} \text{ W/cm}^2 \text{ K}$ and $\ell = 1 \text{ cm}$, the value of the time constant is 207 sec. Hence, for operating periods less than these time constants, the absorbed energy integrates, and the total temperature rise is the sum of increases for each individual pulse.

Optical distortion results from the optical path for a ray transversing the center of the window being different from that for a ray near the edge of the window. This results from greater laser intensities, hence greater temperatures, near the center of the window.¹³ With uniform intensities and uniform heating, there may be an equal change in the optical path for all rays, but no distortion. Estimates for the optical-distortion intensity threshold are made from the change in the optical path through the center of the window:

$$\ell \Delta T \left| \partial_{nT} \right| \cong \lambda / \gamma, \quad (5.3)$$

where γ is typically an integer in the range from 10 to 100 and ∂_{nT} is

$$\partial_{nT} = (\partial n / \partial T)_\sigma + \alpha(1 + \nu)(n - 1) + S, \quad (5.4)$$

where the derivative is taken at constant stress, α is the linear expansion coefficient, ν is the Poisson ratio, and S is a small stress-optic term. The first term is the explicit change in the refractive index with temperature, and the second term results from bulging at the center of the window due to nonuniform heating.

Taking the window thickness equal to 1 cm, Eq. (5.3) is readily solved for the optical distortion temperature rise:

$$\Delta T_o = \lambda / \gamma \left| \partial_{nT} \right|. \quad (5.5)$$

The temperature rise for fracture is given by

$$\Delta T_f = 2\sigma/\alpha ESF, \quad (5.6)$$

where σ is the fracture strength, E is the Young's modulus, and SF is the safety factor usually equal to 4. Values of ΔT_o and ΔT_f are given in Table III for several materials using $\gamma = 40$. Alkaline-earth fluorides generally have small values of ∂_{nT} , and hence, large values of ΔT_o . Depending on the value of ν , which changes with crystal orientation, the first and second terms in Eq. (5.4) for alkaline-earth fluorides may cancel. This possible cancellation is shown as a function of wavelength for CaF_2 in Fig. 10.¹⁴ Oxides tend to have σ/E ratios and large fracture temperatures. However, oxides may suffer two-photon absorption, and this advantage may be lost to a larger absorption coefficient. It is cautioned that one of the major differences between materials is the achievable absorption coefficient. In the following calculation of intensity thresholds, the values $\Delta T_o = 0.1 \text{ K}$ and $\Delta T_f = 10 \text{ K}$ are used as typical values.

The temperature rise upon irradiation is given by

$$\Delta T = (I/C) \int \beta(t) dt, \quad (5.7)$$

where expressions for $\beta(t)$ under various conditions have been derived in the previous section. For a material limited by extrinsic absorption, the expression for $\beta(t)$ from Eq. (4.10) is readily integrated to give

$$\Delta T = \frac{I\beta_0 t}{C} + \frac{I^2\beta_0}{C\hbar\omega} (\sigma_F - \sigma_b) \left[\tau_R' t - \tau_R'^2 + \tau_R'^2 C^{-t/\tau_R'} \right], \text{ impurity.} \quad (5.8)$$

At short times, the absorption coefficient equals β_0 and the temperature rise is linear in I and t . At later times as the impurity levels become depleted, the temperature increases at a faster or slower rate, depending on whether the free-carrier cross section is greater than or less than the bound-electron cross section.

Table III. Comparison of thermal distortion and thermal fracture parameters for some candidate materials.

Material	n	$\alpha (10^{-6} \text{K}^{-1})$	$C (\text{J/cm}^3 \cdot \text{K})$	$K (10^{-2} \text{W/cm} \cdot \text{K})$	$\frac{dn}{dT} (10^{-6} \text{K}^{-1})$	$\Delta T_o (K)$	$\sigma (10^3 \text{psi})$	$E (10^6 \text{psi})$	$\Delta T_F (K)$
LiF	1.40	33.2	4.11	11	-16	~ 1	3.6	12	4.5
MgF ₂	n_o 1.39	13.7	3.14	12	+2.3	8.8	0.098	7.6	24
	n_e 1.40				+1.7				
CaF ₂	1.45	19.7	2.71	10	-9.44	1.6	0.56	6	17
Al ₂ O ₃	1.80	5.6	3.0	23	+17	23	0.039	65	50
		5.0		25					
SiO ₂ (X-tal)	n_o 1.566	7.4	2.0	12	-4.04	2.9	0.46	~ 10	15
	n_e 1.576	13.6		6.8	-5.11				
SiO ₂ (fused)	1.48	0.41	1.7	1.4	+14.1	14	0.061		

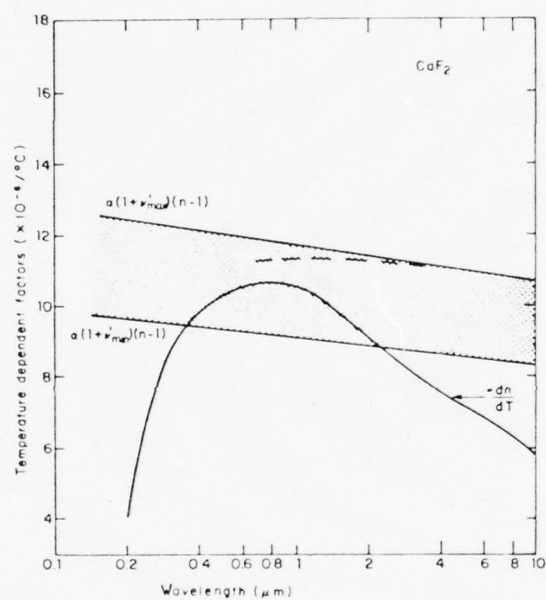


Fig. 10. Wavelength dependence of terms in the thermal distortion expression for CaF_2 demonstrating a possible cancellation in the visible and near uv spectral regions. (From Miles, Ref. 14)

This is illustrated in Fig. 11 using $\beta_0 = 10^{-4} \text{ cm}^{-1}$ and $I = 10^7 \text{ W/cm}^2$. For $\sigma_b = \sigma_F$, the second term in Eq. (5.8) is zero, and the temperature increases linearly with pulse duration reaching $5 \times 10^{-4} \text{ K}$ for $t = 10^{-6} \text{ sec}$. For $\sigma_b = 10^2 \sigma_F$, the bound electrons become depleted after approximately 10^{-9} sec . Subsequently, the absorption coefficient decreases and the temperature again increases linearly in time at a different slope. With the smaller cross section $\sigma_b = 10^{-2} \sigma_F$, depletion does not occur until 10^{-6} sec at this intensity.

In the case where $\sigma_F = \sigma_b$, threshold intensities for optical distortion or thermal fracture are easily obtained from Eq. (5.8):

$$I = C \Delta T / \beta_0 t, \quad \sigma_F = \sigma_b, \quad \text{impurity.} \quad (5.9)$$

For a pulse duration of 10^{-6} sec and an optical distortion temperature rise of 0.1 K , the single-pulse threshold intensity is $2.0 \times 10^9 \text{ W/cm}^2$, using $C = 2 \text{ J/cm}^3 \text{ K}$ and $\beta_0 = 10^{-4} \text{ cm}^{-1}$. For a repetitively pulsed system having a total operating time less than the thermal time constant of the window, the temperature rise is linear in the number of pulses, and the threshold intensity decreases by the same factor. With a system pulsed at 10^3 Hz for 60 sec (6×10^4 pulses), the optical distortion threshold decreases to $3.3 \times 10^4 \text{ W/cm}^2$. The temperature rise of 10 K for thermal fracture is 100 times greater than ΔT_0 , and the thresholds for a single pulse and repeated pulses become $2.0 \times 10^{11} \text{ W/cm}$ and $3.3 \times 10^6 \text{ W/cm}^2$, respectively.

Lower thresholds will be obtained if $\sigma_F > \sigma_b$, and greater thresholds will be obtained if $\sigma_F < \sigma_b$ at the same initial absorption coefficient $\beta_0 = 10^{-4} \text{ cm}^{-1}$. Cases involving other initial values of β_0 or different pulse durations with $\sigma_F = \sigma_b$ can be simply obtained from Eq. (5.9).

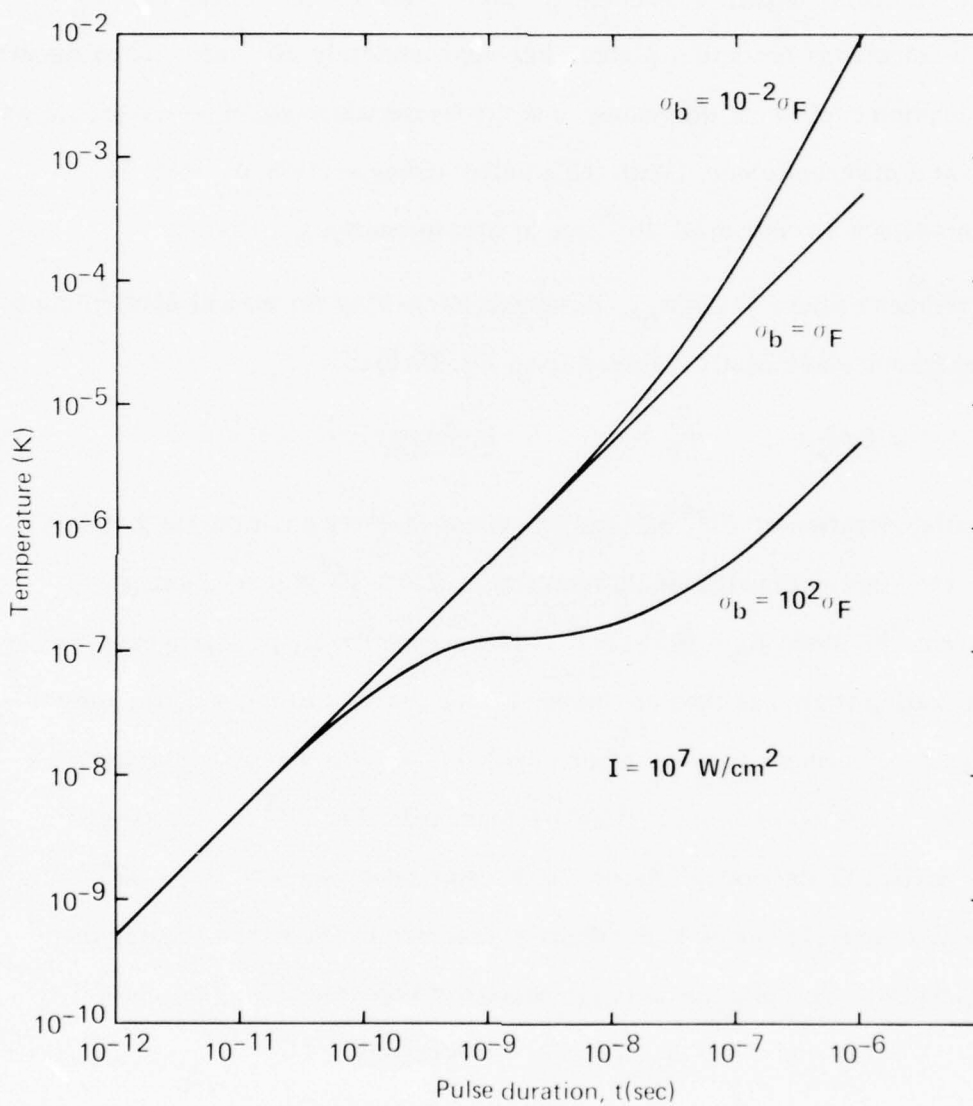


Fig. 11. Temperature rise as a function of time in materials limited by donor-impurity absorption having an initial absorption coefficient of 10^{-4} cm^{-1} and various impurity-absorption cross sections.

Sec. D-V

For all practical cases involving two-photon absorption, depletion of the bound electrons does not occur, and the short-time limit for β in Eq. (4.12) can be used. Integration yields

$$\Delta T = \frac{I_0^2 t}{I_0 C} + \frac{I_0^3 t^2}{4 I_0 C \hbar \omega} (\sigma_F - \sigma_2), \quad t \ll \tau_R', \quad \text{two-photon}, \quad (5.10)$$

Temperature increases are plotted as a function of time for four laser intensities in Fig. 12. At short times in the figure, the temperature rise is due to the creation of electron-hole pairs, and ΔT is linear in time and proportional to I^2 . At longer times depending on the intensity, free-carriers dominate the absorption, and ΔT is proportional to t^2 and I^3 .

At intensities near the single-pulse threshold intensities, the two terms in Eq. (5.10) tend to make comparable contributions to the temperature rise. With long pulse durations comparable to 10^{-6} sec, the second term from free carriers tends to be dominant, yielding the threshold

$$I = \left(\frac{4 I_0 C \hbar \omega \Delta T}{t^2 \sigma_F} \right)^{1/3}, \quad \text{two-photon, single pulse, } t \gtrsim 10^{-7} \text{ sec.} \quad (5.11)$$

Using $I_0 = 1.7 \times 10^8 \text{ W/cm}^2$ and $\sigma_F = 2.4 \times 10^{-18} \text{ cm}^2$, the optical distortion temperature of 0.1 K occurs at an intensity $2.9 \times 10^6 \text{ W/cm}^2$ with a pulse duration of 10^{-6} sec. The single-pulse thermal fracture threshold intensity is $1.4 \times 10^7 \text{ W/cm}^2$ using $\Delta T_f = 10 \text{ K}$.

With repeated pulses or with a single short-duration pulse, the first term in Eq. (5.10) from the free-carrier creation tends to dominate the temperature rise. In these cases, threshold intensities are obtained from

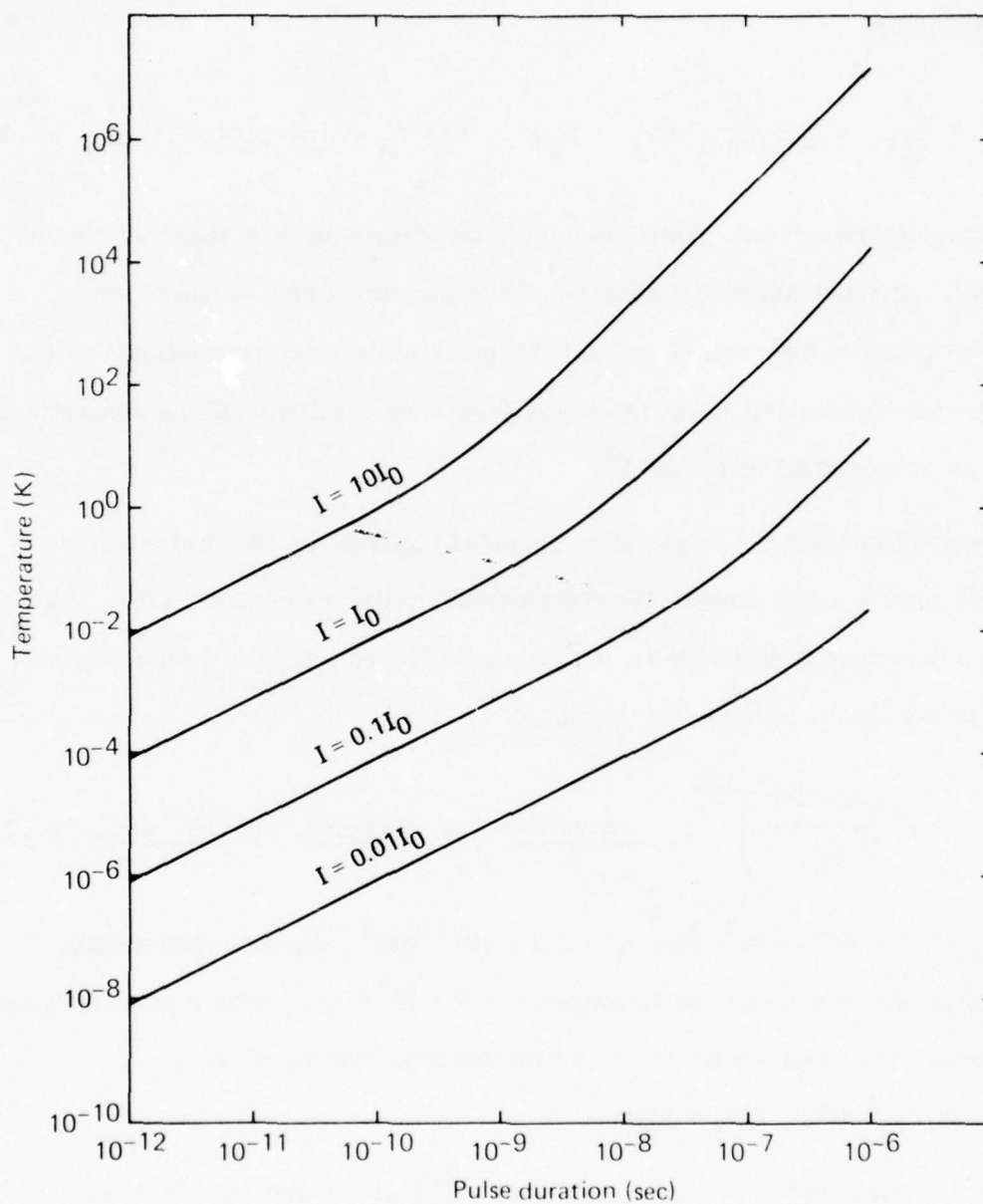


Fig. 12. Temperature rise as a function of time at four laser intensities in a material limited by intrinsic two-photon absorption.

$$I = \frac{I_0 C \Delta T}{q t}^{1/2}, \quad \text{two-photon, repeated-pulse,} \quad (5.12)$$

where q is the number of pulses. For 6×10^4 pulses of 10^{-6} sec duration, the optical-distortion threshold intensity is $2.4 \times 10^4 \text{ W/cm}^2$, and the thermal-fracture threshold intensity is $2.2 \times 10^5 \text{ W/cm}^2$. Because of the square-root dependence on ΔT , the threshold for fracture is a factor of only 10 greater than the optical-distortion threshold, even though the two temperatures differ by a factor of 100. This fractional-power dependence results in the threshold intensities being somewhat insensitive to the value of I_0 . An order of magnitude change in I_0 results in a change of approximately 3 in the threshold.

Similarly, using the short-time limit for the three-photon absorption coefficient from Eq. (4.14), the temperature rise in this case is

$$\Delta T = \frac{I^3 t}{I_{03}^2 C} + \frac{I^4 t^2}{6 I_{03}^2 C \hbar \omega} (\sigma_F - \sigma_3), \quad \text{three-photon, } t \ll \tau_R'. \quad (5.13)$$

Temperature rises are plotted as a function of time in Fig. 13 for four intensities. At short times in the figure, the temperature increases linearly with time and is proportional to I^3 . At later times where the free-carrier contribution dominates the absorption, the temperature rise is proportional to t^2 and I^4 .

In contrast to the results for two-photon absorption, the second, free-carrier, term in Eq. (5.13) dominates the temperature rise for all thresholds of present interest and yields

$$I = \left(\frac{6 I_{03}^2 C \hbar \omega \Delta T}{q t^2 \sigma_F} \right)^{1/4}, \quad \text{three-photon,} \quad (5.14)$$

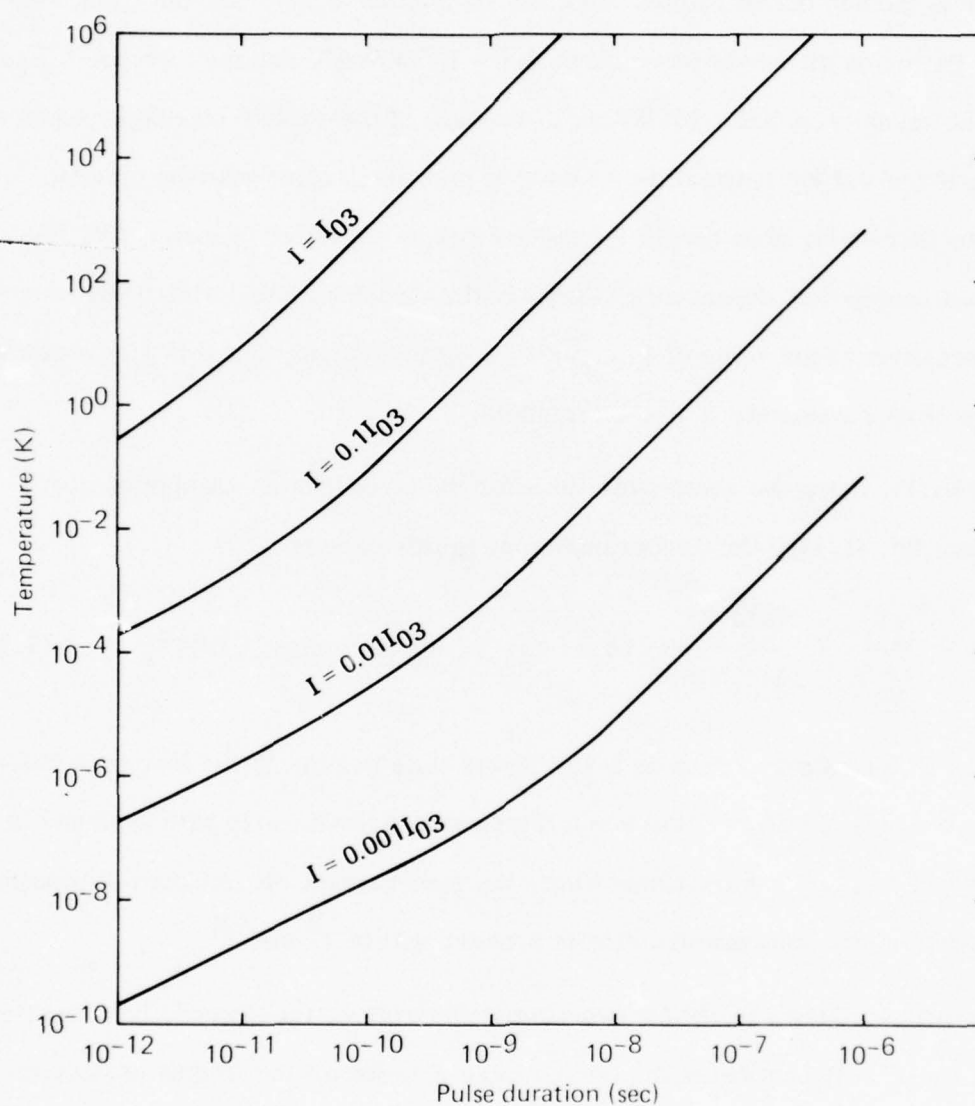


Fig. 13. Temperature rise as a function of time at four laser intensities in a material limited by intrinsic three-photon absorption.

where q is the number of pulses. This dominance of the free-carrier absorption occurs because large numbers of electron-hole pairs are created at the large intensities where the intrinsic three-photon absorption coefficient has moderate values. Using $I_{03} = 3.7 \times 10^{11} \text{ W/cm}^2$ and a pulse duration of 10^{-6} sec , the single-pulse thresholds for optical distortion and thermal fracture are $4.4 \times 10^8 \text{ W/cm}^2$ and $1.4 \times 10^9 \text{ W/cm}^2$, respectively. With a repeated-pulse system having 6×10^4 pulses, these thresholds decrease to $2.8 \times 10^7 \text{ W/cm}^2$ and $9.0 \times 10^7 \text{ W/cm}^2$, respectively.

As with two-photon absorption, the fractional-power dependence of the threshold intensity makes it insensitive to many of the parameters. Increasing the number of pulses by a factor of 10^4 decreases the thresholds by only a factor of 10. On the other hand, if the effective thermal time constant is decreased, perhaps by a factor of 60, using either adaptive optics or a rotating window, the three-photon thermal-distortion threshold increases by a factor of only 2.8. The threshold for a material limited by two-photon absorption would increase by a factor of 7.8 under these conditions, and the threshold for extrinsic absorption would increase by a factor of 60.

VI. NONLINEAR REFRACTIVE INDEX

Optical distortion from the nonlinear refractive index results from intensity dependence of the contribution of bound electrons to the refractive index. In contrast to optical distortion from free carriers which also involves an intensity-dependent refractive index, changes in the refractive index due to the nonlinear index occur instantaneously. The two mechanisms are not completely independent. The imaginary part of the nonlinear susceptibility is responsible for intrinsic multiphonon absorption which may give rise to free carriers. Additionally, at frequencies near half the band gap of a material where two-photon absorption occurs, a resonant enhancement of the nonlinear index is expected. The value of the two-photon enhancement is estimated to be approximately three in LiF.¹

The change in the refractive index is generally written as

$$\delta n = n_2 \langle E^2 \rangle, \quad (6.1)$$

where n_2 is the nonlinear refractive index and $\langle E^2 \rangle$ is the rms electric field strength. Using $I = cn_0 \langle E^2 \rangle / 4\pi$ where c is the velocity of light and n_0 is the linear refractive index, the change in the optical path through a material of thickness l is typically restricted to less than a fraction of a wavelength:

$$\frac{4\pi n_2 I}{cn_0} l \leq \frac{\lambda}{\gamma}, \quad (6.2)$$

where γ is typically an integer in the range from 10 to 100. For a material thickness of 1 cm, the intensity threshold for distortion is

$$I = \frac{n_0 c \lambda}{4\pi \gamma n_2}. \quad (6.3)$$

Sec. D-VI

Neglecting the enhancement in n_2 and using the typical low-frequency value of $n_2 = 10^{-13}$ esu, the intensity threshold is $3.1 \times 10^9 \text{ W/cm}^2$ at 350 nm wavelength with $\gamma = 40$ and $n_0 = 1.5$.

VII. ABSORBING INCLUSIONS

Localized fracture from absorbing inclusions is primarily a single-pulse phenomenon because the energy absorbed by the inclusions tends to reach thermal equilibrium between pulses in repeated-pulse systems. The most troublesome size and type of inclusion are identified in the following analysis for inclusions located in the bulk material.¹⁵ For inclusions located near the surface or near defects, similar most troublesome sizes are expected, although the damage thresholds will be lower than for bulk inclusions.

For wavelengths and pulse durations of interest, the most-troublesome-size inclusion has a radius given by

$$a_{eq} = (2 K_H t / C_I)^{1/2} , \quad (7.1)$$

where K_H is the thermal conductivity of the host material, C_I is the heat capacity of the inclusion material, and t is the pulse duration. Equation (7.1) is approximately valid for both absorbing dielectric and metallic inclusions in a transparent host material. This most-troublesome-size inclusion is the largest size inclusion that is in thermal equilibrium at time t , i.e., heat is being conducted away from the inclusion as rapidly as it is absorbed. Using the typical values $K_H = 10^{-1}$ W/cm K and $C_I = 2$ J/cm³ K in Eq. (7.1) yields

$$a_{eq} = 0.4 t^{1/2} , \quad (7.2)$$

where units of a_{eq} are centimeters for t in seconds. Values of a_{eq} range from 0.1 μ m to 4 μ m for t ranging from 1 ns to 1 μ s.

The absorption cross sections σ_{abs} for metallic and dielectric inclusions in this size range are given by $\pi a^2 (1 - R)$ and $4\beta_I \pi a^3 / 3$, respectively, where R

is the metallic reflectivity and β_I is the absorption coefficient of the dielectric inclusion material. The lowest damage thresholds are obtained for strongly absorbing dielectric inclusions because of their greater absorption cross sections.

The temperature at the center of a dielectric inclusion is given by

$$T = \frac{3\sigma_{\text{abs}} I}{8\pi a K_{\text{eff}}} \quad , \quad (7.3)$$

where $K_{\text{eff}}^{-1} = (2K_H^{-1} + K_I^{-1})/3 \cong K_H^{-1}$. Using Eq. (7.1) and the absorption cross section yields the temperature of the most troublesome size inclusion,

$$T = (\beta_I / C_I) I t \quad (7.4)$$

Assuming that failure occurs at a temperature rise T_F , the energy density for failure is

$$I_F t = (C_I / \beta_I) T_F \quad . \quad (7.5)$$

Using $T_F = 1000$ K and $C_I = 2 \text{ J/cm}^3 \text{ K}$, a failure energy density of less than 2 J/cm^2 is obtained for β_I greater than 10^3 cm^{-1} . Lower failure energy densities can occur for more strongly absorbing inclusions or for inclusions located near the surface or near defects.

This analysis indicates that absorbing inclusions are potentially troublesome at the energy densities of interest. The worst-case damage thresholds calculated above are comparable to those that have been calculated previously for infrared absorption and to those observed experimentally in infrared materials containing such inclusions. However, as experience with high-power infrared materials has demonstrated, care in materials preparation can eliminate at least those absorbing inclusions in the most-troublesome-size range.

VIII. SUMMARY OF SINGLE-PULSE THRESHOLDS

Single-pulse intensity thresholds, for various failure mechanisms calculated in the previous sections, are presented as a function of pulse duration in Fig. 14. The curves are labeled using a scheme where the first two characters denote the number of photons involved in the absorption and the following characters denote the failure mode. For example, 2PFCOD denotes two-photon free-carrier optical distortion. Two of the curves do not fit this scheme. The one labeled Inc. denotes localized fracture from absorbing inclusions, and the one labeled NLI denotes distortion from the nonlinear refractive index.

Those mechanisms arising from extrinsic absorption are presented as dashed curves. In calculating the thresholds, an extrinsic absorption coefficient of 10^{-4} cm^{-1} was used, and it was assumed that the impurity absorption cross section equaled the free-electron absorption cross section of $2.4 \times 10^{-18} \text{ cm}^2$. With this cross section assumption, the extrinsic thresholds involving thermal mechanisms are inversely proportional to the absorption coefficient and, hence, decrease accordingly for larger absorption coefficients. At the same value of the absorption coefficient, the thresholds will decrease if the impurity absorption cross section is less than the free-electron cross section. The extrinsic free-carrier optical distortion curve assumes that there are sufficient electrons available to cause distortion. This may not be valid for strongly absorbing impurities which may not yield enough electrons even when the impurity levels are completely depleted. A failure energy density of 2 J/cm^2 has been used for localized fracture from absorbing inclusions. This threshold should increase with material improvement programs.

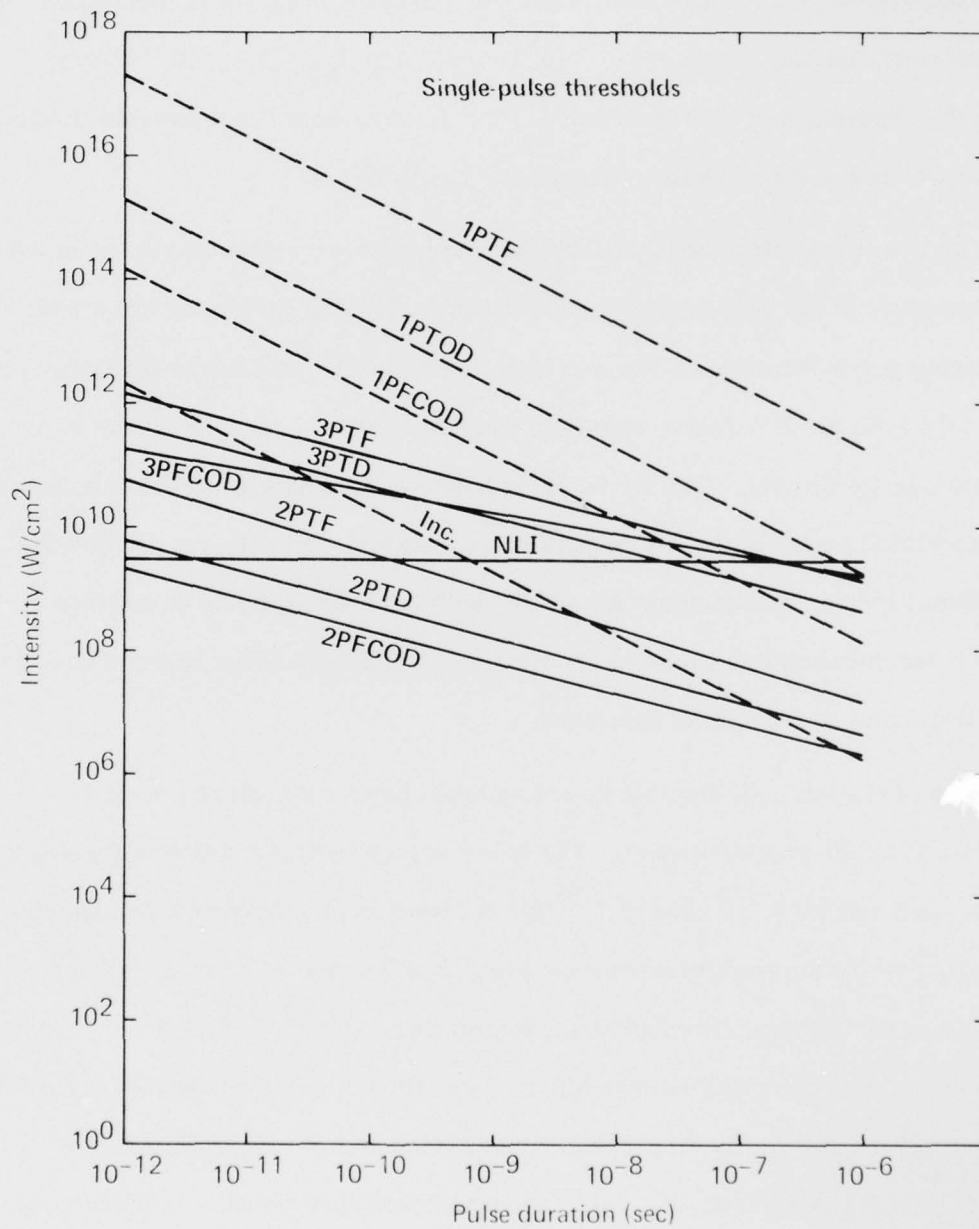


Fig. 14. Summary of single-pulse thresholds for failure as a function of the pulse duration.

Sec. D-VIII

The threshold curves for mechanisms involving intrinsic two-photon and three-photon absorption are drawn as solid curves. In calculating these thresholds, the characteristic intensities $I_0 = 1.7 \times 10^8 \text{ W/cm}^2$ and $I_{03} = 3.7 \times 10^{11} \text{ W/cm}^2$, where the absorption coefficients equal 1 cm^{-1} , were used for materials limited by two-photon and three-photon absorption, respectively.

With the exception of the threshold for the nonlinear refractive index which is independent of the pulse duration, all the intensity thresholds increase with decreasing pulse durations. The extrinsic intensity thresholds are inversely proportional to the pulse duration with the result that these thresholds occur at a constant energy density. The intrinsic multiphoton intensity thresholds increase as a fractional power of the decreasing pulse duration. Hence, energy density for the multiphoton mechanisms decreases with decreasing pulse durations. These pulse duration dependences result in extrinsic absorption being relatively more important at long pulse durations.

Most of the intrinsic multiphoton thresholds have a simple power-law dependence on the pulse duration. The free-carrier optical distortion thresholds are proportional to $t^{-1/2}$ and $t^{-1/3}$ for two-photon and three-photon absorption, respectively. In the regions where the heating is dominated by free-carrier absorption, the thermal thresholds are proportional to $t^{-2/3}$ and $t^{-1/2}$ for two-photon and three-photon absorption, respectively. This occurs for all pulse durations in the figure for three-photon absorption and for pulse durations greater than approximately 10^{-8} sec for two-photon absorption. At pulse durations less than 10^{-8} sec, the two-photon absorption is dominated by the creation of the free carriers, and the thresholds are proportional to $t^{-1/2}$.

It should be cautioned that with a single pulse, thermal distortion and thermal fracture may not occur until after the pulse has passed through the sample. This is because the absorbed energy that went into creating the free carriers is not converted into heat until after the free carriers recombine. Even then it is still necessary for the lattice to expand for the refractive index to change or for fracture to occur.

The intensity thresholds at a pulse duration of 10^{-6} sec are summarized in Fig. 15. The mechanism having the lowest intensity threshold is localized fracture from absorbing inclusions at the threshold value of $2 \times 10^6 \text{ W/cm}^2$. With care in materials preparation, this extrinsic threshold may be able to be increased to 10^8 W/cm^2 . Materials suffering intrinsic two-photon absorption have the thresholds of $2.2 \times 10^6 \text{ W/cm}^2$, $2.9 \times 10^6 \text{ W/cm}^2$ and $1.4 \times 10^7 \text{ W/cm}^2$ for free-carrier optical distortion, thermal distortion, and thermal fracture, respectively. These values are somewhat insensitive to the value used for I_0 , with the free-carrier optical distortion threshold being proportional to $I_0^{1/2}$ and with the thermal thresholds being proportional to $I_0^{1/3}$.

The lowest extrinsic threshold for $\beta = 10^{-4} \text{ cm}^{-1}$ is the free-carrier optical distortion threshold of $1.4 \times 10^8 \text{ W/cm}^2$. This value is greater than the intrinsic two-photon absorption thresholds, and such low levels of impurity absorption will not be a limitation for single pulses in two-photon limited materials. There may not be enough electrons available to cause optical distortion. To achieve the number 2.4×10^{16} electrons required for distortion, the impurity absorption cross section must be less than $4.2 \times 10^{-21} \text{ cm}^2$ at $\beta = 10^{-4} \text{ cm}^{-1}$.

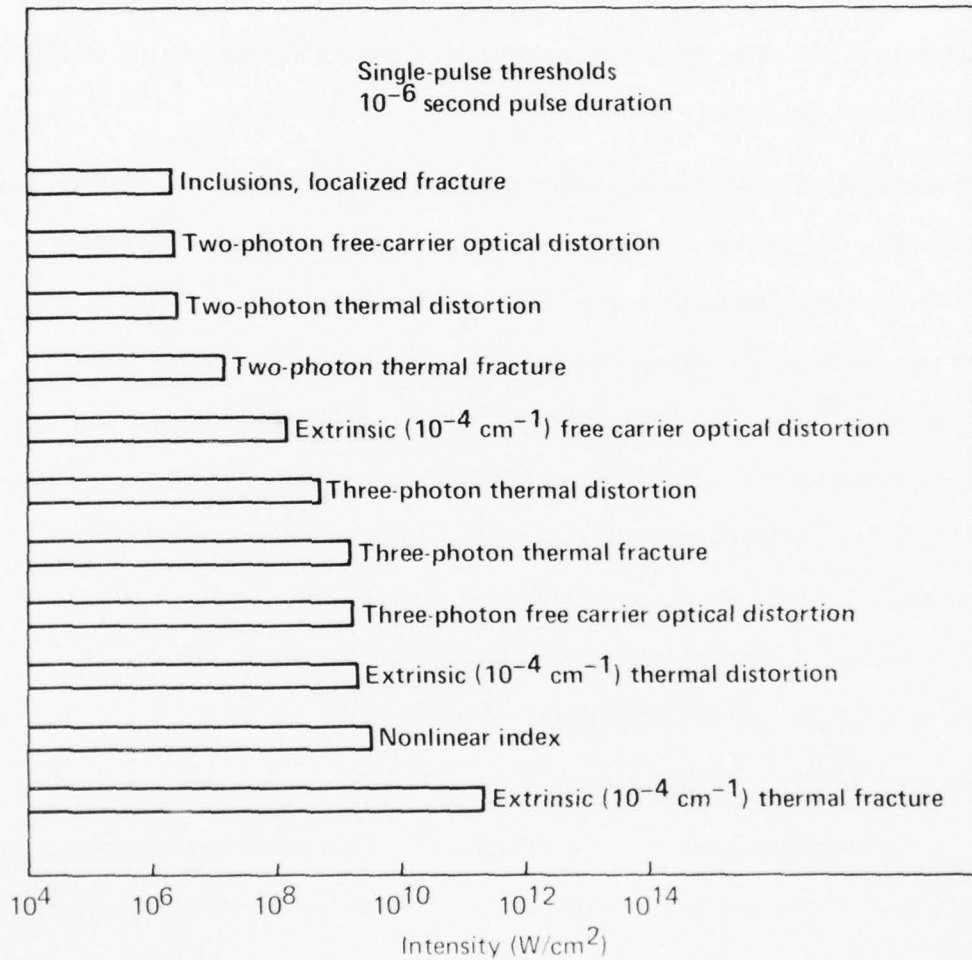


Fig. 15. Summary of single-pulse thresholds for a 10^{-6} sec duration pulse.

For a material limited by intrinsic three-photon absorption and not affected by extrinsic free-carrier optical distortion, the single-pulse thresholds for thermal distortion, thermal fracture, and free-carrier optical distortion are $4.4 \times 10^8 \text{ W/cm}^2$, $1.4 \times 10^9 \text{ W/cm}^2$, and $1.8 \times 10^9 \text{ W/cm}^2$, respectively. With this intrinsic absorption mechanism, the thermal thresholds occur at lower intensities than the free-carrier distortion intensity, as opposed to two-photon and extrinsic absorption which occur in the opposite order. This arises because of the intense heating of the free carriers that occurs at the high intensities associated with three-photon absorption.

The single-pulse intensity thresholds for thermal distortion and thermal fracture with an extrinsic absorption coefficient of 10^{-4} cm^{-1} are $2 \times 10^9 \text{ W/cm}^2$ and $2 \times 10^{11} \text{ W/cm}^2$, respectively. These values are derived assuming equal impurity and free-carrier absorption cross sections and will increase or decrease, depending on the actual value of the impurity cross section.

The nonlinear refractive index yields an optical distortion threshold of $3.1 \times 10^9 \text{ W/cm}^2$. This threshold is greater than other previously considered thresholds at a pulse duration of 10^{-6} sec. At shorter pulse durations this intensity threshold remains constant and becomes relatively more important in comparison to the other thresholds which increase with decreasing pulse durations. At intensities greater than 10^9 W/cm^2 , other nonlinear effects that have not been considered explicitly may occur. Such effects include "optical distortion" from frequency doubling, frequency tripling or Raman shifting of the frequency. Since Raman scattering is an inelastic process, enhanced-stimulated Raman scattering can result in intense heating with the associated thermal effects.

IX. SUMMARY OF REPEATED-PULSE THRESHOLDS

Pulse-intensity thresholds are presented as a function of the pulse duration in Fig. 16 for systems having 6×10^4 pulses within the thermal time constants of the materials. An example is a laser pulsed at 10^3 Hz for a total operating period of 60 sec incident on a 10 cm diameter window whose time constant for edge cooling is 125 sec. The average intensity is the single-pulse intensity multiplied by the pulse duration and the repetition rate. With a repetition rate of 10^3 Hz and a pulse duration of 10^{-6} sec, the average intensity is 10^{-3} times the single-pulse intensity.

Certain failure mechanisms attain equilibrium between pulses and have the same intensity threshold values for single or repeated pulses. Such mechanisms are the nonlinear index, absorbing inclusions, and free-carrier optical distortion which have the same threshold values in Figs. 14 and 16. The equilibrium assumption is well satisfied for the nonlinear index which reaches equilibrium at optical frequencies, and absorbing inclusions which reach equilibrium at times comparable to the pulse duration. However, with free-carrier optical distortion, free carriers from one pulse may persist until the next pulse, depending on the recombination time which may be as long as 10^{-2} sec.

For operating times less than the thermal time constant of the material, the heat induced by the individual pulses integrates, and the thermal distortion and thermal fracture thresholds are reduced accordingly. In materials limited by two-photon absorption, the dominant heating mechanism goes from free-carrier absorption to the two-photon absorption in going from a single pulse to repeated pulses. Free-carrier absorption remains the dominant heating mechanism with

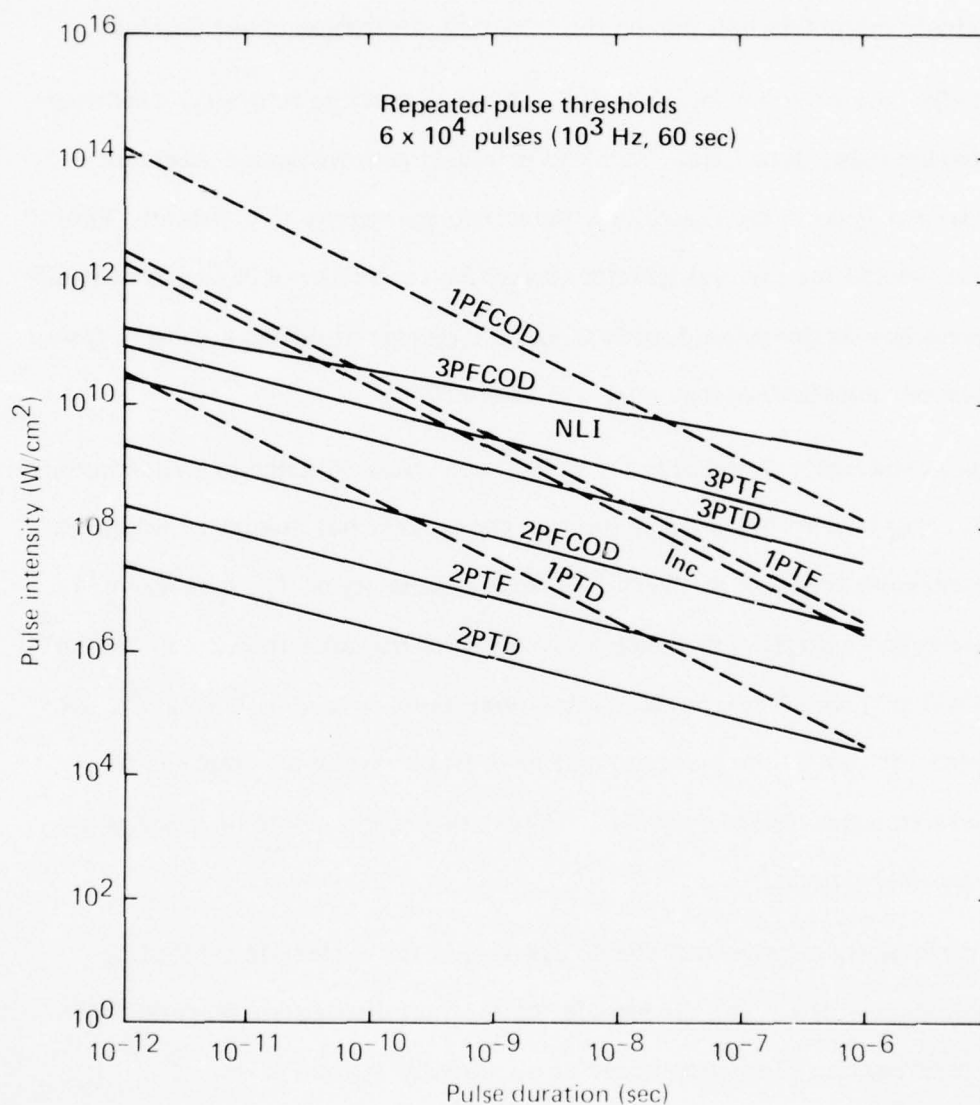


Fig. 16. Summary of repeated-pulse thresholds for failure as a function of pulse duration for a system pulsed at 10^3 Hz for 60 sec. The average intensities for failure are equal to the pulse intensity multiplied by the product of the pulse duration and the repetition rate.

Sec. D-IX

three-photon absorption. The relative contribution of free carriers to the heating in extrinsic materials depends on the impurity absorption cross section.

Generally the pulse energy density, hence the average intensity, decreases with decreasing pulse durations. With the extrinsic absorption mechanisms shown as dashed lines in the figure, the pulse energy density is constant. The intensity thresholds for the multiphoton absorption mechanisms have a fractional-power dependence on the pulse duration, and the energy densities decrease faster than the dashed, constant-energy contours in the figure.

The pulse-intensity thresholds for a 10^{-6} sec pulse duration are summarized in Fig. 17. The lowest threshold is the two-photon thermal distortion threshold at a pulse intensity of $2.4 \times 10^4 \text{ W/cm}^2$ (average intensity of $I_{av} = 24 \text{ W/cm}^2$). Other two-photon absorption thresholds are thermal fracture at $2.2 \times 10^5 \text{ W/cm}^2$ ($I_{av} = 220 \text{ W/cm}^2$) and free-carrier optical distortion at $2.2 \times 10^6 \text{ W/cm}^2$. At the repetition rate used, the material will have fractured by the time the free-carrier distortion threshold is reached. These two mechanisms have the same threshold for 600 pulses.

The intrinsic-absorption thresholds are larger for materials limited by three-photon absorption. The thresholds for thermal distortion, thermal fracture, and free-carrier distortion occur at the closely-spaced values of $2.8 \times 10^7 \text{ W/cm}^2$ ($I_{av} = 2.8 \times 10^4 \text{ W/cm}^2$), $8.9 \times 10^7 \text{ W/cm}^2$ ($I_{av} = 8.9 \times 10^4 \text{ W/cm}^2$) and $4.4 \times 10^8 \text{ W/cm}^2$ ($I_{av} = 4.4 \times 10^5 \text{ W/cm}^2$), respectively.

A potentially serious difficulty is posed by the low thresholds that occur with extrinsic absorption. With an extrinsic absorption coefficient of 10^{-4} cm^{-1} , the thresholds for thermal distortion and thermal fracture are less than those

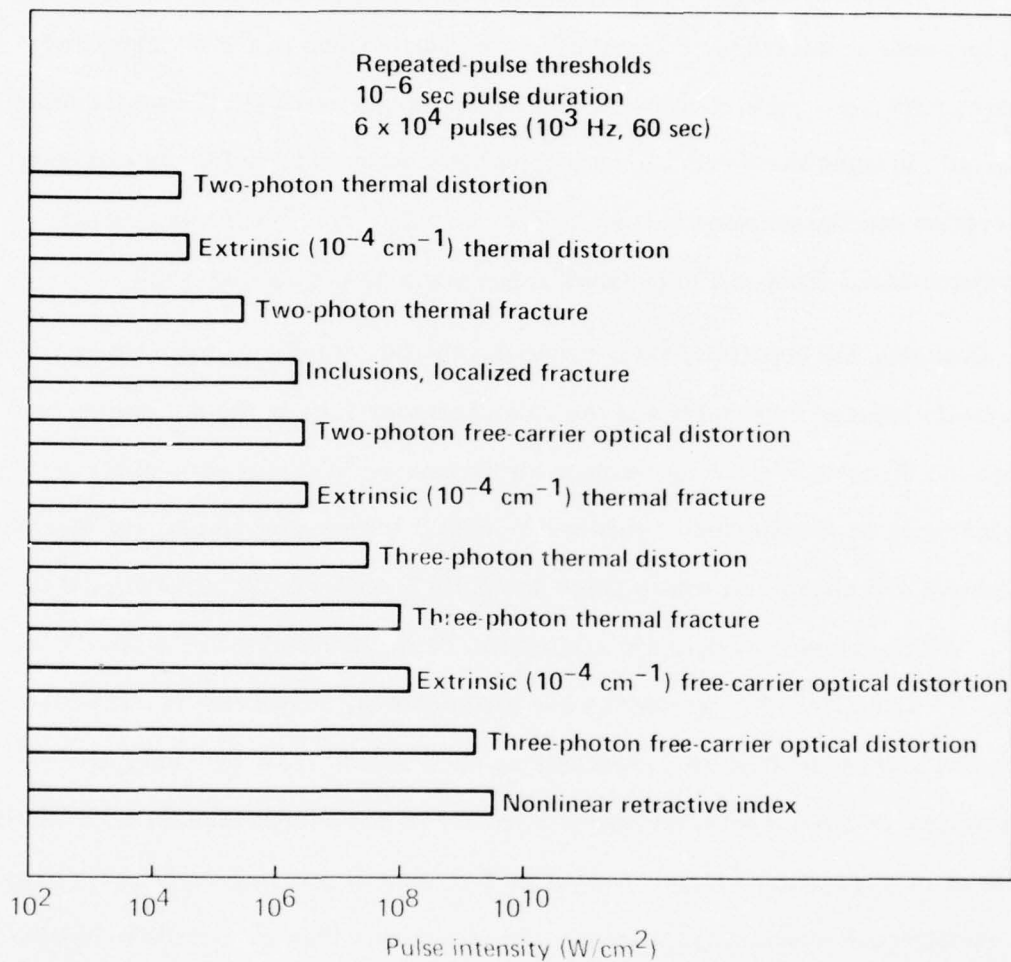


Fig. 17. Summary of repeated-pulse thresholds for 10^{-6} sec duration pulses repeated at 10^3 Hz for 60 sec. The average intensities are 10^{-3} times the pulse intensities.

Sec. D-IX

for three-photon absorption and have the values $3.3 \times 10^4 \text{ W/cm}^2$ ($I_{av} = 33 \text{ W/cm}^2$) and $3.3 \times 10^6 \text{ W/cm}^2$ ($I_{av} = 3.3 \times 10^3 \text{ W/cm}^2$), respectively. These thresholds will increase or decrease, depending on the relative size of the impurity and free-carrier absorption thresholds. In order for the extrinsic thermal-distortion threshold to equal the three-photon thermal-distortion threshold, the extrinsic absorption coefficient must be reduced to $1.2 \times 10^{-7} \text{ cm}^{-1}$ with the present repetition rate. This is a very small value that may not be achievable.

Changing the repetition rate, hence the number of pulses, will change the thermally induced thresholds and the relative importance of the thresholds because the thresholds from the various absorption mechanisms have different dependences on the number of pulses q . With extrinsic absorption, the thermal-distortion and thermal-fracture pulse-intensity thresholds are proportional to q^{-1} . With intrinsic multiphonon absorption, these thresholds are proportional to $q^{-1/2}$ and $q^{-1/4}$ for two-photon and three-photon, respectively. The lesser sensitivity of the multiphonon mechanisms on q arises from the nonlinear dependence of the temperature on the intensity in these mechanisms, with small changes in I producing large changes in T . With decreasing repetition rates, the multiphonon mechanisms become more important than the extrinsic mechanism. The pulse-intensity thresholds for thermal distortion from extrinsic absorption (10^{-4} cm^{-1}) and from three-photon absorption are equal at $q = 71$, e.g., 1.2 Hz for 60 sec. Although the pulse-intensity thresholds decrease with increasing repetition rates, the average intensity generally increases, being independent of q for intrinsic absorption and having the dependences $q^{1/2}$ and $q^{3/4}$ for two-photon and three-photon absorption, respectively.

The effective number of pulses can be changed by reducing the effective thermal time constant to a value less than the total operating time of the laser with the use of adaptive optics or using rotating windows. If the effective thermal time constant is reduced to 1 sec for a laser pulsed at 10^3 Hz for 60 sec, the effective number of pulses is reduced from 6×10^4 to 10^3 . Using the above dependences on q , the extrinsic pulse-intensity threshold for thermal distortion is increased by a factor of 60. This threshold is increased by the lesser factors of 7.8 and 2.8 for two-photon and three-photon absorption, respectively. Over the 60 sec operating period, the average intensities are increased by the same factors. If the thermal time constant is decreased by using a rotating window, the thermal-fracture thresholds will increase by the same factors. In the case where the thermal distortion is compensated by adaptive optics, thermal fracture may become the limiting failure mechanism. Fracture will not occur with the factor of 60 decrease in the effective operating period for thermal distortion in the example, since the resulting factor of 60 temperature increase is less than the ratio of the thermal-fracture temperature to the thermal-distortion temperature.

Sec. D-References

REFERENCES

1. C. J. Duthler in Theoretical Studies of High-Power Ultraviolet and Infrared Materials, Xonics, Inc. Fifth Technical Report, 30 June 1975, under Contract No. DAHC 15-73-C-0127.
2. M. Sparks, J. Appl. Phys. 46, 2134 (1975).
3. R. Braunstein, Phys. Rev. 125, 475 (1962).
4. M. Sparks in Theoretical Studies of High-Power Ultraviolet and Infrared Materials, Xonics, Inc. Third Technical Report, 30 June 1974, under Contract No. DAHC 15-73-C-0127.
5. K. Park and R. G. Stafford, Phys. Rev. Letters 22, 1426 (1969).
6. J. J. Hopfield, J. M. Worlock and K. Park, Phys. Rev. Letters 11, 414 (1963).
7. D. Fröhlich and B. Stagginnus, Phys. Rev. Letters 19, 496 (1967).
8. D. Fröhlich, B. Stagginnus and Y. Onodera, Phys. Stat. Sol. 40, 547 (1970).
9. R. Dinges, D. Fröhlich, B. Stagginnus and W. Stande, Phys. Rev. Letters 25, 922 (1970).
10. B. Stagginnus, D. Fröhlich and T. Caps, Rev. Sci. Inst. 39, 1129 (1968).
11. C. Kittel, Introduction to Solid State Physics (Wiley, New York, 1967), pp 322.
12. C. Kittel, *ibid*, pp. 227.
13. M. Sparks, J. Appl. Phys. 42, 5029 (1971); M. Sparks and H. C. Chow, J. Appl. Phys. 45, 1510 (1974).
14. P. Miles in Proceedings of the Infrared Laser Window Materials Meeting, compiled by C. R. Andrews and C. L. Strecker (Sept. 1976), p. 27.
15. M. Sparks and C. J. Duthler, J. Appl. Phys. 44, 3038 (1973).

Sec. E

E. LASER-INDUCED ELECTRON AVALANCHES IN
INSULATING SOLIDS

T. D. Holstein
Department of Physics
University of California
Los Angeles, California 90024

and

Xonics, Incorporated
Santa Monica, California 90401

In this first phase of investigation of electron-avalanche breakdown, the classical transport equation to be used is derived from the Boltzmann equation. A quasi-isotropy approximation and the Fokker-Planck expansion are used, and a current density, a conductivity tensor, and relaxation rates are introduced. The transport equation is used to derive an expression for the average electron-multiplication rate β . The electron-phonon interaction parameters appearing in β are evaluated. Applications to specific cases of interest will be included in a future report.

I. INTRODUCTION

The preliminary theory of electron-avalanche breakdown presented in the Fifth Technical Report (30 June 1975) explained experimental results satisfactorily for the first time. However, additional work is needed to determine the validity of the theory. The results below represent the results to date on this investigation in which the electron-avalanche process is considered from first principles. The previous technical report contained preliminary results for the transport operation.

In the present report we describe a theoretical approach to the computation of laser-induced electron multiplication insulating solids with special references to alkali-halide crystals. Both the physical contents and the mathematical structure correspond to those contained in treatments¹ of the analogous problem in gases. As in that case, the basic mechanism of multiplication is the non-radiative excitation of electrons from their ground states to a conducting state. In gases this amounts to ionization of individual atoms (or molecules); in insulating solids, the analogue is excitation of electrons from the (filled) valence band to the (empty) conduction band. In either case, the process requires a minimum energy (ionization energy or band-gap energy); this energy is supplied by the laser beam via various electronic processes. Two general mechanisms exist. (1) The free electrons gain energy from the combined action of the laser field and collisions, that is, by the inverse Brehmsstrahlung process. Under steady-state conditions, there exists a characteristic energy distribution for the electrons. In particular, that fraction of electrons whose energy exceeds the above mentioned threshold gives rise to "ionizing" collisions (i.e.,

collisions which produce electrons in the conduction band). This is the prevailing mechanism at sufficiently low laser irradiance. As will be discussed below the major inhibiting factor for this mechanism is the circumstance that, on their upward climb towards the ionization threshold, the free electrons have to transverse the "exciton barrier" (i.e., the energy region above the threshold for exciton formation). The occurrence of exciton-forming collisions, analogous to excitation collisions in gases, entails a severe energy loss by the impacting electrons, in contrast to the relatively small energy loss associated with electron-phonon collisions in the energy region below the exciton threshold. Thus most of the laser energy fed to the electrons ends up in the creation of excitations, rather than in electron multiplication. (2) When the applied laser field is sufficiently strong, the possibility of exciton photoionization in one or two-photon absorption becomes significant. In the case of the above cited treatment of the laser-produced ionization of gases¹, it was found that, under experimental conditions, the photoionization of excited atoms is so efficient that it could be assumed that every excited atom is ionized essentially instantaneously. The ionization rate is then essentially equal to the average rate of excitation collisions per electron.

In the present work, we shall begin by making an analogous assumption for insulating solids. Namely, we assume that every exciton will be photo-ionized instantaneously. With this simplification, the treatment will focus on the inverse-Bremsstrahlung mechanisms present in a typical insulator, in particular, how they determine a steady-state energy distribution. Subsequently, we shall investigate the validity of this assumption. This investigation will involve the

AD-A040 596

XONICS INC SANTA MONICA CALIF
THEORETICAL STUDIES OF HIGH-POWER ULTRAVIOLET AND INFRARED MATE--ETC(U)
DEC 76 M SPARKS, C J DUTHLER

F/G 20/5

DAHC15-73-C-0127

NL

UNCLASSIFIED

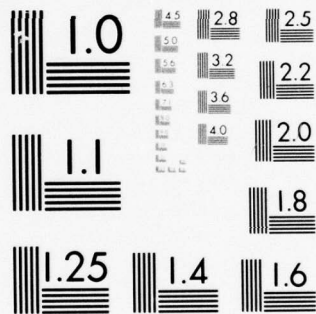
4 OF 4

AD
A040 596



END

DATE
FILMED
7-77



MICROCOPY RESOLUTION TEST CHART
NATIONAL BUREAU OF STANDARDS-1963-A

Sec. E-I

interesting question of the electronic states of the exciton, which, in the case of alkali halides, is self-trapped².

The core of the present treatment is a transport equation for the electron energy distribution function. In its classical form, valid when the laser frequency is sufficiently small, it may be derived from the nonlinear Boltzmann equation. This derivation is presented in Appendix A.

When the external frequency is sufficiently high—in practice, when the quantum of electron energy is comparable to the domain in which the electron energy distribution is found (usually *a posteriori*) to undergo appreciable relative variation — a derivation taking explicit account of the quantal character of the interaction of electrons with the external electromagnetic field is required. This derivation will be included in a subsequent report. As may be expected, the resulting equation reduces to its classical counterpart in the limit of sufficiently small external frequency.

Armed with our transport equation for the energy distribution function, we proceed (in Secs. II and III) to an analysis of the steady-state solution, having in mind the ultimate goal of obtaining the electron multiplication rate as a function of the magnitude and frequency of the external field and of the cross sections, in particular for the alkali-halide crystals. It should here be mentioned that, in order to render the problem tractable, it will be necessary to introduce simplifying model-type assumptions concerning these cross sections. Such a procedure is, in fact, all the more appropriate in view of the lack of even semi-quantitative information on said cross sections in an energy domain from one to ten electron volts, which is far in excess of conventional electron-transport phenomena in insulating solids.

Sec. E-I

We are now in a position to apply our results to specific practical cases of interest and to compare the results with our previous estimates. This will be carried out and the results included in future reports.

II. AVERAGE MULTIPLICATION RATE β

In this section an expression is derived for the average multiplication rate β . As stated in the Introduction, the basis of the treatment is a transport equation for the electron-energy distribution function $f(E)$. In Appendix A, a derivation of the classical form of this equation is given; the result (cf. (A 20)) is

$$N(E) \frac{\partial f(E)}{\partial t} = \frac{\epsilon_0^2}{6} \frac{\partial}{\partial E} \text{Re} \sigma(E, \omega) \frac{\partial f}{\partial E} + \frac{\partial}{\partial E} N(E) \frac{\Delta(E)}{\tau(E)} f(E) \quad (2.1)$$

In this equation ,

$$N(E) = \sum_k \delta(E - E_k) \quad (2.1)$$

is the density of states at an energy E , ϵ_0 the amplitude of the external field ($\epsilon = \epsilon_0 \cos \omega t$), $1/\tau(E)$ is the total collision rate due to electron-phonon interaction, and $\Delta(E)$ is the average energy loss per collision (cf. (A 13)). The remaining undefined quantity, $\sigma(E, \omega)$, is the "monoenergetic" conductivity given by (cf. (A 19) and (A 16b))

$$\sigma(E, \omega) = \sum_k \delta(E - E_k) e^2 \underline{v}_k \underline{\phi}_k(\omega)/3 \quad (2.3)$$

with $\underline{\phi}_k$ the solution of the "monoenergetic" vector-transport equation

$$\underline{v}_k = i\omega \underline{\phi}_k + \sum_{k'} (\underline{\phi}_{k'} - \underline{\phi}_k) \omega(\underline{k}, \underline{k}') \delta(E_k - E_{k'}) \quad (2.4)$$

(where $\omega(\underline{k}, \underline{k}') \delta(E_k - E_{k'})$ is the elastic approximation to the transition rate between states \underline{k} and \underline{k}').

An explicit formula for $\sigma(E, \omega)$ reads (cf. (A 23b))

$$\sigma(E, \omega) = \frac{N(E) c^2 v^2(E) \tau_r(E)/3}{1 + i \omega \tau_r(E)} \quad (2.5)$$

where $v^2(E)$ is an average of v_k^2 over the constant-energy surface, $E = E_k$, and $1/\tau_r(E)$, the "transport" relaxation rate, is given by (cf. (A 25))

$$\frac{1}{\tau_r(E)} = \frac{1}{N(E)} \sum_{kk'} \delta(E - E_k) \delta(E_k - E_{k'}) \omega(k, k') (1 - \underline{v}_k \cdot \underline{v}_{k'} / v_k^2). \quad (2.6)$$

Although approximate, (2.5) turns out to be quite useful, since (a) in the limit $\omega \tau_r(E) \gg 1$ it can easily be shown to coincide with the perturbative solution of (2.4) in powers of $1/\omega \tau_r(E)$, and (b) at $\omega = 0$, it yields a lower bound to the correct $\sigma(E, \omega)$ in the sense of the variational approach to d.c. transport theory. As is known, this approach is powerful and accurate. The energy-transport equation, obtained by substituting (2.5) into (2.1), namely,

$$N(E) \frac{\partial f(E)}{\partial t} = \frac{\epsilon_0^2}{6} \frac{\partial}{\partial E} \left(\frac{N(E) c^2 v^2(E) \tau_r(E)}{1 + \omega^2 \tau_r^2(E)} \frac{\partial f}{\partial E} \right) + \frac{\partial}{\partial E} \left(N(E) \frac{\Delta(E)}{\tau(E)} f(E) \right) \quad (2.7)$$

will therefore be used exclusively in what follows.³

We hasten to remark here that Eqs. (2.1) and (2.7) are not complete in that they do not take account of electron collisions involving the creation of (a) excitons or (b) electron-hole pairs. As pointed out in the Introduction, the role played by the first category depends crucially upon the magnitude of the contribution of multiphoton ionization of the resultant excitons, as compared with that of the direct process, (b). In this paper, we are provisionally assuming that the exciton-photoionization mechanism contributes dominantly to electron-hole formation, and hence to avalanching. As will be seen, this physical situation permits a drastic simplification of the analysis.

Sec. E-II

Initially, however, let us introduce the above-mentioned collision processes into our theory in at least a formal sense. The derivation of the appropriate terms is given in Appendix B. The results (B 1, 4) are, respectively,

$$N(E) \left(\frac{\partial f}{\partial t} \right)_{\text{ex}} = \sum_h \left[\frac{N(E + E_h) f(E + E_h)}{T_h(E + E_h)} - \frac{N(E) f(E)}{T_h(E)} \right], \quad (2.8)$$

and

$$N(E) \left(\frac{\partial f}{\partial t} \right)_{\text{ion}} = \int_0^\infty \left[\frac{N(E + E_g + E')}{\tau_{\text{ion}}(E + E_g + E', E')} - \frac{1}{2} \frac{N(E) f(E)}{\tau_{\text{ion}}(E, E')} \right] dE', \quad (2.9)$$

where the subscript "h" indexes exciton levels, and where (cf. B 3) $dE'/\tau_{\text{ion}}(E, E')$ is the probability per unit time for an electron of energy E to undergo an ionizing collision such that one of the resulting two electrons has energy between E' and $E' + dE'$.

We here note that, for the case where exciton-photoionization plays no role, Eqs. (2.1), (2.8), and (2.9) contain essentially all the physics of the electron-avalanche phenomenon. In the case that exciton photoionization is significant, an additional piece of physical information is required, namely, the photoionization efficiency per exciton, η_{ex} . In what follows, we provisionally confine the discussion to this latter case.

For this purpose we "invent" a population-type term which describes the effect on the distribution function, $f(E, t)$, of the production of photo-electrons (via exciton photoionization). Specifically, we replace (2.9) by a term of the form

$$\left(\frac{\partial f}{\partial t} \right)_{\text{ion}}^{\text{ex}} = D(E, \{f\}), \quad (2.10)$$

Sec. E-II

where $D(E; \{f\})$ is a linear functional of the distribution, $f(E)$. It must satisfy the equation

$$\int_0^{\infty} D(E; \{f\}) dE = \eta_{\text{ex}} \sum_h \int_0^{\infty} \frac{N(E) f(E)}{\tau_h(E)} dE, \quad (2.11)$$

which states that the rate of production of additional electrons is equal to the rate of exciton formation, multiplied by the exciton-photoionization efficiency.

In this paper, we are interested in the steady-state solution of (2.1) (augmented, of course, by (2.8) and (2.10)) for the case of time-independent amplitude, \mathcal{E}_0 , of impressed laser field. (This condition is an idealization, since, in practice, one is interested in avalanching caused by pulsed fields. However, as will become evident later, the readjustment time scale for the electron distribution is much smaller than the pulse width.) As in the analogous problem in gases⁴, we assume that the time dependence of the distribution function is of the form, $e^{\beta t}$. The transport equation then reads:

$$\begin{aligned} \beta N(E) f(E) = & \frac{\mathcal{E}_0^2}{6} \frac{d}{dE} \left(\frac{N(E) c^2 v^2(E) \tau_r(E)}{1 + \omega^2 \tau_r^2(E)} \frac{\partial f}{\partial E} \right) + \frac{d}{dE} \left(N(E) \frac{\Delta(E)}{\tau(E)} + (E) \right) \\ & + \sum_h \left[\frac{N(E+E_h) f(E+E_h)}{\tau_h(E+E_h)} - \frac{N(E) f(E)}{\tau_h(E)} \right] + D(E; \{f(E)\}). \end{aligned} \quad (2.12)$$

The quantity of ultimate interest is the average multiplication rate, β . From the standpoint of Eq. (2.12), it is obtained as the solution of an eigenvalue problem. It turns out that this formulation is of limited utility since, in practice, the β -proportional term is much smaller than the individual terms on the right-hand side of (2.12). A more useful approach is to express β in the form

Sec. E-II

$$\beta = \frac{\int_0^{\infty} D(E; \{f(E)\}) dE}{\int_0^{\infty} N(E) f(E) dE} = \eta_{\text{ex}} \frac{\int_0^{\infty} N(E) f(E) \left(\sum_h 1/\tau_h(E) \right) dE}{\int_0^{\infty} N(E) f(E) dE} \quad (2.13)$$

(obtained by integrating (2.10) over all energies). The problem is then reduced to calculating $f(E)$. It will be found that a solution of sufficient accuracy is obtainable even under the extreme condition in which the β -proportional term of (2.12) is neglected entirely.

Let us now outline a "zeroth-order" procedure for solving (2.12) for $f(E)$ and determining β via (2.13). We divide the total energy interval into two parts, namely, energies above and below the exciton threshold, $E_{\text{ex}} = E_1$. For energies above E_1 we take advantage of the aposteriori result that $f(E)$ will be found to be a rapidly falling function of E , and that the energies of photoelectrons produced by exciton-photoionization will have energies well below E_1 (~ 7 eV in NaCl), to neglect the population terms on the right-hand side of (2.12). Said equation is thereby reduced to an ordinary second-order differential equation, the explicit solution of which, $f_{>}(E)$, depends upon the detailed energy variation of the collision rates. At this point we shall not seek an explicit solution but merely take note of the fact that, to within an arbitrary (normalization) constant, it is uniquely determined by the boundary condition at infinity, $f(E \rightarrow \infty) \rightarrow 0$; the continuity of its logarithmic derivative, $L_{>} \equiv [d \log f_{>}(E)/dE]_{E_1}$, serves as a boundary condition for the solution in the region $E < E_1$.

For energies below E_1 , we write (2.12) as

$$\beta N(E) f(E) - \frac{d}{dE} \left(\frac{e_0^2 c^2}{6} \frac{N(E) v^2(E) \tau_r(E)}{1 + \omega^2 \tau_r^2(E)} \frac{\partial f}{\partial E} \right) - \frac{d}{dE} \left(N(E) \frac{\Delta(E)}{\tau(E)} f(E) \right) = \mathcal{L}(E), \quad (2.14)$$

Sec. E-II

$$\text{where } \mathcal{D}(E) \equiv \sum_h \frac{N(E + E_h) f_{>}(E + E_h)}{\tau_h(E + E_h)} + D(E; \{f_{>}(E)\}) \quad (2.15)$$

(Note that $\mathcal{D}(E)$ is determined by $f_{>}(E)$, i. e., by the solution in the upper energy region, $E > E_1$.)

At this point, we introduce the approximation of dropping the β -proportional term of (2.14). The error thereby incurred will be small provided that β is sufficiently small compared to the rates associated with the retained terms. (In any event, the approximation may be checked by an iterative perturbation calculation.) One may then carry out a first integration to obtain

$$-\frac{\varepsilon_0^2 e^2}{6} \frac{N(E) V^2(E) \tau_r(E)}{1 + \omega^2 \tau_r^2(E)} \frac{\partial f}{\partial E} - N(E) \frac{\Delta(E)}{\tau(E)} f(E) = S(E) \quad (2.16)$$

$$\text{where } S(E) \equiv \int_0^E \mathcal{D}(E') dE' \quad (2.17)$$

We may, at least formally, carry out another integration by treating $S(E)$ as an explicit source term. We introduce the notations

$$G(E) \equiv \frac{e^2 \varepsilon_0^2}{6} \frac{N(E) V^2(E) \tau_r(E)}{1 + \omega^2 \tau_r^2(E)} \quad (2.18a)$$

$$H(E) = N(E) \Delta(E) / \tau(E) \quad (2.18b)$$

Equation (2.17) may then be written as

$$-G(E) \frac{\partial f}{\partial E} - H(E) f = S(E) \quad (2.19)$$

Sec. E-II

the general solution of which is

$$f(E) = e^{-J(E)} \left[\int_E^{E'} \frac{S(E')}{G(E')} e^{J(E')} dE' + \text{const} \right] . \quad (2.20)$$

The integration constant of (2.20) is determined by the requirement of continuity of logarithmic derivatives at $E = E_1$. This yields, finally,

$$f(E) = e^{-J(E)} \left[\int_E^{E_1} \frac{S(E')}{G(E')} e^{J(E')} dE' + \frac{S(E_1) e^{J(E_1)}}{G(E_1)} \times \frac{1}{|L_{>}| - dJ/dE_1} \right] \quad (2.21)$$

where cognizance has been taken of the fact that $L_{>}$ is intrinsically negative.

Focusing now on the evaluation of β , we note that the *integral* in the numerator of (2.13) may be transformed by integration of (2.12) over the domain $E > E_1$. As pointed out above, in this energy domain $\mathcal{L}(E)$ (as given by (2.15)) may be ignored. Dropping the β -proportional term as well, we have as a suitable approximation to (2.12) in the region $E > E_1$,

$$0 = \frac{d}{dE} \left[G(E) \frac{\partial f}{\partial E} + H(E) f(E) \right] - \sum_h \frac{N(E) f(E)}{\tau_h(E)}$$

which, when substituted into the numerator of (2.13), yields

$$\beta = - \eta_{\text{ex}} \frac{G(E_1) \frac{\partial f}{\partial E_1} + H(E_1) f(E_1)}{\int_0^\infty N(E) f(E) dE} = \eta_{\text{ex}} S(E_1) / \int_0^\infty N(E) f(E) dE , \quad (2.22)$$

Sec. E-II

the last equality holding by virtue of (2.19). The determination of the electron-multiplication rate β is thus reduced to the evaluation of (2.21) and (2.22).

We now introduce an additional approximation which is based on the a posteriori-justified inequalities,

$$J(E_1) = \int_0^{E_1} \frac{H(E)}{G(E)} dE \gg 1$$

$$E_1 J'(E_1) = \frac{E_1 H(E_1)}{G(E_1)} \gg 1, \quad (2.23)$$

i. e., on the assumption, to be justified later, that $f(E)$ is a rapidly falling function of energy. Under these circumstances, the integral in the square bracket of (2.21) may be evaluated, viz:

$$\int_E^{E_1} \frac{S(E')}{G(E')} e^{J(E')} dE' \cong \frac{S(E_1)}{G(E_1)} \frac{1}{J'(E_1)} (e^{J(E_1)} - e^{J(E)})$$

$$= \frac{S(E_1)}{H(E_1)} (e^{J(E_1)} - e^{J(E)}).$$

Then, for values of E not too close to E_1 , (2.21) may be written as

$$f(E) \cong e^{-J(E)} \frac{e^{J(E_1)} S(E_1)}{H(E_1)} \left[1 + \frac{1}{|L_{>}| / J'(E) - 1} \right]. \quad (2.24)$$

We may remark that, due to the extreme inelasticity of exciton-producing collisions, which dominate the energy-loss processes in the region $E > E_1$, it turns out that

$$|L_{>}| \gg J'(E_1) \equiv \frac{H(E_1)}{G(E_1)}, \quad (2.25)$$

so that the second term of the square bracket of (2.24) is generally negligible. (A similar situation holds for electron energy distribution in gases.) This means that, in effect, the energy distribution is cut off at the exciton threshold.

Inserting (2.24) into (2.22), we have

$$\beta \cong \frac{\eta_{ex} H(E_1) e^{-J(E_1)}}{\int_0^\infty N(E) e^{-J(E)} dE},$$

where the square bracket of (2.24) has been replaced by unity (in accordance with the preceding remarks). Introducing Eqs. (2.18a, b), we have explicitly

$$\beta \cong \frac{E_1^{1/2} \Delta(E_1)}{\tau(E_1)} \eta_{ex} \times \frac{\exp \left\{ -\frac{6}{e^2 \delta_0^2} \int_0^{E_1} \frac{(1 + \omega^2 \tau_r^2(E)) \Delta(E)}{\tau(E) v^2(E) \tau_r(E)} dE \right\}}{\int_0^\infty E^{1/2} \exp \left[-\frac{6}{e^2 \varepsilon^2} \int_0^E \frac{[1 + \omega^2 \tau_r^2(E')] \Delta(E') dE'}{\tau_r(E') \tau(E') v^2(E')} \right] dE} \quad (2.26)$$

where it has been assumed that $N(E) \propto E^{1/2}$.

This equation (2.26) is the central result for the average multiplication rate β . Further progress in the evaluation of β requires specific knowledge of the collisional functions $1/T_r(E)$ and $\Delta(E)/\tau(E)$. The evaluation of these parameters for NaCl is the subject matter of Section III.

III. ELECTRON-PHONON INTERACTION IN ALKALI-HALIDES

As is known, for low energy electrons ($\sim kT$), the Coulombic interaction with the polar optical modes constitutes the dominant mechanism for electron scattering. However, at the higher energies of interest to us, it is necessary to consider non-Coulombic interactions, regardless of whether the interaction is with an optical or acoustical branch. In what follows, we compute order-of-magnitude expressions for the non-Coulombic contribution to the transport and energy relaxation times, $\tau_r(E)$ and $\tau(E)$. The corresponding expressions for polar scattering will be developed subsequently.

We start from an elementary expression for the electron-phonon scattering rate. The probability $P_q^{(\pm)}(\underline{k} \rightarrow \underline{k}')$ for an electron making a transition from \underline{k} to \underline{k}' , thereby absorbing (emitting) a phonon of wave vector \underline{q} is given by the usual golden-rule expression

$$P_q^{(\pm)}(\underline{k} \rightarrow \underline{k}') = \frac{2\pi}{\hbar} |M_{\underline{k}\underline{k}'}|^2 \left(\frac{\hbar}{2MN\omega_q} \right) \delta_{\underline{k} - \underline{k}' \pm \underline{q}} \delta(E_{\underline{k}} - E_{\underline{k}'} \pm \hbar\omega_q) \\ \times \left(N_q + \frac{1}{2} \mp \frac{1}{2} \right) \quad (3.1)$$

In this expression, $\underline{K} = \underline{k}' - \underline{k}$ is the electron-scattering vector, \underline{g} a reciprocal-lattice vector, and $M_{\underline{k}\underline{k}'}$ is the matrix element for electron-phonon interaction per unit displacement-amplitude of the vibration mode of wave vector \underline{q} , a particular polarization direction left unspecified here, frequency ω_q , and phonon population N_q . We remark that the displacement-amplitude parameter, $\left(\frac{\hbar}{2MN\omega_q} \right)$ is, strictly speaking, appropriate to monatomic lattice; however, we

Sec. E-III

employ it with the proviso that it can always be modified later to take account of the mass difference of the component ions of an alkali-halide crystal.

For the electron-phonon matrix element we use the simplest possible theory, namely, the free-electron diffraction theory described in Ziman's elementary book⁵. This type of theory yields for $M_{kk'}$ the expression

$$M_{kk'} = -i V_a(K) (\mathbf{K} \cdot \mathbf{e}_q) \quad (3.2)$$

where (with n_a = atomic density)

$$V_a(K) = n_a \int e^{-i \mathbf{K} \cdot \mathbf{r}} U_a(\mathbf{r}) d^3r \quad (3.3)$$

is a Fourier coefficient of the potential, $U_a(\mathbf{r})$, associated with a single atomic site-in, e.g., NaCl, this is either Na^+ or Cl^- . Finally, in (3.2), \mathbf{e}_q is the unit polarization vector of the involved lattice-vibration mode.

We note that (3.1) assumes the validity of the Born approximation. In this approximation, one may relate $V_a(\mathbf{K})$ to the differential atomic-scattering cross section via the well-known expression (cf. Ziman, loc. cit., eq. (6.89))

$$\sigma_a(K) = \frac{k'}{k} \left(\frac{m}{2\pi\hbar^2} \right)^2 \frac{1}{n_a^2} |V_a(K)|^2 \quad (3.4)$$

Substituting (3.2) and (3.4) into (3.1), we obtain

$$P_q^{(\pm)}(\mathbf{k} \rightarrow \mathbf{k}') = \frac{2\pi}{\hbar} \left(\frac{2\pi\hbar^2 n_a}{m} \right)^2 \frac{k}{k'} \sigma_a(K) (\mathbf{K} \cdot \mathbf{e}_q)^2 \left(\frac{\hbar}{2MN\omega_q} \right) \left(N_q + \frac{1}{2} \mp \frac{1}{2} \right) \\ \delta_{K, \mathbf{g} \pm \mathbf{q}} \delta(E_k - E_{k'} \pm \hbar\omega_q). \quad (3.5)$$

Sec. E-III

The quantity, $P_g^{(\pm)}(\underline{k} \rightarrow \underline{k}')$, describes the transition rate to a specific final state, \underline{k}' . This has to be summed over all the \underline{k}' 's contained in a differential range of energy, dE' , and solid angle, $d\Omega_{\underline{k}\underline{k}'}$, in \underline{k} -space. We have, using the recipe

$$\begin{aligned} \sum_{\underline{k}'} (---) &= \frac{V}{8\pi^3} k'^2 dk' d\Omega_{\underline{k}\underline{k}'} (---) = \frac{V}{8\pi^3} \frac{m^2 v_{k'}^2}{\hbar^2} \frac{1}{\hbar v_{k'}} d\Omega_{\underline{k}\underline{k}'} (---) \\ &= \frac{N}{n_a} v_{k'} \frac{\hbar}{2\pi} \left(\frac{m}{2\pi\hbar} \right)^2 d\Omega_{\underline{k}'} (---) \end{aligned} \quad (3.6)$$

and integrating over the final energy, the result

$$P^{(\pm)}(\underline{k}, \psi_{\underline{k}\underline{k}'}) d\Omega_{\underline{k}\underline{k}'} = n_a v_{k'} \frac{k}{k'} \sigma_a(K) (\underline{K} \cdot \underline{e}_q)^2 \left(\frac{\hbar}{2M\omega_g} \right) \left(N_g + \frac{1}{2} \mp \frac{1}{2} \right). \quad (3.7)$$

This equation gives the differential scattering rate into an element of solid angle $d\Omega_{\underline{k}\underline{k}'}$, the scattering angle being denoted as $\psi_{\underline{k}\underline{k}'}$.

So far, all the obtained results rely on the Born approximation. We now present a hand-waving argument for the utility of (3.5) and (3.7) beyond the range of validity of the Born approximation. The argument goes as follows:

Suppose we augment the Born amplitude with terms arising from repeated interaction of an electron with a given scattering center. The overall scattering amplitude is then given by a perturbation-like expression, where, however, the matrix element, $\langle \underline{k}' | U_a(\underline{r}) | \underline{k} \rangle$, is replaced by the corresponding t matrix, $t_a(\underline{k}', \underline{k})$ (which expresses the amplitude for repeated interaction of an electron with the atomic potential, $U_a(\underline{r})$, of a given site). When account is

Sec. E-III

taken of the displacements of the scattering centers associated with a given vibration mode, one obtains the same structure factor as in the Born calculation, i.e.,

$$M_{\mathbf{k}'\mathbf{k}} = -i t_a(\mathbf{k}', \mathbf{k})(\mathbf{K} \cdot \mathbf{e}_q) \quad (3.8)$$

in analogy with (3.2). However, the same t matrix also determines the atomic scattering cross section, according to the formula

$$\sigma_a(\mathbf{k}', \mathbf{k}) = \frac{k'}{k} \left(\frac{m}{2\pi\hbar^2} \right)^2 \frac{1}{n_a^2} |t_a(\mathbf{k}', \mathbf{k})|^2 \quad (3.9)$$

in similar analogy with (3.4). Elimination of the t matrix then yields (3.5) and, hence, (3.7).

The deception in this argument, of course, is the neglect of those intermediate interactions which involve the atomic fields of the neighboring atoms. As is known, the inclusion of this wider class of processes would lead to the situation in which, if we still wish to formulate a single-site t -matrix theory, we would have to consider the incoming and outgoing waves as Bloch-type, rather than plane waves. It then follows that the obtained t matrix would not be identifiable with a bonafide atomic-type t matrix; in this eventuality, we would not be able to use experimental atomic cross sections to determine electron-phonon scattering rates from known atomic cross sections.

At this stage of our work, we are principally interested in order-of-magnitude estimates, with the view towards determining qualitative features, such as the magnitude of $\omega\tau_r$ relative to unity. Since most of the scattering will involve transitions between electron states \mathbf{k} and \mathbf{k}' which are not too close to zone

Sec. E-III

boundaries, we simply assume that the Bloch functions in question can be approximated by their plane-wave counterparts. If this is done, we are led to (3.5) and hence (3.7).

Expressions for the transport and energy-loss mean free times, $\tau_r(E)$ and $\tau(E)$, which occur in the theory of Sec. II, will now be obtained. We note that $1/\tau(E)$ is the total scattering rate, with the quantity $\Delta(E)$ of (2.1) playing the role of the average energy loss per collision. Since in our problem most of the scattering involves essentially all the phonon modes (whose frequencies are concentrated principally in the vicinity of the Debye frequency, ω_D), we take

$$\Delta E \approx \hbar \omega_D / (2 N_D + 1) \quad (3.10)$$

(the second factor of (3.10) arising from the circumstance that only the difference between the scattering rates for phonon emission and absorption contributes to the inelasticity). Assuming that $\sigma_a(K)$ is isotropic – this assumption is qualitatively acceptable for the case of non-polar scattering – we have, with $K^2 \cong 2k^2(1 - \cos \psi_{kk'})$,

$$\frac{1}{\tau(E)} = n_a v_k Q_a(E) 2k^2 \left(\frac{\hbar}{2M\omega_D} \right) (2N_D + 1) \quad (3.11)$$

where $Q_a(E)$ is the total atomic cross section and $N_D = \left(e^{\hbar\omega_D/kT} - 1 \right)^{-1}$. For simplicity we have ignored the polarization – this amounts essentially to summing over all polarizations – and have set ω_q equal to the Debye frequency. (We note that there are no small- q divergences, since for small g , the concomitant absence of Umklapp means that $\underline{K} = \underline{q}$).

Sec. E-III

The transport relaxation rate, $1/\tau_r(E)$, brings in an extra factor $(1 - \cos \psi_{kk'})$ in the angular integration, resulting in an overall angle-dependent factor of $(1 - \cos \psi_{kk'})^2$; the angular average of this factor (again with the assumption of isotropic $\sigma_a(K)$) gives simply a factor $3/2$. This

$$\begin{aligned} \frac{1}{\tau_r(E)} &= \frac{3}{2} \frac{1}{\tau(E)} = n_a v_k Q_a(E) 3k^2 \left(\frac{\hbar}{2M\omega_D} \right) (2N_D + 1) \\ &= 3 n_a v(E) Q_a(E) (E/\hbar\omega_D) \frac{m}{M} \coth \frac{\hbar\omega_D}{2kT} . \end{aligned} \quad (2.12)$$

Before undertaking numerical estimates, we supplement the above treatment with comparable calculations for polar scattering. The starting point in an expression for the matrix element of electron-optical-phonon interaction, which we piece together from Eqs. (5.11.14) and (5.11.2) of Ziman's advanced text⁶ we have

$$\begin{aligned} \langle \underline{k}, N_q \mp 1 | H_{int} | N_q, \underline{k}' \rangle &= \left(N_q + \frac{1}{2} \mp \frac{1}{2} \right)^{1/2} \delta_{\underline{k}', \underline{k} \pm \underline{q} + \underline{g}} \\ &\times \frac{-i}{K} \left[\frac{4\pi e^2 \hbar \omega_q}{2V} \left(\frac{1}{\epsilon_\infty} - \frac{1}{\epsilon} \right) \right]^{1/2} \end{aligned} \quad (3.13)$$

where \underline{g} is a reciprocal lattice vector and ϵ_∞ , ϵ are the optical and d.c. dielectric constants. This expression is to be inserted into the formula

$$\begin{aligned} P^{(\pm)}(\underline{k} \rightarrow \underline{k}') &= \sum_q \frac{2\pi}{\hbar} |\langle \underline{k}', N_q \mp 1 | H_{int} | \underline{k}, H_2 |^2 \delta_{\underline{k}', \underline{k} \pm \underline{q} + \underline{g}} \\ &\times \delta(E_k - E_{k'} \pm \hbar\omega_q) . \end{aligned} \quad (3.14)$$

Sec. E-III

One then obtains, upon summing over the final states, \mathbf{k}' , within a solid angle $d\Omega_{\mathbf{k}'}$ and using the recipe (3.6)

$$\begin{aligned} P^{(\pm)}(\mathbf{k}, \psi_{\mathbf{k}\mathbf{k}'}) d\Omega_{\mathbf{k}'} &= v_{\mathbf{k}'} \left(\frac{m}{2\pi\hbar^2} \right)^2 \frac{4\pi c^2 \hbar \omega_{\mathbf{q}}}{2K^2} \left(\frac{1}{\epsilon_{\infty}} - \frac{1}{\epsilon} \right) \left(N_{\mathbf{q}} + \frac{1}{2} \mp \frac{1}{2} \right) \\ &= v_{\mathbf{k}'} \frac{m e^2}{4\pi\hbar^2} \frac{\hbar \omega_{\mathbf{q}} \left(\frac{1}{\epsilon_{\infty}} - \frac{1}{\epsilon} \right)}{E + E' - 2(EE')^{1/2} \cos \psi_{\mathbf{k}\mathbf{k}'}} \left(N_{\mathbf{q}} + \frac{1}{2} \mp \frac{1}{2} \right). \end{aligned} \quad (3.15)$$

With the aid of (3.15) we may now compute the transport and energy-loss relaxation times. For the transport time, no serious error will be incurred by neglecting the inelasticity, i. e., taking $E = E'$, provided, of course we introduce a low-energy cutoff at $E = \hbar\omega_{\text{opt}}$ (where we have introduced the approximation

$$\omega_{\mathbf{q}} \cong \omega_{\text{opt}} \quad (3.16)$$

which is customary for the optical branch). One then has

$$\begin{aligned} \frac{1}{\tau_r^{(\pm)}} &= 2\pi \int (1 - \cos \psi_{\mathbf{k}\mathbf{k}'}) P^{(\pm)}(\mathbf{k}, \psi_{\mathbf{k}\mathbf{k}'}) d\cos \psi_{\mathbf{k}\mathbf{k}'} \\ &= \frac{4\pi v_{\mathbf{k}} m e^2}{4\pi\hbar^2} \hbar \omega_{\text{opt}} \left(\frac{1}{\epsilon_{\infty}} - \frac{1}{\epsilon} \right) \left(N_{\mathbf{q}} + \frac{1}{2} \mp \frac{1}{2} \right) / 2E \end{aligned}$$

which, upon summing over \pm , and expressing $N_{\mathbf{q}}$ explicitly in terms of temperature, yields

$$\frac{1}{\tau_r} = v_{\mathbf{k}} \left(\frac{m e^2}{\hbar^2} \right) \left(\frac{1}{\epsilon_{\infty}} - \frac{1}{\epsilon} \right) \coth \left(\frac{\hbar\omega_{\text{opt}}}{2\hbar T} \right) \left(\frac{\hbar\omega_{\text{opt}}}{2E} \right) \quad (3.17)$$

For the energy loss time, the use of (3.16) establishes that the average energy loss, $\Delta(E)$, is simply $\hbar\omega_{\text{opt}}$, whereas the corresponding effective collision rate is given by

$$\frac{1}{\tau(E)} = \frac{1}{\tau^{(-)}(E)} - \frac{1}{\tau^{(+)}(E)} \quad (3.18)$$

where $\frac{1}{\tau^{(\pm)}(E)}$ is the total scattering rate for the absorption (emission) of an optical phonon. One obtains

$$\frac{1}{\tau^{(\pm)}(E)} = \frac{v(E') m e^2}{\hbar^2} \frac{\hbar\omega_{\text{opt}}}{(EE')^{1/2}} \left(\frac{1}{\epsilon_{\infty}} - \frac{1}{\epsilon} \right) \log \left| \frac{E^{1/2} + E'^{1/2}}{E^{1/2} - E'^{1/2}} \right|^{(N_q + \frac{1}{2} \mp \frac{1}{2})} \quad (3.19)$$

where $E' = E \pm \hbar\omega$. Inserting this result into (3.18), one finally obtains

$$\begin{aligned} \frac{1}{\tau(E)} = & \frac{m e^2}{\hbar^2} \frac{\hbar\omega_{\text{opt}}}{E} v(E) \left(\frac{1}{\epsilon_{\infty}} - \frac{1}{\epsilon} \right) \\ & \times \left[\frac{1}{1 - e^{-\hbar\omega_{\text{opt}}/kT}} \log \left| \frac{E^{1/2} + (E - \hbar\omega_{\text{opt}})^{1/2}}{E^{1/2} - (E - \hbar\omega_{\text{opt}})^{1/2}} \right| \right. \\ & \left. + \frac{1}{e^{\hbar\omega_{\text{opt}}/kT} - 1} \log \left| \frac{E^{1/2} + (E + \hbar\omega_{\text{opt}})^{1/2}}{E^{1/2} - (E + \hbar\omega_{\text{opt}})^{1/2}} \right| \right]. \end{aligned}$$

The remainder of this section will be devoted to obtaining numerical estimates of the various relaxation times, based on above-obtained formulae. We consider the two cases of non-polar and polar scattering in order.

(a) Non-Polar Scattering: From (3.13) it is clear that, barring unusual low-energy behavior of $Q_a(E)$, the transport-relaxation rate is an increasing function of energy. For a relevant estimate we take $E = 8 \text{ eV}$ and $kT = .025 \text{ eV}$ ($\approx 300 \text{ K}$). Material parameters for NaCl are $h\omega_{\text{opt}} = 320 \text{ K} = .027 \text{ eV}$, $M = 16 M_H$, $n_a = 2.2 \times 10^{22} \text{ cm}^{-3}$, $m/M = 2.5 \times 10^{-5}$, $v(E) = .6 \times 10^8 (E_{\text{eV}})^{1/2} \text{ cm/sec} = 1.7 \times 10^8 \text{ cm/sec}$. Under these conditions, (3.13) yields

$$\frac{1}{\tau_r(8 \text{ eV})} = 2 \times 10^{13} Q_a \text{ sec}^{-1} \quad (3.20)$$

where Q_a is measured in square Angstroms.

The estimation of Q_a constitutes a major uncertainty, due to the lack of direct experimental data and/or reliable theory. In our opinion, the most relevant data is provided by the experimentally observed total cross section for HCl (as cited, e.g., in Massey, Burhop, and Gilbody's tome).⁷ If, as seems reasonable, most of the scattering is due to Cl^- , this ion is common to both NaCl and HCl. The only other possibly relevant data known to us is for Cl_2 (loc cit, p 709); we reject this on the grounds that Cl_2 does not present a closed-shell structure, such as Cl^- .

The cited data for HCl gives $Q_a \sim 35 \text{ \AA}^2$. Introducing this number into (3.19) yields

$$\frac{1}{\tau_r(8 \text{ eV})} = 0.7 \times 10^{15} \text{ sec}^{-1} \quad (3.20)$$

(b) Polar Scattering: From (3.17) and (3.18) it is clear that the critical behavior takes place at low energies in that $1/(\tau_r)$ diverges as $E \rightarrow 0$. Actually,

Sec. E-III

caution must be employed in analyzing the classical transport theory of Sec. II to situations wherein the various parameters possess an energy variation which is appreciable over a range of the order of the optical quantum energy, $\hbar\omega$. In this case, the effective transport relaxation rate must be treated quantally. This will be done in a subsequent report. Provisionally, we take quantal effects into account by introducing a low-energy cutoff $\sim \hbar\omega$ into (3.17). Specifically, we take (3.17) to be valid for $E \geq \hbar\omega$; for $E < \hbar\omega$, we replace (3.17) by $1/(\tau_r(E = \hbar\omega))$. Equation (3.18) on the other hand, is assumed to hold for arbitrary energy.

A maximal estimate for $1/\tau_r$ due to polar scattering is, from the above, attained by inserting the cutoff energy, $E \cong \hbar\omega$ with (3.17). Using the data

$$\frac{1}{\epsilon_\infty} - \frac{1}{\epsilon} = 0.259 \quad (3.21)$$

(appropriate to NaCl as obtained from the Handbook of Chemistry & Physics), and $\hbar\omega$ appropriate to $\omega = 10^4 \text{ cm}^{-1}$ (1 micron laser light), i.e., $\hbar\omega = 1.25 \text{ eV}$, $\hbar\omega_{\text{opt}} = .027 \text{ eV} \cong kT$, we obtain

$$\frac{1}{\tau_r(\text{polar})} \sim 0.75 \times 10^{14} \text{ sec}^{-1} . \quad (3.22)$$

Let us now note that, both from (3.22) and (3.20), the parameter $\omega^2 \tau_r^2$ is substantially larger than unity for $\omega \geq 2 \times 10^{15} \text{ sec}^{-1}$ (corresponding to $\lambda \leq 1 \text{ micron}$). It is thus apparent that the high-frequency limit obtains. We note also that correctives to this limit arise (a) explicitly from the non-negligible value of $1/\omega^2 \tau^2$ obtained from the non-polar scattering, and (b) implicitly from the low-energy cutoff for polar scattering ($E_{\text{min}} = \hbar\omega$).

Sec. E-III

In the next section (to be written at some future date) the results of this section will be used in conjunction with Eq. (2.26) of Sec. II to obtain the multiplication rates as a function of frequency and laser field.

Sec. E-Appendix A

APPENDIX A. DEVIATION OF THE CLASSICAL TRANSPORT EQUATION

In this Appendix, we derive the classical transport equation that will be used in the analysis of electron-avalanche breakdown. We start from the Boltzmann transport equation

$$\frac{\partial f}{\partial t} + \frac{e\mathcal{E}(t)}{\hbar} \cdot \text{grad}_{\mathbf{k}} f = \left(\frac{\partial f}{\partial t} \right)_{\text{coll}} . \quad (\text{A.1})$$

Here, $f = f_{\mathbf{k}}(t)$ is the time-dependent electron distribution in \mathbf{k} space,

$\mathcal{E}(t) = \mathcal{E}_0 \cos \omega t$ is the impressed laser field, and

$$\left(\frac{\partial f}{\partial t} \right)_{\text{coll}} = \sum_{\mathbf{k}'} \left[f_{\mathbf{k}'} W(\mathbf{k}' \rightarrow \mathbf{k}) - f_{\mathbf{k}} W(\mathbf{k} \rightarrow \mathbf{k}') \right] , \quad (\text{A.2})$$

where $W(\mathbf{k} \rightarrow \mathbf{k}')$ is the collisional transition probability between states \mathbf{k} and \mathbf{k}' .

We generally have

$$W(\mathbf{k} \rightarrow \mathbf{k}') = \sum_i w_i(\mathbf{k}, \mathbf{k}') \delta(E_{\mathbf{k}} - E_{\mathbf{k}'} - \Delta_{\mathbf{k}\mathbf{k}'}^{(i)}) \quad (\text{A.3})$$

where the subscript, i , refers to a particular type of collision (e.g., electron scattering with emission or absorption of various types of phonons) and where $\Delta_{\mathbf{k}\mathbf{k}'}^{(i)}$, represents the associated energy loss (or gain).

It may be remarked that, for electron-phonon collisions, $\Delta_{\mathbf{k}\mathbf{k}'}$ is relatively small ($\lesssim 0.05$ eV), i.e., the collisions are quasi-elastic. This feature will

Sec. E-Appendix A

permit substantial simplification of the analysis to be given below, especially in the energy region below the threshold for exciton formation, which we now discuss. We rewrite (A.1) in the form

$$\frac{\partial f}{\partial t} + \frac{e\mathcal{E}(t)}{\hbar} \cdot \text{grad}_{\mathbf{k}} f - \left(\frac{\partial f}{\partial t} \right)_{\text{in coll}} = \left(\frac{\partial f}{\partial t} \right)_{\text{el coll}} \quad (\text{A.4})$$

where

$$\left(\frac{\partial f}{\partial t} \right)_{\text{el coll}} = \sum_{\mathbf{k}'} (f_{\mathbf{k}'} - f_{\mathbf{k}}) w(\mathbf{k}, \mathbf{k}') \delta(E_{\mathbf{k}} - E_{\mathbf{k}'}) \quad (\text{A.5})$$

(with $w(\mathbf{k}, \mathbf{k}') \equiv \sum_i w_i(\mathbf{k}, \mathbf{k}')$ taken to be symmetrical with respect to interchange of \mathbf{k} and \mathbf{k}')¹ and $\left(\frac{\partial f}{\partial t} \right)_{\text{in coll}}$ is the remainder of the collision term; it may be written as

$$\begin{aligned} \left(\frac{\partial f}{\partial t} \right)_{\text{in coll}} = \sum_{\mathbf{k}', i} \left[f_{\mathbf{k}'} w_i(\mathbf{k}', \mathbf{k}) [\delta(E_{\mathbf{k}'} - E_{\mathbf{k}} - \Delta_{\mathbf{k}\mathbf{k}'}) - \delta(E_{\mathbf{k}'} - E_{\mathbf{k}})] \right. \\ \left. - f_{\mathbf{k}} w_i(\mathbf{k}, \mathbf{k}') [\delta(E_{\mathbf{k}} - E_{\mathbf{k}'} - \Delta_{\mathbf{k}\mathbf{k}'}) - \delta(E_{\mathbf{k}} - E_{\mathbf{k}'})] \right] . \end{aligned} \quad (\text{A.6})$$

The stage has now been set for introducing the principal assumption of this -- as well as other derivations -- of the energy transport equation, namely, the assumption of quasi-isotropy of the distribution function in \mathbf{k} space. Strictly speaking, this phraseology pertains to the usual case of spherical energy surfaces, for which it describes the situation in which $f_{\mathbf{k}}$ depends principally on the magnitude of \mathbf{k} . In our case, we generalize by writing

$$f_{\mathbf{k}} = f(E_{\mathbf{k}}) + f_{\mathbf{k}}^{(1)} \quad (\text{A.7})$$

Sec. E - Appendix A

where $f_k^{(1)}$ is taken to be small compared to $f(E_k)$, and is ultimately to be determined by a suitably prescribed iteration procedure. We incidentally note that, by definition,

$$f(E) = \frac{\sum_k f_k \delta(E - E_k)}{\sum_k \delta(E - E_k)} \quad (A.8)$$

so that the corresponding integral of $f_k^{(1)}$ vanishes.

Let us integrate (A.4) over a surface of constant energy, E . This is done by multiplying by $\delta(E - E_k)$ and summing over \underline{k} . Introducing the density-of-states function

$$N(E) \equiv \sum_k \delta(E - E_k) \quad (A.9)$$

we have

$$\begin{aligned} N(E) \frac{\partial f(E)}{\partial t} + \sum_k e \underline{\mathcal{E}}(t) \cdot \underline{v}_k \frac{\partial}{\partial E} \delta(E - E_k) f_k^{(1)} \\ = \sum_{\underline{k}\underline{k}',i} \delta(E - E_k) \left[f(E_{k'}) w_i(\underline{k}, \underline{k}') \delta(E_{k'} - E_k - \Delta_{\underline{k}\underline{k}'}^{(i)}) \right. \\ \left. - f(E_k) w_i(\underline{k}, \underline{k}') \delta(E_k - E_{k'} - \Delta_{\underline{k}\underline{k}'}^{(i)}) \right] \\ = \int \left[f(E') K(E', \Delta E) - f(E) K(E, \Delta E) d\Delta E \right] \end{aligned} \quad (A.10)$$

where $E' = E + \Delta E$ and where

$$K(E, \Delta E) \equiv \sum_{\underline{k}\underline{k}',i} \delta(E - E_k) \delta(E - \Delta E - E_{k'}) w_i(\underline{k}, \underline{k}') \delta(E_k - E_{k'} - \Delta_{\underline{k}\underline{k}'}^{(i)}) \cdot \quad (A.11)$$

Sec. E - Appendix A

The Fokker-Planck expansion is now applied to the right-hand side of (A.10), yielding

$$N(E) \frac{\partial f(E)}{\partial t} + \frac{\partial}{\partial E} \langle \tilde{\xi}(t) \cdot \tilde{J}(E, t) \rangle = \frac{\partial}{\partial E} \left[N(E) \frac{\Delta(E)}{\tau(E)} f(E) \right] \quad (A.12)$$

where

$$N(E) \frac{\Delta(E)}{\tau(E)} \equiv \int (\Delta E) K(E, \Delta E) dE = \sum_{kk', i} \delta(E - E_k) w^{(i)}(\underline{k}, \underline{k}') \times \Delta^{(i)}(\underline{k}, \underline{k}') \times \delta(E_k - E_{k'} - \Delta_{kk'}^{(i)}) \quad (A.13)$$

Thus $\Delta(E)$ is the average energy loss per collision (with $1/\tau(E)$ representing the total collision rate). Also

$$\tilde{J}(E, t) \equiv \sum_k \delta(E - E_k) e \underline{v}_k f_k^{(1)}(t) \quad (A.14)$$

is manifestly the "monoenergetic" current density (to be evaluated below). Finally, the braced expression, $\langle \dots \rangle$, is a time average over a period $2\pi/\omega$ of the external laser field. It is thereby assumed that the variation of $f(E)$ over this time interval is negligible.²

An explicit expression for $\tilde{J}(E, t)$ has now to be obtained. To achieve this objective, we consider the equation satisfied by $f_k^{(1)}(t)$, which reads

$$\frac{\partial f_k^{(1)}}{\partial t} + e \tilde{\xi}(t) \cdot \underline{v}_k \frac{\partial f(E)}{\partial E} = \sum_{k'} (f_{k'} - f_k) w(\underline{k}, \underline{k}') \delta(E_k - E_{k'}) \quad (A.15)$$

Equation (A.15) is a linearized version of (A.4), wherein the "small" terms, such as that proportional to $\tilde{\xi}(t)$, have been approximated by the replacement of f_k by $f(E_k)$. (From a logical point of view, an additional "driving" term of this sort,

Sec. E-Appendix A

involving the inelastic collision operator, should have been included. However, as one may readily demonstrate, the resulting contribution to $f_k^{(1)}(t)$ is even with respect to reflection of \underline{k} through the origin, and would hence give no contribution to $J(E, t)$.)

Ignoring the time variation of $f(E_k)$ (as discussed in the text subsequent to (A. 14)), and taking $\underline{\epsilon}(t) = R\underline{\epsilon}_0 \exp(-i\omega t)$, we may replace $\partial/\partial t$ in (A. 15) by $-i\omega$, thereby obtaining

$$-e\underline{\epsilon}_0 \cdot \underline{v}_k \frac{\partial f(E_k)}{\partial E_k} = i\omega f_k + \sum_{k'} \left[f_{k'} - f_k w(\underline{k}, \underline{k}') \delta(E_k - E_{k'}) \right]$$

the formal solution of which is written as

$$f_k = -\phi_k(\omega) \cdot e\underline{\epsilon} \frac{\partial f_0}{\partial E_k} \quad (\text{A. 16a})$$

where $\phi_k(\omega)$ obeys the equation

$$\underline{v}_k = i\omega \phi_k + \sum_{k'} [\phi_{k'} - \phi_k] w(\underline{k}, \underline{k}') \delta(E_k - E_{k'}) \quad (\text{A. 16b})$$

Inserting (A. 16) into (A. 14), we have

$$\begin{aligned} J(E, t) &= \sum_k \delta(E - E_k) e^2 \underline{v}_k \phi_k(\omega) \cdot \frac{\partial f}{\partial E_k} \\ &\equiv -R \left\{ \underline{\sigma}(E, \omega) \cdot \underline{\epsilon}_0 e^{-i\omega t} \frac{\partial f_0}{\partial E} \right\} \end{aligned} \quad (\text{A. 17})$$

where

$$\underline{\sigma}(E, \omega) \equiv \sum_k \delta(E - E_k) e^2 \underline{v}_k \phi_k(\omega)$$

Sec. E-Appendix A

is the monoenergetic conductivity tensor; as is known, for cubic crystals, it reduces to a scalar quantity; i. e.,

$$\underline{J}(E, t) = -R \left\{ \sigma(E, \omega) \underline{\varepsilon}_0 e^{-i\omega t} \frac{\partial f(E)}{\partial E} \right\} \quad (A. 18)$$

with

$$\sigma(E, \omega) = \frac{1}{3} \sum_{\underline{k}} \delta(E - E_{\underline{k}}) e^2 \underline{v}_{\underline{k}} \cdot \underline{\phi}_{\underline{k}}(\omega) \quad (A. 19)$$

We now substitute (A. 18) into (A. 12), obtaining

$$N(E) \frac{\partial f(E)}{\partial t} = \frac{\varepsilon_0^2}{6} \frac{\partial}{\partial E} R \sigma(E, \omega) \frac{\partial f(E)}{\partial E} + \frac{\partial}{\partial E} \left[N(E) \frac{\Delta(E)}{\tau(E)} f(E) \right] \quad (A. 20)$$

Let us note that, in the usual spherical approximation -- with $E_{\underline{k}}$ dependent only on the magnitude of \underline{k} , and with $w(\underline{k}, \underline{k}')$ a function of just the magnitudes of \underline{k} and \underline{k}' and of the angle $\psi_{\underline{k}\underline{k}'}$ between them -- it is always possible to replace the collision integral by a relaxation-time expression, i. e.,

$$\sum_{\underline{k}'} [\underline{\phi}_{\underline{k}'} - \underline{\phi}_{\underline{k}}] w(\underline{k}, \underline{k}') \delta(E_{\underline{k}} - E_{\underline{k}'}) \rightarrow - \frac{\phi_{\underline{k}}}{\tau_r} \quad (A. 21)$$

where

$$1/\tau_r(E) \equiv \sum_{\underline{k}'} w(\underline{k}, \underline{k}') (1 - \cos \psi_{\underline{k}\underline{k}'}) \delta(E_{\underline{k}} - E_{\underline{k}'}) \quad (A. 22)$$

is the "transport" relaxation rate. Introducing (A. 21) into (A. 17), we have

$$\underline{\phi}_{\underline{k}} = \frac{\underline{v}_{\underline{k}} \tau_r}{1 + i\omega \tau_r} \quad (A. 23a)$$

whence

Sec. E-Appendix A

$$\begin{aligned}\sigma(E, \omega) &= \frac{\left[\sum_{\mathbf{k}} \delta(E - E_{\mathbf{k}}) e^2 v_{\mathbf{k}}^2 / 3 \right] \tau_r(E)}{1 - i\omega \tau_r(E)} \\ &= \frac{N(E) e^2 \langle v^2(E) \rangle \tau_r(E) / 3}{1 - i\omega \tau_r(E)}\end{aligned}\quad (\text{A.23b})$$

where $\langle v^2(E) \rangle$ denotes an average of $v_{\mathbf{k}}^2$ over a surface of constant energy.

Upon substituting (A.23) into (A.20), one has

$$\begin{aligned}N(E) \frac{\partial f(E)}{\partial t} &= \frac{e_0^2}{6} \frac{\partial}{\partial E} \left(\frac{N(E) e^2 \langle v^2(E) \rangle \tau_r(E)}{1 + \omega^2 \tau_r^2(E)} \frac{\partial f}{\partial E} \right) \\ &+ \frac{\partial}{\partial E} \left[N(E) \frac{\Delta(E)}{\tau(E)} f(E) \right] \quad .\end{aligned}\quad (\text{A.24})$$

It may be remarked that, in the more general case of cubic symmetry, an expression of the form of (A.24), with $1/\tau_r$ given by the relation

$$\frac{1}{\tau_r(E)} = \frac{1}{N(E)} \sum_{\mathbf{k}, \mathbf{k}'} \delta(E - E_{\mathbf{k}}) \delta(E_{\mathbf{k}} - E_{\mathbf{k}'}) w(\mathbf{k}, \mathbf{k}') (1 - \underline{v}_{\mathbf{k}} \cdot \underline{v}_{\mathbf{k}'} / v_{\mathbf{k}}^2) \quad (\text{A.25})$$

is still a useful approximation; in particular, it has the following two properties:

(1) In the high-frequency limit $\omega \tau_r \gg 1$, it coincides with the first non-vanishing term obtained from a perturbation solution of (A.17) in powers of $(\omega \tau_r)^{-2}$. (2) In the d.c. limit, variational theory may be used to show that the coefficient of $\partial f / \partial E$ in the square bracket of (A.24) is a lower bound to the correct $\sigma(E, 0)$, with an error quadratic in the deviation of the "trial" function, $\phi_{\mathbf{k}}(\text{var}) = \underline{v}_{\mathbf{k}}$ from the actual solution of (A.16).

Sec. E-Appendix A

Equation (A.20) and its approximate form (A.24) (with some subsequent straightforward modifications introduced in the text) constitute the basis of the classical energy-transport theory used in this paper.

It remains, finally, to carry out some estimate of the validity of the approximation of generalized quasi-isotropy introduced with Eq. (A.7). Our task is to demonstrate the relative smallness of $f_k^{(1)}$ (as given, e.g., by (A.16a) and (A.23a)) compared to $f(E)$. For this purpose it is clearly necessary to know $\partial f / \partial E$ as a function of primary parameters. As pointed out above, experience has shown that this is feasible only on an aposteriori basis. In what follows, we give the simplest illustrative example; the state of affairs in other cases of interest will be discussed in due course.

Let us consider the situation in which exciton and electron-hole forming collisions may be ignored. Then, Eq. (A.24), with $\partial f / \partial t = 0$, applies. A first integration can immediately be carried out, yielding

$$0 = \frac{\epsilon_0^2}{6} \frac{e^2 v^2(E) \tau_r(E)}{1 + i \omega^2 \tau_r^2(E)} \frac{\partial f}{\partial E} + \frac{\Delta(E)}{\tau(E)} f(E) \quad (\text{A.26})$$

where the constant of integration has been set equal to zero, to assure $f(E) \rightarrow 0$ as $E \rightarrow \infty$. From (A.26) we obtain an explicit expression for $\partial f / \partial E$ in terms of $f(E)$ and the primary parameters. Introducing this expression into (A.23a) and (A.16a), we have, for the component of $f_k^{(1)}$ in phase with the external field (which we denote as $f_k^{(1)'}$)

$$\begin{aligned} f_k^{(1)'} / f(E) &= \frac{e \epsilon_0 v(E) \tau_r}{1 + \omega^2 \tau_r^2} \frac{6(1 + \omega^2 \tau_r^2(E))}{\epsilon_0^2 e^2 v^2(E) \tau_r(E)} \frac{\Delta(E)}{\tau(E)} \\ &= \frac{6 \Delta(E)}{e \epsilon_0 v(E) \tau(E)} \end{aligned} \quad (\text{A.27})$$

Sec. E-Appendix A

To extract some physical meaning from this result, we define an effective energy-dependent electron temperature via the equation

$$\frac{1}{kT_e(E)} = - \frac{d \log f(E)}{dE} \quad . \quad (A.28)$$

Equation (A.28) together with (A.26) yields

$$kT_e(E) = \frac{e^2 \epsilon_0^2}{6} \frac{v^2(E) \tau_r(E) \tau(E)}{(1 + \omega^2 \tau_r^2) \Delta(E)}$$

or

$$e \epsilon_0 v(E) = \left[\frac{6(1 + \omega^2 \tau_r^2(E)) \Delta(E)}{\tau_r(E) \tau(E)} \right]^{1/2} (kT_e(E))^{1/2}$$

which, when inserted into (A.27), gives

$$\frac{f_k^{(1)'}}{f(E)} = \left[\frac{\Delta(E)}{\tau(E)} \frac{\tau_r(E)}{1 + \omega^2 \tau_r^2} \frac{1}{kT_e(E)} \right]^{1/2} \lesssim \left(\frac{\Delta(E)}{kT_e(E)} \right)^{1/2} \quad (A.29)$$

if we take $\tau_r(E) \sim \tau(E)$. The parameter contained in square brackets is usually quite small. In fact, if we consider $kT_e(E)$ as characterizing the energy spread of the distribution function, the parameter on the right-hand side of (A.29) is known to be small – at least in the energy region below the exciton threshold.

APPENDIX B. CONTRIBUTION OF ELECTRONICALLY INELASTIC COLLISIONS TO THE TRANSPORT EQUATION

1. Excitation Collisions. We consider a collision event which leads to the creation of an exciton in the h^{th} level. Let $1/\tau_h(E)$ be the probability per unit time for an electron of energy, E , to suffer a collision event of this type; the energy of the scattered electron will be $E - E_h$. We may then write

$$N(E) \left[\frac{\partial f}{\partial t} \right]_{\text{exc}} = \sum_h \left[\frac{N(E + E_h) f(E + E_h)}{\tau(E + E_h)} - \frac{N(E) f(E)}{\tau_h(E)} \right], \quad (\text{B. 1})$$

where the sum goes over all the electronically bound states of the exciton.

Equation (B. 1) is easily proved by writing down a general equation of the same form as that of (A. 10), with

$$K(E, \Delta E) = \sum_h \delta(E_h - \Delta E) / \tau_h(E).$$

Integration over ΔE then leads directly to (B. 1).

2. Ionizing Collisions. We obtain $N(E) [\partial f / \partial t]_{\text{ion}}$ by suitable generalization of (B. 1). Two steps are involved: (a) Replacement of E_h by a continuous variable, $E_g + E^{(e)}$, where E_g is the minimum energy for the creation of an electron pair (vertical-gap energy), and $E^{(e)}$ is the energy of the ejected electron. (b) We must take account of the fact that the ejected electron also contributes to the electron energy distribution. We thus write

Sec. E-Appendix B

$$\begin{aligned}
 N(E) \left[\frac{\partial f}{\partial t} \right]_{\text{ion}} = & \int_0^{E-E_g} \frac{-N(E) f(E) dE}{\tau_i} + \int_0^{\infty} \frac{N(E+E_g+E^{(e)}) f(E+E_g+E^{(e)})}{\tau_i(E+E_g+E^{(e)}, E^{(e)})} dE^{(e)} \\
 & + \int_0^{\infty} \frac{N(E+E^{(s)}+E_g) f(E+E^{(s)}+E_g)}{\tau_i(E+E^{(s)}+E_g, E)} dE^{(s)}, \quad (B.2)
 \end{aligned}$$

where $E^{(s)}$ is the energy of the scattered electron. But we now want to incorporate the basic indistinguishability between scattered and ejected electrons. We do this by redefining our ionization rate as

$$\frac{dE'}{\tau_{\text{ion}}(E, E')} = \frac{dE'}{\tau_i(E, E')} + \frac{dE'}{\tau_i(E, E-E_g-E')} \quad , \quad (B.3)$$

where $dE'/\tau(E, E')$ is seen to represent the probability per unit time that a primary electron of energy E suffers an ionizing collision such that any one of the two emerging electrons has energy between E' and $E'+dE'$, and the other automatically has energy $E-E_g-E'$. We may now write,

$$\begin{aligned}
 N(E) \left[\frac{\partial f}{\partial t} \right]_{\text{ion}} = & -\frac{1}{2} \int_0^{E-E_g} \frac{N(E) f(E) dE'}{\tau_{\text{ion}}(E, E')} + \int_0^{\infty} \frac{N(E+E_g+E') f(E+E_g+E')}{\tau_{\text{ion}}(E+E_g+E', E')} dE', \quad (B.4)
 \end{aligned}$$

where the factor $1/2$ in front of the "depopulation" term is introduced to avoid double counting.

Finally, we give an expression for the average ionization rate β resulting from the above-described electron-collision process. It is obtained by integration of (B.4) over all energies, E , and dividing by the total number of electrons; it reads

Sec. E-Appendix B

$$\beta = \frac{\int_{E_g}^{\infty} \frac{N(E) f(E) dE}{\tau_{ion}(E)}}{\int_0^{\infty} N(E) F(E) dE}, \quad (B.5)$$

where

$$\frac{1}{\tau_{ion}(E)} = \frac{1}{2} \int_0^{E-E_g} \frac{dE'}{\tau_{ion}(, E')} \quad (B.6)$$

is the total probability per unit time for an electron of energy E to undergo an ionizing collision.

Sec. E-References

REFERENCES

1. This property is certainly valid in the Born approximation, in which it is possible to treat all electron-phonon collisions.
2. This approximation is valid when energy loss and gain processes are slow, relative to the external frequency, ω ; said condition is hereby assumed to hold once and for all.

OVERVIEW OF MATERIALS FOR HIGH-POWER VISIBLE AND ULTRAVIOLET LASERS*

M. Sparks

Xonics, Incorporated, Santa Monica, California 90401

The useful frequency range of metallic reflectors extends from ~ 0 to ~ 14 eV, and the absorptance on this range is great, varying from approximately eight percent at 7.2 eV to approximately one-half percent at $10.6 \mu\text{m}$. Neither higher operating frequencies nor significantly lower values of metallic absorptance are expected to be obtained since these values are near the intrinsic limits. The useful frequency region of transparent materials extends from ~ 0 to ~ 11.8 eV, and the values of the bulk absorption coefficient on this range are extrinsic, the lowest experimental values varying from $\sim 5 \times 10^{-5} \text{ cm}^{-1}$ at $2\text{--}10 \mu\text{m}$, to $\sim 10^{-6} \text{ cm}^{-1}$ at $1.06 \mu\text{m}$, to $\sim 10^{-1} \text{ cm}^{-1}$ at 7.2 eV. For frequencies greater than 14 eV, grazing incidence reflection from dense materials, and in some cases Bragg reflection, can be used, but fundamental limitations preclude the development of highly transparent materials. Multilayer-dielectric reflectors have much lower intrinsic absorptance than do metallic reflectors. Technical difficulties, including orders of magnitude typical greater absorptance of materials in film form than in bulk form, currently limit the absorptance of deposited films to a few times 10^{-4} .

The shift of interest in the last 10 years from low-power to high-power optical systems has had great impact on optical materials, particularly infrared materials. It appears that we are now at the beginning of another period of a shift in interest, this time from high power at a few isolated frequencies to a range of frequencies spread throughout the optical spectrum and indeed even to high-power sources that are tunable from the infrared at $\sim 10 \mu\text{m}$ to the X-ray region at $\sim 0.1 \text{ nm}$. The infrared region has of course received great attention, and Duthler and Sparks¹ have recently discussed vacuum-ultraviolet materials. In the present paper a broad overview of the expected performance and problems of materials for use at high power levels from the infrared through the vacuum-ultraviolet regions is given.

First consider metallic reflectors. Here metallic reflector will mean uncoated metal and normally incident radiation. It will be shown that the useful range of metallic reflectors extends from near zero frequency to approximately 14 eV, and that the absorptance on this range is great, varying from approximately eight percent at 7.2 eV

Sec. F

to approximately one-half percent at $10.6\mu\text{m}$. Neither higher operating frequencies nor significantly lower values of metallic absorptance are expected to be obtained since these values are near the intrinsic limits.

Recall that the xenon laser, which operates at 7.2 eV, or 172 nm, was materials limited from its first operation.^{2,1} The laser-mode pattern was burned into the cavity mirror, which consisted of a thin aluminum film deposited on a magnesium fluoride substrate. The important fact here is that the failure is a result of the great absorptance of the aluminum. The commercially available films had approximately 20 percent absorptance, and H. C. Chow and M. Sparks³ have shown that the intrinsic limit of the absorptance of aluminum is approximately eight percent. There are no metals with lower absorptance in the ultraviolet or vacuum-ultraviolet regions. This value of eight percent is to be compared with a typical desired value of 10^{-4} for high-power systems.

In Table 1 it is seen that the intrinsic absorptance of aluminum is \sim eight to 10 percent from \sim 500 nm (green) to 7.2 eV (or 172 nm, for xenon). In the visible and infrared regions, silver has the lowest absorptance, but the values are still quite large, ranging from approximately one-half percent at $10.6\mu\text{m}$ to approximately two percent at 500 nm. It is emphasized that these values are near the intrinsic limits,⁴ that these limits are quite high, and that significantly lower values of metallic absorptance at these wavelengths are not expected to be obtainable.

For both metallic reflectors and transparent dielectrics, it is helpful to think of two aspects of the usefulness of a material. The first is the approximate useful wavelength region. For metallic reflectors, this useful range extends from the plasma frequency (15.3 eV for aluminum) down to zero frequency, as illustrated schematically in Fig. 1. Metals are not useful as normal-incidence reflectors at frequencies greater than the plasma frequency because the reflectance becomes quite small. Notice that there is no limit on the low-frequency side. It has been argued that metals having plasma frequencies greater than that of aluminum (15.3 eV) or vacuum-ultraviolet absorptance less than that of aluminum (\sim eight percent) are not likely to be found.³

The second aspect of the usefulness of materials is how good they are in the useful range. For example, how low is the absorptance A for metals and how small is

Sec. F

Table 1. Lowest measured values of absorptance of silver and aluminum, showing the great intrinsic values of metallic absorptance.

Wavelength (μm)	10.6	1.06	0.50	0.32	0.172 (7.2 eV)
Absorptance of Ag (%)	<u>0.47</u>	<u>0.64</u>	<u>2.1</u>	~85	>80
Absorptance of Al (%)	1.2	~4.3	10	<u>9</u>	<u>8</u>

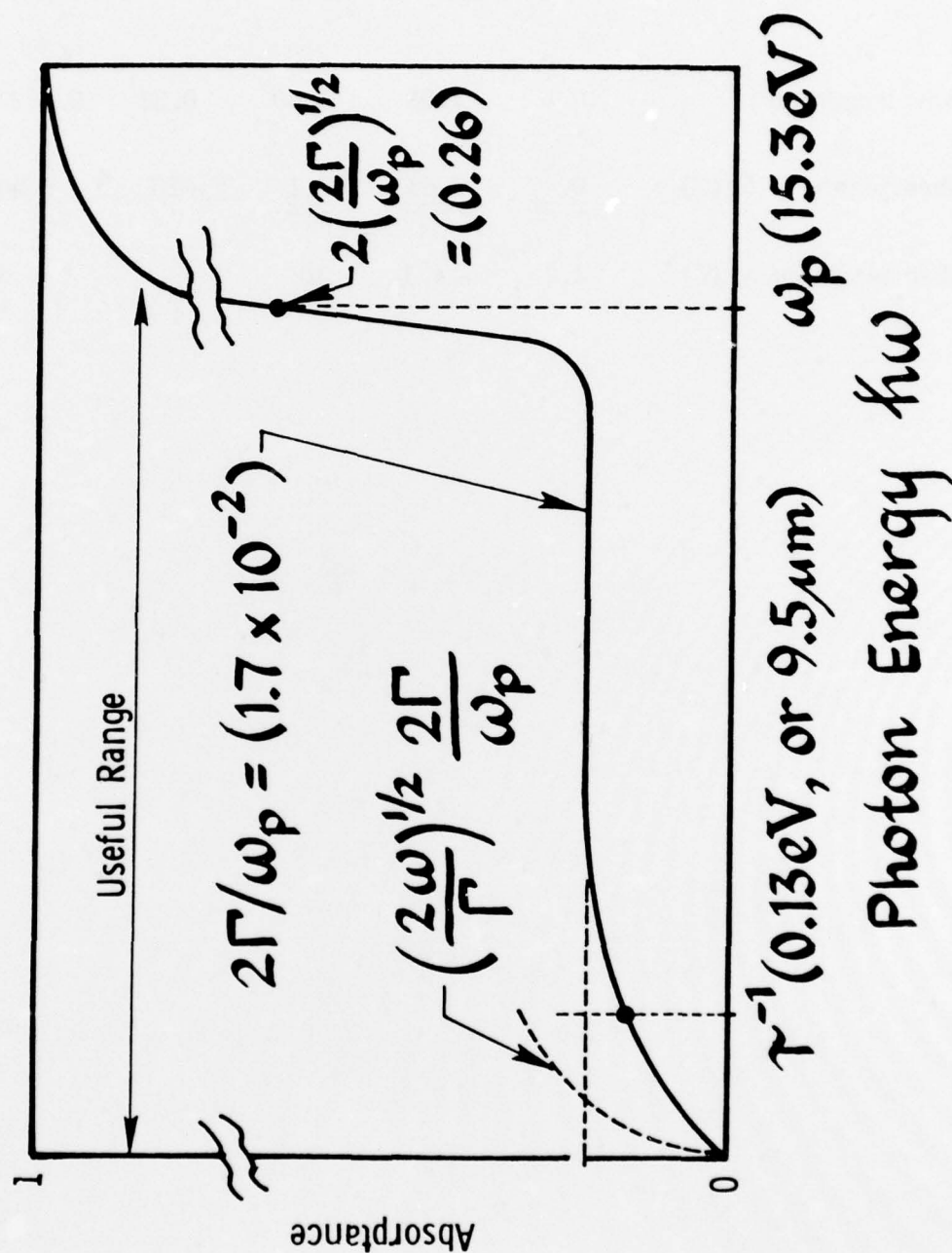


Fig. 1. Schematic illustration of metallic absorptance in the free-electron approximation, showing the useful frequency range, $0 < \omega < \omega_p$, and the great intrinsic values of absorptance on this range. Numbers in parentheses are for aluminum (neglecting the interband contribution to the absorptance).

Sec. F

the absorption coefficient for transparent materials. For aluminum in the useful range $\omega < \omega_p$, the free-electron approximation gives $A \cong 0.02$ from near ω_p to $\sim 10 \mu\text{m}$, and the absorptance decreases at longer wavelengths. The difference between this value of two percent and the above value of eight percent is that inter-band transitions are not included in the free-electron approximation.

Before leaving the subject of metallic reflectors, it is worth mentioning that they are expected to remain useful in spite of lower multilayer-dielectric-reflector absorptance (possibly by orders of magnitude), as discussed below. Merits of metallic reflectors include the following: Great cooling is possible. They may be more damage resistant than are dielectric reflectors in short-pulse operation. Diamond-turned metallic reflectors have received considerable recent attention. The useful wavelength region of a given reflector is generally greater for metallic reflectors than for multilayer-dielectric reflectors. Strongly aspheric optics are difficult to construct by multilayer-dielectric techniques, which also suffer from the lack of materials with different values of n_r for $\omega \gtrsim 8 \text{ eV}$. Coatings can be used to reduce the absorptance. Dielectrics may fail in such hostile environments as laser-fusion chambers and space.

It will be shown below that dielectrics become highly absorbing at frequencies greater than 11.8 eV. Thus there are neither good normal-incidence reflectors nor transparent materials for use at frequencies greater than $\sim 14 \text{ eV}$. Grazing-incidence reflection from dense materials and in some cases Bragg reflection can be used at frequencies greater than 14 eV, but fundamental limitations preclude the development of highly transparent materials for such high frequencies.

Since the values of metallic absorptance are quite high for use at high power levels, it is appropriate to consider alternate reflectors. Multilayer-dielectric reflectors are currently the most promising. Total-internal-reflection devices offer interesting possibilities,⁵ but the long optical path lengths through the material generally make the failure-intensity thresholds low. However, for the usual case in which antireflection coatings on the surfaces of the total-internal-reflection devices are not required, the technical difficulties of deposition are avoided.

Multilayer-dielectric reflectors have lower intrinsic absorptance than do metallic reflectors. As an illustration, for a dielectric reflector with thickness $\ell_f = 5 \mu\text{m}$ and absorption coefficient $\beta_f = 10^{-4} \text{ cm}^{-1}$, the absorptance is $A_f \cong \beta_f \ell_f = 5 \times 10^{-8}$,

Sec. F

which is an extremely low value. The lowest measured values reported to date at any wavelength are a few times 10^{-4} . For example, a value of 7×10^{-4} was obtained at $10.6 \mu\text{m}$ at the Hughes Research Laboratory. It should be technically less difficult to obtain low absorptance at $1.06 \mu\text{m}$ and in the visible region than at $10.6 \mu\text{m}$. It is emphasized that technical difficulties, including orders of magnitude greater absorptance of materials in film form than in bulk form, not fundamental limitations, currently limit the absorptance of deposited coatings (including multilayer-dielectric reflectors).^{6,7} The solution to the technical problems, perhaps by the methods suggested elsewhere,^{6,7} would be extremely important both for obtaining improved high-power reflectors and for obtaining satisfactory antireflection coatings for high-power windows.

Transparent materials are of course used for windows, antireflection coatings, multilayer-dielectric reflectors, and reflection-enhancing coating for metals. It will be shown that the useful range of transparent materials extends from approximately $45 \mu\text{m}$ to 11.8 eV (105 nm), that values of the bulk absorption coefficient β on this range are extrinsic, and that the lowest experimental values vary from $\sim 5 \times 10^{-5} \text{ cm}^{-1}$ at $2\text{--}10 \mu\text{m}$, to $\sim 10^{-6} \text{ cm}^{-1}$ at $1.06 \mu\text{m}$, to $\sim 10^{-1} \text{ cm}^{-1}$ at 7.2 eV . Higher operating frequencies are not expected to be obtained, but lower-frequency operation ($\lambda > 45 \mu\text{m}$) is possible by using materials with high Reststrahl frequencies and operating below the Reststrahl frequency.

The useful range of transparent materials is limited at high frequencies by absorption across the electronic band gap and at low frequencies by multiphonon and direct Reststrahl absorption, as illustrated schematically in Fig. 2, which was previously used in discussions of window materials.^{8,9} The high-frequency useful region is extended by using light-element crystals that are ionically bonded in order to increase the band gap.^{8,9} Lithium fluoride has the highest electronic absorption edge of 11.8 eV at room temperature. The frequency range is extended on the lower frequency end by using heavy-element ionically bonded crystals such as potassium bromide and potassium chloride.^{8,9} The absorption coefficient of potassium bromide is $\sim 10 \text{ cm}^{-1}$ at $45 \mu\text{m}$. Transparent materials can be used at lower frequencies ($\lambda > 45 \mu\text{m}$) by choosing a material with a high Reststrahl frequency and operating below the Reststrahl frequency (to the left of $\omega/\omega_f = 1$ in Fig. 2). The values of the absorption coefficient in the useful range are extrinsic, and the lowest experimental

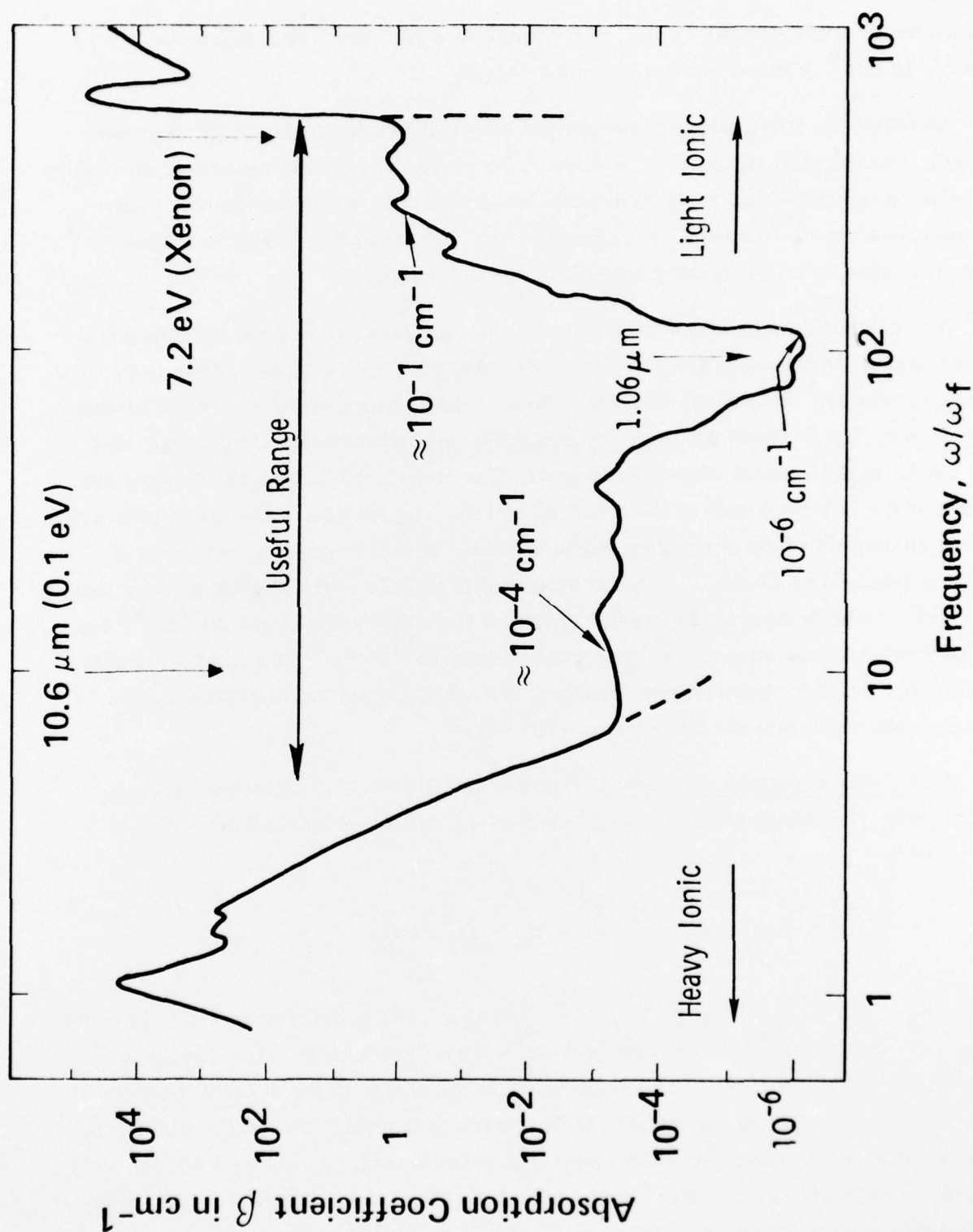


Fig. 2. Schematic illustration of the frequency dependence of the absorption of a dielectric material, showing the useful range and the extrinsic absorption on this range.

Sec. F

values range from $\sim 5 \times 10^{-5} \text{ cm}^{-1}$ at $2\text{-}10 \mu\text{m}$, to $\sim 10^{-6} \text{ cm}^{-1}$ at $1.06 \mu\text{m}$, to $\sim 10^{-1} - 10 \text{ cm}^{-1}$ in the vacuum-ultraviolet region.

Consider the limitations of transparent materials in the useful range in greater detail. The infrared region has, of course, received the greatest attention, with many absorption mechanisms having been considered in detail. Examples include multi-phonon absorption,¹⁰ damage and absorption resulting from absorbing inclusions,¹¹ and absorption by impurity molecules and molecular ions.¹²

The mechanisms by which materials fail at high intensities in the vacuum-ultraviolet region, particularly for a single 10 ns pulse of 7.2 eV radiation, have been studied recently,¹ as already mentioned above. The results are summarized briefly as follows: Fig. 3 shows the impurity-absorption spectra of several materials that are useful in the vacuum-ultraviolet region. The steep Urbach absorption edges are shown at the left-hand ends of the spectra, and the long extrinsic absorption tails are shown coming off of the absorption edges at values of the absorption coefficient β ranging from ~ 1 to 50 cm^{-1} . Typical values of β at 7.2 eV are slightly greater than 10^{-1} cm^{-1} . The heating of the crystal resulting from this value of $\beta = 10^{-1} \text{ cm}^{-1}$ can cause fracture at an intensity slightly greater than 10^{10} W/cm^2 . If a conduction electron is generated for each photon absorbed, the resulting optical distortion by the electron plasma limits the intensity to $\sim 10^8 \text{ W/cm}^2$.

This electron-plasma defocusing¹⁴ arises as follows: The refractive index n_r of the crystal is changed when the conduction electrons are generated according to the relation

$$n_r = \epsilon^{1/2} = \left(\epsilon_0 - \omega_p^2 / \omega^2 \right)^{1/2} \cong n_0 - \omega_p^2 / 2 n_0 \omega^2$$

where $n_0 = \epsilon_0^{1/2}$. The change $\delta n_r = -\omega_p^2 / 2 n_0 \omega^2$ in the index of refraction has the value $\delta n_r \cong -3 \times 10^{-4}$ for $\lambda = 1 \mu\text{m}$ and $\omega_p^2 = 4 \pi n e^2 / m$ with electron density $n = 10^{18} \text{ cm}^{-3}$. The decrease in the value of n_r at the center of the beam (for the usual case in which the intensity is greater at the center of the beam than at the beam edge) causes a defocusing since the optical path $n_r \ell$ is decreased, just as it is for a ground lens that is thinner in the center than at the edge. For a one-centimeter-thick, five-centimeter-radius R window with $n_r = -3 \times 10^{-4} (1 - \rho^2 / R^2)$, the angular distortion $\theta = -d(n_r \ell) / d\rho$ has the value $\theta = 10^{-4}$ radians, which is a factor of 10 greater than

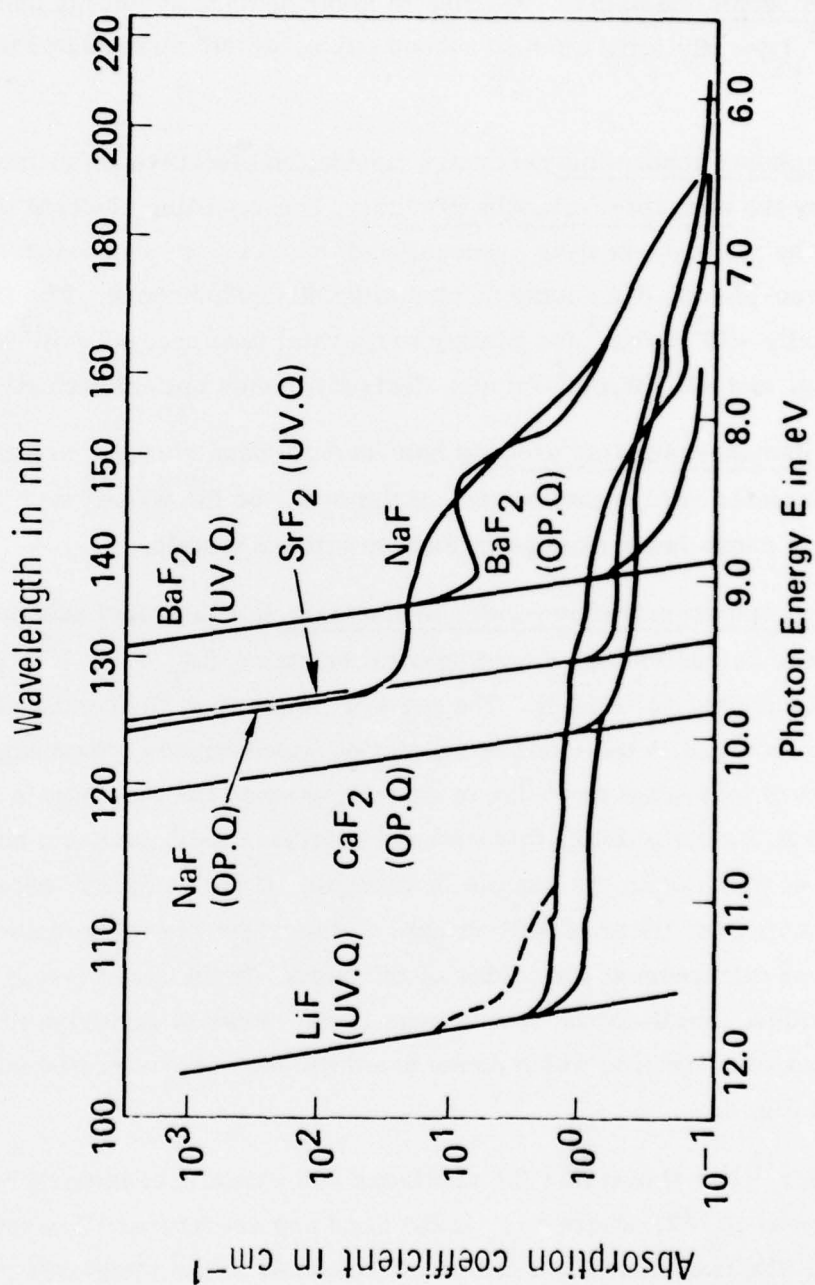


Fig. 3. Impurity absorption in several alkali halides near the absorption edge, showing the long extrinsic absorption "tails" and the sample to sample variation. From Tomiki and Miyata.¹³

Sec. F

a typical value at which failure occurs. For Gaussian beams, the distortion is somewhat worse than for the parabolic decrease to zero used in the illustrative example.

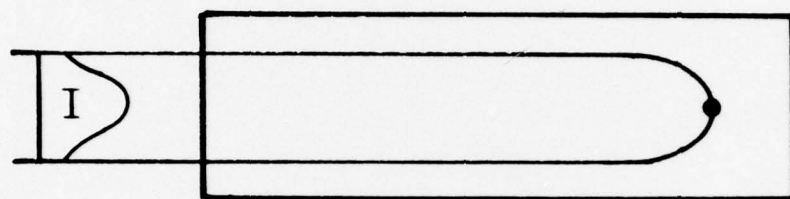
Microscopic inclusions give rise to laser damage at energy densities of $\sim 2 \text{ J/cm}^2$ typically for a ten nanosecond pulse, which corresponds to intensity $I = 0.2 \text{ GW/cm}^2$.¹⁰

Two-photon absorption generates conduction electrons which can be amplified in number by the electron-avalanche process. The resulting electron density can absorb radiation by the Joule-heating process, and the electrons can defocus the radiation by the electron-plasma defocusing mechanisms discussed above. The failure intensities are typically $\sim 10^9 \text{ W/cm}^2$ for heating to thermal fracture, $\sim 2 \times 10^9 \text{ W/cm}^2$ for heating to melting, and $\sim 10^8 \text{ W/cm}^2$ for the electron-plasma optical distortion.

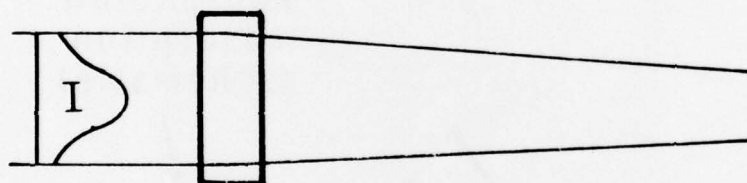
The Raman-scattering process has recently been shown¹⁵ to have a highly unstable character at high intensities, of the order of 10^9 W/cm^2 typically, which is expected to cause laser damage in Raman-active crystals.

The nonlinear-refractive-index mechanism is illustrated schematically in Fig. 4. The index of refraction has a nonlinear contribution $\delta n_r = n_2 \langle E^2 \rangle$ proportional to the square of the electric field E . The greater intensity at the center of a typical beam causes an increase in the index of refraction which causes a focusing of the beam, which in turn increases the index of refraction since the intensity is increased. If the sample is sufficiently thick, this process continues until the beam collapses to a small diameter at which point the sample is damaged. If the sample is not sufficiently thick for beam collapse, there is still an optical distortion resulting from the increase in the index of refraction at the center of the beam. In the glass lasers used in laser-fusion studies, small spatial fluctuations in the intensity give rise to local variations in the index of refraction which cause beam breakup as illustrated schematically in the bottom of Fig. 4.

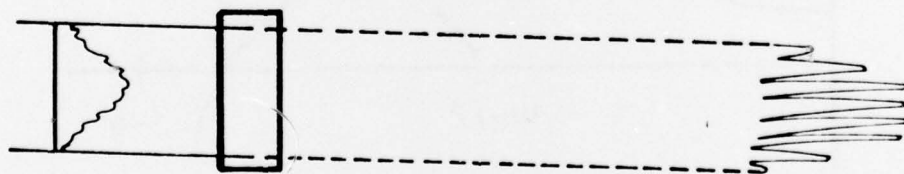
Duthler¹⁶ has shown that the nonlinear index can be considerably greater at frequencies near $\omega_g/2$, where $\hbar\omega_g$ is the band gap energy, as illustrated schematically in Fig. 5. The two-photon absorption corresponds to the imaginary part of a contribution to the dielectric constant. The enhancement of the nonlinear index corresponds to the real part of this contribution.



Self Focusing (thick)



Overall Distortion (thin)



Beam Breakup (thin)

Fig. 4. Schematic illustration of the effects of the nonlinear index of refraction $n_2 \langle E^2 \rangle$.

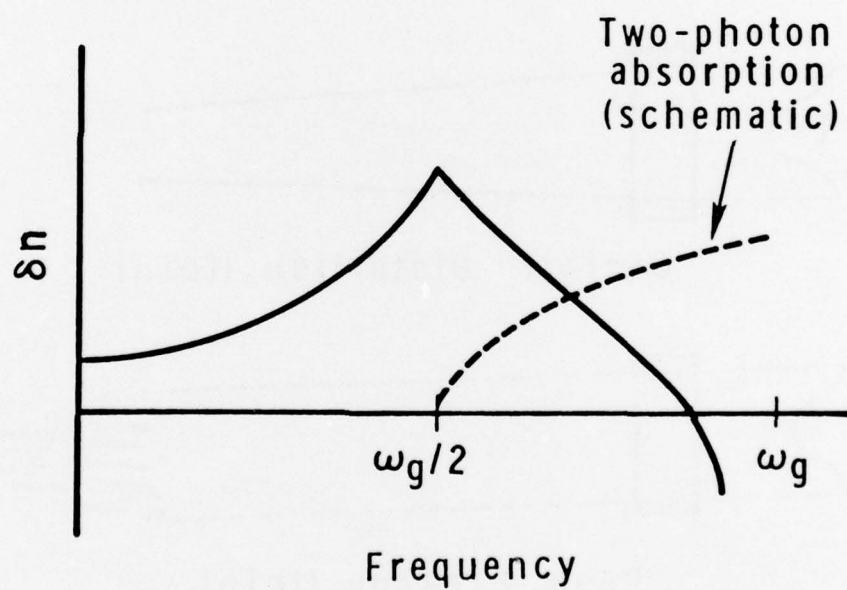


Fig. 5. Schematic illustration of the enhancement in the nonlinear refractive index $\delta n = n_2 \langle E^2 \rangle$.

Sec. F

The intensities for failure by these various mechanisms are collected in bar-graph form in Fig. 6. The lowest failure threshold ($\sim 20 \text{ MW/cm}^2$) is the metallic failure by melting. The lowest failure intensity for transparent materials is that of the one-photon-absorption, electron-plasma optical-distortion process. This value of failure intensity ($\sim 50 \text{ MW/cm}^2$) could be increased if the large value of 0.1 cm^{-1} for the absorption coefficient could be reduced by, say, purifying the materials. However, only a factor of approximately three would be gained since the failure intensities for the two-photon-absorption, electron-plasma optical distortion and the macroscopic inclusions are only slightly greater than that of the one-photon electron-plasma optical-distortion process. The value of the nonlinear absorption coefficient for the two-photon absorption process has been estimated only to within an order of magnitude or so since the electron wavefunctions are not well known. It is emphasized that the results in Fig. 6 apply to a 7.2 eV, 10 ns pulse, and that both the values of the intensities and the relative importance of the mechanisms change in general when the wavelength or pulse duration is changed.

At the present time such detailed results as those of Fig. 6 have not been obtained for other wavelengths and other pulse durations. Color-center absorption and color-center generation in the ultraviolet and visible regions have, of course, been studied in detail. The secondary-exponential absorption region for disordered materials also has been studied in some detail, as have the limits imposed by scattering. Pulsed laser damage at ruby and a few other optical frequencies have received considerable attention in recent years. However, neither the intrinsic nor the extrinsic values of failure intensities are known for the ultraviolet and visible wavelength regions. Such results as those of Fig. 6 for 7.2 eV, 10 ns pulses are needed for wavelengths throughout the visible, ultraviolet, and vacuum-ultraviolet regions and for a range of pulse durations.

References

* Talk at DARPA Conference on Infrared Laser Window Materials, Boulder, Colo., July 12, 1976.

1. M. Sparks and C. J. Duthler in "Proceedings of the Fourth Annual Conference on Infrared Laser Window Materials," Tucson, Arizona, November 1974 (Advanced Research Projects Agency, January 1975); C. J. Duthler and M. Sparks in "Laser Induced Damage in Optical Materials: 1975," NBS Special Publication 435 (U. S. Department of Commerce, 1976).
2. N. Basov, V. Denilychev, and Y. Popov, *Sov. J. Quantum Electron.* **1**, 18 (1971); P. W. Hoff, J. C. Swingle, and C. K. Rhodes, *Appl. Phys. Lett.* **23**, 245 (1973); J. B. Gerardo and A. W. Johnson, *J. Appl. Phys.* **44**, 4120 (1973); W. M. Hughes, J. Shannon, A. Kolb, E. Ault, and M. Bhaumik, *Appl. Phys. Lett.* **23**, 385 (1973).

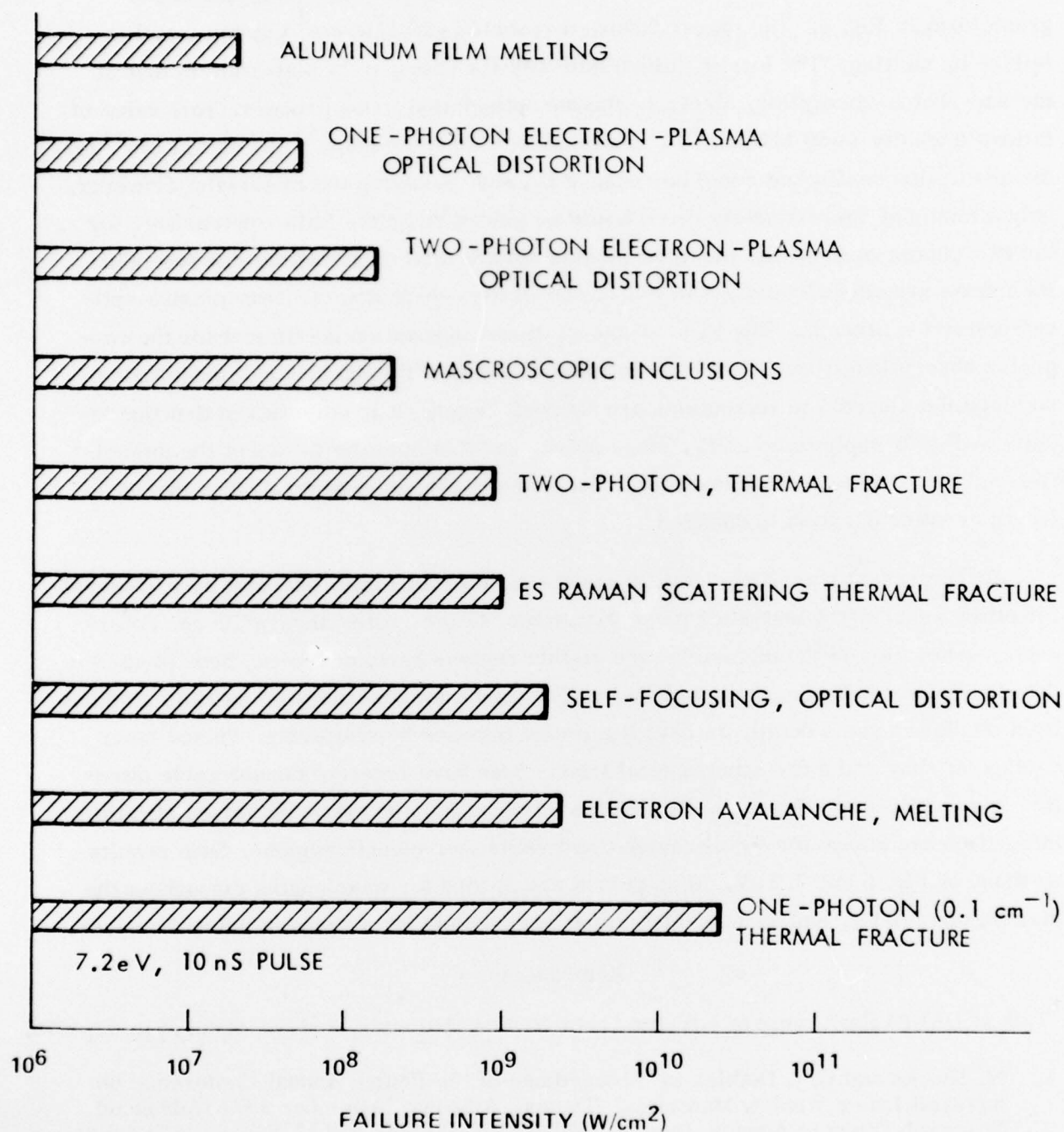


Fig. 6. Intensities at which transparent materials fail by various mechanisms for a single 7.2 eV, 10 ns pulse. Changing the frequency or the pulse duration changes the values of the intensities and the relative importance of the mechanisms.

Sec. F-References

3. H. C. Chow and M. Sparks, J. Appl. Phys. 46, 1307 (1975).
4. H. E. Bennett and coworkers at China Lake have been instrumental in reducing metallic absorptance to the intrinsic limits.
5. C. J. Duthler, Sec. E of M. Sparks and C. J. Duthler, Xonics, Inc. Third Technical Report, Contract DAHC15-73-C-0127, June 1974.
6. M. Sparks, "Proceedings of 8th Annual Symposium on Optical Materials for High Power Lasers," Boulder, Colorado, July 1976 (to be published).
7. M. Sparks, Xonics, Inc. Sixth Technical Report, Contract DAHC15-73-C-0127, December 1975.
8. M. Sparks, "Physical Principles, Materials Guidelines, and Materials Lists for High-Power 10.6μ Windows," Rand Report No. R-863-PR, September 1973.
9. M. Sparks, Xonics, Inc. Quarterly Technical Progress Report No. 1, Contract DAHC15-72-C-0129, March 1972.
10. M. Sparks, Xonics, Inc. Quarterly Technical Progress Report No. 1, Contract DAHC15-72-C-0129, March 1972; M. Sparks and L. J. Sham, Solid State Commun. 11, 1451 (1972); M. Sparks and L. J. Sham, Phys. Rev. B 8, 3037 (1973); D. L. Mills and A. A. Maradudin, Phys. Rev. B 8, 1617 (1973); T. C. McGill, R. W. Hellwarth, M. Mangir, and H. V. Winston, J. Phys. Chem. Solids 34, 2105 (1973); B. Bendow, S. C. Ying, and S. P. Yukon, Phys. Rev. B 8, 1679 (1973); K. V. Namjoshi and S. S. Mitra, Phys. Rev. B 9, 815 (1974); L. L. Boyder, J. A. Harrington, M. Hass, and H. B. Rosenstock, Phys. Rev. B 11, 1665 (1975); C. J. Duthler, Phys. Rev. (to be published).
11. C. J. Duthler and M. Sparks, J. Appl. Phys. 44, 3038 (1973).
12. C. J. Duthler, J. Appl. Phys. 45, 2668 (1974).
13. T. Tomiki and T. Miyata, J. Phys. Soc. Japan 27, 658 (1969).
14. R. W. Hellwarth, National Bureau of Standards Special Publication 341, p. 67 (U. S. Department of Commerce, 1970).
15. M. Sparks, J. Appl. Phys. 46, 2134 (1975); M. Sparks, Phys. Rev. Lett. 32, 450 (1974); M. Sparks and J. H. Wilson, Phys. Rev. B 12, 4493 (1975).
16. C. J. Duthler, Sec. C of M. Sparks and C. J. Duthler, Xonics, Inc. Fourth Technical Report, Contract DAHC15-73-C-0127, December 1974.